TESIS DE LA UNIVERSIDAD DE ZARAGOZA

2021

126

Lorenzo Vallan

Fluorescent polymeric carbon dots: from synthesis and elucidation of chemical struture towards photoactive hybrid materials

Director/es

Benito Moraleja, Ana M.

Maser, Wolfgang K.

ISSN 2254-7606

Prensas de la Universidad Universidad Zaragoza

ISSN 2254-7606

Universidad Zaragoza
1542

Tesis Doctoral

FLUORESCENT POLYMERIC CARBON DOTS: FROM SYNTHESIS AND ELUCIDATION OF CHEMICAL STRUTURE TOWARDS PHOTOACTIVE HYBRID MATERIALS

Autor

Lorenzo Vallan

Director/es

Benito Moraleja, Ana M.
Maser, Wolfgang K.

UNIVERSIDAD DE ZARAGOZA
Escuela de Doctorado

Programa de Doctorado en Ingeniería Química y del Medio Ambiente

2019

FLUORESCENT POLYMERIC CARBON DOTS: FROM SYNTHESIS AND ELUCIDATION OF CHEMICAL STRUCTURE TOWARDS PHOTOACTIVE HYBRID MATERIALS

TESIS DOCTORAL

Lorenzo Vallan

2018

CONSEJO SUPERIOR DE INVESTIGACIONES CIENTÍFICAS (CSIC)

INSTITUTO DE CARBOQUÍMICA

FLUORESCENT POLYMERIC CARBON DOTS: FROM SYNTHESIS AND ELUCIDATION OF CHEMICAL STRUCTURE TOWARDS PHOTOACTIVE HYBRID MATERIALS

Memoria presentada en el marco del Programa de Doctorado de Ingeniería Química y Tecnologías del Medio Ambiente de la Universidad de Zaragoza, para optar al grado de Doctor por:

Lorenzo Vallan

Diciembre 2018

Directores:

Ana Maria Benito Moraleja

Wolfgang Maser

Ana María Benito Moraleja y Wolfgang Maser

Investigadores Científicos del Consejo Superior de

Investigaciones Científicas

CERTIFICAN

Que la Memoria, titulada

“Preparation and investigation of fluorescent carbon dots and carbon dots-based materials”

ha sido realizada bajo nuestra dirección en el Instituto de Carboquimica de Zaragoza (CSIC) por D. Lorenzo Vallan, autorizando su presentación.

Y para que así conste, firmamos el presente certificado en Zaragoza, a 12 de diciembre de 2018

Dr. Wolfgang Maser

Dra. Ana María Benito Moraleja

This work has received funding from the European Union's Horizon 2020 Research and Innovation Programme under the Marie Skłodowska-Curie grant agreement No. 642742.

Aknowledgement

To my supervisors Ana and Wolfgang, or Wolfgang and Ana, it goes equally and sincerely my deepest gratitude. My scientific formation at ICB and the results achieved owe you a lot, for all your help and advices of every sort, for the freedom you gave me to take decisions, for the peaceful and relaxed environment you create in the group and for your tact and empathy in the personal relations.

I want to thank with all my heart Ana Santidrián and Emin Istif, whose encounter and friendship cannot be described in other ways except as a big stroke of luck.

I would like to thank Esteban Urriolabeitía for the generosity and infinite patience with which he helped me far beyond taking NMR spectra (that would have been a lot anyway).

I would like to thank my friends and colleagues at the Instituto de Carboquímica, José Miguel González Domínguez, Sandra Victor, Eduardo Colom, Alejandro Anson, Javier Hernandez-Ferrer and Enrique García Bordejé for the pleasant and constructive environment they contributed to create in our group.

I'm very grateful to Rubén Canton-Vitoria, for the incredible synergism in the laboratory that he made possible thanks to his strong commitment as well as to his good heart and enthusiasm.

I would also like to express my deep gratitude to Dr. Nikos Tagmatarchis and his group for the great collaboration during my secondment in National Hellenic Research Foundation, Greece. In particular, I would like to thank Antonia Kagkoura, that together with Rubén made my time in Athens a nice memory.

I would like to thank Fernando Ruiperéz and Jon Mattin Matxain, respectively from POLYMAT and Kimia Facultatea in Euskadi, for their great and fundamental contribution to this work.

I would like to thank Habtom B. Gobeze and Youngwoo Yang for our fruitful collaboration.

I would like to thank all the people from the Enabling Excellence network for creating the best possible teamwork and for the fruitful collaborations. Especially I would like to thank

Chris Ewels for all the effort and positivity he put on leading the network and Raul Arenal, for its important and enthusiastic contribution to the studies.

I would like to acknowledge to European Union's Horizon 2020 research and innovation program for its funding under the Marie Skłodowska-Curie grant agreement No 642742.

I would like to thank all the people that made my life in Spain rich and beautiful. Thank you Esteban, Barbara, Neus, Glòria, Riccardo, Silvia, Miguel, Benjamin, Olga, Gonzalo, thank you Adrià and thank you Sara!

And last but most important, I wish to thank my parents, Lucilla and Flavio, and my sister Chiara, for supporting me and loving me from Italy!

This turkey found that, on his first morning at the turkey farm, he was fed at 9 a.m. However, being a good inductivist, he did not jump to conclusions. He waited until he had collected a large number of observations of the fact that he was fed at 9 a.m., and he made these observations under a wide variety of circumstances, on Wednesdays and Thursdays, on warm days and cold days, on rainy days and dry days. Each day, he added another observation statement to his list. Finally, his inductivist conscience was satisfied and he carried out an inductive inference to conclude, "I am always fed at 9 a.m.". Alas, this conclusion was shown to be false in no uncertain manner when, on Christmas Eve, instead of being fed, he had his throat cut.

(From an anecdote of Bertrand Russel, via: Alan Chalmers, What is this thing called Science, 2nd edition, University of Queensland Press, St. Lucia, 1982)

Content

List of Figures

List of Schemes

List of Tables

List of abbreviations and acronyms

2D: Two dimensional

AcOEt: Ethyl Acetate

AFM: Atomic Force Microscopy

APT: Attached Proton Test

BOC: tert-Butoxycarbonyl

CA: Citric acid

CDs: Carbon dots

CEE: Crosslink-Enhanced Emission

CV: Cyclic voltammetry

DCM: Dichloromethane

DFT: Density Functional Theory

DIC: N,N′-Diisopropylcarbodiimide

DLS: Dynamic light scattering

DMF: Dimethylformamide

DOSY: Diffusion ordered spectroscopy

EDA: Ethylenediamine

EDC: N-(3-Dimethylaminopropyl)-N′-ethylcarbodiimide hydrochloride

EDS: Energy-dispersive X-ray spectroscopy

EELS: Electron Energy Loss Spectroscopy

FTIR: Fourier-transform infrared spectroscopy

HB: Hydrogen Bond

HMBC: Heteronuclear Multiple Bond Correlation

HOMO: Highest occupied molecular orbital

HAADF-STEM: high-angle annular dark-field scanning transmission electron microscopy

HRTEM: High resolution transmission electron microscopy

HSQC: heteronuclear Single Quantum Correlation

LUMO: Lowest unoccupied molecular orbital

MeOH: Methanol

MWCO: Molecular weight cut-off

NHS: N-hydroxysuccinimide

NMR: Nuclear magnetic resonance

PTFE: Polytetrafluoroethylene

QY: Quantum Yield

SEC: Size exclusion chromatography

TA: Tricarballylic acid

TDDFT: Time Dependent Density Functional Theory

TEM: Transmission electron microscopy

TMDs: Transition metal dichalcogenides

THF: Tetrahydrofuran

TGA: Thermogravimetric analysis

UV/Vis: Ultraviolet/visible spectroscopy

XPS: X-ray photoelectron spectroscopy

ABSTRACT

Carbon dots (CDs) are an emerging class of organic nano-sized particles, whose exceptional photoluminescence surely is one of the most intriguing properties. Thanks to their photo-induced energy transfer and charge transfer ability, CDs are an extremely valuable material for the preparation of photocatalysts and donor-acceptor composites for energy conversion applications. Moreover, the presence of metal ions as well as organic species affects heavily the CDs' photoluminescence intensity. For this reason, CDs are widely employed for the design of highly sensitive sensors and biosensors. Finally, CDs demonstrated to be a safe and biocompatible material, perfectly suitable for medical applications such as imaging and drug delivery.

Despite their consistent use for various applications, the chemical nature of CDs and its relationship with their outstanding optical properties is still a topic under debate, being the actual knowledge incomplete and at times contradictory. In fact, the wide variety of precursors and synthetic methods employed for the preparation of CDs is reflected in the high variability of their structures, hampering the identification of the common fundamental elements behind the fluorescence emission. Additionally, the lack of understanding and control on the synthetic process undermines the ability to design and tailor the CDs structure, which instead is a key point for improving their properties or making them suitable for further applications.

In this thesis, the first part is focused on fundamental structural and optical studies on citric acid-based CDs, which, jointly with theoretical calculations, provided new insights into the CDs chemical nature and furnished a general explanation for their blue fluorescence emission. Next, these findings were exploited for the development of a novel room-temperature and versatile synthesis method, which allows the rational design of the CDs polymer structure and at the same time their *in-situ* functionalization, granting in this way the full control on the final chemical structure. In the last part of the thesis, the preparation of CDs-based material and their chemical and optical characterization is reported. In here non-covalent and covalent approaches were both employed for combining CDs with transition metal dicalchogenides (TMDs) and creating photo-active donor-acceptor materials for energy applications.

Chapter 1 provides a general overview regarding CDs and CDs based materials. It includes a chronological review on the fundamental studies investigating the CDs chemical nature from their discovery until the actual state of the art, as well as a presentation of the parallel development of theories about the origin of the fluorescence. Next, the most common methods of synthesis and functionalization of CDs are presented. Finally, together with many examples, the employment of CDs in the field of sensing, medicine, catalysis and energy conversion is described.

Chapter 2 consists of an accurate structural and optical investigation of polymeric CDs. In here, the choice of the precursors and synthetic methods employed was determinant for identifying the structural features responsible for the bright blue fluorescence emission. By sample comparison, it was proved that the polycondensation between citric acid and ethylenediamine into a polyamide is the only necessary condition for obtaining the excitation-independent blue emission. In order to confirm these results and understand the role of the organic moieties involved in the fluorescence, DFT calculations based on the experimental results were performed. The computational models showed that strong intra-molecular H-bonds are responsible for the high conformational rigidity of CDs, which hampers vibrations and rotations, promoting thus the radiative relaxation. Additionally, amide and carboxylic acids were identified respectively as HOMO and LUMO of the fluorescent process, which consists of an intra-molecular charge transfer.

Chapter 3 presents a novel, versatile pathway towards the rational design of a wide variety of polymeric fluorescent CDs with well-defined structures. The exploited reaction consists of the room-temperature carbodiimide-mediated condensation between citric acid and amines. Moreover, this method allows the *in-situ* introduction of several types of desired moietes onto the surface of the CDs, thus achieving the CDs synthesis and functionalization in only one step.

Chapter 4 focuses on the preparation, characterization, and study of the photophysical and electrocatalytical properties of CDs/MoS_2 electrostatic complexes. Negatively charged CDs prepared from microwave irradiation of citric acid and ethylenediamine were employed in the titration essay of a dispersion of positively charged MoS_2 oligolayers. The optical properties of the forming electrostatic complex were studied ongoing. Efficient fluorescence quenching of CDs by MoS_2 was observed and ascribed to photoinduced electron and/or energy transfer as the decay mechanism for the transduction of the singlet excited state of CDs. Finally, the

electrocatalytic performance of CDs/MoS_2 was assessed towards the hydrogen evolution reaction and found superior as compared to that owed to the individual CDs species.

Chapter 5 covers the preparation of covalent CDs-TMDs (MoS_2 and WS_2) hybrids and their characterization, including spectroscopic, thermal and electron microscopy imaging methods. The preparation of the material was started by functionalizing CDs with disulfide moietes. Thus, the high affinity of disulfide groups towards Mo and W was exploited for attaching CDs onto the metal atoms defects located at the exfoliated TMDs edges. Steady-state and time-resolved fluorescence spectroscopy determined the occurrence of fast energy and/or charge transfer processes between CDs and TMDs. Furthermore, transient absorption spectroscopy studies revealed that upon MoS_2 photoexcitation charge transfer from an exciton dissociation path of MoS_2 to CDs, within CD-MoS_2, was observed. In contrast, CD-WS_2 did not display such behavior due to energetic reasons. The electronic processes taking place in this novel material certainly can be of interest for the development of donor-acceptor components in view of energy conversion applications.

Finally, *Chapter 6* provides the general conclusion of the findings and an outlook in what concerns possible opportunities and future research work.

RESUMEN

Los Puntos de Carbono, en inglés Carbon Dots (CDs), son una clase de partículas orgánicas nanométricas, cuya excepcional fluorescencia es ciertamente una de sus propiedades más fascinantes. Gracias a propiedades como la transferencia de energía y/o de carga, los CDs resultan ser materiales muy atractivos para la preparación de foto-catalizadores y compuestos donor-aceptor para aplicaciones en el campo de la conversión de energía. Además, la presencia de iones metálicos así como de especies orgánicas puede afectar considerablemente a la intensidad de la fluorescencia de los CDs. Por esta razón, los CDs se utilizan ampliamente para el desarrollo de sensores y biosensores altamente sensibles. Finalmente, los CDs son materiales seguros y biocompatibles, perfectamente adecuados para aplicaciones médicas como agentes de contraste o vectores de fármacos.

A pesar de su amplio uso en varias aplicaciones, la naturaleza química de los CDs y la relación con sus increíbles propiedades ópticas son todavía argumento de debate, siendo el conocimiento actual incompleto y a veces contradictorio. Esto se debe también a la gran variedad de precursores y métodos de síntesis empleados en la preparación de los CDs, lo que se refleja en la dificultad de identificar los elementos fundamentales y comunes relacionados con el proceso de fluorescencia. Además, la falta de comprensión y de control sobre el proceso sintético limita la posibilidad de diseñar y modificar la estructura de los CDs, lo que es un factor clave para mejorar sus propiedades o adaptarlas para aplicaciones específicas.

La primera parte de este trabajo de tesis se centra en estudios fundamentales de la estructura y propiedades ópticas de los CDs derivados de ácido cítrico y etilendiamina. Resultados experimentales de esta investigación junto a cálculos teóricos han aportado nuevo conocimiento con respecto a la naturaleza química de los CDs y también han contribuido a dar una explicación general a su emisión de fluorescencia azul. Posteriormente, se han aprovechado estos descubrimientos para el desarrollo de un nuevo y versátil método de síntesis, que consigue el diseño de la estructura polimérica de los CDs y, al mismo tiempo, su funcionalización *in-situ*, asegurando de esta manera un control completo sobre la estructura química final. En la última parte de la tesis, se reporta la preparación de materiales basados en los CDs y su caracterización química y óptica. Aquí se han utilizado estrategias de enlace covalente y non-covalente se han utilizado para combinar los CDs con dicalcogenuros mono-capa de metales de transición (TMDs: transition metal dichalcogenides) y crear materiales donor-aceptor fotoactivos para aplicaciones energéticas.

El *Capítulo 1* consiste en un resumen general en relación a los CDs y a sus materiales derivados. Incluye un repaso cronológico de los estudios fundamentales que investigaron la naturaleza química de los CDs desde su descubrimiento hasta el momento actual, así como una descripción del desarrollo paralelo de teorías sobre el origen de la fluorescencia.

El *Capítulo 2* presenta una rigurosa investigación estructural y óptica de los CDs. Aquí, la elección de los precursores y de los métodos sintéticos ha sido determinante para identificar los componentes estructurales responsables de la intensa emisión de fluorescencia azul. Comparando los resultados de las diferentes muestras, se ha establecido que la policondensación entre ácido cítrico y etilendiamina es la única reacción necesaria para la obtención de fluorescencia independiente de la excitación. Para confirmar estos resultados y para entender el papel de los grupos organicos involucrados en la fluorescencia, se han realizado cálculos de DFT (teoría funcional de la densidad) basados en los datos experimentales. Los modelos computacionales enseñan que hay fuertes enlaces de hidrogeno intra-moleculares responsables de la alta rigidez conformacional de los CDs, lo que limita la vibración y rotación de enlaces implicados, fomentando así la relajación radiativa. Además, amidas y acidos carboxílicos se han identificado respectivamente como HOMO y LUMO del proceso fluorescente, que consiste en una transferencia de carga intra-molecular.

El *Capítulo 3* presenta un camino nuevo y versátil hacia la síntesis racional de una amplia variedad de CDs fluorescentes con estructuras poliméricas bien definidas. La reacción utilizada consiste en la condensación a temperatura ambiente mediada por carbodiimida entre ácido cítrico y etilenodiamina. Además, este método posibilita la introducción *in-situ* de distintos tipos de grupos funcionales en la superficie de los CDs, logrando así síntesis y funcionalización en un solo paso.

El *Capítulo 4* se enfoca en la preparación, caracterización y estudio de las propiedades fotofísicas y electro-catalíticas de complejos electroestáticos de CDs/MoS_2. CDs cargados negativamente, preparados por irradiación en microondas de ácido cítrico y etilendiamina, se han empleado en el ensayo de valoración de una dispersión de oligo-capas de MoS_2 cargadas positivamente. Asimismo, se han estudiado las propiedades ópticas del compuesto electroestático durante la formación. Se ha observado una eficiente desactivación (quenching) de la fluorescencia de los CDs por parte del MoS_2, lo que se ha atribuido a un mecanismo de decaimento desde el estado excitado de singlete de los CDs, consistente en una trasferencia de

carga y/o energia. Por último, el rendimiento electro-catalitico de CDs/MoS_2 se ha evaluado para la reacción de desarrollo de hidrogeno y se ha encontrado que es más alto que el rendimiento en los CDs solos.

El *Capítulo* 5 cubre la preparación de híbridos covalentes CDs-TMDs (MoS_2 y WS_2) y su caracterización, que incluye métodos espectroscópicos, térmicos y de microscopia electrónica. La preparación del material ha comenzado con la funcionalización de los CDs con disulfuros. Posteriormente, la alta afinidad de los grupos disulfuros hacia Mo y W se ha explotado para conectar covalentemente los CDs a los defectos de los atomos metálicos localizados en los bordes de los TMDs exfoliados. Las técnicas de espectroscopía de fluorescencia en estado estacionario y resuelta en el tiempo han determinado la presencia de transferencia de energía y/o de carga entre los CDs y los TMDs. Asimismo, los estudios de espectroscopía de absorción transitoria han revelado que en CD-MoS_2, bajo foto-excitación, se observa transferencia de carga desde MoS_2 hasta los CDs. Por contra, CD-WS_2 no muestra este comportamiento por razones energéticas. Los procesos electrónicos que ocurren en este nuevo material pueden ser seguramente de interés para el desarrollo de componentes donor-aceptor en vista de aplicaciones en conversión de energía.

Por último, el *Capítulo 6* aporta las conclusiones generales a los resultados conseguidos y también una perspectiva futura con respecto a las oportunidades que estos resultados puedan conllevar.

1. LITERATURE OVERVIEW

1.1.Definition of carbon dots

Carbon dots (CDs) are organic particles of size generally smaller than 10 nm whose main characteristic is to be highly fluorescent. The structure of CDs is amorphous (polymeric), but often it can include carbonized or even graphitic domains, depending on the synthetic method employed for the synthesis. CDs'precursors always contain carbon and oxygen, frequently nitrogen and sometimes other elements such as sulfur or phosphorus. Clearly this definition is quite broad and accommodates a wide number of materials, different in structure and properties. Furthermore it is not an official definition. In fact, despite some efforts in this respect[1], it is still missing an unambiguous nomenclature for these materials and CDs are called as well carbon nanodots (CNDs), C-dots or Carbon quantum dots (CQDs). Nevertheless, not all these terms are perfectly equivalent, since "CQDs" generally implies the presence of graphene-like structures inside the nanoparticles, while CDs, CNDs and C-dots terms do not, albeit they neither exclude the possibility. Moreover CDs should not be confused with graphene quantum dots (GQDs), which are also nano-sized fluorescent particles, but obtained from pure sp^2 carbon structures, such as graphite, graphene oxide and carbon nanotubes, and therefore showing different optoelectronic properties.

Photoluminescence (PL) is one of the most exciting features of CDs. Different types of PL have been documented for this class of nanoparticles, including fluorescence, phosphorescence[2], chemiluminescence[3] and electrochemiluminescence.[4] Fluorescence is by far the most observed type of PL and therefore also the most investigated and exploited for the preparation of CDs-based technologies. The understanding of the relationship between CDs optical properties and chemical nature has been intensively pursued until the present days; however yet there is no consense in what concerns the structural origin of the bright fluorescence emission has not been reached yet. In the next section, a chronological approach towards the problematic of the fluorescence is presented jointly with a personal point of view, in order to provide to the reader a better comprehension of the CDs optical and chemical nature.

1.2. Understanding CDs chemical nature and optical properties: a chronological approach

1.2.1. Introduction

After 14 years from the first report, carbon dots (CDs, also referred to as C-dots or carbon nanodots) have become a prominent material for numerous nanotechnology applications, including sensing, bio-imaging, drug delivery and energy conversion. From 2008 to 2018, around 4000 articles having "carbon dots" in the title were published (Figure 1.1). In this time, the term carbon dots developed and evolved, as new synthetic approaches were explored and more reports on the CDs chemical nature appeared. Today, it refers to a rather diffuse definition, including every new type of organic photoluminescent nano-sized particle. However, in spite of the different synthetic approaches and the variety of precursor employed, it was observed that CDs share very similar and common optical properties. The effort to ascribe them to common chemical features was the driving force for the blossoming of many theories about the nature of the PL. In this chapter, the main stages that contributed to the birth and evolution of these theories are shortly reported by a chronological approach, with the intention of highlighting the historical background behind the actual state of the art. Next, the validity limits of some established interpretations are discussed under the light of the latest discoveries, re-defining and updating old points of view. In this way, a fresh set of interpretations for well-known CDs structural and optical features are proposed, in particular regarding the role of the carbonization and the role of the nitrogen in the PL, and the causes for the PL excitation-dependency.

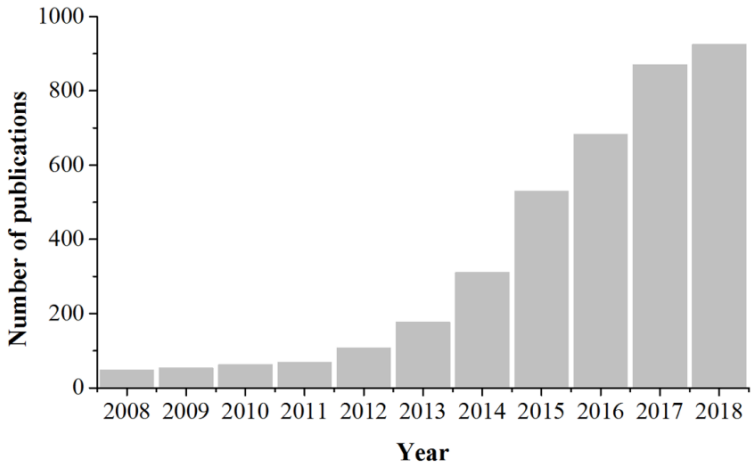

Figure 1.1. number of publications containing the words "carbon dots" in the title from 2008 to 2018, source: Scopus).

1.2.2. Chronological presentation

Carbon dots (CDs) were mentioned for the first time in 2004, by the group of W. A. Scrivens upon investigating an electrophoretic method for the purification of single-walled carbon nanotubes produced by arch-discharge.[5] The nanotubes were first treated with an oxidative HNO_3 solution and then separated from the impurities by electrophoresis. This process revealed the presence of a fluorescent fraction, which was later characterized and found to consist of carbonaceous fluorescent nanoparticles. Two years later, an electrochemical method was developed for the synthesis of blue emitting carbon particles.[6] In here multi walled carbon nanotubes were deposited on the surface of the work electrode and several redox cycles were applied, causing the fragmentation and oxidation of the material into particles of around 3 nm size, called by the authors nanocrystals (Figure 1.2).

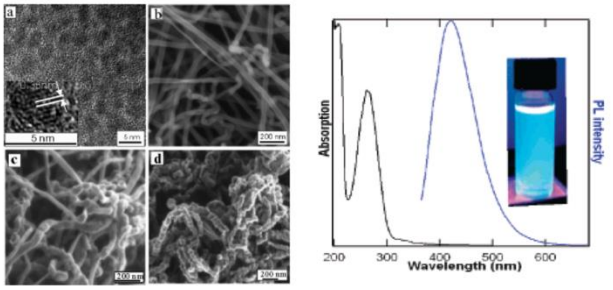

Figure 1.2. (left) TEM images of nanocrystals and other carbonaceous material, (right) absorption and emission of the nanocrystals, from ref. [6]).

During the same period, other synthetic strategies were explored with similar results: laser ablation and electro-oxidation have been established as top-down approaches for producing multicolor fluorescent dots.[7-10] As a result of interesting properties such as photoluminescence (PL), photo-stability, water-solubility and presumed biocompatibility, these new materials were identified as promising candidates for medical applications, offering a safer alternative to the toxic semiconductor quantum dots (QDs). Possibly due to this intentional parallelism, the name "carbon dots" flourished and furtherly referred to particles with very distinct chemical nature obtained from different synthetic procedures. However, in these first stage works, CDs showed low quantum yield, and the synthetic methods were involving complex processes and producing small quantities of material. In 2006, the group of Y.-P. Sun discovered a procedure for switching-on the fluorescence emission of CDs produced by laser ablation and acid oxidation.[9] The as-produced nanoparticles were heated at 120 °C for 72 h in presence of amine-terminated PEG, obtaining the passivation of the particles' surface with organic material (Figure 1.3). After this process, the quantum yield raised from zero up to 10%. In order to explain these observations and to identify the fluorescence origin, the authors suggested that the fluorescence may be attributed to the presence of surface energy traps, which become emissive upon stabilization as a result of the surface passivation.

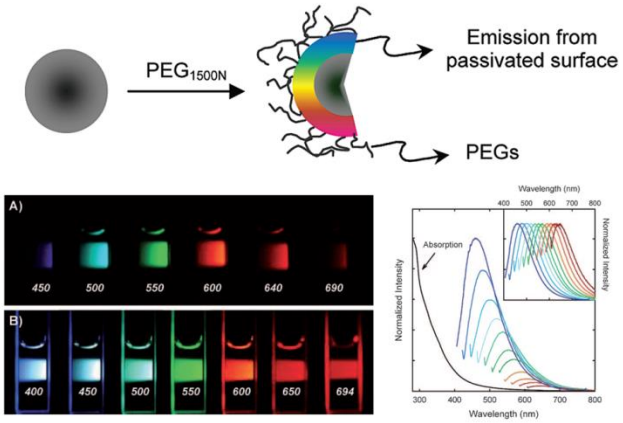

Figure 1.3. PL emission of PEG_{1500N} passivated CDs, excited at different wavelengths (from ref. [9]).

In the following years, passivation with organic molecules became a routinary step in the synthesis of CDs.[11-16] In 2008, passivation was performed *in-situ*, by laser treatment of graphite in a solution of PEG_{200N}.[8] By a comparative analysis between this sample and a blank obtained by laser irradiation of graphite in water, amide moietes, detected only in the former one, were determined to play a fundamental role in the fluorescence activation.

In these pioneering works, some common points should be highlighted. The carbon source employed here consisted of pure carbon materials, such as graphite, carbon nanotubes and active carbon. The synthetic procedures involved the destruction and oxidation of the material, aiming to create the defects acting as surface traps. Additionally the fluorescence emission of the as-produced nanoparticles commonly showed an excitation-dependent behavior. Considering that these CDs are expected to have large sp^2 conjugated domains delimited by oxygenated groups, the excitation-dependent PL was attributed to the variety of trap states on the particles surface, as well as to the quantum size effect, i.e. the radiative recombination of excitons whose energy depends from the size of the conjugated domain. With these premises, passivation was considered to play a role in the stabilization of the energy traps, enhancing the emission.

In 2008, the group of P. Giannelis et al. reported an entirely different approach for the synthesis of photoluminescent organic nanoparticles[17-18]. Citrate ammonium salts and other molecular precursors were heated at 300 °C by hydrothermal treatment or pyrolysis, obtaining nanoparticles of <10 nm size and quantum yield (QY) of 3%. Their optical properties showed many similarities with the ones of the CDs obtained from fragmentation and oxidation of carbon materials and an analogy with them was made. Thus, it was suggested that the carbonization of the molecular precursor leads to the formation of a carbon core, composed by co-existing aromatic and aliphatic regions, similarly to graphite oxide. Additionally, TEM images, high water solubility and the presence of amide bonds proved that a polymeric corona covers the surface of the nanoparticles. Therefore, polymerization was proposed to be the reaction step preceding the core carbonization.

The following studies explored more synthetic routes, finding that hydrothermal treatment[19-21], pyrolysis by microwave irradiation[22-24] and strong acid treatment[11] were all effective one-step methodologies for the obtaining of fluorescent nanoparticles, achieving better quantum yields and avoiding annoying oxidation and passivation steps with respect to the top-down approaches. Possibly because these new materials resembles in size and optical properties the firsts fluorescent carbon nanoparticles discovered, they were as well called carbon dots (or C-dots, carbon nanodots, carbon quantum dots etc.), widening and blurring the limits of this definition. This vagueness most likely was encouraged by looking for transversal principles beyond the PL, and the attention was initially focused on the carbonized core and its interaction with the amorphous surface, since the synthetic procedures were generally harsh and high temperature unavoidable forms sp^2 unpredictable structures.

The complex fluorescence behavior of bottom-up synthetized CDs is often described as a combination of processes, covering excitons recombination (Figure 1.4a), presence of trap states which may promote the radiative decay (Figure 1.4b), and interaction of the oxygenated groups at the edges with the conjugated domains[25]. Nevertheless, these hypothesis imply (and the dictionary suggests) the existence of highly delocalized states, i.e. a semi-conducting band from where the electron can decay through different pathways. Under this point of view, the existence of a graphitized core, offering dlocalized ground and excited states, is the necessary condition for the appearance of PL, while oxygenated groups simply promote the radiative decay acting as localized acceptor traps for the excited electrons. Moreover in this framework nitrogen is commonly depicted as a dopant ("N-doped carbon dots" appeared more than 200 times in the article titles between 2010 and 2018; source: Scopus), suggesting its participation in the process of electron delocalization.

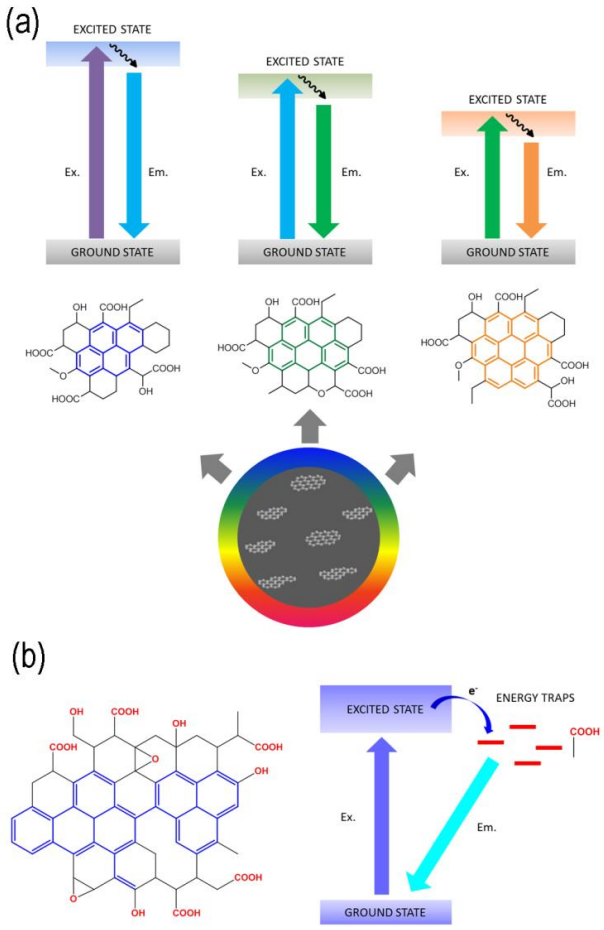

Figure 1.4. (a) PL due to the quantum size effect. The sum of different conjugated domains with distinct energy band gaps can be responsible for the observed excitation-dependent PL behavior. (b) Oxygen groups located at the edges of the conjugated domains can act as localized energy traps, which promote the radiative relaxation.

However, in 2012 P. Giannelis et al. studied the formation of CDs by pyrolysis of citric acid and ethanolamine at different temperatures and observed that carbonization only starts above 200 °C.[26] Interestingly, CDs prepared at lower temperatures display very intense PL emission independent from the excitation (QY=50%). Increasing the temperature, this features drastically fall, almost disappearing at 300 °C, while with the growth of the carbonized core a new type of excitation-dependent PL is observed, but with considerably lower quantum yield (4% at 300 °C). Thus, it was proposed that at relatively low temperature (<200 °C) the formation of molecular fluorophores occurs. Increasing the temperature the fluorophore is consumed by the carbonization process, and the excitation-dependent PL rises at the expenses of the excitation-independent component. Further studies brought additional arguments for the existence of the molecular fluorophores[27-29].

The structural recognition of the molecular fluorophore is largely pursued and since 2015 several reports linked the PL to particular aromatic structures, formed when citric acid and amines precursors were employed. The first report in this direction, by B. Yang et al., recognized the origin of the molecular state fluorescence in the IPCA conjugated molecule (imidazo[1,2-a]pyridine-7-carboxylic acid), which was found attached to the carbon core and whose optical properties are in good agreement with the CDs excitation-independent blue PL (Figure 1.5a,b).[30-31] Naturally, the fluorophore structure depends on the reagents employed (Figure 1.5c,d). Many publications identified similar pyridine-like/carboxylic acid structures as origin of the molecular state PL[32-36], also underlining the influence of supramolecular H-bond or aggregation.

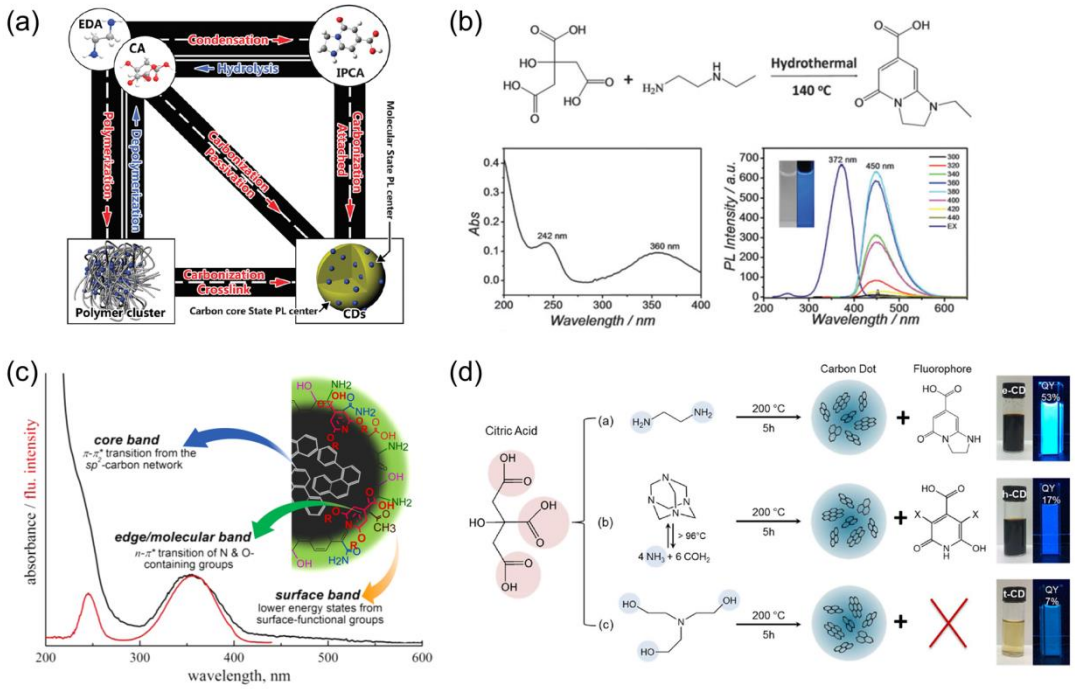

Figure 1.5. reactions that occur during the hydrothermal treatment of citric acid and ethylenediamine towards the formation of molecular fluorophores, polymer clusters and the carbonized core (from ref. [30]) (b) IPCA fluorophore and its optical properties (from ref. [30]). (c) molecular fluorophore and core contributions to the absorption of CDs (from ref [36]). (d) the hydrothermal treatment of citric acid with different amines produces molecular fluorophores (from ref. [32]).

Nevertheless, in the last few years another relevant type of PL process was discussed in relation to the CDs optical behavior. It was established that non-conjugated polymers are capable of displaying bright PL emission in condition of high rigidity. Aggregation[37-38], hyperbranching[39-40], self-assembly[41] or crosslinking[40, 42] are some of the conditions that enable the PL emission in non-conjugated polymers (Figure 1.6). This phenomenon was therefore called crosslink enhanced emission (CEE) effect. B. Yang documented strong PL emission in various CDs systems prepared in mild conditions, regardless the absence of carbon core or simple C=C double bonds and thus excluding also the presence of aromatic molecular fluorophores[2, 43-46]. The PL of CDs was therefore related to the immobilization of the so-called sub-fluorophores located on the polymer structure, which are organic chromophores (such as C=O, C=N, N=O, corresponding for example to amide and carboxylic acid groups) that, due to the crosslinked and rigid structure of the CDs, become able to re-emit the absorbed photons by means of radiative pathways.

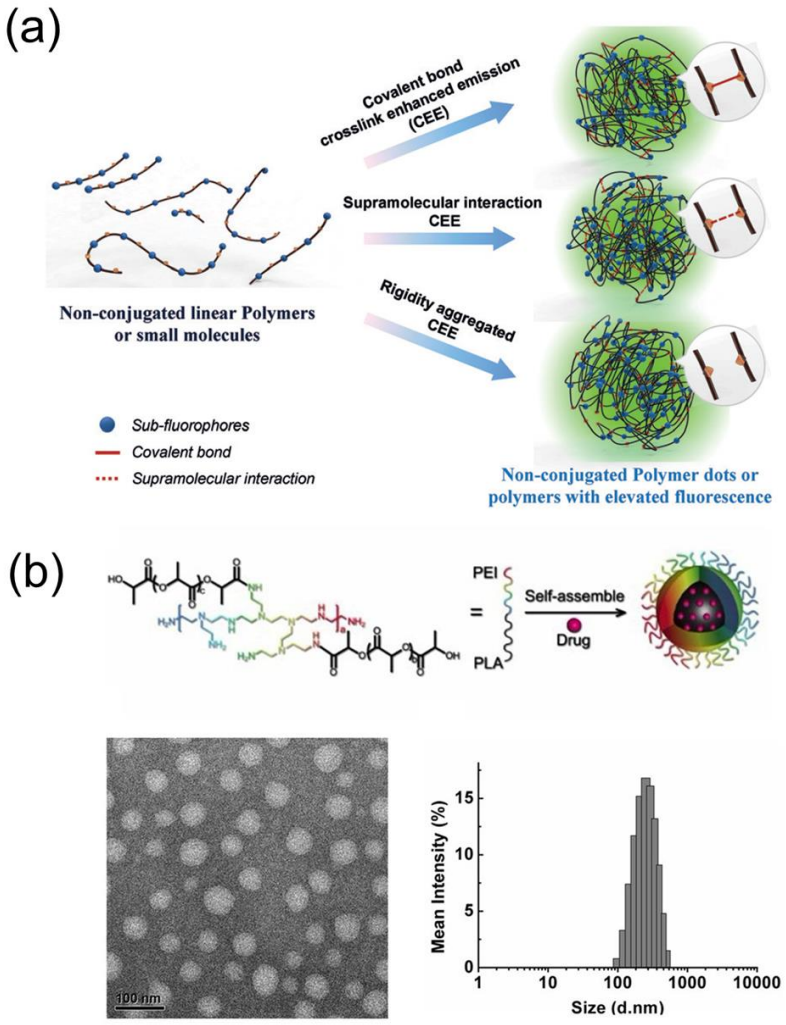

Figure 1.6. (a) some examples of interactions responsible for the CEE effect (from ref. [43]). (b) a fluorescent crosslinked copolymer from polyethyleneimine and polylactic acid (from ref. [40]).

The emission due to the CEE effect may be affected or not from the excitation wavelength employed (Figure 1.7). When the energy distribution of the polymer conformations originating the PL is narrow, i.e. the PL centers are similar, the emission is independent from the excitation. On the other hand, when the emitting states are originated from different conformations, emission can be tuned by excitation. In fact, the lowering of the excitation energy leaves the various higher emission energy levels inaccessible and the exclusion of their contribution from the total PL is not only reflected in the intensity decrease, but also the emission red-shift[47]. The rate of aggregation can also broaden the energy levels and make PL dependent from excitation[37].

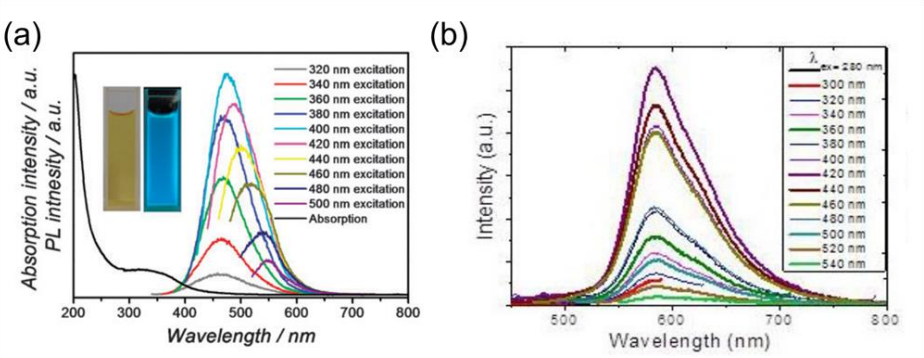

Figure 1.7. (a) excitation dependent PL from non-conjugated crosslinked PEI nanoparticles (from ref. [44]), (b) excitation independent PL from non-conjugated polyamide nanoparticles (from ref. [48]).

1.2.3. Discussion

From the CDs discovery up to now, four coexisting interpretations of the PL phenomena were formulated in the following chronological order:

1. Quantum size effect of aromatic domains with different sizes (excitation dependent).
2. Trap states from oxygen moieties and from passivation by nitrogen containing molecules (excitation dependent or independent, according to the energy distribution of the traps).
3. Conjugated molecular fluorophores attached on the CDs surface (excitation independent).
4. CEE effect of non-conjugated polymer (excitation dependent or independent, according to the distribution of conformations and aggregation effects).

Naturally, the listed PL emitters are not mutually exclusive. On the contrary, the complex optical behavior of the CDs has been frequently described as the sum of different contributions. Nevertheless, the gathered information can be exploited to discuss in hindsight the way that statements about the fluorescence-structure relationship should be argued from the experimental data. A revision of the most widespread interpretations in favour of an updated point of view that considers and includes the latest findings is highly desirable for providing better basis for the future development of the field of CDs.

As aforementioned, the PL due to quantum size effect, trap states and passivation implies the presence of large conjugated domains in the CDs structure. When CDs were discovered, the employed methods generally involved the use of pure carbon material as precursor, as well as very high temperatures and harsh treatments. Thus, it is reasonable that the observed PL in

these nanoparticles has to be somehow related to their conjugated structures. Nowadays these materials are most likely classified as GQDs, a class of carbon nanoparticles consisting of nano-sized single or multilayer of graphene oxide. The bottom-up approaches however afford completely different results: the use of organic molecules as precursors requires diverse procedures, which generally involve two consequential synthetic steps: the formation of the polymer nanoparticles and their partial carbonization. Possibly due to the fact that the bottom-up approach followed chronologically the top-down approach, carbonization has been considered for long time the key step for enabling the PL properties of CDs and it has been pursued by employing harsh procedures, with temperatures not lower than 150-250 °C. High temperatures promote dehydration and decarboxylation, which are reactions required for the formation of aromatic structures. As previously reported, these structures may involve individual conjugated molecular fluorophores, whose PL is independent from the excitation, or, at higher temperature, random graphitic domains. PL dependency from the excitation has been generally related to these last products of carbonization. However excitation dependency should not be considered a proof of the contribution of graphitic domains to the PL, since comparable excitation-dependent emission was also reported for pure non-conjugated polymer nanoparticles. On the contrary, since polymerization is the preliminary step for the carbonization (Figure 1.8a), the hypothesis that PL emission is due to the CEE effect should be considered first, assuming that the synthetic method does not achieve the complete carbonization (>300 °C) (Figure 1.8b).

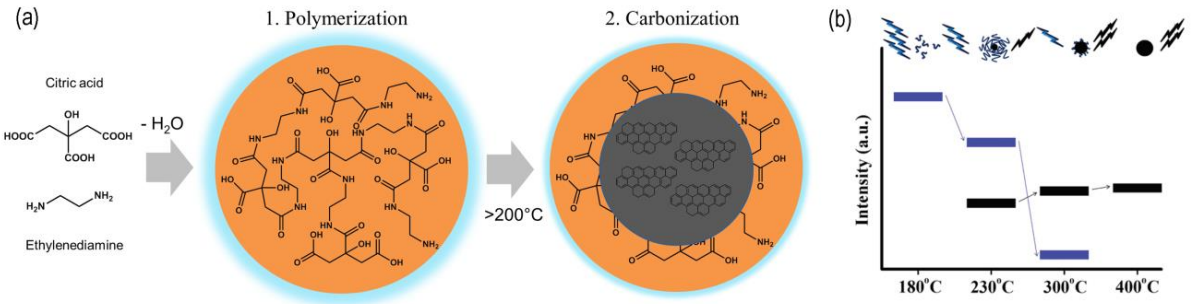

Figure 1.8. (a) polymerization and carbonization step for citric acid-based CDs. (b) Schematic representation of the emission characteristics of three photoactive species produced from the thermal treatment of mixture of citric acid and ethanolamine. During pyrolysis, the organic fluorophores (blue groups) are consumed for the buildup of the carbonized core (black sphere) so that the PL component that corresponds to the carbonized core (black bars) increases at the expenses of the component that arises from the organic fluorophores (blue bars) (from ref. [26]).

Additionally, even the simple presence of graphitized domains should be proved carefully. It was reported that also polymers can form crystalline structure inside the CDs, which could be potentially mistaken as graphite lattice when analyzed by TEM and XRD (Figure 1.9).[48] These techniques are employed routinely for demonstrating the CDs graphitic nature, jointly with XPS analysis. However XPS structural attribution is rarely supported by other techniques for the precise determination of the carbon structures and therefore it has a somewhat arbitrary taste. For an improved structural characterization, NMR spectroscopy can offer a wide choice of experiments that allow the recognition of the CDs features, easily revealing the rate and the type of carbonized structures, as well as improving the understanding of the polymer component. Finally, the passivation process should be discussed under the light of the CEE effect. Passivation with amine-containing molecules or polymers has been largely exploited for originating or enhancing the PL of carbon nanoparticles carrying carboxylic acids. This process, promoted by heating, has been frequently related to the stabilization of the trap states, as well as to the doping of the conjugated structures. Nevertheless, amide is known to increase the molecule structural rigidity, possibly promoting the CEE effect, and could also participate to the PL emission as subfluorophore. A role of nitrogen atoms, independent from the presence of conjugated systems, should be certainly considered when amines and carboxylic acids are found among the CDs precursors.

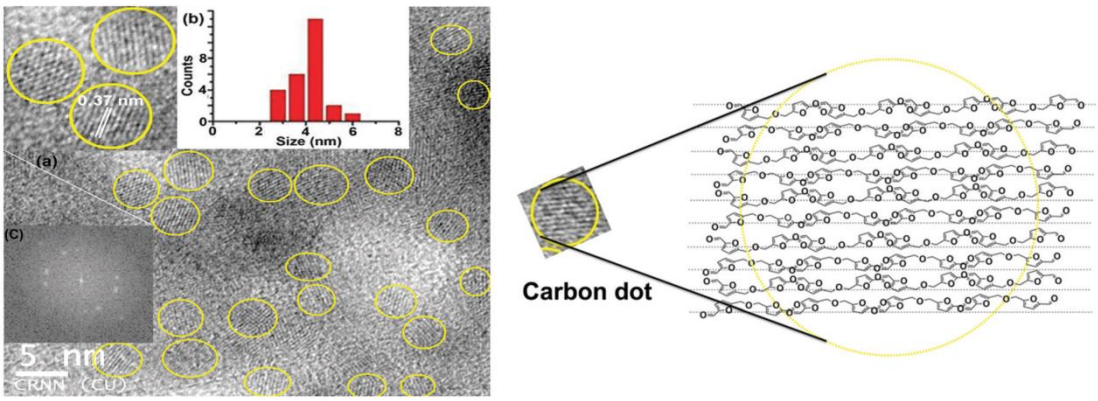

Figure 1.9. (left) TEM image and (right) plausible aggregation pattern of polymer CDs, resembling graphite lattice (from ref. [48]).

1.2.4. Conclusion

In summary, a brief chronological report was intended to draw the attention of the reader on the interconnection between birth and evolution of the CDs synthesis approaches and the development of theories regarding the structure/PL relationship. Under the light of the latest

findings, the validity limits of some established interpretations concerning the PL chemical nature of CDs were reconsidered, pointing the attention on the underestimated role of the polymer component, which, in contrast to the carbonized core, is always present when molecular precursor are employed in the synthesis. In particular, it is shown that facts such as PL dependence from the excitation and presence of C=C double bonds cannot be presented as the sole evidences of a contribution from the carbonized component to the PL, when the presence of the polymer component could furnish alone a self-sufficient explanation. For equivalent reasons it is proposed to consider nitrogen not only for its possible electronic participation on the conjugated structures, but also and primarily as amide, when carboxylic acids and amines are employed in the CDs synthesis. Amide in fact could play a role in the PL process independently from the existence of a carbonized core. Finally, a wider use of the NMR spectroscopy is encouraged for safely ascertaining the presence and the extent of the carbonized component, as well as the nature of the polymer structure.

1.3.Precursors and synthesis methods of CDs

1.3.1. Introduction

In this chapter a description of the precursors and the synthetic methods employed for the synthesis of CDs is presented. In fact, these two points are fundamental for understanding their chemical and optical properties and they also will furnish an idea of the extreme variety of structures and materials that goes by the name of CDs.

1.3.2. Precursors

Fluorescent nanoparticles have been produced from many and very different precursors. Indeed, any oxygen- and nitrogen-containing organic molecule can be employed, without neither the need of complex synthetic processes nor difficult purificiation steps (basically, the majority of these procedures involves the simple heating of the starting material in solution, as described in the following sections). For this reason, researchers were very imaginative at the moment of the precursors choice. For example natural substances were extensively explored as source for the obtaining of CDs and included grass[49], hair fibers[50], orange juice[51], melon peel[52], rice flour[53], papaya[54] and urine[55] (pee-dots). Nevertheless, more ordinary reagents are usually preferred. Actually, CDs are normally obtained from simple molecules rich in oxygen groups, typically sugars, aminoacids, ascorbic acid and citric acid. Probably, citric acid is the most common reagent; so much that citrate-based CDs recently deserved

alone a full review.[56] It is widely accepted that the presence of nitrogen is responsible for a strong enhancement of the fluorescence emission and therefore nitrogen-containing molecules are also normally found among the precursors. In particular ammonia[32], urea[57], ethylenediamine[45] and other simple amines are often employed. Also L-lysine has been used for this purpose[58-60], while L-cysteine is added when the introduction of sulfur is desired.[61-62] Finally, polymers constitute another exploited category of precursor, among which polysaccharides (such as chitosan)[63], polyethylene glycol[64], polyacids[45] and polyamines[44]. In general, the use of molecular precursors is more widespread with respect to natural materials and polymers, probably because it allows the obtaining of simpler structures with better defined properties.

1.3.3. Synthetic methods

Due to the increasing ability to understand the relationship between structure and fluorescence of CDs, some older synthetic procedures (such as laser ablation/oxidation route, combustion, additional passivation steps) were replaced along the years with more efficient approaches (see Chapter 1.2 for details). In general, the majority of the employed methodologies involve harsh temperature conditions, in order to achieve the condensation and dehydration reactions responsible for the growth of the CDs. In this section the most nowadays common procedures for the obtaining of CDs, i.e. hydrothermal treatment, microwave irradiation, other carbonization procedures and polymerization, are described and illustrated with few examples.

1.3.3.1 Hydrothermal treatment

The hydrothermal method is based on the employment of autoclave (Figure 1.10) for treating at high temperature and high pressure the water solution containing the precursors. Typically the reported synthesis temperatures for CDs are found between 150-250 °C and the time of reaction is usually comprised between 1-6 hours. This method is probably the most widespread, because it allows to obtain nanoparticles with controllable size, surface modifications and high stability.[32, 51, 60-62, 64-70] B. Yang et al. exploited the hydrothermal method for synthetizing a wide variety of CDs from citric acid and different amines.[27] Moreover they performed the synthesis at different temperatures, from 150 to 250 °C, observing a trend in the quantum yield, which laid the basis for the understanding of the polymer structure role in the fluorescence behavior.

Figure 1.10. Disassembled autoclave reactor.

1.3.3.2 Microwave irradiation

Microwave irradiation is a very energy efficient way for the synthesis of CDs.[57-58, 71-74] Precursors irradiation accomplishes the formation of the nanoparticles in few minutes, with a good control on temperature and pressure. The microwave irradiation accelerates and facilitates many organic reactions that in normal conditions would be kinetically hindered or not allowed at all, resulting in the fast polymerization/carbonization of the starting material. Through this procedure, Q. Wang et al. prepared an efficient sensor for the selective detection of Ce^{3+}.[75] The CDs synthesis involved a typical microwave-mediated protocol: citric acid and urea were dissolved in water and irradiated for 3 minutes at 800 W (Figure 1.11). The CDs were separated from the carbonized larger particles through centrifugation, dialysis and precipitation in ethanol.

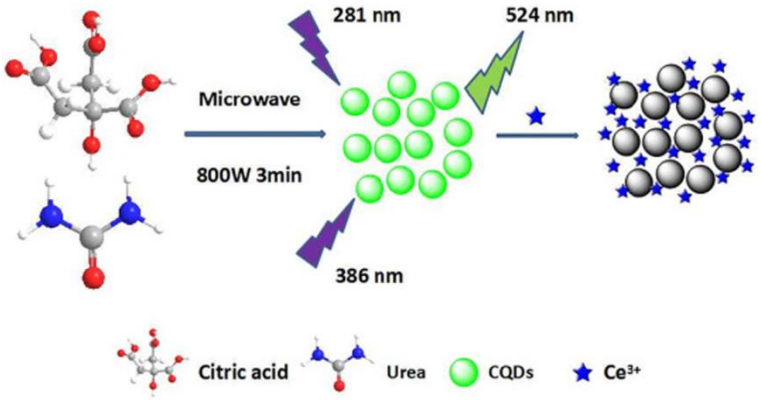

Figure 1.11. microwave synthesis of CDs for Ce^{3+} sensing (from ref. [75]).

1.3.3.3 Pyrolytic or acid-promoted carbonization and other similar procedures

Pyrolysis is an inexpensive and convenient method for the production of CDs from biological materials. It consists of heating the precursor at high temperatures in air or inert atmosphere, followed by dissolution of the product in an appropriate solvent, such as water, and by uptake of the nano-sized material through a process of filtration and purification.[52, 63] Alternatively, the material can be carbonized in concentrated acid[76], or simply by prolonged heating in water[59, 77], obtaining similar results. Although with some differences, all these methods promote the condensation, dehydration and decarboxylation reactions that enable the CDs growth and carbonization.

1.3.3.4 Polymerization and crosslinking

The non-conjugated polymer structure has not been widely recognized yet as an important contribution to the CDs fluorescence, which is most commonly related to the sole carbonized structure. For this reason, only few studies reported the preparation of CDs by polymerization or crosslinking, although similar processes effectively take place also in the previously described methods. An interesting example of CDs synthesis by polymerization is given by the work of S. Dai et al.[78] In here carbon tetrachloride and ethylenediamine were polymerized inside a porous zeolite matrix, obtaining nano-sized fluorescent non-conjugated polymers. B. Yang et al. employed instead a branched polyethylenimine for the crosslinking reaction with carbon tetrachloride (Figure 1.12).[44] Also in this case the formed nanoparticles showed high fluorescence emission due to their non-conjugated structure.

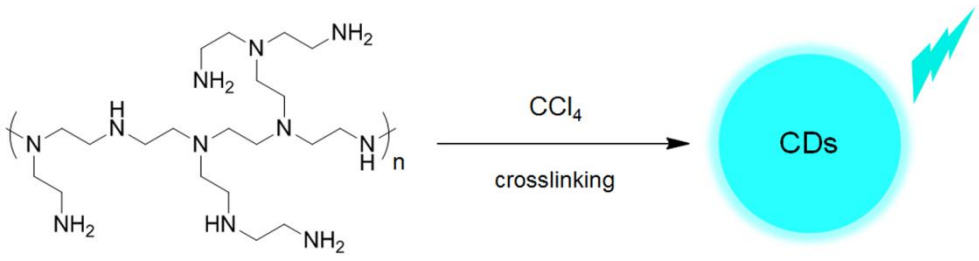

Figure 1.12. CDs synthesis by branched polyethyleneimine crosslinking.

1.4. Quenching of the CDs fluorescence

1.4.1. Introduction

Quenching, i. e. the decrease of the fluorescence intensity due to an external agent, is a common and well-documented process in CDs, thus its comprehension is of great interest for the design of sensors and biosensors. Typical quenching mechanisms observed in CDs can be related to different phenomena, such as Förster resonance energy transfer (FRET), photoinduced electron transfer (PET) or the inner filter effect (IFE). In this chapter, a short guide for the recognition of these phenomena with some CDs-related examples is provided.

1.4.2. FRET, PET and IFE in CDs

1.4.2.1 Förster resonance energy transfer (FRET)

In the proximity of an ion or molecular specie, an excited fluorophore can relax to the ground state transferring on it the absorbed energy through a non-radiative process, which is an alternative path to the fluorescence emission. The requirement for the occurrence of this phenomenon, called FRET, is that the emission of the donor (i.e. the fluorophore) matches with the absorbance of the acceptor, in the way that the two spectroscopic features are at least partially overlapped. In addition, the donor-acceptor distance is crucial, since the FRET probability is inversely proportional to R^6, where R is the distance between the donor and the acceptor. FRET processes have been frequently observed in CDs. The group of R. Sun investigated the quenching mechanism of CDs prepared from hydrothermal treatment of chitosan.[79] Several nitroaromatic molecules, such as 2,4,6-trinitrophenol (TNP), were tested as quenchers, at various concentrations. For all the nitroaromatics, the Stern-Volmer plot showed a linear correlation between the ratio I_0/I and their concentration. Moreover the quenching rate of the different nitroaromatics was correlated with the overlap rate of their absorption with the CDs emission, which takes place around 400 nm, as well as with the corresponding decrease of lifetime. Finally, a CDs spectroelectrochemical investigation excluded the contribution of electron transfer phenomena to the quenching mechanism, since nor oxidation or reduction of the nanoparticles alone decreased the fluorescence intensity, proving that the dynamic quenching observed in these CDs is due to a FRET process.

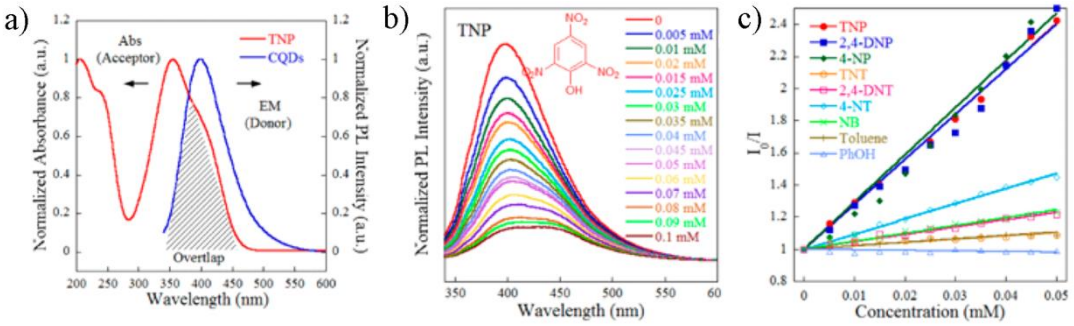

Figure 1.13. a) overlap between CDs emission and TNP absorbance, b) CDs emission at different concentrations of TNP, c) Stern-Volmer plots for different nitroaromatics (figures from ref. [79]).

FRET processes induced by metal ions and organic molecules have been widely exploited for the preparation of fluorescent sensors.[80-83] As an illustrative example, Chen et al. employed the FRET mechanism of CDs for detecting Co^{2+}.[84] CDs were prepared by hydrothermal treatment of citric acid and L-cysteine. Next, cysteine was used for chelating the cobalt ions, forming the complex ($Co(cys)_3^{2+}$), which shows a wide absorption in the range of the CDs emission and therefore its concentration is finely reflected in the CDs fluorescence quenching, occurring by FRET (Figure 1.14). Furthermore the electrostatic interactions between negatively charged CDs and positively charged ($Co(cys)_3^{2+}$) intensify the collision probability, thus increasing the CDs sensitivity.

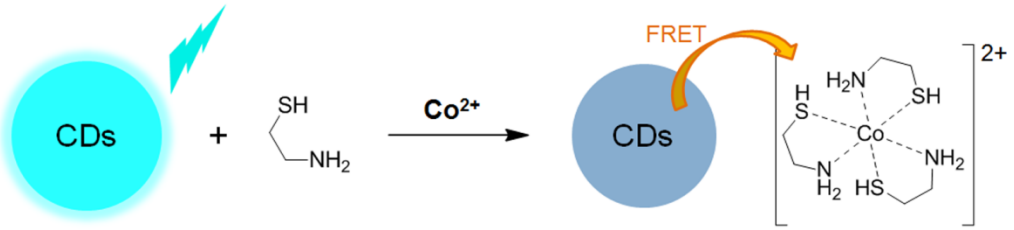

Figure 1.14. FRET between CDs and the complex ($Co(cys)_3^{2+}$).

1.4.2.2 Photoinduced electron transfer (PET)

In PET, an electron is transferred from the donor excited state to an acceptor, from where it goes back to the donor ground state. The charge separation is involved in this mechanism and therefore the formation of a cation radical and an anion radical. Depending if the fluorophore is the donor or the acceptor, the process is called oxidative or reductive PET respectively. Thus, the presence of PET implicates the quenching of the fluorescence emission, since a new non-radiative decay is provided for the excited electron of the fluorophore.

The PET phenomenon was exploited by Z. He et al. in the preparation of a CDs-based "off–on" fluorescent probe for the selective detection of phytic acid (Figure 1.16).[60] The fluorescent nanoparticles were prepared by hydrothermal treatment of citric acid and lysine. Next, Fe(III) was added and the quenching of the CDs fluorescence was attributed to the photo-induced electron transfer enabled by the strong interaction between Fe^{3+} and the organic moieties on the CDs surface. Having a greater affinity towards Fe^{3+}, the addition of phytic acid can be quantified by the corresponding increasing of the CDs fluorescence. Numerous additional works report the occurrence of PET as the principle behind the sensing ability of various CDs.[85-88]

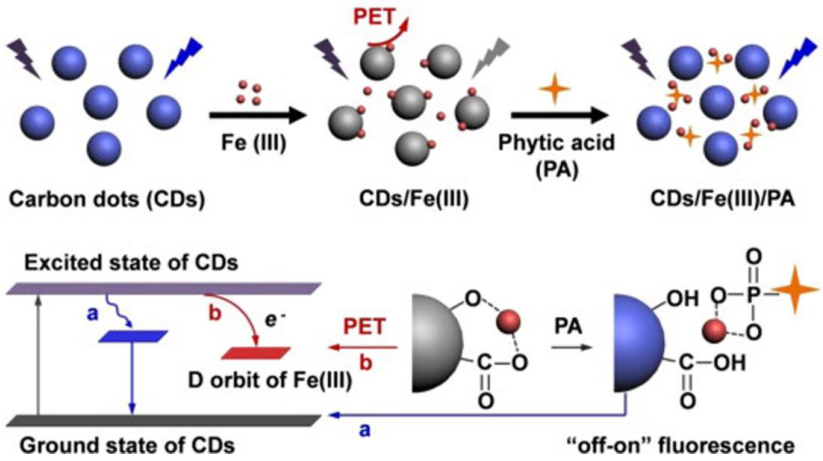

Figure 1.15. sensing mechanism of phytic acid based on the PET quenching of CDs by Fe^{3+} (from ref. [60]).

1.4.2.3 Inner filter effect (IFE)

IFE consists of the re-adsorption of the fluorophore emission from the quencher and it is sometimes called apparent quenching, i.e. the fluorescence emission is not affected in its mechanism, but rather filtered along the cuvette path (Figure 1.17). Thus, absorbance and lifetime of the excited state are not affected by IFE. The only condition for observing the IFE is that the emission of the fluorophore partially or totally overlaps the absorption of the quencher, which could also be the fluorophore itself. Even though it cannot be considered a proper quenching mechanism, IFE can be exploited for the preparation of fluorescent probes.

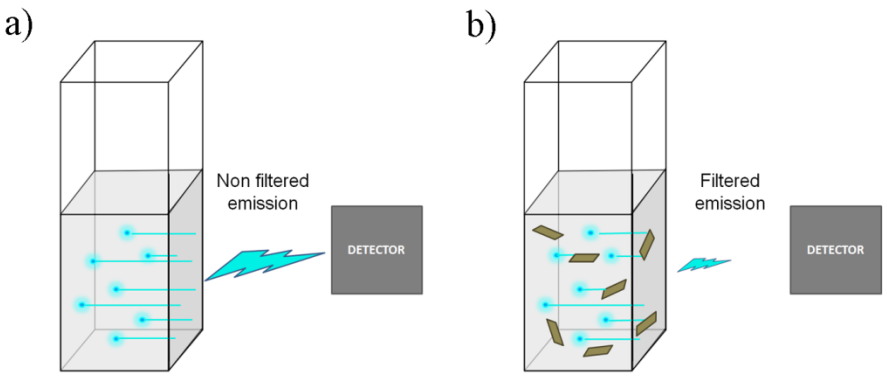

Figure 1.16. illustration of the inner filter effect: while in a) the whole emitted light can reach the detector, in b) an additional specie is able to absorb it. The result is the decrease of the output emission.

In the work of X. Chen et al., a "Switch-On" fluorescent sensor based on IFE between CDs and MnO_2 was prepared.[89] in fact the absorption of MnO_2 nanosheets overlaps the emission of CDs prepared by hydrothermal treatment of sodium citrate and ammonium bicarbonate. The quenching observed after the addition of MnO_2 to a CDs solution was related to IFE by applying the Parker equation, which describes the change of fluorescence intensity in function of optical parameters (absorbance, excitation and emission wavelengths of the species) and instrumental parameters (thickness of the laser beam and size of the cuvette). Next, the probe was prepared, consisting of a non-fluorescent system obtained by mixing CDs and MnO_2 in solution. Finally it was proved that the addition of ascorbic acid to the system causes the reduction of MnO_2 to Mn^{2+}, whose absorbance is not anymore matching with the CDs emission. Therefore the IFE is attenuated by the addition of ascorbic acid and the fluorescence detection increases proportionally. The as-fabricated fluorescent sensing system was successfully applied to the analysis of ascorbic acid in several types of food samples. Many other studies report the preparation of CDs fluorescent probes based on the IFE effect.[90-93]

1.4.3. Conclusions

Many different factors can affect the CDs fluorescence emission, therefore the processes behind the quenching phenomenon should be examined carefully. Change in absorption, emission, quantum yield and lifetime in accordance with the mathematical models as well as the study of the photoelectrochemical properties provide useful hints for the identification of the quenching mechanism. This knowledge can be easily exploited for the preparation of CDs-based fluorescent nanosensors.

1.5. Toxicity of CDs

Since their discovery, CDs have been immediately recognized as an interesting alternative to semiconductor quantum dots (QDs) in biological and medical applications. In fact, while the employment of QDs is limited by the intrinsic toxicity associated to their metallic composition, CDs are made of biocompatible elements and therefore offer a safer choice. Several studies were performed in order to assess the toxicity of various CDs *in vitro* and *in vivo*. Y. Zhang et al. monitored the growth of green beans in a CDs solution, in a CdTe QDs solution and in water.[94] While the bean sprouts resulted pathological in the QDs solution, their growth was comparable in the CDs solution and in water. The fluorescence properties of the bean plant proved that CDs are able to permeate throughout the plant cells with good biocompatibility and that they are non-toxic and do not hinder plant growth. In the work of D. Cui et al. the acute toxicity, subacute toxicity and genotoxicity of CDs was systematically tested, concluding that no significant toxicity effects were detected in mice organs.[95] Other studies reported the employment of CDs for *in vivo* and *in vitro* imaging of various tumor cell lines, without finding any significant toxicity.[96] Also other cell types were investigated. S. K. Kailasa used CDs as probes for imaging of bacterial and fungal cells.[97] In both cases the internalization occurred successfully without any toxic effect on the cells. CDs also proved to be able to decrease the toxicity of other drug vectors. Polyethyleneimine (PEI) is an efficient vector for gene delivery, but its use is associated with cytotoxicity. In the work of W. Liu et al., PEI-passivated CDs showed a DNA transfection efficiency *in vitro* comparable to PEI alone, but with decreased cytotoxicity.[98] Finally, a deep study on the pharmacokinetic of PEG-functionalized CDs was performed by the group of X. Chen.[99] The effects of intravenous, intramuscular and subcutaneous routes were compared, observing that in the three cases CDs are rapidly concentrated in kidneys and liver and efficiently excreted from the body, without showing appreciable toxicity.

In conclusion, even if CDs chemical structure and properties can be different from one another due to the different precursors and methods employed for their synthesis, a huge amount of toxicity studies *in vitro* and *in vivo* on numerous types of cells and in mice indicates that these nanoparticles are generally safe and biocompatible. Also for this reason the impact of CDs on the preparation of nanotechnologies and materials for bioimaging, biosensing, drug delivery and other medical applications is potentially high and thus this field is rapidly developing.

1.6.Functionalization of CDs for biomedical applications

1.6.1. Introduction

Many interesting applications are perfectly suited for the employment of CDs, including metal sensing, biomolecule sensing, bioimaging and drug delivery. Indeed bright photoluminescence and high water solubility and biocompatibility makes CDs very promising candidates for analytical and medical purposes. However, in view of their use a critical requirement is that the nanoparticles must be selective, that is to say that CDs should display a strongly preferential interaction with the target to reach/analyze. Actually, the method and the precursors frequently employed for the synthesis of CDs do not confer them the desired selectivity, and the pristine material lacks of organic groups for the specific recognition of metals or biological systems. For this reason further modification strategies have had an important role for the developing of novel CDs-based materials and a large number of studies in the last two-three years reported the use of functionalized CDs for sensing and bioimaging. A widespread strategy is based on the CDs covalent functionalization, which exploits the chemical reactivity of the organic groups on the CDs surface in order to form the chemical bond with the moieties intended for the molecular recognition. Moreover this approach can tailor or enhance the photoluminescence features of the nanoparticles.

1.6.2. Functionalization through amide bond

Among all the types of covalent functionalization reported in literature, the amide bond formation is without any doubt the most common. In fact the precursors employed for the CDs synthesis frequently carry carboxylic acids, amines or they are treated in oxidizing conditions. Therefore a very simple strategy such as the EDC/NHS (N-(3-Dimethylaminopropyl)-N′-ethylcarbodiimide hydrochloride/N-hydroxysuccinimide)
activation of carboxylic acids provide a useful path for the amide bond formation (Figure 1.18).

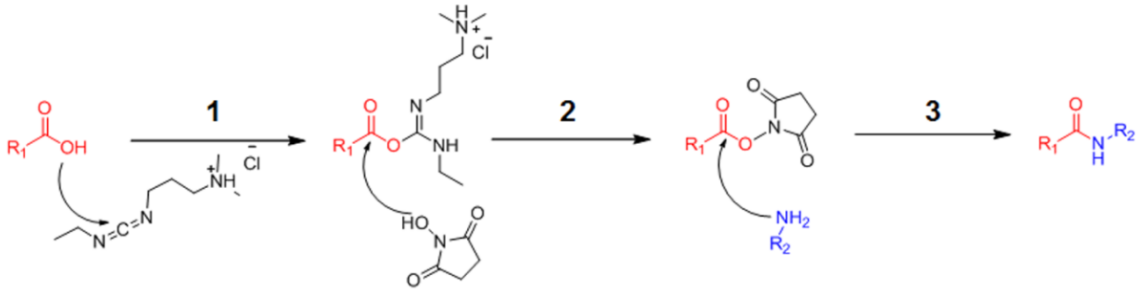

Figure 1.17. mechanism of the amide bond formation catalyzed by EDC/NHS. Carboxylic acid reacts with 1-Ethyl-3-(3-dimethylaminopropyl)carbodiimide hydrochloride (EDC), forming an unstable intermediate (1). The addition of *N*-Hydroxysuccinimide (NHS) cause the cleavage of the EDC bond and a less labile NHS ester is formed (2). Finally an amine is added (3) and the amide bond is achieved.

Furthermore, some studies reported an enhancement of the fluorescence emission after the formation of the amides, thus revealing an additional advantage of this covalent approach. For example Dong et al. activated by EDC/NHS coupling the carboxylic acids of CDs obtained from hydrothermal treatment of glucose and functionalized them with ethylenediamine.[100] The amide bond formation improved the QY from 1.3 to 3.0%. CDs sensitivity towards certain metal ions is often high due to the facility with which those can quench the fluorescence, but selectivity must be improved. For example polyamine molecules such as triethylenetetramine (TETA) are good chelants for copper ions. Therefore the group of Yang used the EDC/NHS protocol for attaching TETA on the carboxylic acids of CDs made from citric acid and urea.[101] The as-produced material was used for the detection of Cu^{2+} and GSH (glutathione). In fact, Cu^{2+} could bind the CDs surface and quench the PL emission. Further addition of GSH can recover it, due to the stronger ability of GSH to bind the copper ions. In this way GSH concentrations of 0.2-175 µM were detected and the modified CDs were also applied in living yeast cells for detecting Cu^{2+} and GSH. Similar experiments were performed by Chen et al., who prepared CDs from citric acid and ethylenediamine hydrothermal treatment and coupled them with 1,4,8,11 tetraazacyclotetradecane cyclam through the EDC chemistry.[80] Cyclam ring was exploited for hosting copper ions and the CDs fluorescence was completely quenched (Figure 1.19). This material was used in HeLa cells for monitoring the concentration of S^{2-} ions, which are able to remove the copper from cyclam and recover the fluorescence. In this way a concentration range of 0-15 µM of S^{2-} could be detected.

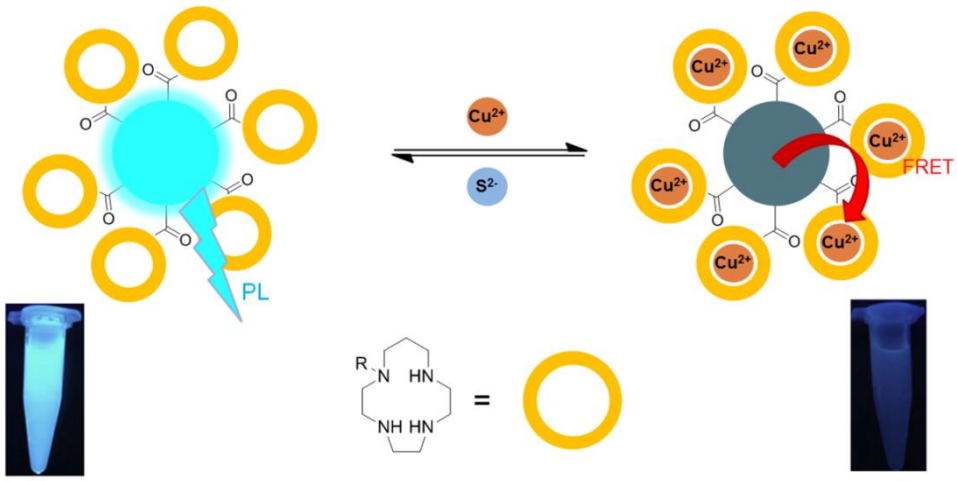

Figure 1.18. fluorescence quenching and recovery of cyclam-functionalized CDs, respectively by Cu^{2+} and S^{2-} ions (vials pictures from ref. [80]).

An example of CDs-based biosensor is the material prepared by Chai et al., who conjugated CDs carrying –COOH moieties with dopamine through catalyzed amide bond formation.[102] This material was used to detect the concentration/activity of tyrosinase, an enzyme that catalyzes the oxidation of the dopamine di-hydroxy phenyl ring to the corresponding quinone.[103] The dopapine quinone is able to quench the CDs fluorescence as a result of an intramolecular photo-induced charge transfer and, therefore, the decrease in fluorescence emission is proportional to the tyrosinase activity. Zhong et al. attached instead the glycopeptide antibiotic Vancomycin on CDs made from citric acid and urea, also in this case exploiting the presence of carboxylic groups for the conjugation.[104] Vancomycin is able to selectively target the bacteria *Staphylococcus aureus*, because its terminal peptide sequence D-Ala-D-Ala binds specifically the gram-positive bacteria cell walls. Once vancomycin was covalently linked to the CDs, a quenching was measured because of the bacteria presence, which concentration could be therefore quantitatively determined in the range of 3.18×10^5 – 1.59×10^8 cfu mL^{-1}. Similarly, the group of Wang developed a fluorometric essay for the gram-negative bacteria *Salmonella typhimurium.*[105] The sensor was prepared by coupling to the CDs a specific aptamer, able to recognize the bacteria's outer membrane proteins. The contact of the functionalized CDs with the bacteria induced a measurable loss of PL emission, corresponding to the bacteria concentration. CDs-based sensors for small biomolecules were also prepared resorting to the amide functionalization. Cyclodextrin has a ring-like molecular structure, where the internal part is hydrophobic while the external hydrophilic, thus promoting the host-guest interaction with hydrophobic molecules such as *p*-nitrophenol,

which is a quencher of the CDs emission. Therefore Sun et al. functionalized the CDs with 6-aminoethylamino-β-cyclodextrin via EDC/NHS coupling and filled it with p-nitrophenol.[106] The as-prepared material showed excellent sensing properties towards cholesterol, which can replace p-nitrophenol as the cyclodextrin guest molecule, causing a proportional enhancement of the CDs fluorescence (Figure 1.20).

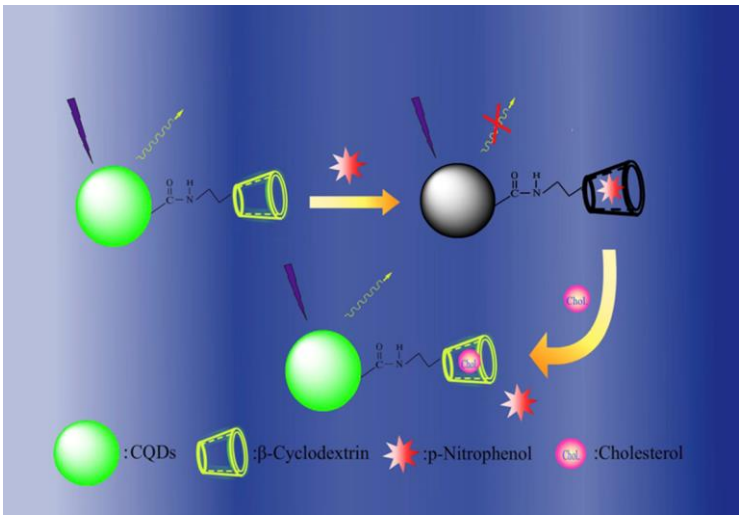

Figure 1.19. sensing mechanism based on the host-guest interaction of p-nitrophenol and cholesterol with β-cyclodextrin-functionalized CDs (from ref. [106]).

An equivalent sensing strategy was exploited by Luo et al., that synthetized CDs from citric acid and cysteine and conjugated them with cyclodextrin. Ferrocenylmethyl trimethylammonium iodide was used as a guest molecule in order to quench completely the CDs emission. This system was then successfully employed for the detection of testosterone, which, being less polar then the ferrocene compound, forms better host-guest interaction with cyclodextrin and could quantitatively recover the fluorescence emission.

1.6.3. Other covalent functionalizations

Alternative methods to the amide bond formation for the CDs covalent functionalization involve esterification or sulfonylation. For example, Algarra et al. used mercaptosuccinic acid for functionalizing CDs made from lactose, exploiting therefore the alcohol moieties for the further esterification (Figure 1.21).[107] The functionalized CDs could selectively sense Ag^+ concentrations of 0-30 µM in water, thanks to the ability of the thiol group to form a complex with silver, which is responsible for the static quenching of the CDs.

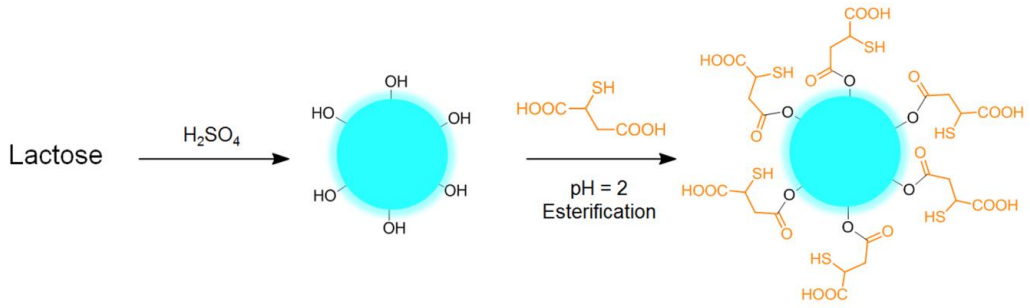

Figure 1.20. Mercaptosuccinic acid in acid conditions is used for the CDs functionalization. The as-produced nanoparticles are selectively quenched by Ag^+ ions (ref. [107]).

Amino-containing CDs can be modified by sulfonylation, i. e. using sulfonyl chloride compounds for the formation of the sulfonamide. In this way, Wang et al. attached 2,4-dinitrobenzene, a specific ligand for selenocysteine, to the nanoparticles, resulting in the complete quenching of their fluorescence.[108] Selenocysteine was able to restore the fluorescence, cleaving by nucleophilic substitution the 2,4-dinitrobenzene functionalities, while cysteine, homocysteine, glutathione and others aminoacids didn't show almost any effect on the CDs emission (Figure 1.22). Therefore the as-prepared sensor showed to be capable of selectively imaging selenol in living cells in a linear range of 0.2-30 µM.

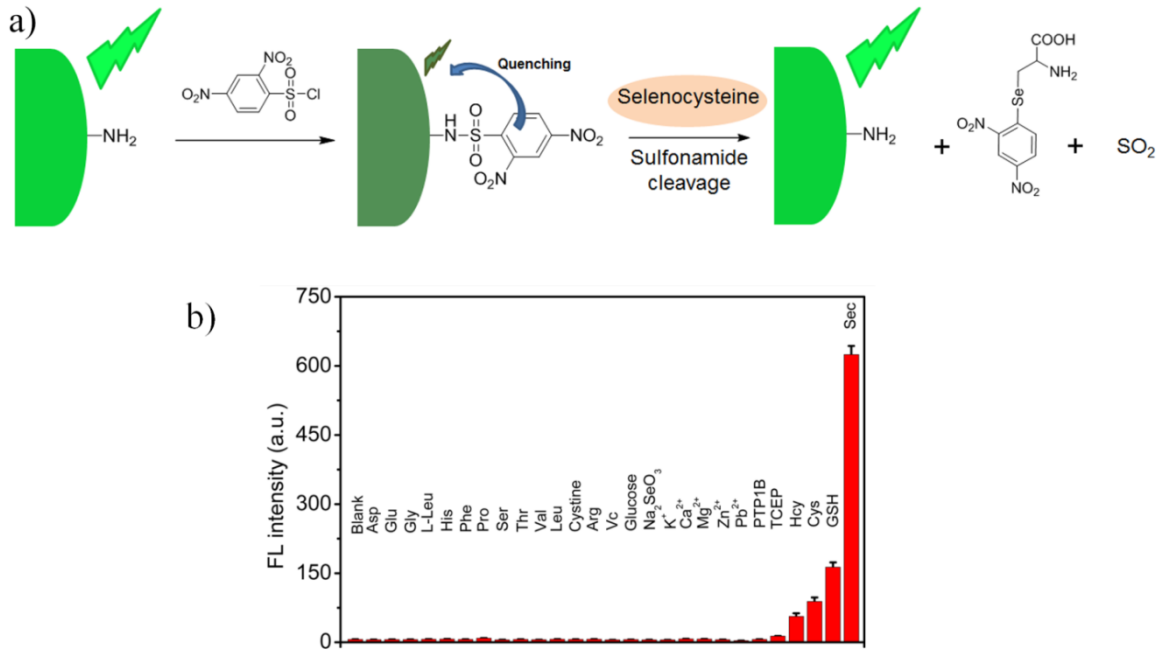

Figure 1.21. a) sulfonamide bond formation and cleavage on CDs from ref. [108] and fluorescence dependence. b) selectivity towards selenocysteine (Sec).

1.7. CDs in photocatalysis and solar cells

1.7.1. introduction

PL phenomena in CDs are the most evident sign of interesting underlying properties, including charge separation and donor-acceptor behavior, photocatalytic activity and photon harvesting ability. The early and rapid discovery of all these properties immediately drew the attention from the energy conversion field. Nowadays researchers are widely employing CDs for the preparation of photocatalysts and solar cells layer components, disclosing step by step their potentiality and revealing the extreme versatility and easiness of processing that are peculiar of this material. In this chapter a description of the CDs role in energy application is given, jointly with few examples.

1.7.2. Photocatalysis

Thanks to their special optical behavior, as well as to the high water solubility, excellent environmental compatibility and easiness of production, CDs have been exploited for the preparation of several efficient photocatalysts, in fact CDs acceptor ability stabilizes the photo-induced charge separation occurring on other materials, displacing the electrons and therefore delaying the electron-hole recombination. In the work of S.-Y. Kwak et al. CDs prepared from hydrothermal treatment of ascorbic acid were embedded with mesoporous hematite clusters and the photocatalytic degradation of methylene blue was studied.[109] The remarkably higher degradation efficiency of the composite with respect to the hematite alone highlighted the role of CDs, which were able to transfer the electron from hematite to the oxygen specie that starts the methylene blue degradation mechanism. A similar behavior is observed in the CDs/CdS heterojunction prepared by H.-L. Zhang et al., which showed improved photocatalytic ability towards *p*-nitrobenzene reduction. In here, the CDs were prepared by heating L-cysteine at 280 °C for 5 minutes and mixed with CdS quantum dots *via* an electrophoretic and sequential chemical bath deposition method, achieving the formation of the heterojunction.[110] Upon visible light irradiation, electron-hole separation occurs on CdS and electrons are accepted by CDs, which efficiently catalyze the *p*-nitrobenzene reduction (Figure 1.23).

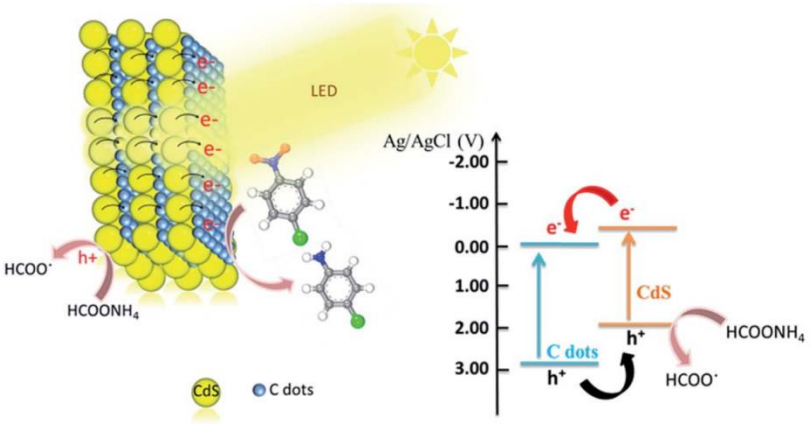

Figure 1.22. illustration of the CDs/CdS heterojunction and its photocatalytic activity towards *p*-nitrobenzene (from ref. [110]).

One last example of the versatility of CDs in photocatalysis, the work of R. Chen et al. reports the evaluation of the photocatalytic activity of the monolayered 2D material $BiMoO_6$ mixed in solution with CDs synthetized from hydrothermal treatment of citric acid and ethylenediamine.[111] The efficient degradation under visible light of four pollutants, i.e. ciprofloxacin, bisphenol A, tetracycline hydrochloride, and methylene blue was achieved, promoted by the electron acceptor role of CDs.

1.7.3. Solar cells

CDs have been extensively employed in solar cell for covering multiple roles, including as electrode components, mixed in the transport layer or acting as photosensitizer and spectrum converter. H.-S. Choi synthetized CDs by microwave irradiation of citric acid and urea.[112] The CDs were used as initiators for the dendritic growth of Au, obtaining in this way the material further employed as counter electrode for the ZnO nanowire/CdS/CdSe quantum dot-sensitized solar cell. The as-prepared counter-electrode showed better performance with respect to commonly used Au-sputtered counter electrodes, increasing the power conversion efficiency from 3.6% to 5.4%. The higher performance of the CDs/Au counter electrode was ascribed to its much larger surface area than the Au-sputtered counter electrode, and therefore to an increase in the number of electrocatalytic active sites. The group of E. Palomares instead employed the CDs in the preparation of the hole-transport layer of perovskite solar cells.[113] CDs were synthetized by hydrothermal treatment of citric acid and *p*-phenylenediamine. Next they were included in the solar cell fabrication process as hole-transport material on top of the perovskite layer. In fact, the measured HOMO and LUMO energies of CDs were found to be adequate on one side for ensuring the hole transfer and blocking the electron transfer on the

other. The as-prepared device showed a power conversion efficiency of 3%, proving the capability of CDs as hole-transporter material. In the study of M. Q. Zhang et al. CDs were used for increasing the harvesting efficiency of the solar cell, widening its absorption spectrum (Figure 1.24).[114] In fact, the absorption of CDs prepared from the hydrothermal treatment of ascorbic acid and silane is found in the UV range, while their fluorescence emission is blue. Blue light matches with the response curve of the active layer, consisting of poly(3-hexylthiophene): [6,6]-phenyl-C61-butyric acid methyl ester (P3HT:PCBM), while UV light does not. Therefore the presence of CDs allows the active layer to partially collect also the UV light, increasing the power conversion efficiency of the device.

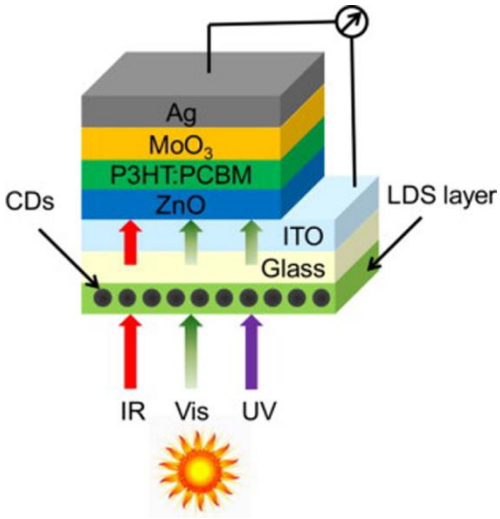

Figure 1.23. photovoltaic device in which the CDs layer acts as spectral converter (from ref. [114]).

1.8. References

1. Cayuela, A.; Soriano, M. L.; Carrillo-Carrión, C.; Valcárcel, M., Semiconductor and carbon-based fluorescent nanodots: the need for consistency. *Chemical Communications* **2016,** *52* (7), 1311-1326.
2. Feng, T.; Zhu, S.; Zeng, Q.; Lu, S.; Tao, S.; Liu, J.; Yang, B., Supramolecular Cross-Link-Regulated Emission and Related Applications in Polymer Carbon Dots. *ACS Applied Materials & Interfaces* **2018,** *10* (15), 12262-12277.
3. Shah, S. N. A.; Lin, J.-M., Recent advances in chemiluminescence based on carbonaceous dots. *Advances in Colloid and Interface Science* **2017,** *241*, 24-36.
4. Xu, Y.; Liu, J.; Gao, C.; Wang, E., Applications of carbon quantum dots in electrochemiluminescence: A mini review. *Electrochemistry Communications* **2014,** *48*, 151-154.
5. Xu, X.; Ray, R.; Gu, Y.; Ploehn, H. J.; Gearheart, L.; Raker, K.; Scrivens, W. A., Electrophoretic Analysis and Purification of Fluorescent Single-Walled Carbon Nanotube Fragments. *Journal of the American Chemical Society* **2004,** *126* (40), 12736-12737.

6. Zhou, J.; Booker, C.; Li, R.; Zhou, X.; Sham, T.-K.; Sun, X.; Ding, Z., An Electrochemical Avenue to Blue Luminescent Nanocrystals from Multiwalled Carbon Nanotubes (MWCNTs). *Journal of the American Chemical Society* **2007,** *129* (4), 744-745.
7. Liu, H.; Ye, T.; Mao, C., Fluorescent Carbon Nanoparticles Derived from Candle Soot. *Angewandte Chemie International Edition* **2007,** *46* (34), 6473-6475.
8. Hu, S.-L.; Niu, K.-Y.; Sun, J.; Yang, J.; Zhao, N.-Q.; Du, X.-W., One-step synthesis of fluorescent carbon nanoparticles by laser irradiation. *Journal of Materials Chemistry* **2009,** *19* (4), 484-488.
9. Sun, Y.-P.; Zhou, B.; Lin, Y.; Wang, W.; Fernando, K. A. S.; Pathak, P.; Meziani, M. J.; Harruff, B. A.; Wang, X.; Wang, H.; Luo, P. G.; Yang, H.; Kose, M. E.; Chen, B.; Veca, L. M.; Xie, S.-Y., Quantum-Sized Carbon Dots for Bright and Colorful Photoluminescence. *Journal of the American Chemical Society* **2006,** *128* (24), 7756-7757.
10. Zhao, Q.-L.; Zhang, Z.-L.; Huang, B.-H.; Peng, J.; Zhang, M.; Pang, D.-W., Facile preparation of low cytotoxicity fluorescent carbon nanocrystals by electrooxidation of graphite. *Chemical Communications* **2008,** (41), 5116-5118.
11. Peng, H.; Travas-Sejdic, J., Simple Aqueous Solution Route to Luminescent Carbogenic Dots from Carbohydrates. *Chemistry of Materials* **2009,** *21* (23), 5563-5565.
12. Qiao, Z.-A.; Wang, Y.; Gao, Y.; Li, H.; Dai, T.; Liu, Y.; Huo, Q., Commercially activated carbon as the source for producing multicolor photoluminescent carbon dots by chemical oxidation. *Chemical Communications* **2010,** *46* (46), 8812-8814.
13. Gonçalves, H.; Jorge, P. A. S.; Fernandes, J. R. A.; Esteves da Silva, J. C. G., Hg(II) sensing based on functionalized carbon dots obtained by direct laser ablation. *Sensors and Actuators B: Chemical* **2010,** *145* (2), 702-707.
14. Anilkumar, P.; Wang, X.; Cao, L.; Sahu, S.; Liu, J.-H.; Wang, P.; Korch, K.; Tackett Ii, K. N.; Parenzan, A.; Sun, Y.-P., Toward quantitatively fluorescent carbon-based "quantum" dots. *Nanoscale* **2011,** *3* (5), 2023-2027.
15. Liu, Y.; Liu, C.-y.; Zhang, Z.-y., Synthesis and surface photochemistry of graphitized carbon quantum dots. *Journal of Colloid and Interface Science* **2011,** *356* (2), 416-421.
16. Sachdev, A.; Matai, I.; Gopinath, P., Implications of surface passivation on physicochemical and bioimaging properties of carbon dots. *RSC Advances* **2014,** *4* (40), 20915-20921.
17. Bourlinos, A. B.; Stassinopoulos, A.; Anglos, D.; Zboril, R.; Karakassides, M.; Giannelis, E. P., Surface Functionalized Carbogenic Quantum Dots. *Small* **2008,** *4* (4), 455-458.
18. Bourlinos, A. B.; Stassinopoulos, A.; Anglos, D.; Zboril, R.; Georgakilas, V.; Giannelis, E. P., Photoluminescent Carbogenic Dots. *Chemistry of Materials* **2008,** *20* (14), 4539-4541.
19. Hsu, P.-C.; Chang, H.-T., Synthesis of high-quality carbon nanodots from hydrophilic compounds: role of functional groups. *Chemical Communications* **2012,** *48* (33), 3984-3986.
20. Hu, S.; Tian, R.; Dong, Y.; Yang, J.; Liu, J.; Chang, Q., Modulation and effects of surface groups on photoluminescence and photocatalytic activity of carbon dots. *Nanoscale* **2013,** *5* (23), 11665-11671.
21. Kozák, O.; Datta, K. K. R.; Greplová, M.; Ranc, V.; Kašlík, J.; Zbořil, R., Surfactant-Derived Amphiphilic Carbon Dots with Tunable Photoluminescence. *The Journal of Physical Chemistry C* **2013,** *117* (47), 24991-24996.
22. Yin, J.-Y.; Liu, H.-J.; Jiang, S.; Chen, Y.; Yao, Y., Hyperbranched Polymer Functionalized Carbon Dots with Multistimuli-Responsive Property. *ACS Macro Letters* **2013,** *2* (11), 1033-1037.

23. Zhu, H.; Wang, X.; Li, Y.; Wang, Z.; Yang, F.; Yang, X., Microwave synthesis of fluorescent carbon nanoparticles with electrochemiluminescence properties. *Chemical Communications* **2009,** (34), 5118-5120.
24. Chandra, S.; Pathan, S. H.; Mitra, S.; Modha, B. H.; Goswami, A.; Pramanik, P., Tuning of photoluminescence on different surface functionalized carbon quantum dots. *RSC Advances* **2012,** *2* (9), 3602-3606.
25. Wang, L.; Zhu, S.-J.; Wang, H.-Y.; Qu, S.-N.; Zhang, Y.-L.; Zhang, J.-H.; Chen, Q.-D.; Xu, H.-L.; Han, W.; Yang, B.; Sun, H.-B., Common Origin of Green Luminescence in Carbon Nanodots and Graphene Quantum Dots. *ACS Nano* **2014,** *8* (3), 2541-2547.
26. Krysmann, M. J.; Kelarakis, A.; Dallas, P.; Giannelis, E. P., Formation Mechanism of Carbogenic Nanoparticles with Dual Photoluminescence Emission. *Journal of the American Chemical Society* **2012,** *134* (2), 747-750.
27. Zhu, S.; Meng, Q.; Wang, L.; Zhang, J.; Song, Y.; Jin, H.; Zhang, K.; Sun, H.; Wang, H.; Yang, B., Highly Photoluminescent Carbon Dots for Multicolor Patterning, Sensors, and Bioimaging. *Angewandte Chemie International Edition* **2013,** *52* (14), 3953-3957.
28. Wang, J.; Zhang, P.; Huang, C.; Liu, G.; Leung, K. C.-F.; Wáng, Y. X. J., High Performance Photoluminescent Carbon Dots for In Vitro and In Vivo Bioimaging: Effect of Nitrogen Doping Ratios. *Langmuir* **2015,** *31* (29), 8063-8073.
29. Deng, L.; Wang, X.; Kuang, Y.; Wang, C.; Luo, L.; Wang, F.; Sun, X., Development of hydrophilicity gradient ultracentrifugation method for photoluminescence investigation of separated non-sedimental carbon dots. *Nano Research* **2015,** *8* (9), 2810-2821.
30. Song, Y.; Zhu, S.; Zhang, S.; Fu, Y.; Wang, L.; Zhao, X.; Yang, B., Investigation from chemical structure to photoluminescent mechanism: a type of carbon dots from the pyrolysis of citric acid and an amine. *Journal of Materials Chemistry C* **2015,** *3* (23), 5976-5984.
31. Zhu, S.; Zhao, X.; Song, Y.; Lu, S.; Yang, B., Beyond bottom-up carbon nanodots: Citric-acid derived organic molecules. *Nano Today* **2016,** *11* (2), 128-132.
32. Schneider, J.; Reckmeier, C. J.; Xiong, Y.; von Seckendorff, M.; Susha, A. S.; Kasák, P.; Rogach, A. L., Molecular Fluorescence in Citric Acid-Based Carbon Dots. *The Journal of Physical Chemistry C* **2017,** *121* (3), 2014-2022.
33. Zhang, W.; Shi, L.; Liu, Y.; Meng, X.; Xu, H.; Xu, Y.; Liu, B.; Fang, X.; Li, H.-B.; Ding, T., Supramolecular interactions via hydrogen bonding contributing to citric-acid derived carbon dots with high quantum yield and sensitive photoluminescence. *RSC Advances* **2017,** *7* (33), 20345-20353.
34. Fang, Q.; Dong, Y.; Chen, Y.; Lu, C.-H.; Chi, Y.; Yang, H.-H.; Yu, T., Luminescence origin of carbon based dots obtained from citric acid and amino group-containing molecules. *Carbon* **2017,** *118*, 319-326.
35. Ehrat, F.; Bhattacharyya, S.; Schneider, J.; Löf, A.; Wyrwich, R.; Rogach, A. L.; Stolarczyk, J. K.; Urban, A. S.; Feldmann, J., Tracking the Source of Carbon Dot Photoluminescence: Aromatic Domains versus Molecular Fluorophores. *Nano Letters* **2017,** *17* (12), 7710-7716.
36. Sharma, A.; Gadly, T.; Neogy, S.; Ghosh, S. K.; Kumbhakar, M., Molecular Origin and Self-Assembly of Fluorescent Carbon Nanodots in Polar Solvents. *The Journal of Physical Chemistry Letters* **2017,** *8* (5), 1044-1052.
37. Viallat, A.; Bom, R. P.; Cohen-Addad, J. P., Charge-transfer interaction and chain association in poly(ether imide) solutions: a fluorescence spectroscopic study. *Polymer* **1994,** *35* (13), 2730-2736.
38. Zhao, E.; Lam, J. W. Y.; Meng, L.; Hong, Y.; Deng, H.; Bai, G.; Huang, X.; Hao, J.; Tang, B. Z., Poly[(maleic anhydride)-alt-(vinyl acetate)]: A Pure Oxygenic Nonconjugated Macromolecule with Strong Light Emission and Solvatochromic Effect. *Macromolecules* **2015,** *48* (1), 64-71.

39. Yang, W.; Pan, C.-Y.; Luo, M.-D.; Zhang, H.-B., Fluorescent Mannose-Functionalized Hyperbranched Poly(amido amine)s: Synthesis and Interaction with E. coli. *Biomacromolecules* **2010,** *11* (7), 1840-1846.
40. Sun, Y.; Cao, W.; Li, S.; Jin, S.; Hu, K.; Hu, L.; Huang, Y.; Gao, X.; Wu, Y.; Liang, X.-J., Ultrabright and Multicolorful Fluorescence of Amphiphilic Polyethyleneimine Polymer Dots for Efficiently Combined Imaging and Therapy. *Scientific Reports* **2013,** *3*, 3036.
41. Guo, C. X.; Xie, J.; Wang, B.; Zheng, X.; Yang, H. B.; Li, C. M., A new class of fluorescent-dots: long luminescent lifetime bio-dots self-assembled from DNA at low temperatures. *Scientific Reports* **2013,** *3*, 2957.
42. Yang, J.; Zhang, Y.; Gautam, S.; Liu, L.; Dey, J.; Chen, W.; Mason, R. P.; Serrano, C. A.; Schug, K. A.; Tang, L., Development of aliphatic biodegradable photoluminescent polymers. *Proceedings of the National Academy of Sciences* **2009,** *106* (25), 10086-10091.
43. Zhu, S.; Song, Y.; Shao, J.; Zhao, X.; Yang, B., Non-Conjugated Polymer Dots with Crosslink-Enhanced Emission in the Absence of Fluorophore Units. *Angewandte Chemie International Edition* **2015,** *54* (49), 14626-14637.
44. Zhu, S.; Wang, L.; Zhou, N.; Zhao, X.; Song, Y.; Maharjan, S.; Zhang, J.; Lu, L.; Wang, H.; Yang, B., The crosslink enhanced emission (CEE) in non-conjugated polymer dots: from the photoluminescence mechanism to the cellular uptake mechanism and internalization. *Chemical Communications* **2014,** *50* (89), 13845-13848.
45. Tao, S.; Song, Y.; Zhu, S.; Shao, J.; Yang, B., A new type of polymer carbon dots with high quantum yield: From synthesis to investigation on fluorescence mechanism. *Polymer* **2017,** *116*, 472-478.
46. Tao, S.; Lu, S.; Geng, Y.; Zhu, S.; Redfern, S. A. T.; Song, Y.; Feng, T.; Xu, W.; Yang, B., Design of Metal-Free Polymer Carbon Dots: A New Class of Room-Temperature Phosphorescent Materials. *Angewandte Chemie International Edition* **2018,** *57* (9), 2393-2398.
47. Wang, Y.; Kalytchuk, S.; Zhang, Y.; Shi, H.; Kershaw, S. V.; Rogach, A. L., Thickness-Dependent Full-Color Emission Tunability in a Flexible Carbon Dot Ionogel. *The Journal of Physical Chemistry Letters* **2014,** *5* (8), 1412-1420.
48. Gude, V.; Das, A.; Chatterjee, T.; Mandal, P. K., Molecular origin of photoluminescence of carbon dots: aggregation-induced orange-red emission. *Physical Chemistry Chemical Physics* **2016,** *18* (40), 28274-28280.
49. Liu, S.; Tian, J.; Wang, L.; Zhang, Y.; Qin, X.; Luo, Y.; Asiri, A. M.; Al-Youbi, A. O.; Sun, X., Hydrothermal Treatment of Grass: A Low-Cost, Green Route to Nitrogen-Doped, Carbon-Rich, Photoluminescent Polymer Nanodots as an Effective Fluorescent Sensing Platform for Label-Free Detection of Cu(II) Ions. *Advanced Materials* **2012,** *24* (15), 2037-2041.
50. Sun, D.; Ban, R.; Zhang, P.-H.; Wu, G.-H.; Zhang, J.-R.; Zhu, J.-J., Hair fiber as a precursor for synthesizing of sulfur- and nitrogen-co-doped carbon dots with tunable luminescence properties. *Carbon* **2013,** *64*, 424-434.
51. Sahu, S.; Behera, B.; Maiti, T. K.; Mohapatra, S., Simple one-step synthesis of highly luminescent carbon dots from orange juice: application as excellent bio-imaging agents. *Chemical Communications* **2012,** *48* (70), 8835-8837.
52. Zhou, J.; Sheng, Z.; Han, H.; Zou, M.; Li, C., Facile synthesis of fluorescent carbon dots using watermelon peel as a carbon source. *Materials Letters* **2012,** *66* (1), 222-224.
53. Zhang, Z.; Duan, Y.; Yu, Y.; Yan, Z.; Chen, J., Carbon quantum dots: synthesis, characterization, and assessment of cytocompatibility. *Journal of Materials Science: Materials in Medicine* **2015,** *26* (7), 213.

54. Wu, H.; Mi, C.; Huang, H.; Han, B.; Li, J.; Xu, S., Solvothermal synthesis of green-fluorescent carbon nanoparticles and their application. *Journal of Luminescence* **2012,** *132* (6), 1603-1607.
55. Essner, J. B.; Laber, C. H.; Ravula, S.; Polo-Parada, L.; Baker, G. A., Pee-dots: biocompatible fluorescent carbon dots derived from the upcycling of urine. *Green Chemistry* **2016,** *18* (1), 243-250.
56. Shan, D.; Hsieh, J.-T.; Bai, X.; Yang, J., Citrate-Based Fluorescent Biomaterials. *Advanced Healthcare Materials* **2018,** *7* (18), 1800532.
57. Simões, E. F. C.; Leitão, J. M. M.; da Silva, J. C. G. E., Carbon dots prepared from citric acid and urea as fluorescent probes for hypochlorite and peroxynitrite. *Microchimica Acta* **2016,** *183* (5), 1769-1777.
58. Choi, Y.; Thongsai, N.; Chae, A.; Jo, S.; Kang, E. B.; Paoprasert, P.; Park, S. Y.; In, I., Microwave-assisted synthesis of luminescent and biocompatible lysine-based carbon quantum dots. *Journal of Industrial and Engineering Chemistry* **2017,** *47*, 329-335.
59. Arad, E.; Bhunia, S. K.; Jopp, J.; Kolusheva, S.; Rapaport, H.; Jelinek, R., Lysine-Derived Carbon Dots for Chiral Inhibition of Prion Peptide Fibril Assembly. *ADVANCED THERAPEUTICS* **2018,** *1* (4), 1800006.
60. Gao, Z.; Wang, L.; Su, R.; Huang, R.; Qi, W.; He, Z., A carbon dot-based "off–on" fluorescent probe for highly selective and sensitive detection of phytic acid. *Biosensors and Bioelectronics* **2015,** *70*, 232-238.
61. Zhang, Y.; He, J., Facile synthesis of S, N co-doped carbon dots and investigation of their photoluminescence properties. *Physical Chemistry Chemical Physics* **2015,** *17* (31), 20154-20159.
62. Li, F.; Li, Y.; Yang, X.; Han, X.; Jiao, Y.; Wei, T.; Yang, D.; Xu, H.; Nie, G., Highly Fluorescent Chiral N-S-Doped Carbon Dots from Cysteine: Affecting Cellular Energy Metabolism. *Angewandte Chemie International Edition* **2018,** *57* (9), 2377-2382.
63. Liu, X.; Pang, J.; Xu, F.; Zhang, X., Simple Approach to Synthesize Amino-Functionalized Carbon Dots by Carbonization of Chitosan. *Scientific Reports* **2016,** *6*, 31100.
64. Fan, R.-J.; Sun, Q.; Zhang, L.; Zhang, Y.; Lu, A.-H., Photoluminescent carbon dots directly derived from polyethylene glycol and their application for cellular imaging. *Carbon* **2014,** *71*, 87-93.
65. Yang, Z.-C.; Wang, M.; Yong, A. M.; Wong, S. Y.; Zhang, X.-H.; Tan, H.; Chang, A. Y.; Li, X.; Wang, J., Intrinsically fluorescent carbon dots with tunable emission derived from hydrothermal treatment of glucose in the presence of monopotassium phosphate. *Chemical Communications* **2011,** *47* (42), 11615-11617.
66. Yan, H.; Tan, M.; Zhang, D.; Cheng, F.; Wu, H.; Fan, M.; Ma, X.; Wang, J., Development of multicolor carbon nanoparticles for cell imaging. *Talanta* **2013,** *108*, 59-65.
67. Chen, Y.; Wu, Y.; Weng, B.; Wang, B.; Li, C., Facile synthesis of nitrogen and sulfur co-doped carbon dots and application for Fe(III) ions detection and cell imaging. *Sensors and Actuators B: Chemical* **2016,** *223*, 689-696.
68. Wang, B.; Tang, W.; Lu, H.; Huang, Z., Hydrothermal synthesis of ionic liquid-capped carbon quantum dots with high thermal stability and anion responsiveness. *Journal of Materials Science* **2015,** *50* (16), 5411-5418.
69. Qu, K.; Wang, J.; Ren, J.; Qu, X., Carbon Dots Prepared by Hydrothermal Treatment of Dopamine as an Effective Fluorescent Sensing Platform for the Label-Free Detection of Iron(III) Ions and Dopamine. *Chemistry – A European Journal* **2013,** *19* (22), 7243-7249.
70. Liu, H.; Li, Z.; Sun, Y.; Geng, X.; Hu, Y.; Meng, H.; Ge, J.; Qu, L., Synthesis of Luminescent Carbon Dots with Ultrahigh Quantum Yield and Inherent Folate Receptor-Positive Cancer Cell Targetability. *Scientific Reports* **2018,** *8* (1), 1086.

71. Qin, X.; Lu, W.; Asiri, A. M.; Al-Youbi, A. O.; Sun, X., Microwave-assisted rapid green synthesis of photoluminescent carbon nanodots from flour and their applications for sensitive and selective detection of mercury(II) ions. *Sensors and Actuators B: Chemical* **2013,** *184*, 156-162.
72. Wang, Q.; Liu, X.; Zhang, L.; Lv, Y., Microwave-assisted synthesis of carbon nanodots through an eggshell membrane and their fluorescent application. *Analyst* **2012,** *137* (22), 5392-5397.
73. Jaiswal, A.; Ghosh, S. S.; Chattopadhyay, A., One step synthesis of C-dots by microwave mediated caramelization of poly(ethylene glycol). *Chemical Communications* **2012,** *48* (3), 407-409.
74. Zhai, X.; Zhang, P.; Liu, C.; Bai, T.; Li, W.; Dai, L.; Liu, W., Highly luminescent carbon nanodots by microwave-assisted pyrolysis. *Chemical Communications* **2012,** *48* (64), 7955-7957.
75. Li, X.; Zheng, Y.; Tang, Y.; Chen, Q.; Gao, J.; Luo, Q.; Wang, Q., Efficient and visual monitoring of cerium (III) ions by green-fluorescent carbon dots and paper-based sensing. *Spectrochimica Acta Part A: Molecular and Biomolecular Spectroscopy* **2019,** *206*, 240-245.
76. Liu, Y.; Liu, C.-y.; Zhang, Z.-y., Synthesis of highly luminescent graphitized carbon dots and the application in the Hg2+ detection. *Applied Surface Science* **2012,** *263*, 481-485.
77. Yin, B.; Deng, J.; Peng, X.; Long, Q.; Zhao, J.; Lu, Q.; Chen, Q.; Li, H.; Tang, H.; Zhang, Y.; Yao, S., Green synthesis of carbon dots with down- and up-conversion fluorescent properties for sensitive detection of hypochlorite with a dual-readout assay. *Analyst* **2013,** *138* (21), 6551-6557.
78. Qiao, Z. A.; Huo, Q.; Chi, M.; Veith, G. M.; Binder, A. J.; Dai, S., A "ship-in-a-bottle" approach to synthesis of polymer dots@silica or polymer dots@carbon core-shell nanospheres. *Adv Mater* **2012,** *24* (45), 6017-21.
79. Liang, Z.; Kang, M.; Payne, G. F.; Wang, X.; Sun, R., Probing Energy and Electron Transfer Mechanisms in Fluorescence Quenching of Biomass Carbon Quantum Dots. *ACS Applied Materials & Interfaces* **2016,** *8* (27), 17478-17488.
80. Chen, J.; Li, Y.; Lv, K.; Zhong, W.; Wang, H.; Wu, Z.; Yi, P.; Jiang, J., Cyclam-functionalized carbon dots sensor for sensitive and selective detection of copper(II) ion and sulfide anion in aqueous media and its imaging in live cells. *Sensors and Actuators B: Chemical* **2016,** *224*, 298-306.
81. Ganiga, M.; Cyriac, J., FRET based ammonia sensor using carbon dots. *Sensors and Actuators B: Chemical* **2016,** *225*, 522-528.
82. Kong, D.; Yan, F.; Han, Z.; Xu, J.; Guo, X.; Chen, L., Cobalt(ii) ions detection using carbon dots as an sensitive and selective fluorescent probe. *RSC Advances* **2016,** *6* (72), 67481-67487.
83. Zu, F.; Yan, F.; Bai, Z.; Xu, J.; Wang, Y.; Huang, Y.; Zhou, X., The quenching of the fluorescence of carbon dots: A review on mechanisms and applications. *Microchimica Acta* **2017,** *184* (7), 1899-1914.
84. Chen, Y.; Shang, P.; Dong, Y.; Chi, Y., Regulating the overlap between the absorption spectrum of metal ion-chromogenic agent and the emission spectrum of carbon-based dots to improve the sensing performance for metal ions. *Sensors and Actuators B: Chemical* **2017,** *242*, 1210-1215.
85. Liu, Y.; Zhou, Q.; Li, J.; Lei, M.; Yan, X., Selective and sensitive chemosensor for lead ions using fluorescent carbon dots prepared from chocolate by one-step hydrothermal method. *Sensors and Actuators B: Chemical* **2016,** *237*, 597-604.
86. Purbia, R.; Paria, S., A simple turn on fluorescent sensor for the selective detection of thiamine using coconut water derived luminescent carbon dots. *Biosensors and Bioelectronics* **2016,** *79*, 467-475.

87. Miao, H.; Wang, L.; Zhuo, Y.; Zhou, Z.; Yang, X., Label-free fluorimetric detection of CEA using carbon dots derived from tomato juice. *Biosensors and Bioelectronics* **2016,** *86*, 83-89.
88. Huang, Y.; Zhou, J.; Feng, H.; Zheng, J.; Ma, H.-M.; Liu, W.; Tang, C.; Ao, H.; Zhao, M.; Qian, Z., A dual-channel fluorescent chemosensor for discriminative detection of glutathione based on functionalized carbon quantum dots. *Biosensors and Bioelectronics* **2016,** *86*, 748-755.
89. Liu, J.; Chen, Y.; Wang, W.; Feng, J.; Liang, M.; Ma, S.; Chen, X., "Switch-On" Fluorescent Sensing of Ascorbic Acid in Food Samples Based on Carbon Quantum Dots–MnO2 Probe. *Journal of Agricultural and Food Chemistry* **2016,** *64* (1), 371-380.
90. Zhang, H.-Y.; Wang, Y.; Xiao, S.; Wang, H.; Wang, J.-H.; Feng, L., Rapid detection of Cr(VI) ions based on cobalt(II)-doped carbon dots. *Biosensors and Bioelectronics* **2017,** *87*, 46-52.
91. Chen, J.; Liu, J.; Li, J.; Xu, L.; Qiao, Y., One-pot synthesis of nitrogen and sulfur co-doped carbon dots and its application for sensor and multicolor cellular imaging. *Journal of Colloid and Interface Science* **2017,** *485*, 167-174.
92. Zou, S.; Hou, C.; Fa, H.; Zhang, L.; Ma, Y.; Dong, L.; Li, D.; Huo, D.; Yang, M., An efficient fluorescent probe for fluazinam using N, S co-doped carbon dots from l-cysteine. *Sensors and Actuators B: Chemical* **2017,** *239*, 1033-1041.
93. Barati, A.; Shamsipur, M.; Abdollahi, H., Hemoglobin detection using carbon dots as a fluorescence probe. *Biosensors and Bioelectronics* **2015,** *71*, 470-475.
94. Xu, M.; He, G.; Li, Z.; He, F.; Gao, F.; Su, Y.; Zhang, L.; Yang, Z.; Zhang, Y., A green heterogeneous synthesis of N-doped carbon dots and their photoluminescence applications in solid and aqueous states. *Nanoscale* **2014,** *6* (17), 10307-10315.
95. Wang, K.; Gao, Z.; Gao, G.; Wo, Y.; Wang, Y.; Shen, G.; Cui, D., Systematic safety evaluation on photoluminescent carbon dots. *Nanoscale Research Letters* **2013,** *8* (1), 122.
96. Zhang, J.; Yu, S.-H., Carbon dots: large-scale synthesis, sensing and bioimaging. *Materials Today* **2016,** *19* (7), 382-393.
97. Kasibabu, B. S. B.; D'Souza, S. L.; Jha, S.; Singhal, R. K.; Basu, H.; Kailasa, S. K., One-step synthesis of fluorescent carbon dots for imaging bacterial and fungal cells. *Analytical Methods* **2015,** *7* (6), 2373-2378.
98. Liu, C.; Zhang, P.; Zhai, X.; Tian, F.; Li, W.; Yang, J.; Liu, Y.; Wang, H.; Wang, W.; Liu, W., Nano-carrier for gene delivery and bioimaging based on carbon dots with PEI-passivation enhanced fluorescence. *Biomaterials* **2012,** *33* (13), 3604-3613.
99. Huang, X.; Zhang, F.; Zhu, L.; Choi, K. Y.; Guo, N.; Guo, J.; Tackett, K.; Anilkumar, P.; Liu, G.; Quan, Q.; Choi, H. S.; Niu, G.; Sun, Y.-P.; Lee, S.; Chen, X., Effect of Injection Routes on the Biodistribution, Clearance, and Tumor Uptake of Carbon Dots. *ACS Nano* **2013,** *7* (7), 5684-5693.
100. Dong, W.; Zhou, S.; Dong, Y.; Wang, J.; Ge, X.; Sui, L., The preparation of ethylenediamine-modified fluorescent carbon dots and their use in imaging of cells. *Luminescence* **2015,** *30* (6), 867-871.
101. Yang, R.; Guo, X.; Jia, L.; Zhang, Y., A fluorescent "on-off-on" assay for selective recognition of Cu(II) and glutathione based on modified carbon nanodots, and its application to cellular imaging. *Microchimica Acta* **2017,** *184* (4), 1143-1150.
102. Chai, L.; Zhou, J.; Feng, H.; Tang, C.; Huang, Y.; Qian, Z., Functionalized Carbon Quantum Dots with Dopamine for Tyrosinase Activity Monitoring and Inhibitor Screening: In Vitro and Intracellular Investigation. *ACS Applied Materials & Interfaces* **2015,** *7* (42), 23564-23574.

103. Palanisamy, S.; Ku, S.; Chen, S.-M., Dopamine sensor based on a glassy carbon electrode modified with a reduced graphene oxide and palladium nanoparticles composite. *Microchimica Acta* **2013,** *180* (11), 1037-1042.
104. Zhong, D.; Zhuo, Y.; Feng, Y.; Yang, X., Employing carbon dots modified with vancomycin for assaying Gram-positive bacteria like Staphylococcus aureus. *Biosensors and Bioelectronics* **2015,** *74*, 546-553.
105. Wang, R.; Xu, Y.; Zhang, T.; Jiang, Y., Rapid and sensitive detection of Salmonella typhimurium using aptamer-conjugated carbon dots as fluorescence probe. *Analytical Methods* **2015,** *7* (5), 1701-1706.
106. Sun, Q.; Fang, S.; Fang, Y.; Qian, Z.; Feng, H., Fluorometric detection of cholesterol based on β-cyclodextrin functionalized carbon quantum dots via competitive host-guest recognition. *Talanta* **2017,** *167*, 513-519.
107. Algarra, M.; Campos, B. B.; Radotić, K.; Mutavdžić, D.; Bandosz, T.; Jiménez-Jiménez, J.; Rodriguez-Castellón, E.; Esteves da Silva, J. C. G., Luminescent carbon nanoparticles: effects of chemical functionalization, and evaluation of Ag+ sensing properties. *Journal of Materials Chemistry A* **2014,** *2* (22), 8342-8351.
108. Wang, Q.; Zhang, S.; Zhong, Y.; Yang, X.-F.; Li, Z.; Li, H., Preparation of Yellow-Green-Emissive Carbon Dots and Their Application in Constructing a Fluorescent Turn-On Nanoprobe for Imaging of Selenol in Living Cells. *Analytical Chemistry* **2017,** *89* (3), 1734-1741.
109. Yu, B. Y.; Kwak, S.-Y., Carbon quantum dots embedded with mesoporous hematite nanospheres as efficient visible light-active photocatalysts. *Journal of Materials Chemistry* **2012,** *22* (17), 8345-8353.
110. Chai, N.-N.; Wang, H.-X.; Hu, C.-X.; Wang, Q.; Zhang, H.-L., Well-controlled layer-by-layer assembly of carbon dot/CdS heterojunctions for efficient visible-light-driven photocatalysis. *Journal of Materials Chemistry A* **2015,** *3* (32), 16613-16620.
111. Di, J.; Xia, J.; Ji, M.; Li, H.; Xu, H.; Li, H.; Chen, R., The synergistic role of carbon quantum dots for the improved photocatalytic performance of Bi2MoO6. *Nanoscale* **2015,** *7* (26), 11433-11443.
112. Dao, V.-D.; Kim, P.; Baek, S.; Larina, L. L.; Yong, K.; Ryoo, R.; Ko, S. H.; Choi, H.-S., Facile synthesis of carbon dot-Au nanoraspberries and their application as high-performance counter electrodes in quantum dot-sensitized solar cells. *Carbon* **2016,** *96*, 139-144.
113. Paulo, S.; Stoica, G.; Cambarau, W.; Martinez-Ferrero, E.; Palomares, E., Carbon quantum dots as new hole transport material for perovskite solar cells. *Synthetic Metals* **2016,** *222*, 17-22.
114. Huang, J. J.; Zhong, Z. F.; Rong, M. Z.; Zhou, X.; Chen, X. D.; Zhang, M. Q., An easy approach of preparing strongly luminescent carbon dots and their polymer based composites for enhancing solar cell efficiency. *Carbon* **2014,** *70*, 190-198.

2. ELUCIDATION OF THE RELATIONSHIP BETWEEN POLYMER STRUCTURE AND BLUE FLUORESCENCE OF CARBON DOTS

2.1. Abstract

The CDs obtained by the employment of carboxylic acid and amine precursors frequently show bright blue fluorescence emission, independent from the excitation wavelength. The polymer structural rigidity was recognized to play a key role in this phenomenon, nevertheless the knowledge of the CDs structure is still inadequate for its comprehension. In this work three synthetic procedures were carried out to obtain blue fluorescent CDs from carboxylic acids and amines. The full elucidation of the chemical structures and their comparison allowed ascribing unequivocally their similar fluorescent behaviors to the presence of a compact and entangled polyamide network. In here, hydrogen bond-mediated intramolecular interactions were found to significantly enhance the polymer conformational rigidity. Density functional theory calculations of this structure confirmed its rigid and compact nature. Moreover a photo-induced intramolecular charge transfer taking place between amide and carboxylic acid moietes was recognized as the mechanism responsible for the fluorescence emission. Finally, the photoinduced charge-transfer processes could easily explain the performance of CDs in applications as revealed in studies on metal ion sensing.

2.2. Introduction

The most common synthesis procedures of fluorescent CDs are generally harsh, involving the hydrothermal treatment or microwave irradiation of organic molecules and/or polymers. These conditions are reflected in the heterogeneous structure of the obtained nanoparticles, which are composed by random polymerization products as well as a certain degree of carbonization. Indeed, at high temperature the molecular precursors condensation, dehydration and other random and unpredictable reactions are expected. However, despite their large variety and uncertain chemical structure, most of the as-produced CDs reveal a unique blue fluorescence emission as common unifying feature. In the last years, some authors related this excitation-independent type of emission to the presence of conjugated molecular fluorophores that are forming on the polymer skeleton during the synthesis process.[1-7] Neverthless, B. Yang et al. focused their attention on the non-conjugated polymer structure itself, claiming its key-role in the CDs fluorescence. In fact it is known that also non-conjugated polymers can display fluorescence in condition of high structural rigidity. Here the rigidity of the polymer network, achieved by cross-linking, aggregation or immobilization decreases the vibrational and rotational freedom of subfluorophores such as

C=O, N=O, C=N heteroatom-containing double bonds, facilitating their radiative relaxation. This process goes by the name of cross-link enhanced emission (CEE) effect. [8-13] Unfortunately, the difficulty to assign a precise chemical structure to CDs and the major role attributed to the presence of conjugated features diverted the bulk of the attention from the polymer contribution to the CDs fluorescence.

The following study proposes a deep investigation on the origin of the excitation-independent blue fluorescence that is commonly observed in a huge variety of CDs. To this end, model types of blue fluorescent CDs with a well-defined structure, consisting of commonly employed carboxylic acid and amine functional groups are synthesized through microwave irradiation or a novel room-temperature synthesis route, exploiting reactions based on carbodiimide chemistry. All the routes produced highly blue emitting fluorescent CDs, whose comparable structural characterization allowed to determine unequivocally their non-conjugated polymer structure and its direct relationship with the optical properties. Density functional theory (DFT) analysis confirmed the experimental data interpretation and provided the mechanism behind the fluorescent behavior, identifying the organic groups involved.

2.3.Experimental Section

2.3.1. Materials

Citric acid anhydrous (≥99.5%), tricarballylic acid (99%), ethylendiamine (99+%), N,N'-diisopropylcarbodiimide (99%), nickel (II) nitrate hexahydrate (98.5%), iron (III) chloride (97%), cobalt (II) nitrate hexahydrate (98%), zinc (II) chloride (≥97%), magnesium (II) nitrate hexahydrate (99%), calcium (II) chloride dihydrate (99%), copper (II) nitrate hemi(pentahydrate) (98%), lead (II) nitrate (≥99%), mercurium (II) nitrate hydrate (98%), were used without further purifications. Dialysis tubes with molecular weight cut-off (MWCO) 0.5-1 KDa were bought from Spectrum Labs.

2.3.2. Characterization techniques

- The microwave-assisted reaction was performed in a CEM Discover SP reactor employed in open-batch modality.
- Atomic force microscopy (AFM) images were acquired in air under ambient conditions using a NT-MDT Aura NTEGRA instrument operating in tapping mode at 110 kHz resonance with Au tips HA_NC ETALON (10nm curvature radius). Samples

were prepared on silica substrates by drop casting of diluite water solutions. Particle height distribution analysis was carried out by using the Gwyddion software.

- Size exclusion chromatography was performed on a system composed by: pump (Izasa Scientific), automatic injector (Izasa Scientific), PL aquagel column OH-mixed-H (Agilent) and refractive index detector T-REX (Wyatt Technology). The mobile phase (0.1 M sodium acetate) was flowed at 1ml/min at 35°C. For the calibration, PEO/PEG polymers were used in the range of 1970-44400 g/mol. The samples were dissolved in the mobile phase at concentration around 1mg/ml. The DLS measurements were recorded on a Malvern Nano Zetasizer HT, on a 10 mm path-length plastic cuvette.
- Elemental analyses were performed in a Thermo Flash EA 1112 instrument with ~3 mg of powder samples.
- Infrared absorption measurements were performed on powder samples pressed with KBr into pellets with a Bruker Vertex 70 spectrometer.
- ^{1}H and ^{13}C NMR spectra were recorded in D_2O solutions at 25 ^{o}C on a Bruker AV500 spectrometer (δ in ppm and J in Hz) at a ^{1}H NMR operating frequency of 500.13 MHz. ^{1}H and ^{13}C NMR spectra were referenced using the solvent signal as an internal standard. The assignment of the ^{1}H NMR signals and the corresponding ^{13}C NMR peaks was carried out using standard $^{1}H–^{13}C$ edited-HSQC and $^{1}H–^{13}C$ HMBC (J_{HC} = 8 Hz) 2D-experiments. The determination of the diffusion coefficients D (m^2/s) was performed at controlled temperature (300 K) in spinning solutions of the corresponding compounds in D_2O (concentrations about 2 mM). The values of delta (δ) and delta (Δ) were optimized for each sample. In the case of δ the values found were in the range 1.7-2.0 ms, while for Δ the optimized values ranged from 0.17-0.20 s.
- X-ray photoelectron spectroscopy (XPS) measurements were taken with an ESCAPlus spectrometer using a Mg anode (1253.5 eV) and a power of 225 W. XPS data analysis was performed with casaXPS software.
- UV/Vis absorption spectra were recorded on a Shimadzu UV-2401 PC spectrophotometer.
- Photoluminescence excitation and emission spectra were recorded on a Horiba Jobin Yvon Fluoromax-P, slits of excitation and emission at 1 mm. All the spectra were recorded at room temperature using 10 mm path-length quartz cuvette.

- Pico-second time-resolved fluorescence spectra were measured by the time-correlated-single-photon-counting (TCSPC) method on a Nano-Log spectrofluorometer (Horiba JobinYvon), by using a laser diode as an excitation source (NanoLED, 375 nm) and a UV-Vis detector TBX-PMT series (250-850 nm) by Horiba JobinYvon. Lifetimes were evaluated with the DAS6 Fluorescence-Decay Analysis Software.

2.3.3. Synthesis of CDs1-3

2.3.3.1 Synthesis procedures

Synthesis of CDs1. 2.0 g of citric acid monohydrate (CA, 9.5 mmol, 1 eq.) were dissolved in 15 mL of ultrapure water. Upon addition of 0.64 mL of ethylenediamine (EDA, 1 equiv.) the solution was heated up to 140°C through microwave irradiation (stirring, open batch), provoking the evaporation of the water. The temperature was kept constant for one minute, after that the irradiation was stopped and the mixture redissolved in 10 mL of water. The same process was repeated two times more, for a total of three minutes at 140°C. The solid product was diluted with ultrapure water, filtrated through a 0.45 µm PTFE membrane and dialyzed against ultrapure water (MWCO = 0.5-1.0 KDa, 3 days, twice a day), yielding in a brownish powder, with a yield in mass of 35%.

Synthesis of CDs2. 2.0 g of tricarballylic acid (TA, 11.4 mmol, 1 equiv.) were dissolved in 15 mL of ultrapure water. Upon addition of 0.76 mL of EDA (1 equiv.) the solution was heated up to 140°C through microwave irradiation (stirring, open batch), provoking the evaporation of the water. The temperature was kept constant for 3 minutes, after that the irradiation was stopped and the mixture cooled down. The solid product was diluted with ultrapure water, filtrated through a 0.45 µm PTFE membrane and dialyzed against ultrapure water (MWCO = 0.5-1.0 KDa, 3 days, twice a day), yielding in a brownish powder with a yield in mass of 27%.

Synthesis of CDs3. 1.0 g of anhydrous citric acid (5.2 mmol, 1 equiv.) was dissolved in 5.0 mL of DMF. The solution was cooled in an ice bath and 2.6 mL of diisopropyl carbodiimide (DIC, 3 equiv.) were added. Subsequently, 0.35 mL of EDA (1 eq.) in 5 mL of water were slowly added and the reaction was stirred for 30 minutes at room temperature, during which the mixture turns its color from slightly yellow to red. The filtered reaction was stopped by adding slowly during a time of 3 hours a NaOH solution at pH=10, until no formation of DIC-urea precipitate was observed. The crude was diluted in ultrapure water, filtered and washed

with ethyl acetate. During these operations the coupling agent urea byproduct, in the form of a white precipitate, was removed. The water phase was dialyzed against ultrapure water (MWCO = 0.5-1.0 KDa, 3 days, twice a day). The dry product was obtained by freeze-drying, with a yield in mass of 29 wt. %. It appears as a brownish powder.

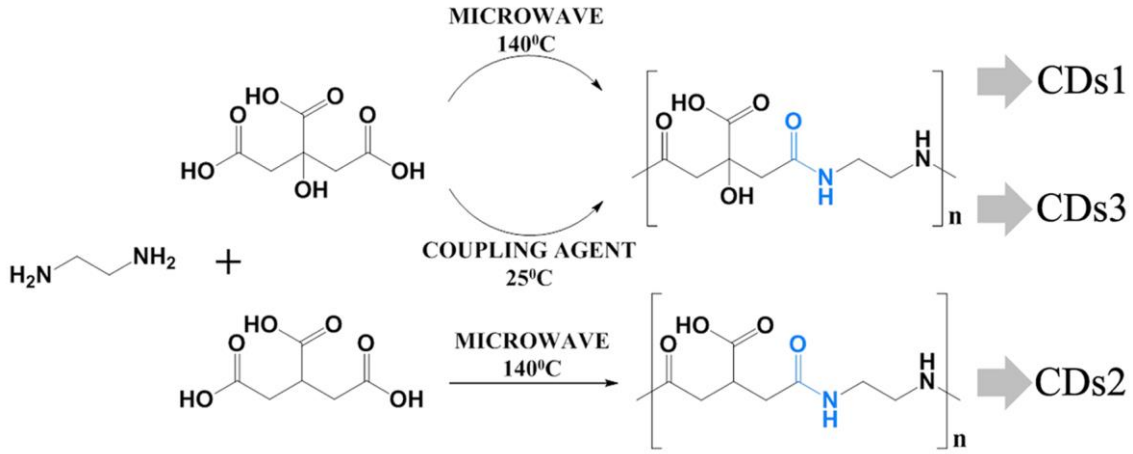

Scheme 2.1. (Top) reaction of EDA with CA through two synthetic pathways to form CDs1 and CDs3. (Bottom) reaction of EDA with TA to form CDs2.

2.3.3.2 Comments to the synthesis procedures

- CA and EDA in a ratio 1:1 were chosen as starting material for the synthesis of **CDs1**, expecting the amide bond formation via condensation between carboxylic acid and amine groups. The employed reaction conditions are the result of a pre-study aimed to investigate the effect of the reaction time on the structural and optical properties of the CDs (see Appendix B).
- **CDs2** are obtained through an identical procedure, but using TA in place of CA. The reason is that at high temperature the hydroxyl group in CA could in principle lead to unpredictable products. Thus, the replacement of CA with TA ensures that reactions involving the –OH group are excluded, while the plausible formation of the amide bond is unaffected.
- Reaction temperature is an additional crucial parameter to keep under control during the synthesis, since high temperatures enable a wider range of unpredictable reaction pathways. For this reason, **CDs3** is achieved by amide bond formation at room temperature, selectively catalyzed by a carbodiimide coupling agent.

- All the water solutions of the three products display blue photoluminescence when irradiated by UV-light.

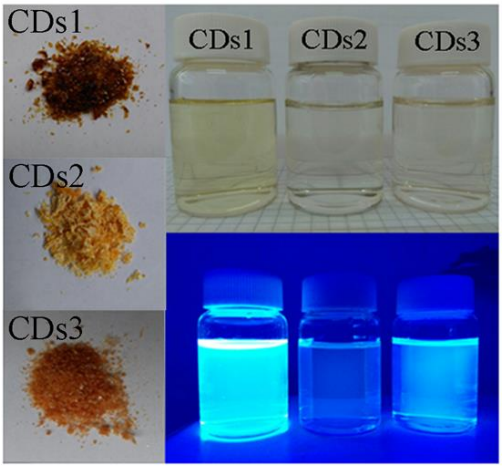

Figure 2.1. Photographs of CDs1, CDs2 and CDs3 in solid and in water solution (0.5 mg/mL), with and without UV irradiation.

2.4. Results and discussion

2.4.1. Size determination of CDs1-3

The three samples were analyzed by AFM (Figure 2.2), DLS (Figure 2.3) and DOSY (Figure 2.4, Table 2.1), finding that they are composed of nanoparticles of around 1.0-1.6 nm.

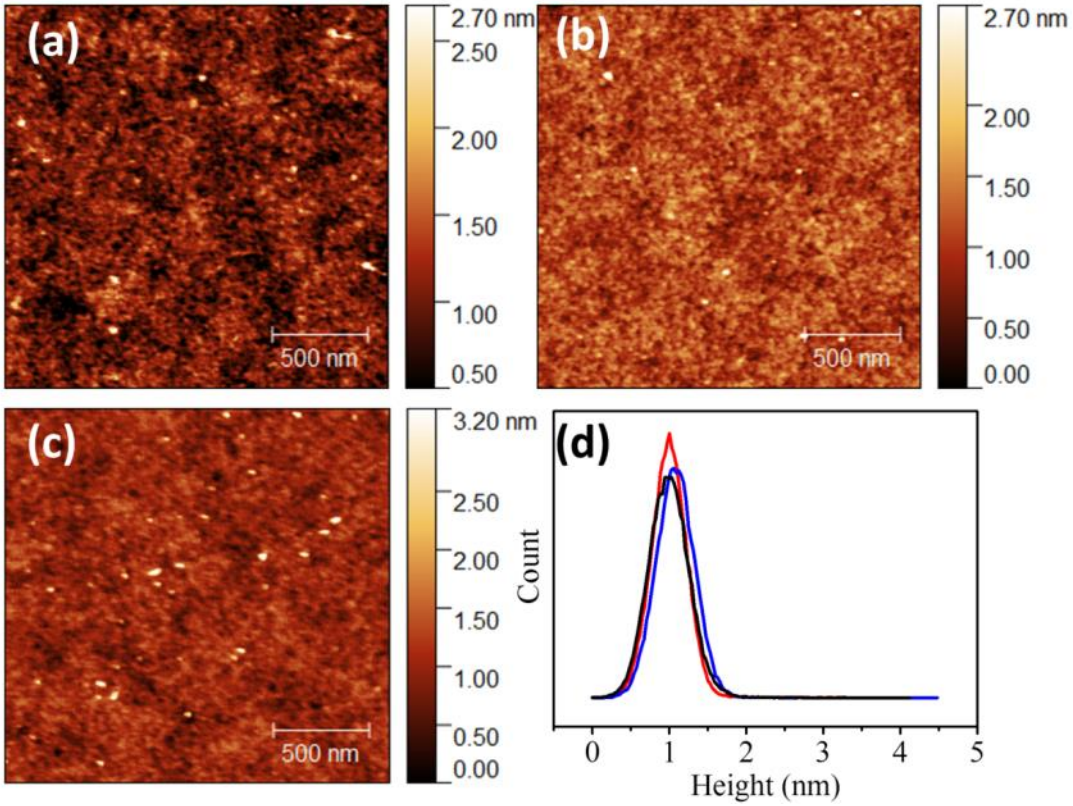

Figure 2.2. AFM images of CDs1 (a), CDs2 (b), CDs3 (c) and their respective height distribution (d) in black, blue and red, respectively. The average height is found at around 1 nm for all the samples.

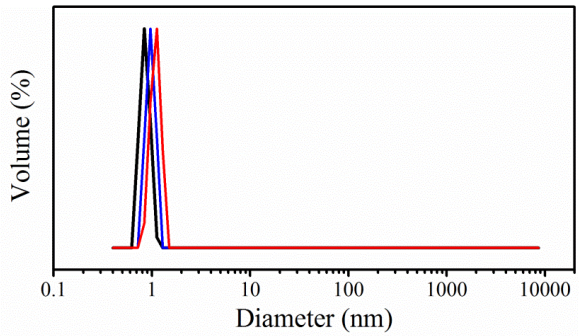

Figure 2.3. DLS size distribution of CDs1 (black), CDs2 (blue), CDs3 (red). All the samples show a diameter of about 1 nm.

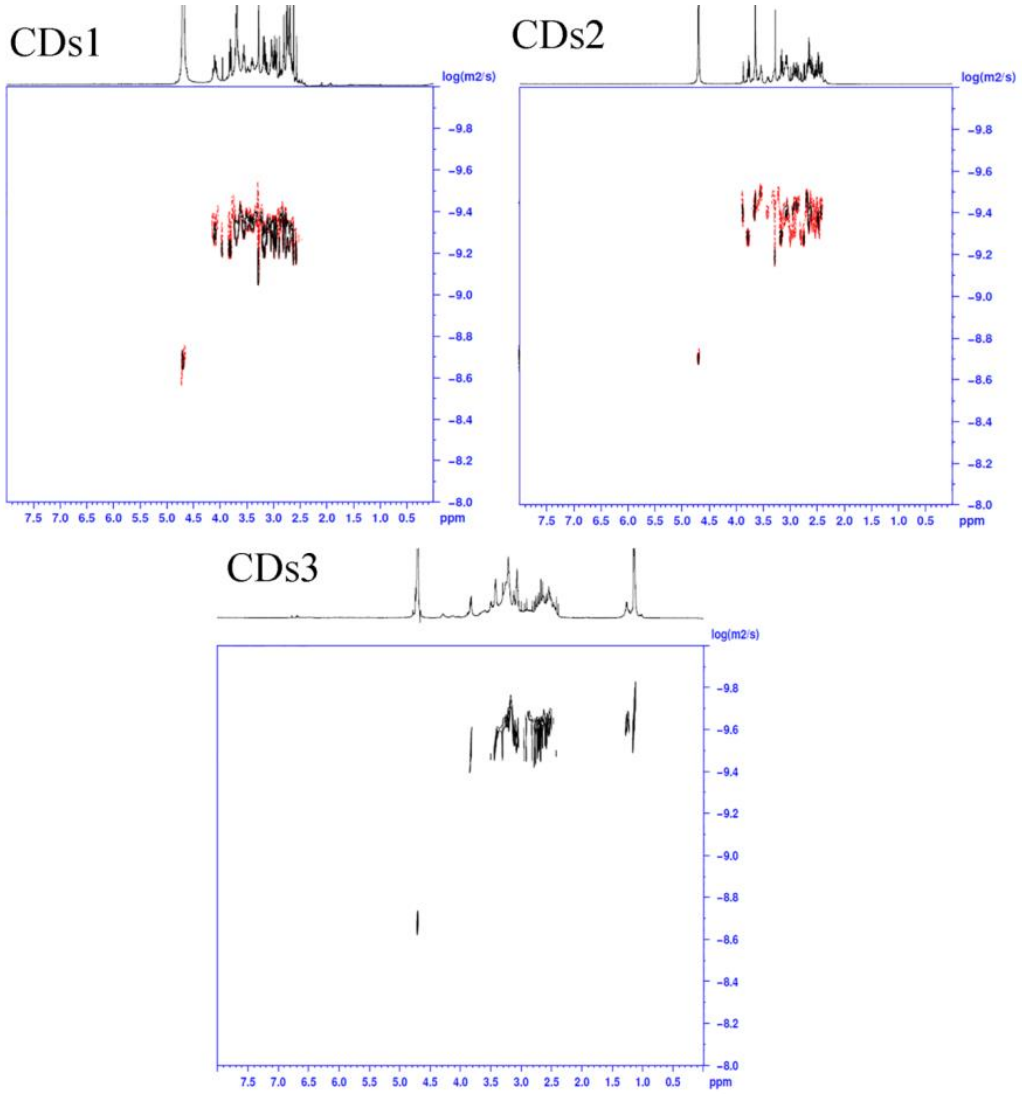

Figure 2.4. DOSY spectra of CDs1, CDs2, and CDs3.

The hydrodynamic radius (rH) was calculated through the Stokes-Einstein equation (Annex A,), and ranges from 1.2 to 1.6 nm for all the three samples (Table 2.1)

Table 2.1. Measured diffusion coefficient (D), calculated hydrodynamic radius (rH) and diameter of CDs1, CDs2, and CDs3. All samples show a diameter between 1.2-1.6 nm.

	D (m^2/s)	rH (nm)	Diameter (nm)
CDs1	$10^{-9.4}$	0.6	1.2
CDs2	$10^{-9.4}$	0.6	1.2
CDs3	$10^{-9.5}$	0.8	1.6

2.4.2. Optical properties of CDs1-3

The optical properties of **CDs1**, **CDs2** and **CDs3** were investigated by UV/Vis spectroscopy (Figure 2.5a), steady state photoluminescence spectroscopy (Figure 2.5b,c) and time-resolved photoluminescence spectroscopy (Figure 2.6a). A peculiar absorption band in the range of 350 - 390 nm appears in the UV/Vis spectra of the three types of CDs, which is directly related to the photoluminescence emission. In fact, the maximum emission intensity, found at 445 nm for **CDs1** and **CDs3** and at 470 nm for **CDs2**, is achieved by exciting exactly in the same region (360-390 nm depending on the CDs sample, see Figure 2.5b). Remarkably, emission spectra of **CDs1**, **CDs2** and **CDs3** taken at different excitation wavelengths do not reveal a wavelength dependency (Figure 2.5c). Although small shifts of the maximum position are found between the different types of CDs, their absorbance, excitation and emission are highly comparable and can be related to the same radiative process.

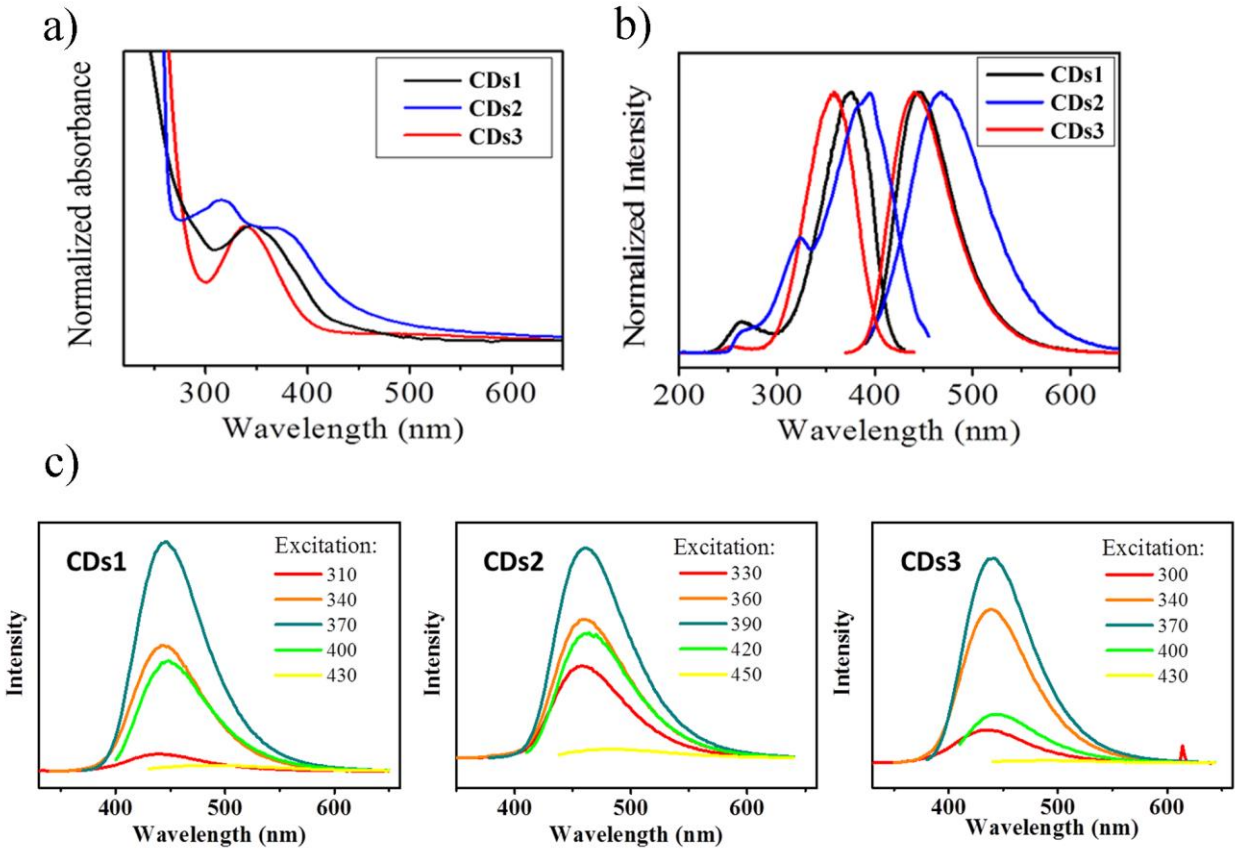

Figure 2.5. (a) UV/Vis, (b) Excitation and emission spectra of CDs1 (black), CDs2 (blue) and CDs3 (red). (c) Emission in CDs1-3 at different excitation wavelengths.

The calculated photoluminescence lifetimes are also similar, being 14.7 ns for **CDs1**, 11.5 ns for **CDs2** and 10.4 ns for **CDs3**. The fast lifetimes indicate that the radiative relaxation occurs by means of fluorescence. The quantum yield is very high for **CDs1**, reaching 64%, and yet still remarkable in **CDs2** (7%) and in **CDs3** (13%) (Figure 2.6b). The higher quantum yield of **CDs1** and **CDs3** with respect to **CDs2** could be related to the presence of the hydroxyl group. In fact, even if not directly involved in the fluorescence emission itself the ability of this group to form H-bonds may contribute to provide enhanced rigidity to the polymer structure and thus assists to suppress non-radiative decay channels.

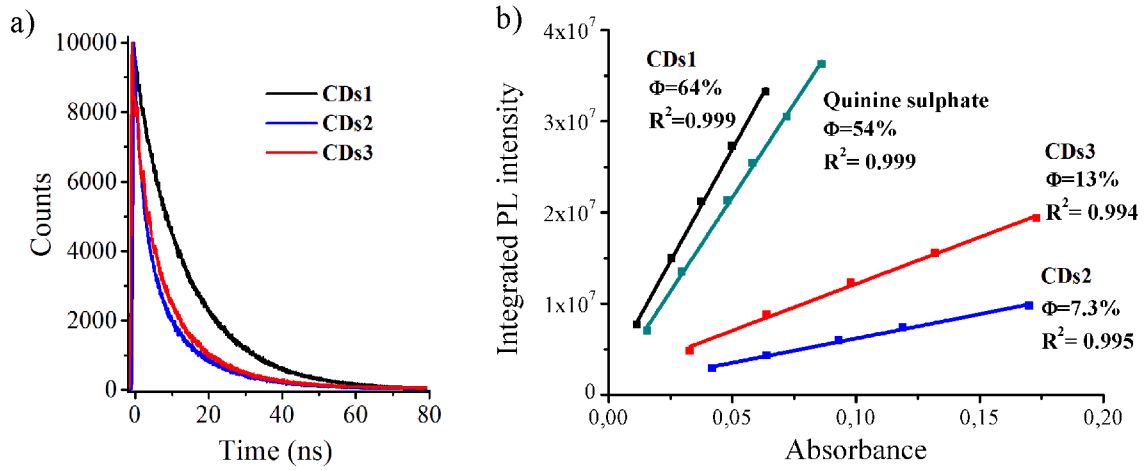

Figure 2.6. PL decay of CDs1 (black), CDs2 (blue) and CDs3 (red). (b) Different concentrations of CDs1 (black), CDs2 (blue), CDs3 (red) and quinine sulfate (cyan), plotted by integrated PL intensity vs. absorbance and fitted for calculating the quantum yield, expressed in %.

The optical properties of **CDs1-CDs3** are very similar to those obtained from different amine and carboxylic acid precursors, as reported in the literature.[4, 6-7, 14-33] This coincidence implies a common principle behind the optical properties, suggesting the involvement of amides, amines and carboxylic acids. Consequently, any alteration of the polymer conformation thus should lead to a modification of the fluorescence behavior. Therefore, absorbance and emission measurements of **CDs1** at various pH were performed. A highly basic solution of **CDs1** (pH>14) was treated dropwise with a HCl solution up to pH<1. A sudden decrease in the absorbance and the emission of **CDs1** is observed between pH 5 and pH 3 (Figure 2.7a,b,e). Switching the pH between basic and acidic conditions, a reversible loss of fluorescence intensity is detected, even during several cycles (Figure 2.7c,d,f). These facts, ascribable to the carboxylic acid protonation-deprotonation, underline the role of H-bonds and/or electrostatic forces in the interaction originating the fluorescence.

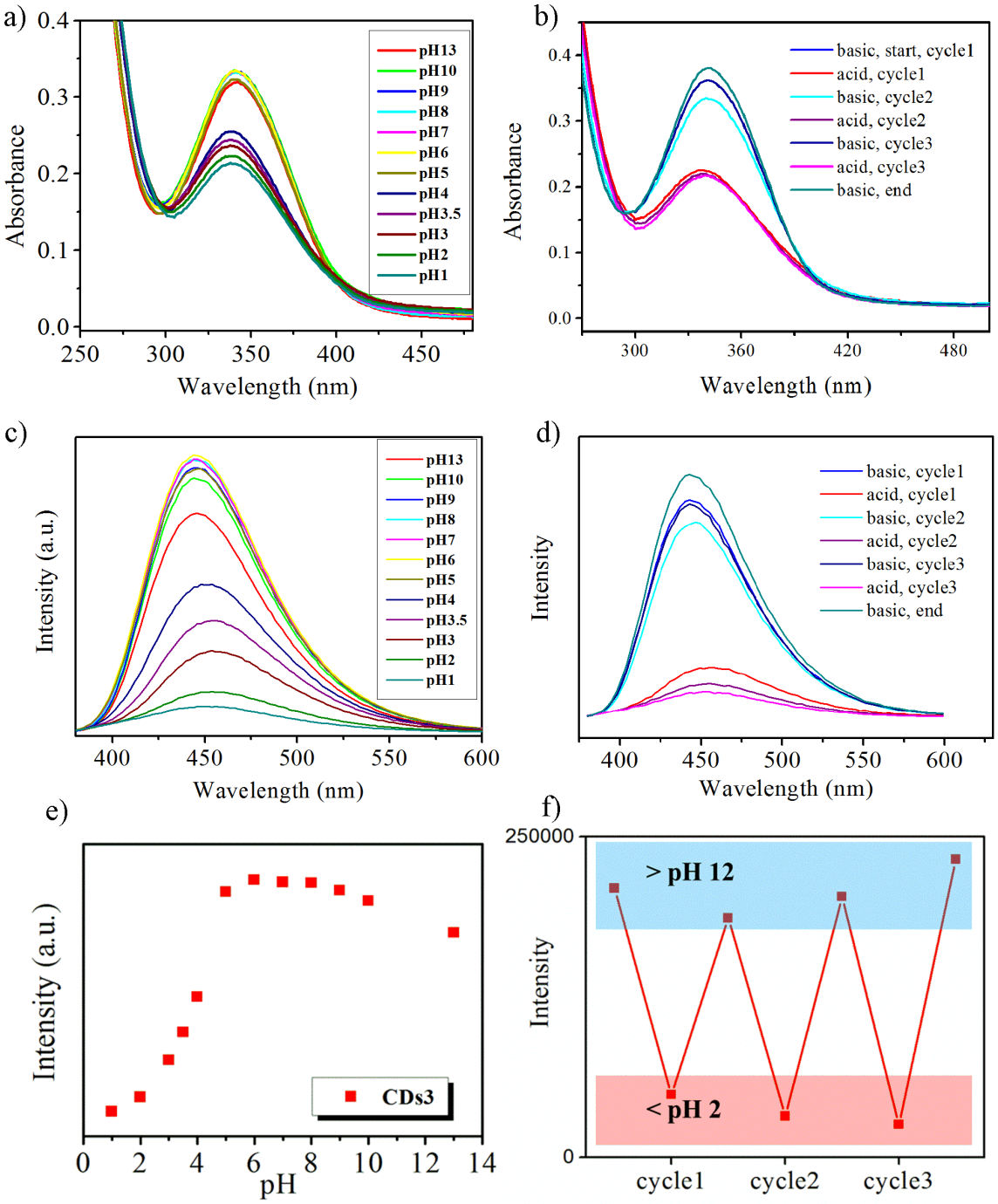

Figure 2.7. (a) Absorbance, (c) emission (λ_{ex}=370 nm) and (e) fluorescence intensity of CDs1 at different pH. (b) Absorbance, (d) emission (λ_{ex}=370 nm) and (f) fluorescence intensity of CDs1 switching repeatedly the pH from basic to acidic conditions and vice-versa.

2.4.3. Structural characterization of CDs1-3

In order to shine light on the chemical interactions behind the fluorescence, a detailed structural characterization of **CDs1**, **CDs2** and **CDs3** was performed by means of elemental analysis, IR, NMR and XPS.

Results of elemental analyses of **CDs1** and **CDs3** (Table 2.2) match with a formula of $C_8H_{12}N_2O_5$, indicating that a stoichiometric copolymer is formed by condensation of CA and EDA in a 1:1 molar ratio. The same correspondence is found for **CDs2** revealing a stoichiometric formula of $C_8H_{12}N_2O_4$ (Figure 2.8). These facts provide a good starting point for the understanding of the chemical structure of the formed CDs.

Table 8. 2.2. Elemental analysis of CDs1, CDs2 and CDs3 and the calculated percentage (mol%) for the repetitive unit of the corresponding polymeric condensation products.

	C (mol%)	H (mol%)	N (mol%)	O (mol%)
CDs1	30,0	44,3	8,0	17,7
CDs3	26,5	48,0	7,0	18,5
$C_8H_{12}N_2O_5$	29,6	44,4	7,4	18,5
CDs2	30,8	45,4	8.4	15.4
$C_8H_{12}N_2O_4$	30,8	46,2	7.7	15.4

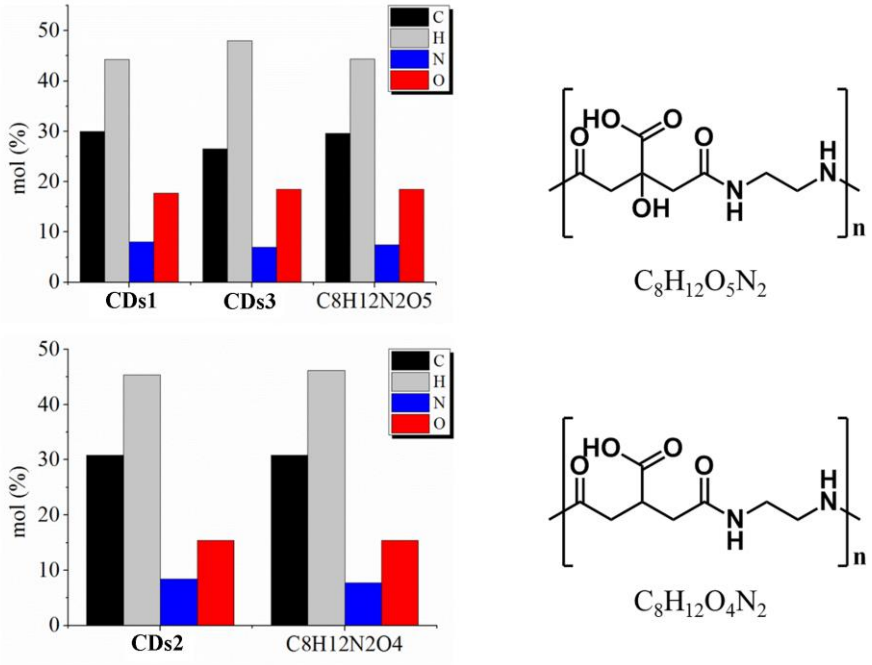

Figure 2.8. Mole percentages of C, H, N, O in CDs1, CDs2 and CDs3, and the calculated percentages for the repetitive unit of the corresponding polymeric condensation product.

In the IR spectrum of **CDs1** (Figure 2.9, black) the typical C=O stretching mode of the carboxylic group splits in two bands. The band at 1710 cm^{-1} reflects the carboxylic acid involved in H-bond, while the band at 1780 cm^{-1} is the free form. The former exhibits a significantly higher intensity than the latter one. This indicates that almost all of the carboxylic groups are involved in H-bonds. The amide vibrational modes I and II are found at 1653 and 1560 cm^{-1}, respectively. Their shifted position is comparable to the peptide bond vibrational modes and reflects the amide participation in H-bonds that increases the rigidity of the polymer.[34-35] More features, such as O-H and N-H stretching, are observed at 3500-2900 cm^{-1} and C-O and C-N stretching at 1438, 1402, 1341 cm^{-1}. Therefore, IR spectroscopy reveals that the structure of **CDs1** encompasses a high involvement of H-bonds and ionic supramolecular interactions that contribute to enhance the rigidity of the system. Identical considerations apply to the cases of **CDs2** and **CDs3**, which both exhibit very similar IR profiles.

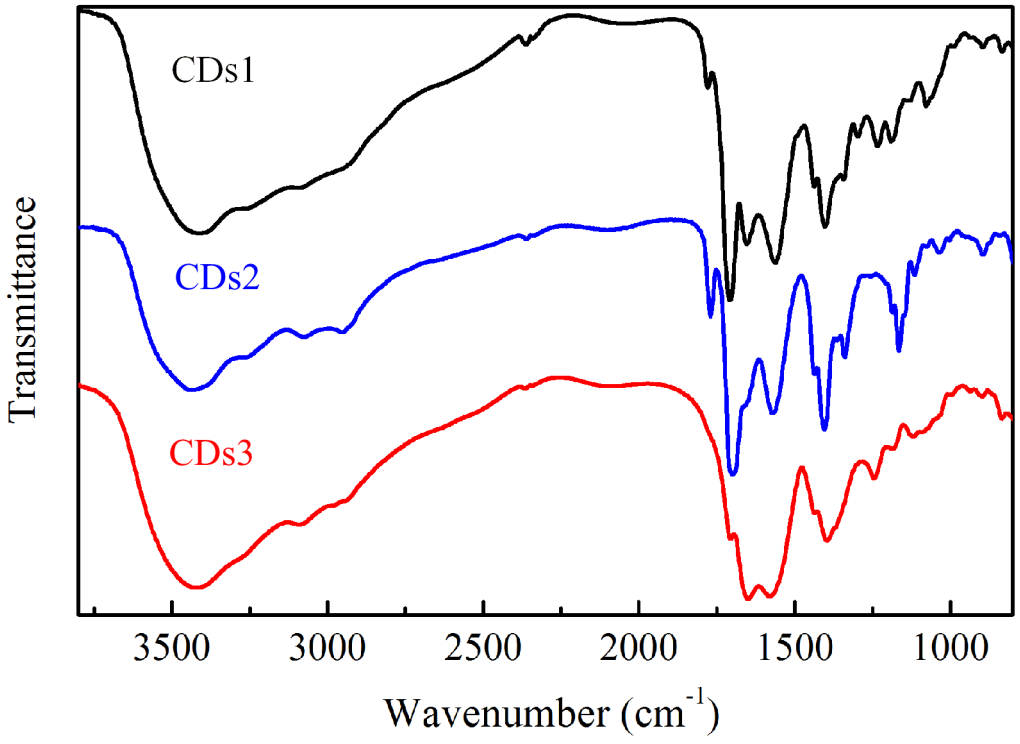

Figure 2.9. (a) IR spectra of CDs1 (black), CDs2 (blue) and CDs3 (red).

The XPS results of **CDs1**, **CDs2** and **CDs3** (Figure 2.10) fit very well with the presence of the above-described structural features. The C 1s peak was deconvoluted into five contributions (Figure 2.10b, first raw), the C-C (284.9 eV), C-N (285.7 eV), C-OH (286.3 eV, absent in **CDs2**), N-C=O (286.8 eV) and –COOH (288.2 eV). The O 1s peak consists of three components corresponding to amide (531.7 eV), carboxylic acid (532.2 eV) and hydroxyl

group (533.0 eV) (Figure 2.10b, second raw). The N 1s peak is the sum of the amide (399.4 eV) and the amine contribution (400.1 eV) (Figure 2.10b, third raw).

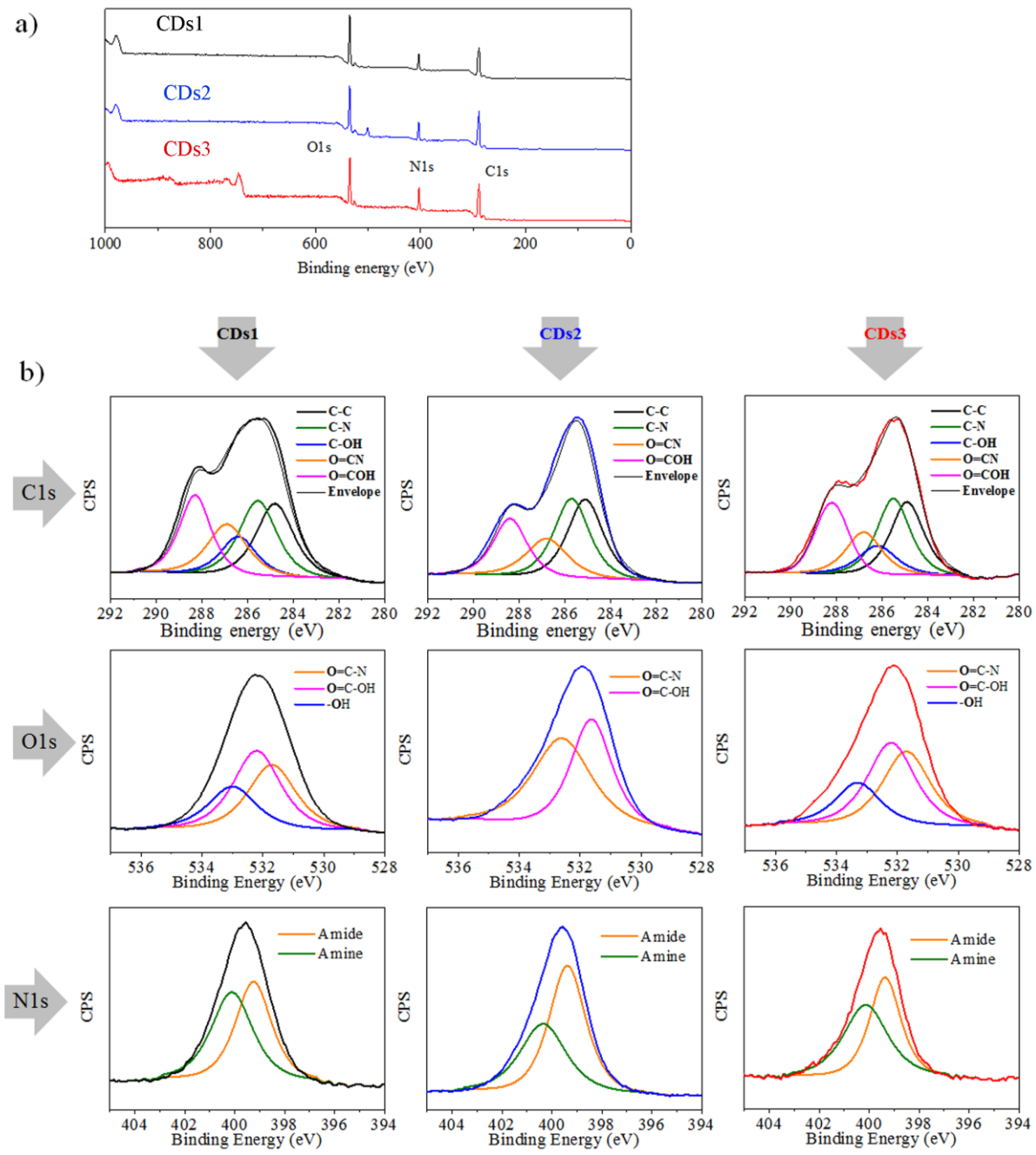

Figure 2.10. (a) XPS survey of CDs1 (black), CDs2 (blue) and CDs3 (red). (b) C1s, O1s and N1s spectra of CDs1 (left), CDs2 (center), CDs3 (right).

Proton (^{1}H) and carbon (^{13}C, APT: attached proton test) standard NMR experiments, as well as two-dimensional correlation experiments ^{1}H-^{13}C HSQC (heteronuclear single-quantum coherence) and ^{1}H-^{13}C HMBC (heteronuclear multiple-bond correlation), of the CDs were measured in D_2O and allowed to gather determinant information about the chemical structure

and connectivity. An individual structure interpretation of **CDs1-3** is first presented (Figures 1.11-1.13), subsequently some general observations are drawn.

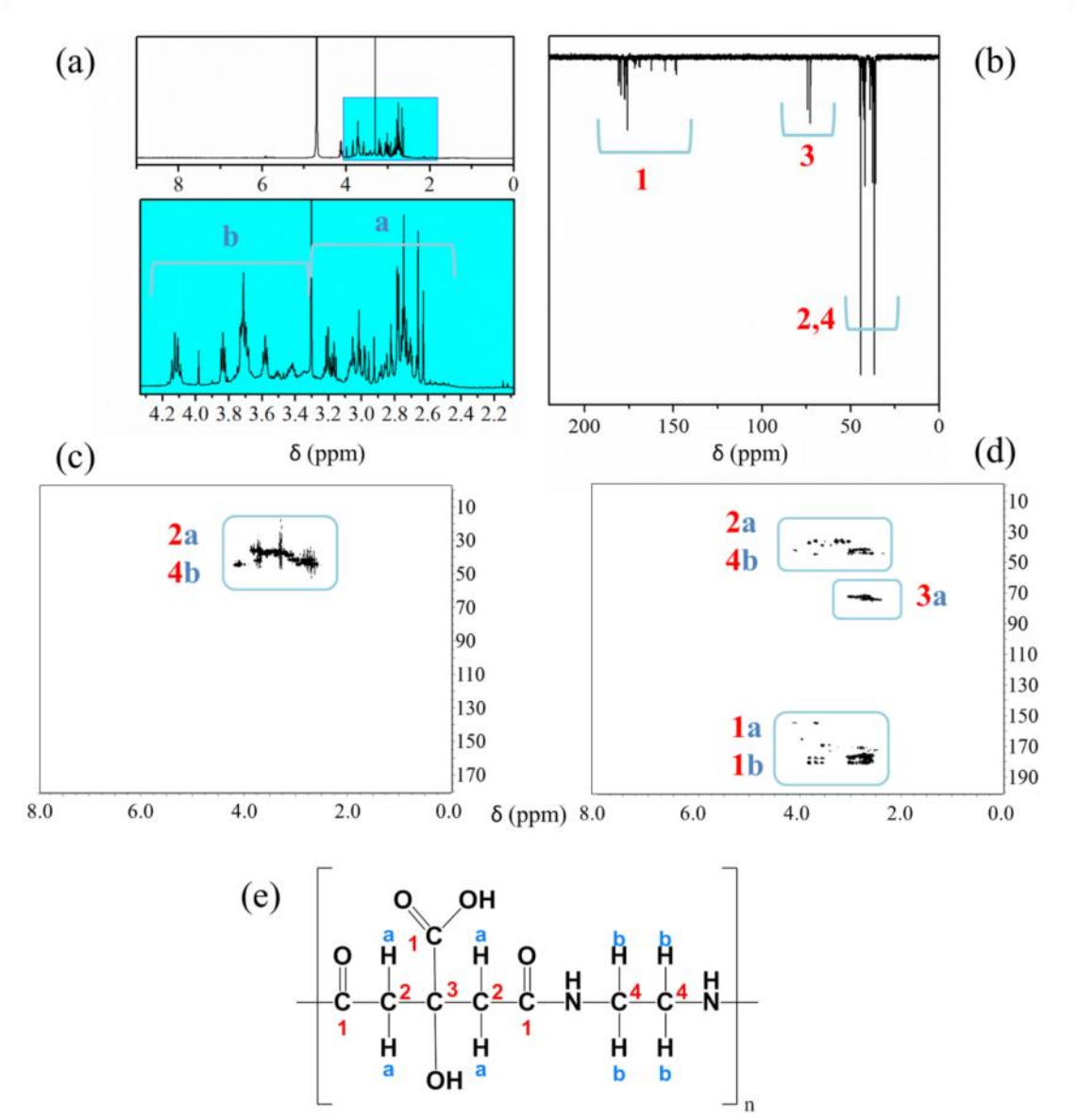

Figure 2.11. (a) ^{1}H NMR. (b) APT ^{13}C NMR, (c) ^{1}H-^{13}C HSQC and (d) ^{1}H-^{13}C HMBC spectra of CDs3. (e) one of the possible chain isomers of the CDs1 repetitive unit, with C and H assignation.

NMR interpretation for CDs1: ^{1}H NMR. Hb: 4.2-3.4 ppm (m), EDA 3.3 ppm (s), Ha: 3.2-2.5 ppm (s or d). APT ^{13}C NMR shows in-phase signals, belonging to secondary or quaternary carbons. C1: 182-148 ppm, C2 and C4: 46-35 ppm, C3: 75-71 ppm. ^{1}H-^{13}C HSQC shows the ^{1}J coupling of Ha and Hb with C2 and C4 respectively. ^{1}H-^{13}C HMBC shows the ^{2}J of Ha with C3, the ^{2}J and ^{3}J coupling of Ha with C1 and C2, the ^{3}J coupling of Hb with C1 and C4.

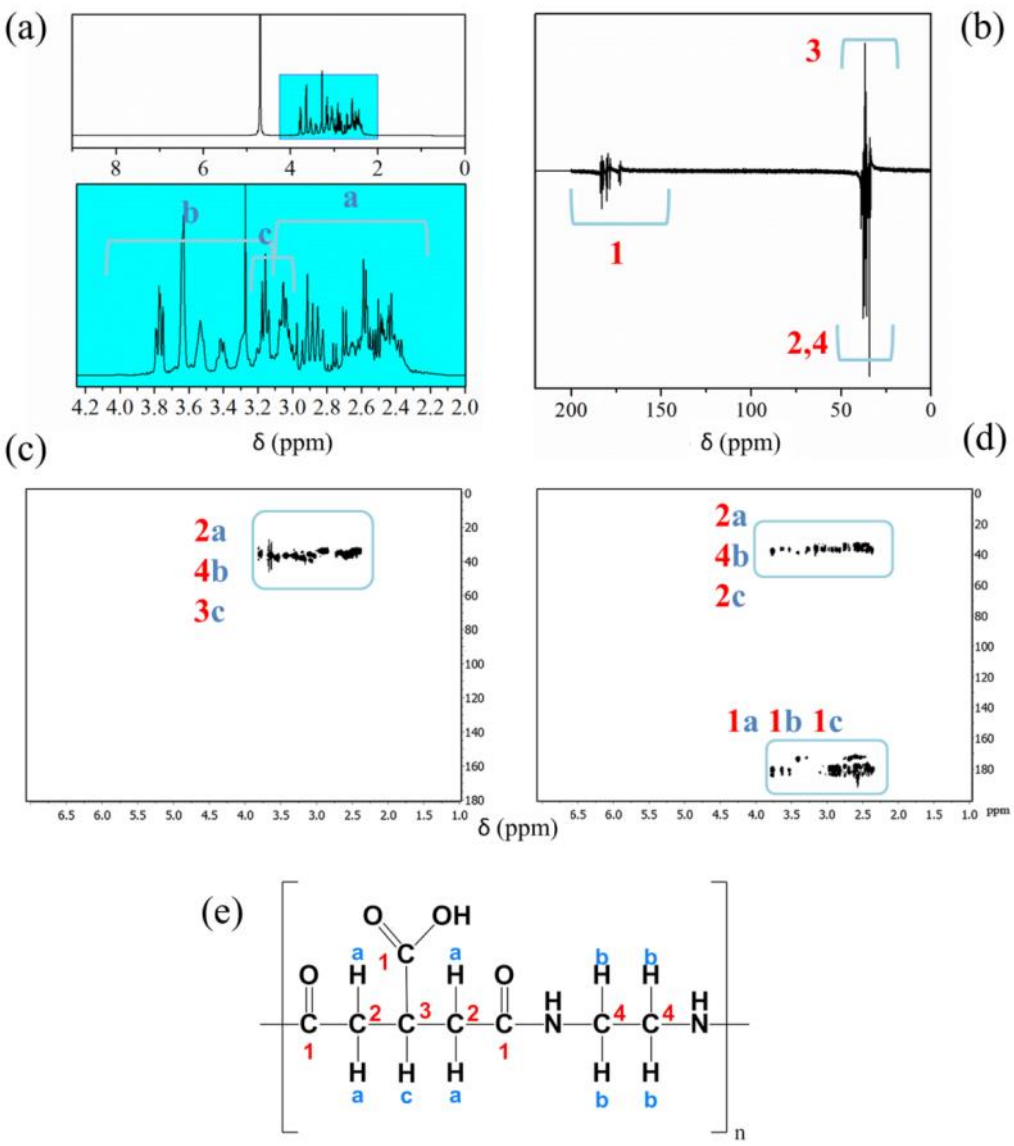

Figure 2.12. (a) ^{1}H NMR. (b) APT ^{13}C NMR, (c) ^{1}H-^{13}C HSQC and (d) ^{1}H-^{13}C HMBC spectra of CDs3. (e) one of the possible chain isomers of the CDs2 repetitive unit, with C and H assignation.

NMR interpretation for CDs2: ^{1}H NMR. Hb: 3.8-3.3 ppm (t), EDA 3.25 ppm (s), Hc: 3.2-3.0 ppm (m), Ha: 3.2-2.3 ppm (s or d). APT ^{13}C NMR shows in-phase signals, belonging to secondary or quaternary carbons. APT also shows an antiphased signal, assigned to C3, at about 36 ppm. C1: 184-171 ppm, C2 and C4: 40-32 ppm, C3: 38-34 ppm. ^{1}H-^{13}C HSQC shows the ^{1}J coupling of Ha, Hb and Hc with C2, C4 and C3 respectively. ^{1}H-^{13}C HMBC shows the ^{2}J of Ha with C3, the ^{2}J coupling of Hc with C1 and C2, the ^{2}J and ^{3}J coupling of Ha with C1 and C2, the ^{3}J coupling of Hc with C1 and the ^{3}J coupling of Hb with C1 and C4.

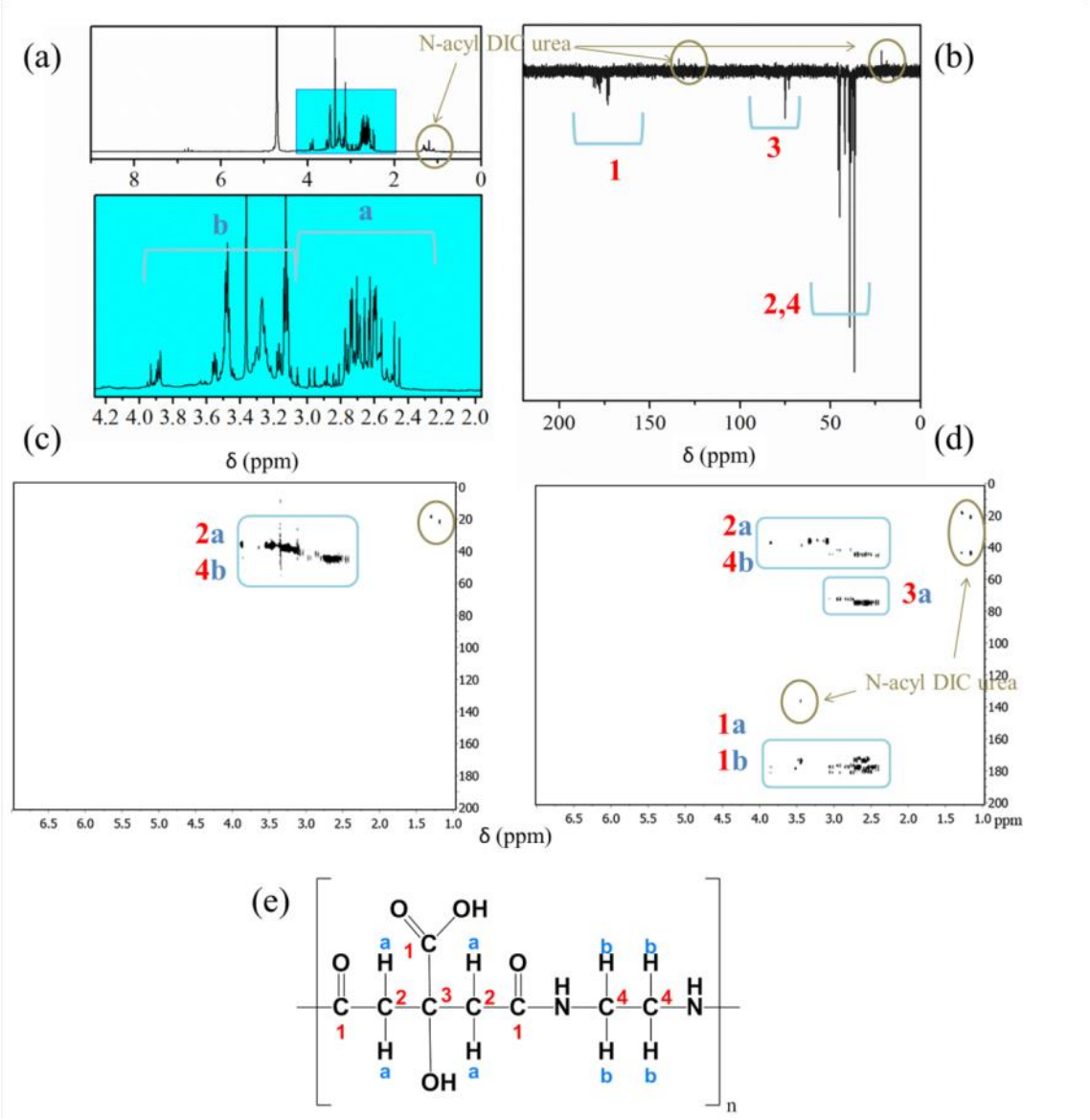

Figure 2.13. (a) ^{1}H NMR. (b) APT ^{13}C NMR, (c) ^{1}H-^{13}C HSQC and (d) ^{1}H-^{13}C HMBC spectra of CDs3. (e) one of the possible chain isomers of the CDs3 repetitive unit, with C and H assignation.

NMR interpretation for CDs2: ^{1}H NMR. Hb: 4.0-3.2 ppm (m), EDA 3.35 ppm (s), Ha: 3.2-2.4 ppm (s or d). APT ^{13}C NMR shows in-phase signals, belonging to secondary or quaternary carbons. C1: 182-171 ppm, C2 and C4: 47-35 ppm, C3: 76-71 ppm. ^{1}H-^{13}C HSQC shows the ^{1}J coupling of Ha and Hb with C2 and C4 respectively. ^{1}H-^{13}C HMBC shows the ^{2}J of Ha with C3, the ^{2}J and ^{3}J coupling of Ha with C1 and C2, the ^{3}J coupling of Hb with C1 and C4. N-acyl DIC urea side-product has formed in little amount during the reaction, incorporated into the CDs5 structure (1H NMR: 1.20, 1.32, 6.72 ppm, in APT: 137, 21 ppm). Some of the proton signals of **CDs3** are right-shifted with respect to **CDs1**, probably because of the different charged form due to the final addition of NaOH.

Despite the differences in the synthesis methods, the NMR profiles of **CDs1** and **CDs3** are remarkably similar, showing that in both cases the same type of polymer structure is obtained. The NMR spectra of **CDs2** are also highly comparable, taking into account the differences due to the absence of the hydroxyl group. Merging the information obtained from all the NMR experiments, the chemical structure of **CDs1**, **CDs2** and **CDs3** is unambiguously identified as a non-conjugated polymer consisting of the product of condensation of CA and EDA for **CDs1** and **CDs3**, and of TA and EDA for **CDs2.** The comparison of the NMR spectra also proves that unassigned minor features, specific to each one of the employed synthetic route, are not common to all the samples, and thus cannot form the basis of the fluorescent behavior. Furthermore, NMR experiments provided valuable information regarding the conformation of the polymeric dots. In the ^{1}H NMR spectra, the sharp lineshape of the peaks (singlets and triplets) strongly suggests a compact and static structure, in fast motion with respect to the time of response of the technique. The ^{1}H-^{13}C HSQC spectra show that the methylene carbons couple with a rather condensed set of proton signals. The high density of sharp signals is related to the variety of static chemical environments that surrounds these protons and can be explained with the presence of various chain isomers of the repetitive unit that coexist in the polymer, as well as with the existence of different ionized forms. These data highlight the branched and rigid conformation of the polymeric CDs.

2.4.4. DFT and TDDFT calculations

In order to achieve a deeper understanding of the structure and photoluminescence of these nanoparticles, DFT calculations have been performed based on the **CDs1** and **CDs3** polymeric $[C_8H_{12}O_5N_2]_n$ units (see Annex B for details). For the analysis of the structural features that may be responsible of the CEE effect, clusters of different size have been studied, in particular the dimer (n = 2), octamer (n = 8) and decamer (n = 10). The latter is a good approximation of the **CDs1** real chain, whose molecular mass was measured to be 2300 Da by size exclusion chromatography (SEC/RI, Annex B), while the polymeric unit weights 216 Da. The optimized structures show that the main characteristic is a very intricate network due to the establishment of both intra- and intermolecular hydrogen bonds. In Figure 2.14a two dimeric chains (n = 2) are represented and it is clear the degree of entanglement, both within and between chains. In Figure 2.14b is represented one decameric chain (n = 10) that also shows a highly intricate structure due to the intramolecular hydrogen bonding (HB). This feature is reflected in the size of the nanoparticle. The calculated diameters are 1.564 nm and

1.670 nm for the octamer and the decamer, respectively, in good agreement with the particle size measured experimentally.

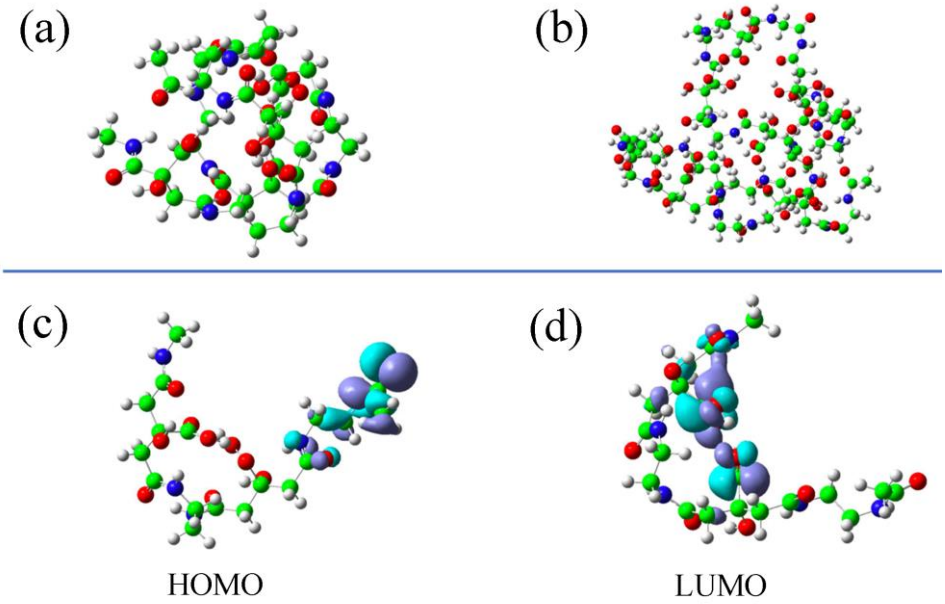

Figure 2.14. Optimized molecular structures of (a) two dimer (*n* = 2) chains and (b) one decamer (*n* =10) chain. (c) HOMO and (d) LUMO molecular orbitals involved in the fluorescence phenomenon.

As it has been previously mentioned, this aggregation of the chains is responsible of the enhancement of the fluorescence in these systems, due to a restriction of the vibrational or rotational degrees of freedom that may favor a non-radiative relaxation. In order to corroborate this statement, the optical properties of four representative systems have been calculated, namely, three dimers and one octamer. The first dimer has only one chain, while the others comprise two dimeric chains to generate two conformers, where either the intramolecular or the intermolecular HB is favored. The use of one or two chains, as well as two different conformers, allows studying the influence of the intra- and intermolecular interactions independently. The octamer has been used in order to relieve the computational effort. In Table 2.3 are gathered the absorption and emission energies, and the corresponding wavelengths.

Table 2.3. Absorption (E_{abs}) and emission (E_{em}) energies

	E_{abs} (eV)	E_{em} (eV)
Dimer (one chain)	5.1811	---
Dimer of two chains (HB intramolecular)	4.8794	---
Dimer of two chains (HB intermolecular)	5.1382	1.8317
Octamer	4.6142	1.9602

It is observed that the four models absorb in the UV, with wavelengths in the range of λ_{abs} = 239 – 269 nm. The nature of the transition has been characterized by the analysis of the molecular orbitals involved, which is depicted in Figures 2.14c and 2.14d for the dimer, in order to facilitate the visualization. The HOMO has its main contribution from the amide moiety (-CONH-), while the LUMO is centered in the carboxylic groups (-COOH) and it is from HOMO to LUMO where excitation takes place. This means that HOMO and LUMO molecular orbitals are confined at very specific sites, that they are well separated, and that the fluorescence is a charge transfer process. This process is enhanced for the large models due to the sum of all local charge transfer processes occurring in each amide-carboxyl pair of the chain. Experimental evidence for these findings is provided by the results of our photoluminescence studies. First, the large Stokes-shift of about 1 eV (see Figure 2.5b) should be related to a considerable change in the dipole moment between ground state and excited state, being consistent with the typical photo-induced charge transfer mechanism.[54-57] Second, the protonation dependency of the emission intensity (see Figure 2.7) reveals the important role of the carboxylic acids in the fluorescence process: They affect the rigidity of the overall polymer network structure via hydrogen bonding or electrostatic interactions, as discussed above. Concomitantly, they act as electron acceptor in the charge transfer process. The observation of a strong decay of the fluorescence in an acidic environment is a consequence of the weakening of the carboxyl acids intramolecular interactions, which create the emitting state (see Figure 2.14c,d). On the contrary, strengthening the carboxylic intramolecular chain interactions, as obtained under neutral and basic conditions, leads to the recovery of the carboxylic acids intramolecular chain interactions, favoring charge-transfer and the fluorescence process.

Regarding the emission, a striking behavior is found. Both the dimer with one chain and that with two chains where the main interaction is the intramolecular HB, show transitions that are

remarkably redshifted. In fact, the emission takes place in a region where the singlet excited state and the ground state potential energy surfaces cross, known as internal conversion (IC), involving a non-radiative relaxation and, hence, no fluorescence will be observed.

Considering the dimer with two chains, in which the intermolecular HB is favored, a clear redshift of the emission energy is observed with respect to the absorption, arising from a singlet excited state well separated from the ground state (1.8317 eV above the ground state). This emission takes place in the visible region (λ_{em} = 676.9 nm). These results suggest that, in a small chain like a dimer, the crosslink generated by the intramolecular HB is not enough to avoid the non-radiative relaxation by vibration or rotation of the chain, and the main confinement is exerted by the intermolecular interactions. Nevertheless, this prominent feature disappears when longer chains are considered and a larger number of intramolecular interactions are allowed. Thus, inspecting the results for the octamer (single chain), a similar redshift is observed and the emission also take place in the visible (λ_{em} = 632.5 nm). This means that the intramolecular crosslink is strong enough to hinder the vibration and rotation of the chain, and fluorescence is observed. At this point it is worthwhile to outline that the theoretical calculations are based on simplified models, which do not take into account several effects of experimental relevance, such as polymer branching, influence of additional chains, solvent effects, nor those related to the presence of free amines or charged states. These parameters contribute to enhance the rigidity of the polymer and thus may lead to further important down shifts of the calculated emission wavelengths towards the blue wavelength range. Importantly, despite quantitative shortfalls, our models yet provide a solid base to qualitatively explain the origin of the fluorescence of the CDs.

2.4.5. Interpretation of the CDs sensing ability

The identification of charge-transfer processes between well-defined and spatially separated functional groups as origin of the fluorescence in polymer CDs now provides a powerful toolbox towards an improved understanding of their use in technological applications. This is demonstrated at hand of studies on the sensing of metal ions in aqueous solutions. To this end, the fluorescence of an aqueous solution of **CDs3** (0.4 mg/mL) was measured in the presence of several types of metal ions at a concentration of 1mM. A high affinity (i.e. high quenching rate) towards Fe^{3+}, Cu^{2+}, and Hg^{2+}, and other types of metal ions to a lower content is observed (Figure 2.15). Similar results were obtained for **CDs1** and **CDs2**, which are also in agreement with those observed for CDs of unknown chemical structure.[58-60] These findings

clearly confirm that the high sensitivity can be ascribed to the common chemical structure of polymer CDs. In fact, the same groups identified to be involved in the charge transfer process can act also as chelating agents, in a similar way to EDA, EDTA and citrate. Carboxylic acids, amides and amines are therefore interacting strongly with the metal ions and the binding provides favorable non-radiative relaxation pathways, which compete with the intramolecular charge-transfer process and drastically reduce the photoluminescence emission. This study not only proves the existence of photoinduced charge-transfer processes between spatially separated amide and carboxylic moieties in polymer CDs, but also explains how to successfully exploit this mechanism in other types of applications of technological relevance.

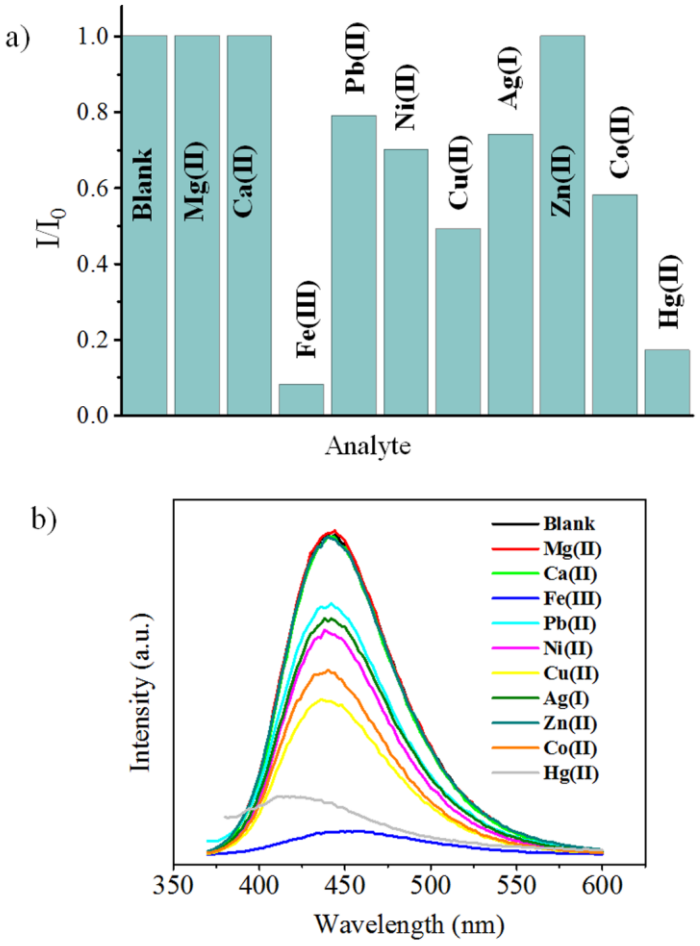

Figure 2.15. (a) Relative fluorescence intensity of CDs3 where I and Io are the intensities in presence and absence of the metal ions. (b) Emission spectra of a CDs3 water solution in the presence of 1mM concentration of Mg^{2+}, Ca^{2+}, Fe^{3+}, Pb^{2+}, Ni^{2+}, Cu^{2+}, Ag^{2+}, Zn^{2+}, Co^{2+}, Hg^{2+}.

2.5. Conclusion

The synthesis of blue fluorescent model polymer CDs was obtained from CA and EDA as well as from TA and EDA by microwave irradiation, and from CA and EDA by a novel coupling agent-mediated condensation at room temperature. The optical features of the three types of model CDs of 1 – 1.5 nm in size are remarkably similar, suggesting that the copolymerization of the reagents by amide bond is a sufficient condition for the formation of the fluorophore in polymer CDs. This hypothesis was further confirmed by a detailed structural characterization of the materials, which revealed that the presence of H-bonds and electrostatic interactions goes along with the high conformational rigidity of the polymeric chain. DFT and TDDFT calculations of the octamer of this structure indeed show that supramolecular H-bond mediated interactions cause the rigid entanglement of the chains, hindering vibration and rotation, and facilitate the radiative relaxation process. Finally, the amide and the carboxylic groups are recognized as the moieties, which respectively provide the main contribution to the HOMO and the LUMO molecular orbitals. Photoinduced charge-transfer between these spatially separated groups, assisted by H-bond mediated supramolecular interactions in the entangled polyamide network therefore is identified as origin of the fluorescence phenomena in polymer carbon dots.

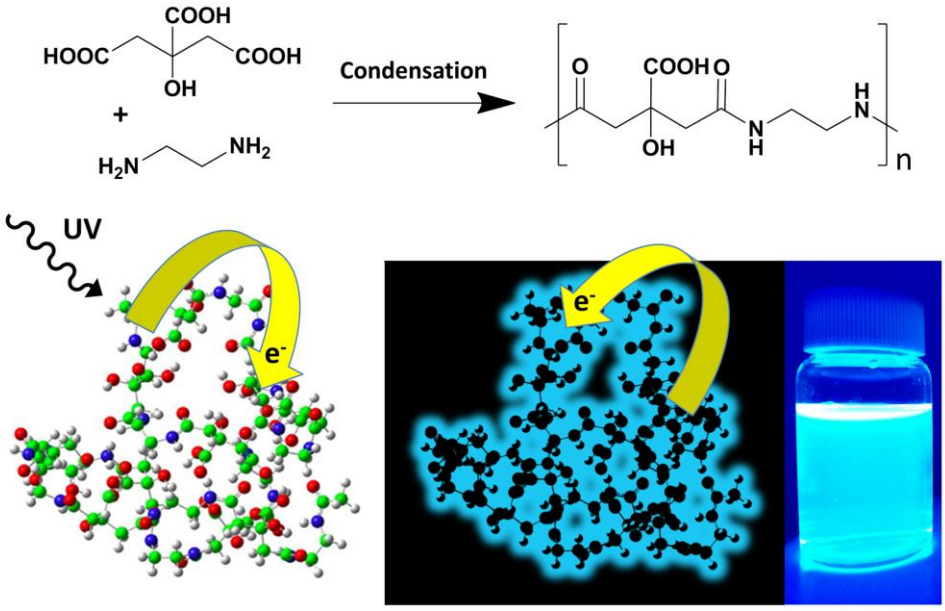

Figure 2.16. Illustration of the CDs formation and of the photo-induced charge transfer phenomenon.

It is proposed that this single emitter type process provides a universal explanation for the CDs' blue fluorescence observed in the vast and increasing amount of reports where these

nanoparticles are prepared from carboxylic acids and amines. However, this process becomes masked by the contribution of additional fluorescent emitters, typically obtained when employing harsher conditions, resulting in an excitation dependent emission behavior. Additionally these findings explain the performance of polymer CDs in existing technological applications. Moreover, it paves the way to exploit novel synthetic bottom-up routes to obtain polymer CDs with tailored properties uncovering yet unexploited opportunities.

2.6. References

1. Song, Y.; Zhu, S.; Zhang, S.; Fu, Y.; Wang, L.; Zhao, X.; Yang, B., Investigation from chemical structure to photoluminescent mechanism: a type of carbon dots from the pyrolysis of citric acid and an amine. *Journal of Materials Chemistry C* **2015,** *3* (23), 5976-5984.
2. Zhu, S.; Zhao, X.; Song, Y.; Lu, S.; Yang, B., Beyond bottom-up carbon nanodots: Citric-acid derived organic molecules. *Nano Today* **2016,** *11* (2), 128-132.
3. Dhenadhayalan, N.; Lin, K.-C.; Suresh, R.; Ramamurthy, P., Unravelling the Multiple Emissive States in Citric-Acid-Derived Carbon Dots. *The Journal of Physical Chemistry C* **2016,** *120* (2), 1252-1261.
4. Schneider, J.; Reckmeier, C. J.; Xiong, Y.; von Seckendorff, M.; Susha, A. S.; Kasák, P.; Rogach, A. L., Molecular Fluorescence in Citric Acid-Based Carbon Dots. *The Journal of Physical Chemistry C* **2017,** *121* (3), 2014-2022.
5. Shi, L.; Yang, J. H.; Zeng, H. B.; Chen, Y. M.; Yang, S. C.; Wu, C.; Zeng, H.; Yoshihito, O.; Zhang, Q., Carbon dots with high fluorescence quantum yield: the fluorescence originates from organic fluorophores. *Nanoscale* **2016,** *8* (30), 14374-14378.
6. Fang, Q.; Dong, Y.; Chen, Y.; Lu, C.-H.; Chi, Y.; Yang, H.-H.; Yu, T., Luminescence origin of carbon based dots obtained from citric acid and amino group-containing molecules. *Carbon* **2017,** *118*, 319-326.
7. Ehrat, F.; Bhattacharyya, S.; Schneider, J.; Löf, A.; Wyrwich, R.; Rogach, A. L.; Stolarczyk, J. K.; Urban, A. S.; Feldmann, J., Tracking the Source of Carbon Dot Photoluminescence: Aromatic Domains versus Molecular Fluorophores. *Nano Letters* **2017,** *17* (12), 7710-7716.
8. Zhu, S.; Song, Y.; Zhao, X.; Shao, J.; Zhang, J.; Yang, B., The photoluminescence mechanism in carbon dots (graphene quantum dots, carbon nanodots, and polymer dots): current state and future perspective. *Nano Research* **2015,** *8* (2), 355-381.
9. Zhu, S.; Song, Y.; Shao, J.; Zhao, X.; Yang, B., Non-Conjugated Polymer Dots with Crosslink-Enhanced Emission in the Absence of Fluorophore Units. *Angewandte Chemie International Edition* **2015,** *54* (49), 14626-14637.
10. Zhao, E.; Lam, J. W. Y.; Meng, L.; Hong, Y.; Deng, H.; Bai, G.; Huang, X.; Hao, J.; Tang, B. Z., Poly[(maleic anhydride)-alt-(vinyl acetate)]: A Pure Oxygenic Nonconjugated Macromolecule with Strong Light Emission and Solvatochromic Effect. *Macromolecules* **2015,** *48* (1), 64-71.
11. Qiao, Z. A.; Huo, Q.; Chi, M.; Veith, G. M.; Binder, A. J.; Dai, S., A "ship-in-a-bottle" approach to synthesis of polymer dots@silica or polymer dots@carbon core-shell nanospheres. *Adv Mater* **2012,** *24* (45), 6017-21.
12. Tao, S.; Song, Y.; Zhu, S.; Shao, J.; Yang, B., A new type of polymer carbon dots with high quantum yield: From synthesis to investigation on fluorescence mechanism. *Polymer*.

13. Tao, S.; Lu, S.; Geng, Y.; Zhu, S.; Redfern, S. A. T.; Song, Y.; Feng, T.; Xu, W.; Yang, B., Design of Metal-Free Polymer Carbon Dots: A New Class of Room-Temperature Phosphorescent Materials. *Angewandte Chemie International Edition* **2018,** *57* (9), 2393-2398.
14. Xiao, Q.; Liang, Y.; Zhu, F.; Lu, S.; Huang, S., Microwave-assisted one-pot synthesis of highly luminescent N-doped carbon dots for cellular imaging and multi-ion probing. *Microchimica Acta* **2017,** *184* (7), 2429-2438.
15. Gao, F.; Ma, S.; Li, J.; Dai, K.; Xiao, X.; Zhao, D.; Gong, W., Rational design of high quality citric acid-derived carbon dots by selecting efficient chemical structure motifs. *Carbon* **2017,** *112*, 131-141.
16. Zhang, Y.; Wang, Y.; Feng, X.; Zhang, F.; Yang, Y.; Liu, X., Effect of reaction temperature on structure and fluorescence properties of nitrogen-doped carbon dots. *Applied Surface Science* **2016,** *387*, 1236-1246.
17. Xu, Z.-Q.; Lan, J.-Y.; Jin, J.-C.; Dong, P.; Jiang, F.-L.; Liu, Y., Highly Photoluminescent Nitrogen-Doped Carbon Nanodots and Their Protective Effects against Oxidative Stress on Cells. *ACS Applied Materials & Interfaces* **2015,** *7* (51), 28346-28352.
18. He, J.; Zhang, H.; Zou, J.; Liu, Y.; Zhuang, J.; Xiao, Y.; Lei, B., Carbon dots-based fluorescent probe for "off-on" sensing of Hg(II) and I−. *Biosensors and Bioelectronics* **2016,** *79*, 531-535.
19. Ogi, T.; Aishima, K.; Permatasari, F. A.; Iskandar, F.; Tanabe, E.; Okuyama, K., Kinetics of nitrogen-doped carbon dot formation via hydrothermal synthesis. *New Journal of Chemistry* **2016,** *40* (6), 5555-5561.
20. Zhang, F.; Feng, X.; Zhang, Y.; Yan, L.; Yang, Y.; Liu, X., Photoluminescent carbon quantum dots as a directly film-forming phosphor towards white LEDs. *Nanoscale* **2016,** *8* (16), 8618-8632.
21. Rong, M.; Feng, Y.; Wang, Y.; Chen, X., One-pot solid phase pyrolysis synthesis of nitrogen-doped carbon dots for Fe3+ sensing and bioimaging. *Sensors and Actuators B: Chemical* **2017,** *245*, 868-874.
22. Bhattacharyya, S.; Ehrat, F.; Urban, P.; Teves, R.; Wyrwich, R.; Döblinger, M.; Feldmann, J.; Urban, A. S.; Stolarczyk, J. K., Effect of nitrogen atom positioning on the trade-off between emissive and photocatalytic properties of carbon dots. *Nature Communications* **2017,** *8* (1), 1401.
23. Bagheri, Z.; Ehtesabi, H.; Rahmandoust, M.; Ahadian, M. M.; Hallaji, Z.; Eskandari, F.; Jokar, E., New Insight into the Concept of Carbonization Degree in Synthesis of Carbon Dots to Achieve Facile Smartphone Based Sensing Platform. *Scientific Reports* **2017,** *7* (1), 11013.
24. Tong, G.; Wang, J.; Wang, R.; Guo, X.; He, L.; Qiu, F.; Wang, G.; Zhu, B.; Zhu, X.; Liu, T., Amorphous carbon dots with high two-photon fluorescence for cellular imaging passivated by hyperbranched poly(amino amine). *Journal of Materials Chemistry B* **2015,** *3* (4), 700-706.
25. Liu, Y.; Zhou, L.; Li, Y.; Deng, R.; Zhang, H., Facile synthesis of nitrogen-doped carbon dots with robust fluorescence in a strongly alkaline solution and a reversible fluorescence 'off-on' switch between strongly acidic and alkaline solutions. *RSC Advances* **2016,** *6* (110), 108203-108208.
26. Yang, M.; Li, B.; Zhong, K.; Lu, Y., Photoluminescence properties of N-doped carbon dots prepared in different solvents and applications in pH sensing. *Journal of Materials Science* **2018,** *53* (4), 2424-2433.
27. Zhang, W.; Shi, L.; Liu, Y.; Meng, X.; Xu, H.; Xu, Y.; Liu, B.; Fang, X.; Li, H.-B.; Ding, T., Supramolecular interactions via hydrogen bonding contributing to citric-acid

derived carbon dots with high quantum yield and sensitive photoluminescence. *RSC Advances* **2017,** *7* (33), 20345-20353.
28. Hu, Y.; Yang, J.; Tian, J.; Yu, J.-S., How do nitrogen-doped carbon dots generate from molecular precursors? An investigation of the formation mechanism and a solution-based large-scale synthesis. *Journal of Materials Chemistry B* **2015,** *3* (27), 5608-5614.
29. Wang, J.; Zhang, P.; Huang, C.; Liu, G.; Leung, K. C.-F.; Wáng, Y. X. J., High Performance Photoluminescent Carbon Dots for In Vitro and In Vivo Bioimaging: Effect of Nitrogen Doping Ratios. *Langmuir* **2015,** *31* (29), 8063-8073.
30. Sharma, A.; Gadly, T.; Neogy, S.; Ghosh, S. K.; Kumbhakar, M., Molecular Origin and Self-Assembly of Fluorescent Carbon Nanodots in Polar Solvents. *The Journal of Physical Chemistry Letters* **2017,** *8* (5), 1044-1052.
31. Zhang, Y.; Liu, X.; Fan, Y.; Guo, X.; Zhou, L.; Lv, Y.; Lin, J., One-step microwave synthesis of N-doped hydroxyl-functionalized carbon dots with ultra-high fluorescence quantum yields. *Nanoscale* **2016,** *8* (33), 15281-15287.
32. Kundu, A.; Lee, J.; Park, B.; Ray, C.; Sankar, K. V.; Kim, W. S.; Lee, S. H.; Cho, I.-J.; Jun, S. C., Facile approach to synthesize highly fluorescent multicolor emissive carbon dots via surface functionalization for cellular imaging. *Journal of Colloid and Interface Science* **2018,** *513*, 505-514.
33. Wang, J.; Li, Q.; Zhou, J.; Wang, Y.; Yu, L.; Peng, H.; Zhu, J., Synthesis, characterization and cells and tissues imaging of carbon quantum dots. *Optical Materials* **2017,** *72*, 15-19.
34. Myshakina, N. S.; Ahmed, Z.; Asher, S. A., Dependence of Amide Vibrations on Hydrogen Bonding. *The Journal of Physical Chemistry B* **2008,** *112* (38), 11873-11877.
35. Barth, A., Infrared spectroscopy of proteins. *Biochimica et Biophysica Acta (BBA) - Bioenergetics* **2007,** *1767* (9), 1073-1101.

3. A VERSATILE METHOD FOR THE CONTROLLABLE ROOM-TEMPERATURE SYNTHESIS AND IN-SITU FUNCTIONALIZATION OF FLUORESCENT CARBON DOTS

3.1. Abstract

Carbon dots' (CDs) suitability for analytical and medical applications critically depends on their chemical structure and functional groups. Gaining control on these key issues remains a major challenge for synthesis routes employed today. The here proposed method offers a versatile pathway toward the rational design of a wide variety of polymeric fluorescent carbon dots with well-defined structures by exploiting the room-temperature carbodiimide-mediated condensation between citric acid and amines. Moreover, the quenching step of the polymerization process furnishes a unique opportunity for the introduction of any desired moiety onto the surface of the CDs, thus enabling the *in-situ* functionalization of this important family of nanoparticles.

3.2. Introduction

The choice of the precursors is defining the CDs chemical properties and is therefore crucial in view of specific applications. For example, for drug delivery particular functional groups are desirable for the conjugation of biomolecules on the CDs surface. Furthermore, the CDs ability for sensing and biosensing depends largely from the sensitivity and the specificity of the chemical interaction between the nanoparticle and the analyte[1]. Also solubility, biocompatibility and fluorescence intensity are important factors that in principle could be adjusted by the selection of the CDs precursors. Nevertheless, the rational tuning of all these properties is still at his infant phase, being largely undermined by the unpredictability of the CDs chemical structure under the harsh conditions that are generally employed during the synthesis. In fact, high temperature brings to the formation of numerous and heterogeneous structures, whose chemical nature can be hardly scrutinized. To overcome this problem and achieve better control on the CDs properties, it is frequently necessary to apply further chemical modifications, involving covalent and non-covalent strategies[1]. Among these, modifications via amide coupling reaction are certainly the most common[2-12]: in here, carboxylic acid or amine groups located on the CDs surface are exploited for the functionalization through amide bond formation, employing a standard EDC/NHS protocol for the carboxylic acid activation. In this way, a large number of molecules, including biomolecules, peptides, antibodies and dyes were conjugated on the CDs, making them suitable for sensing and medical application. However these modifications require at least one more synthesis step and extra purification procedures.

In this work, it is proposed a simple and effective method for the synthesis and the *in situ* functionalization of highly fluorescent polymer CDs. Knowing from our recent studies[13] that fluorescent polymer structures can be synthetized by polycondensation between citric acid and ethylenediamine, here, we expand and demonstrate the clear versatility of the new synthetic route: the employment of a coupling agent drives the reaction at room temperature conditions and allows working with a wide number of different amines. The resulting CDs structure is thus finely programmed by the reagents choice. Moreover the *in situ* functionalization of the nanoparticles is easily obtained by adding in the reaction any nucleophilic amine, which acts as quencher and at the same time introduce the moiety desired for further applications.

3.3.Experimental section

3.3.1. Materials

N,N′-Diisopropylcarbodiimide (≥98%) (DIC), N-(3-Dimethylaminopropyl)-N'-ethylcarbodiimide hydrochloride (≥99%) (EDC), O-(7-Azabenzotriazol-1-yl)-N,N,N',N'-tetramethyluronium hexafluorophosphate (99%) (HATU), Thionyl chloride (97%) ($SOCl_2$), Citric acid anhydrous (≥99.5%) (CA), ethylendiamine (99+%) (EDA), diethylenetriamine(≥99%), triethylenetetramine(≥97%), tris(2-aminoethyl)amine (96%), *o*-phenylenediamine (≥99%), *m*-phenylenediamine (99%), *p*-phenylenediamine (99%), n-butylamine (≥99%), N,N-Diethylethylenediamine (≥99%), aniline (≥99.5%), cysteamine (95%), N-Boc-ethylenediamine (≥98%), were used without further purifications. Dialysis tubes with molecular weight cut-off (MWCO) 0.5-1 KDa were bought from Spectrum Labs.

3.3.2. Characterization techniques

- Atomic force microscopy (AFM) images were acquired in air under ambient conditions using a NT-MDT Aura NTEGRA instrument operating in tapping mode at 110 kHz resonance with Au tips HA_NC ETALON (10nm curvature radius). Samples were prepared on silica substrates by drop casting of diluite water solutions and dried at 50 ^{o}C. Particle height distribution analysis was carried out by using the Gwyddion software.

- Elemental analyses were performed in a Thermo Flash EA 1112 instrument with ~3 mg of powder samples. Infrared absorption measurements were performed on powder samples pressed with KBr into pellets with a Bruker Vertex 70 spectrometer.
- ^{1}H and ^{13}C NMR spectra were recorded in D_2O solutions at 25 ^{o}C on a Bruker AV500 spectrometer (δ in ppm and J in Hz) at a ^{1}H NMR operating frequency of 500.13 MHz. ^{1}H and ^{13}C NMR spectra were referenced using the solvent signal as an internal standard. The assignment of the ^{1}H NMR signals and the corresponding ^{13}C NMR peaks was carried out using standard $^{1}H–^{13}C$ edited-HSQC and $^{1}H–^{13}C$ HMBC (J_{HC} = 8 Hz) 2D-experiments. The determination of the diffusion coefficients D (m^2/s) was performed at controlled temperature (300 K) in spinning solutions of the corresponding compounds in D_2O (concentrations about 2 mM). The values of delta (δ) and delta (Δ) were optimized for each sample. In the case of δ the values found were in the range 1.7-2.0 ms, while for Δ the optimized values ranged from 0.17-0.20 s.
- UV/Vis absorption spectra were recorded on a Shimadzu UV-2401 PC spectrophotometer. Photoluminescence excitation and emission spectra were recorded on a Horiba Jobin Yvon Fluoromax-P, slits of excitation and emission at 1 mm. All the spectra were recorded at room temperature using 10 mm path-length quartz cuvette.

3.4. Results and discussion

The fluorescence emission in polymer CDs is the effect of the rigid environment in which organic groups such as carboxylic acids, amines and amides are found inside the polymer structure. Hydrogen bonds and electrostatic interactions play a fundamental role in determining the entanglement and the conformations that promote the photo-induced radiative emission with respect to other types of non-radiative relaxation[13-14]. Taking into account these premises, the here reported experiments aim to synthetize well-defined CDs, whose chemical structures can be rationally predicted by the choice of the reagents. Among the possible polyacids, citric acid was chosen as common precursor because of its ubiquity in CDs literature. Thus, the polycondensation between citric acid (CA) and ethylenediamine (EDA) in ratio 1:1 was performed through four different methods at room temperature, involving the carboxylic acid activation with a) N,N'-diisopropylcarbodiimide (DIC), b) N-(3-Dimethylaminopropyl)-N′-ethylcarbodiimide hydrochloride (EDC), c)

hexafluorophosphate azabenzotriazole tetramethyl uronium (HATU) and the acyl chloride formation with d) thionyl chloride (Scheme 3.1, for the procedures see Annex C). Purification was easily achieved by washing with organic solvent, filtration and dialysis. In the case of the reactions a), b) and c), the final addition of NaOH is necessary to restore the carboxylic acids from the activated form, quenching the growth of the nanoparticles and stopping the reaction.

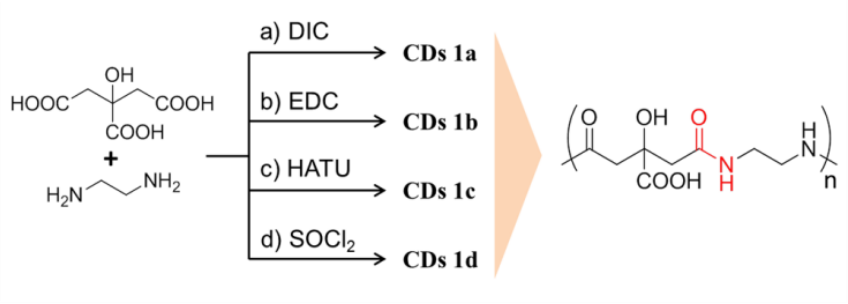

Scheme 3.1. Polycondensation of CA and EDA through four synthetic pathways, for the obtaining of CDs 1a-d.

CDs 1a-d were characterized by atomic force microscopy (AFM, Figure 9.3) and diffusion ordered spectroscopy (DOSY, Figure 9.4 and Table 9.1). According to both techniques, all the samples consist of nanoparticles of size comprised between 1 and 2 nm. The structural characterization of **CDs 1a-1d** was performed by means of elemental analysis, infrared (IR) and nuclear magnetic resonance (NMR) spectroscopy. Elemental analysis shows similar ratios of C, H, N and O in the four compounds consistent with the formula $C_8H_{12}N_2O_5$, indicating that a stoichiometric copolymer is formed by condensation of CA and EDA in a 1:1 molar ratio (Table 9.2 and Figure 9.5). IR bands position is the same for **CDs 1a-1d**, and reveals the presence of alcohols, amines, carboxylic acids and amides (Figures 9.6-9.9). Finally, proton (^{1}H) and carbon (^{13}C, APT: attached proton test) NMR experiments, as well as two-dimensional correlation experiments ^{1}H-^{13}C HSQC (heteronuclear single-quantum coherence) and ^{1}H-^{13}C HMBC (heteronuclear multiple-bond correlation) furnished the decisive information for the understanding of the chemical structure and connectivity (Figures 9.10-9.25). The high degree of spectral resemblance merits a more detailed discussion. The absence of signals in the aromatic part of the proton and carbon spectra indicates that the polymer structure is completely non-conjugated. In fact, all the protons are methylenes and they are found between 3.9 and 2.3 ppm, matching with the presence of the polymerized CA and EDA –CH_2-. The other two sets of ^{13}C signals correspond to the quaternary carbon of CA (76-72 ppm) and the carboxylic acids and amides carbon (181-170 ppm), which in fact couple

with the methylenes in the ^{1}H-^{13}C HMBC spectra but not in the ^{1}H-^{13}C HSQC spectra. Gathering all these structural information, it appears clear that all the four methods employed accomplished the synthesis of polymer nanoparticles whose structure consists of the condensation products between CA carboxylic acids and EDA amines. In spite of the structural similarity, an investigation of the **CDs 1a-1d** optical properties showed that the fluorescence intensity depends considerably on the synthetic method. UV/Vis spectra of **CDs 1a**, **CDs 1b** and **CDs 1d** present an absorption band at 340 nm, while for **CDs 1c** the same feature has its maximum at 310 nm (Figure 3.1a). Probably in **CDs 1c** the shift is not real, due to the fact that the considered absorption band is very small with respect to the absorption of the C=O groups at <300 nm. The emitting behavior of the four samples shows indeed a correlation with the quantum yield (QY). In **CDs 1a** (QY=17.7%) and **1b** (QY=8.6%) the emission takes place around 445 nm and is approximately independent from the excitation, while in **CDs 1c** and **1d** the QY is remarkably lower (respectively 2.2% and 4.0%) and the emission is excitation-dependent (Figure 3.1b). These observations suggest that the main contribution to the fluorescence intensity is independent from the excitation. Additionally some effects produce the excitation dependency in all the samples. However, their influence only becomes noticeable when the main absorption contribution is weak, as in the case of **CDs 1c** and **1d**. The excitation dependency in these cases could be ascribed to heterogeneity of the emitting centers, possibly due to crosslinking or aggregation effects[14].

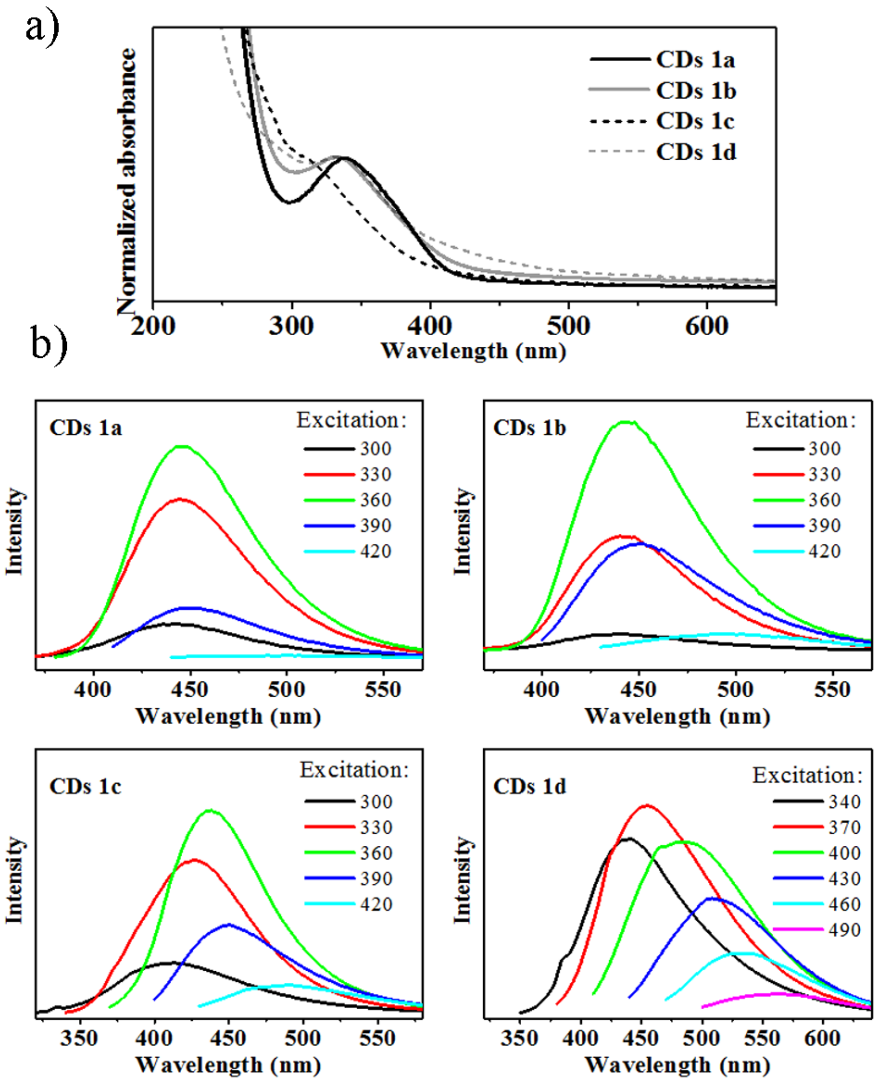

Figure 3.1. a) absorption spectra of CDs 1a-d. b) emission of CDs 1a-d for different excitation wavelengths.

Once attested that the DIC- and EDC-mediated condensation are, among the methods considered, the most effective for the synthesis of highly fluorescent nanoparticles from CA and EDA, the same procedure was tested employing different aliphatic and aromatic polyamines in the place of EDA, again in a ratio 1:1 with respect to CA. In this way the synthesis of **CDs 2a-f** was accomplished (Scheme 3.2, Table 3.1).

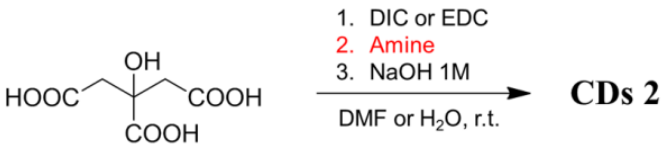

Scheme 3.2. Synthesis of CDs 2a-f.

Table 3.1. amines employed for the polycondensation, emission maximum, QY and pictures (in water, UV light off and on) of CDs 2a-f.

Sample	Amine	Emission maximum (nm)	QY (%)	Picture (0.3 mg/ml)
2a	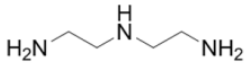	443	24.5	
2b	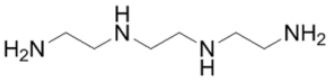	435	7.3	
2c	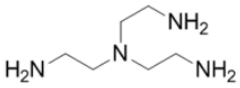	452	4.7	
2d	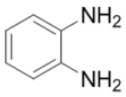	433	3.9	
2e	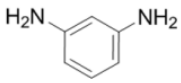	440	1.6	
2f	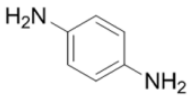	440	0.8	

The as-produced materials **CDs 2a-f** were characterized by AFM (Figure 9.32) and DOSY (Figure 9.33 and Table 9.3). Accordingly to both techniques, all the samples consist of nanoparticles of size comprised between 1.0 and 2.5 nm, with the exception of **CDs 2c**, which shows a size of around 2 nm by AFM, but of 4.8 nm by DOSY. The as-produced materials were characterized by elemental analysis, IR and NMR spectroscopy. Also for **CDs 2a-c**, the C, H, N and O percentages strongly suggest that the formed copolymers are made of a ratio 1:1 between CA and the employed amine (Tables 9.4-9.6 and Figures 9.34-9.36), while this stoichiometry is not respected for **CDs 2d-f**, presumably due to the lower and co-dependent reactivity of the aromatic di-amines (Table 9.7 and Figure 9.37), but also to the presence of unknown impurities (Figures 9.56, 9.60, 9.64). IR spectra (Figures 9.38-9.43) show C=O

stretching for carboxylic acids and amides, as previously observed for **CDs 1a-d**. Moreover **CDs 2d-f** present the typical aromatic C=C stretching between 1516-1497 cm^{-1} (Figures 9.41-9.43). Finally, ^{1}H, ^{13}C APT, ^{1}H-^{13}C HSQC and ^{1}H-^{13}C HMBC experiments confirmed the copolymer connectivity via amide as the results of the condensation between citric acid and the respective amine (Figures 9.44-9.67). For **CDs 2d-f** are also well visible the aromatic signals, between 7.5-6.5 ppm in the proton spectra and 147-109 ppm in the carbon spectra. The fact that the results of the structural characterization conclusively confirm the expected polyamide structures emphasizes the versatility of our synthetic procedure. Concerning the optical properties of **CDs 2a-f**, it can be observed that the emission wavelength does not change consistently with the amine employed and it is found between 433 and 452 nm depending on the sample (Figures 9.69-9.74). On the other hand the QY of **CDs 2a-c**, with aliphatic amines, is higher than in **CDs 2d-f**, with aromatic amines (Table 3.1). It is reasonable to say that the polymer conformation responsible for the radiative decay can be hampered by the locked configuration of the amines in *o*-, *m*- or *p*- position. Among these, *o*-position could be the most favorable, resembling one of the EDA conformations, and in fact **CDs 2d** QY is higher than **CDs 2e** QY, which in turn is higher than the one of **CDs 2f**, whose substituents do not allow the compact folding needed for the formation of the fluorophore.

The finding that the polycondensation catalyzed by carbodiimides can be successfully exploited for the synthesis of different fluorescent nanoparticles as a function of the type of amine group employed, allowing thus the control on the final chemical structure, provided a unique opportunity to perform an additional study testing the possibility to functionalize *in-situ* the as-produced materials. Since the growth of the nanoparticles is mediated by the activation of the carboxylic acids via coupling agents, it can be interrupted at any moment adding an excess of a strong nucleophile. In the previous experiments, NaOH was used to restore the carboxylic acids and quench the polymerization. Nevertheless, primary amines are equally good candidates for this purpose. Moreover, the employment of an amine offers the possibility to attach onto the surface of the CDs virtually any moiety that is stable and soluble in the reaction medium. The *in-situ* functionalization was tested by the addition of five different primary amines during the polycondensation reaction between CA and EDA mediated by DIC (Scheme 3.3, Table 3.2).

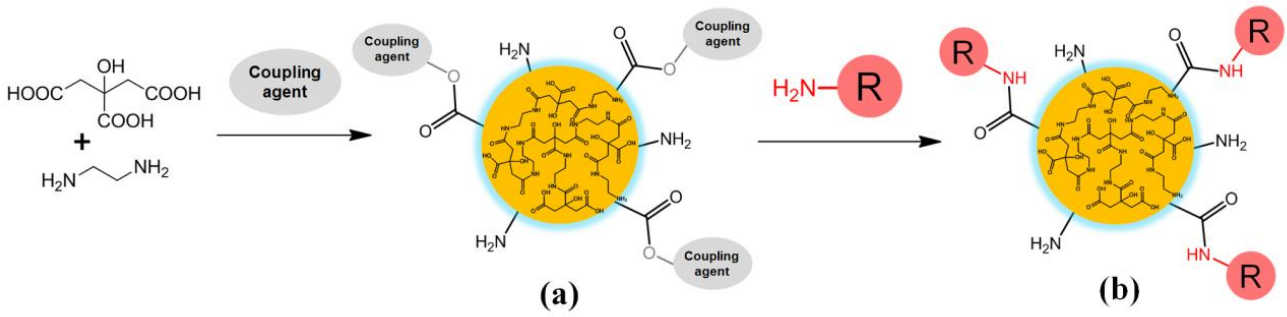

Scheme 3.3. a) polycondensation of CA and EDA mediated by coupling agent. b) the addition of a primary amine consumes the activated carboxylic acids and stops the polymerization.

Table 3.2. amine employed for the functionalization, emission maximum, QY and pictures (in water, UV light off and on) of CDs 3a-e.

Sample	H_2N–R	Emission maximum (nm)	QY (%)	Picture (0.3 mg/ml)
3a	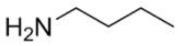	445	8.6	
3b	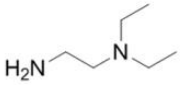	445	8.4	
3c	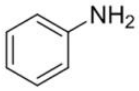	434	5.8	
3d	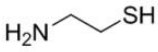	433	25.2	
3e	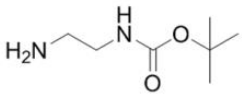	430	4.7	

Similarly to **CDs 1a-d**, **CDs 3a-e** reveal sizes between 1.0-2.6 nm, as probed by AFM (Figure 9.76) and DOSY (Figure 9.77, Table 9.8). The structural characterization proved the effective functionalization. Elemental analysis shows that the functionalized materials **CDs 3a-e** present lower molar percentages of oxygen compared to **CDs 1a**, as a consequence of the successful functionalization (Table 9.9 and Figure 9.78). In parallel, in the infrared spectra of **CDs 3a-3d** (Figures 9.79-9.83) the carboxylic acid C=O stretching at 1704 cm^{-1} is weaker than in **CDs 1a** or not visible, due to the consumption of the majority of the carboxyl groups by means of the functionalization. In **CDs 3e** this effect is not appreciable because of the

presence of the carbamate C=O stretching band, which is found at similar wavenumbers of the carboxylic one. Additionally it is observed in **CDs 3c** the C=C stretching at 1545 cm^{-1} due to the aromatic ring. ^{1}H, ^{13}C APT, ^{1}H-^{13}C HSQC and ^{1}H-^{13}C HMBC experiments confirmed the introduction on **CDs 3a-3e** of the corresponding functionalities (Figures 9.84-9.103). The performed structural modifications only slightly affect the absorption (Figure 9.104) and emission maximum position (Figures 9.105-9.109), meaning that they are not directly involved in the fluorescence mechanism. However different QY are obtained depending on the functionalization. Rigid and bulky groups, such as in **CDs 2c** and **3d**, decrease the fluorescence intensity. In contrast, the QY benefits from the thiol functionalization, possibly due to its involvement in the H-bond interactions that play a role in the formation of the polymer conformation needed for the obtaining of the fluorescent behavior.

3.5. Conclusion

In summary, we illustrated the versatility of a novel approach for the synthesis of fluorescent CDs, consisting in the coupling agent-mediated condensation between citric acid and amines at room temperature. This strategy enables the synthesis of a wide variety of polymeric nanoparticles whose chemical structure is determined only by the choice of the reagents. Furthermore, the method allows the *in-situ* functionalization of the CDs, supplying an additional level of control on the final chemical structure and avoiding further functionalization steps otherwise needed for many applications. Therefore this method provides an easy and efficient pathway for controlling the structure and the chemical properties of the polymer nanoparticles, furnishing an extremely versatile tool for the design of CDs-based material such as sensors and drug nanocarriers.

3.6.References

1. Yan, F.; Jiang, Y.; Sun, X.; Bai, Z.; Zhang, Y.; Zhou, X., Surface modification and chemical functionalization of carbon dots: a review. *Microchimica Acta* **2018,** *185* (9), 424.
2. Fu, C.; Qian, K.; Fu, A., Arginine-modified carbon dots probe for live cell imaging and sensing by increasing cellular uptake efficiency. *Materials Science and Engineering: C* **2017,** *76*, 350-355.
3. Chai, L.; Zhou, J.; Feng, H.; Tang, C.; Huang, Y.; Qian, Z., Functionalized Carbon Quantum Dots with Dopamine for Tyrosinase Activity Monitoring and Inhibitor Screening: In Vitro and Intracellular Investigation. *ACS Applied Materials & Interfaces* **2015,** *7* (42), 23564-23574.

4. Zhong, D.; Zhuo, Y.; Feng, Y.; Yang, X., Employing carbon dots modified with vancomycin for assaying Gram-positive bacteria like Staphylococcus aureus. *Biosensors and Bioelectronics* **2015,** *74*, 546-553.
5. Krishna, A. S.; Radhakumary, C.; Antony, M.; Sreenivasan, K., Functionalized carbon dots enable simultaneous bone crack detection and drug deposition. *Journal of Materials Chemistry B* **2014,** *2* (48), 8626-8632.
6. Zhang, J.; Zhao, X.; Xian, M.; Dong, C.; Shuang, S., Folic acid-conjugated green luminescent carbon dots as a nanoprobe for identifying folate receptor-positive cancer cells. *Talanta* **2018,** *183*, 39-47.
7. Yang, L.; Wang, Z.; Wang, J.; Jiang, W.; Jiang, X.; Bai, Z.; He, Y.; Jiang, J.; Wang, D.; Yang, L., Doxorubicin conjugated functionalizable carbon dots for nucleus targeted delivery and enhanced therapeutic efficacy. *Nanoscale* **2016,** *8* (12), 6801-6809.
8. Yang, R.; Guo, X.; Jia, L.; Zhang, Y., A fluorescent "on-off-on" assay for selective recognition of Cu(II) and glutathione based on modified carbon nanodots, and its application to cellular imaging. *Microchimica Acta* **2017,** *184* (4), 1143-1150.
9. Chen, J.; Li, Y.; Lv, K.; Zhong, W.; Wang, H.; Wu, Z.; Yi, P.; Jiang, J., Cyclam-functionalized carbon dots sensor for sensitive and selective detection of copper(II) ion and sulfide anion in aqueous media and its imaging in live cells. *Sensors and Actuators B: Chemical* **2016,** *224*, 298-306.
10. Luo, M.; Hua, Y.; Liang, Y.; Han, J.; Liu, D.; Zhao, W.; Wang, P., Synthesis of novel β-cyclodextrin functionalized S, N codoped carbon dots for selective detection of testosterone. *Biosensors and Bioelectronics* **2017,** *98*, 195-201.
11. Mohammadi, S.; Salimi, A.; Hamd-Ghadareh, S.; Fathi, F.; Soleimani, F., A FRET immunosensor for sensitive detection of CA 15-3 tumor marker in human serum sample and breast cancer cells using antibody functionalized luminescent carbon-dots and AuNPs-dendrimer aptamer as donor-acceptor pair. *Analytical Biochemistry* **2018,** *557*, 18-26.
12. Sun, Q.; Fang, S.; Fang, Y.; Qian, Z.; Feng, H., Fluorometric detection of cholesterol based on β-cyclodextrin functionalized carbon quantum dots via competitive host-guest recognition. *Talanta* **2017,** *167*, 513-519.
13. Vallan, L.; Urriolabeitia, E. P.; Ruipérez, F.; Matxain, J. M.; Canton-Vitoria, R.; Tagmatarchis, N.; Benito, A. M.; Maser, W. K., Supramolecular-Enhanced Charge Transfer within Entangled Polyamide Chains as the Origin of the Universal Blue Fluorescence of Polymer Carbon Dots. *Journal of the American Chemical Society* **2018**.
14. Feng, T.; Zhu, S.; Zeng, Q.; Lu, S.; Tao, S.; Liu, J.; Yang, B., Supramolecular Cross-Link-Regulated Emission and Related Applications in Polymer Carbon Dots. *ACS Applied Materials & Interfaces* **2018,** *10* (15), 12262-12277.

4. ELECTRONIC INTERACTIONS IN CDs/MoS_2 ELECTROSTATIC COMPLEX

4.1. Abstract

In this chapter, a study on the electronic interactions between carbon dots (CDs) and functionalized molybdenum disulfide (MoS_2) oligolayers is reported. For this purpose, a solution of negatively charged CDs obtained from the microwave irradiation of citric acid and ethylenediamine was titrated with ammonium-functionalized positively charged MoS_2, and the optical properties of the forming electrostatic complex were studied ongoing. Efficient fluorescence quenching of CDs by MoS_2 was observed and attributed to photoinduced electron/energy transfer as the decay mechanism for the transduction of the singlet excited state of CDs. Finally, the CD/MoS_2 complex was tested as catalyst towards the hydrogen evolution reaction and found to be superior to that of individual CDs species.

4.2. Introduction

MoS_2 is a member of the layered-transition metal dichalcogenides (TMDs), a group to which belong also tungsten disulfide (WS_2), tantalum(IV) sulfide (TaS_2), titanium disulfide (TiS_2), tungsten diselenide (WSe_2), molybdenum diselenide ($MoSe_2$), and many others.[1] These materials consist of pseudo-2D crystal layers held together by non-covalent interactions. The number of layers is directly related to the TMDs optical and electronic properties, which therefore can be tailored as a result of an exfoliation process of the bulk material. For example, bulk MoS_2 shows semi-conducting properties, having a band gap of 1.3 eV. Depending on the exfoliation process, oligolayered or monolayered MoS_2 can be obtained, and decreasing the number of layers the band gap increases, up to 1.8 eV for the single layered material. Furthermore, the width of the band gap is directly related to the optical properties of the TMDs: increasing the bandgap energy in MoS_2 results in changes in photoconductivity, absorption and photoluminescence. From bulk to monolayer, MoS_2 shows an increase of photoluminescence quantum yield by a factor of up to 10^4.[2] Clearly, the photoelectronic response of MoS_2 can be of great interest for the design of optoelectronic devices, such as photo-transistor[3], diodes[4], chemical sensors[5] and LEDs.[6] Moreover, the direct bandgap energy is located in the visible range, allowing the use of MoS_2 in solar cells and energy conversion.[7-9] However, just like many 2D materials, the processing of MoS_2 has some draw-backs. In fact, the MoS_2 single layers are hardly dispersible and once in solution they are not well stabilized by the solvent, thus they rapidly aggregate

and precipitite as a result of the energetically favorable stacking between layers. To overcome this problem, several approaches, both covalent and non-covalent functionalization with organic molecules, were explored. For example, the group of Tagmatarchis achieved the covalent bonding of 1,2-dithiolanes on the edges of semiconducting MoS_2 under mild conditions.[10] In here, dithiolanes are reacting with the MoS_2 edges, where the reactive sulphur vacancies are mostly found, thus preserving the basal plane optoelectronic properties. Furthermore, this method allows introducing charged organic groups, such as ammonium salts, on the MoS_2 layers, improving on one side the dispersibility in polar solvents and on the other side providing suitable moieties for the facile coupling with other photoactive materials via electrostatic interactions. In this way, hybrid systems with new optoelectronic properties can be easily prepared.

In this work, the photophysical and electrocatalytic properties of CDs/MoS_2 complexes are investigated. CDs bearing carboxylic acids were prepared by a standard microwave irradiation protocol from citric acid and ethylenediamine. Afterwards, the negatively charged carboxylate form was obtained by mild alkaline treatment. In parallel, positively charged MoS_2 monolayers were prepared in a two-steps procedure, involving first the covalent functionalization of exfoliated MoS_2 with 1,2-dithiolane tert-butyl carbamate and second its acidic deprotection yielding the positively charged ammonium salt. Next, the titration of the negative CDs with the positive MoS_2 was followed by UV/vis spectroscopy, steady-state and time-resolved photoluminescence spectroscopy, allowing to scrutinize the intraensemble electronic interactions between the two species. Finally, overpotentials and Tafel slopes were evaluated for the assessment of the electrocatalytic activity of CD/MoS_2 toward the hydrogen evolution reaction (HER).

4.3. Experimental section

4.3.1. Materials

Molybdenum disulfide powder (>99%), chlorosulfonic acid (99%), citric acid anhydrous (≥99.5%) and ethylendiamine (99+%) were used without further purifications. Dialysis tubes with molecular weight cut-off (MWCO) 0.5-1 KDa were bought from Spectrum Labs.

4.3.2. Characterization techniques

- Steady-state UV-Vis electronic absorption spectra were recorded on a PerkinElmer (Lambda 19) UV-Vis-NIR spectrophotometer.
- Steady-state emission spectra were recorded on a Fluorolog-3 JobinYvon-Spex spectrofluorometer (model GL3-21).
- Picosecond time-resolved fluorescence spectra were measured by the time-correlated-single-photon-counting (TCSPC) method on a Nano-Log spectrofluorometer (Horiba JobinYvon), by using a laser diode as an excitation source (NanoLED, 375 nm) and a UV-Vis detector TBX-PMT series (250-850 nm) by Horiba JobinYvon. Lifetimes were evaluated with the DAS6 Fluorescence-Decay Analysis Software.
- Mid-infrared spectra in the region 500−4500 cm^{-1} were obtained on a Fourier transform IR spectrometer (Equinox 55 from Bruker Optics) equipped with a single reflection diamond ATR accessory (DuraSamp1IR II by SensIR Technologies). A drop of the solution was placed on the diamond surface, followed by evaporation of the solvent, in a stream of nitrogen, before recording the spectrum. Typically, 100 scans were acquired at 2 cm^{-1} resolution.
- Micro-Raman scattering measurements were performed at room temperature in the backscattering geometry using a RENISHAW inVia Raman microscope equipped with a CCD camera and a Leica microscope. A 2400 lines mm^{-1} grating was used for all measurements, providing a spectral resolution of ± 1 cm^{-1}. As an excitation source the Ar^{+} laser (514 nm with less than 0,092 mW laser power) was used. Measurements were taken with 15 seconds of exposure times at varying numbers of accumulations. The laser spot was focused on the sample surface using a long working distance 50x objective. Raman spectra were collected on numerous spots on the sample and recorded with Peltier cooled CCD camera. The data were collected and analyzed with Renishaw Wire and Origin software.
- Thermogravimetric analysis was performed using a TGA Q500 V20.2 Build 27 instrument by TA in a nitrogen (purity >99.999%) inert atmosphere.
- The microwave-assisted reaction was performed in a CEM Discover SP reactor employed in open-batch modality.

- Atomic force microscopy (AFM) images were acquired in air under ambient conditions using a MultiMode AFM with NanoScope V controller (Bruker Nano Surfaces Division, Santa Barbara, CA) operating in tapping mode with Si tips Bruker AFM probe RTESPA PART MPP-11120-10. Samples were prepared on mica substrates. Particle height distribution analysis was carried out by using the Nanoscope Analysis Version 1.5 software (Veeco Ins).
- The DLS measurements were recorded on a Malvern Nano Zetasizer HT, on a 10 mm path-length plastic cuvette.
- ^{1}H NMR spectra were recorded in D_2O solutions at 25 ^{o}C on a Bruker AV500 spectrometer. Electrochemical measurements were carried out at room temperature in N_2-saturated 0.5 M H_2SO_4 in a standard three-compartment electrochemical cell using an EG&G Princeton Applied Research potensiostat/galvanostat (Model PARSTAT^{R} 2273A). As counter electrode, a platinum wire was used and as reference a $Hg/HgSO_4$ (0.5 M K_2SO_4) electrode was placed into Luggin capillary. The working electrode was a glassy carbon disk with geometric surface area of 0.071 cm^2. Linear sweep voltammetry measurements were conducted with a scan rate of 5 mV s^{-1}.

4.3.3. Synthesis of the materials and characterization

4.3.3.1. Synthesis of CDs^{-} 4

2.0 g of citric acid monohydrate (9.5 mmol) were dissolved in 16 mL of ultrapure water. Upon addition of 0.64 mL of ethylenediamine (9.5 mmol, 1 equiv.), the solution was heated up through microwave irradiation. The mixture was irradiated in order to keep the temperature at 140°C for 6 minutes, after that, the irradiation was stopped. This yields a reddish, transparent solid product, highly soluble in water. The product was dialyzed against ultrapure water (MWCO = 0.5-1.0 KDa, 3 days, twice a day). The dry material CDs **4** was obtained by freeze-drying, with a yield in mass of 58 wt. %. CDs **4** were charged negatively by dissolution in a pH=8 NaOH solution followed by dialysis again untrapure water (MWCO = 0.5-1.0 KDa, 3 days, twice a day) and freeze-drying.

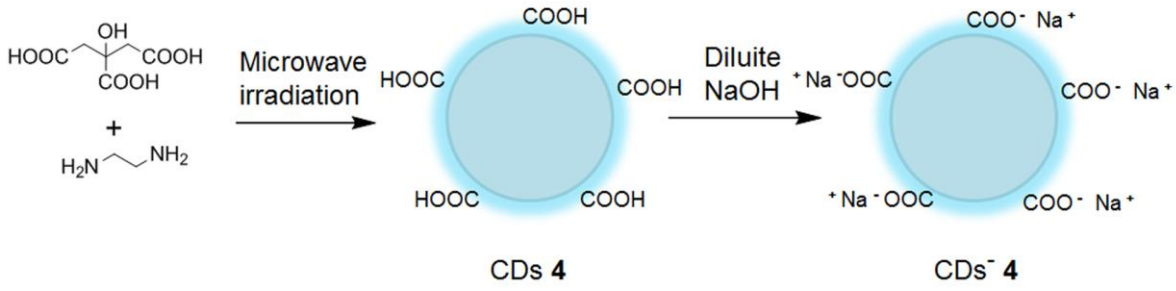

Scheme 4.1. Preparation of CDs^- 4.

4.3.3.2. Preparation of exfoliated MoS_2

Bulk MoS_2 (200 mg) was dispersed in chlorosulfonic acid and sonicated for 2 hours at room temperature. The solution was left under stirring during a month, occasionally sonicating for 30 seconds. Afterwards cold water was added to the solution under stirring, drop by drop and extremely carefully. Please notice that the reaction is exothermic and releases gaseous HCl. Next, the mixture was filtrated on a PTFE filter of 0.2 μm pore-size and washed with a good amount of methanol and acetone. The solid compound was added to N-methyl pyrrolidone and sonicated for 1 hour (tip sonication at 30-35% of amplitude (100% of 200 W)). After 3 days the supernatant was taken, filtrated on PTFE filter (0.2 μm pore-size) and washed with a large amount of methanol, acetone and dichloromethane.

4.3.3.3 Preparation of MoS_2-based materials 2 and 3.

In a round bottom flask, exfoliated MoS_2 (35 mg) and 1,2-dithiolane derivative **1** (15 mg) in DMF (10 mL) were stirred at 70 °C for 40 hours. After that period, the reaction mixture was filtered through a PTFE membrane (0.2 μm pore size), the solid residue was extensively washed with DMF and dichloromethane to obtain material **2**. Then, 15 mg of **2** were redisperse in dichloromethane and treated with gaseous HCl for 2 minutes. The reaction mixture was left under stirring for 12 hours and then filtered through a PTFE membrane (0.2 μm pore size). The solid residue was extensively washed with DMF and dichloromethane to obtain the ammonium derivatized MoS_2-based material **3**.

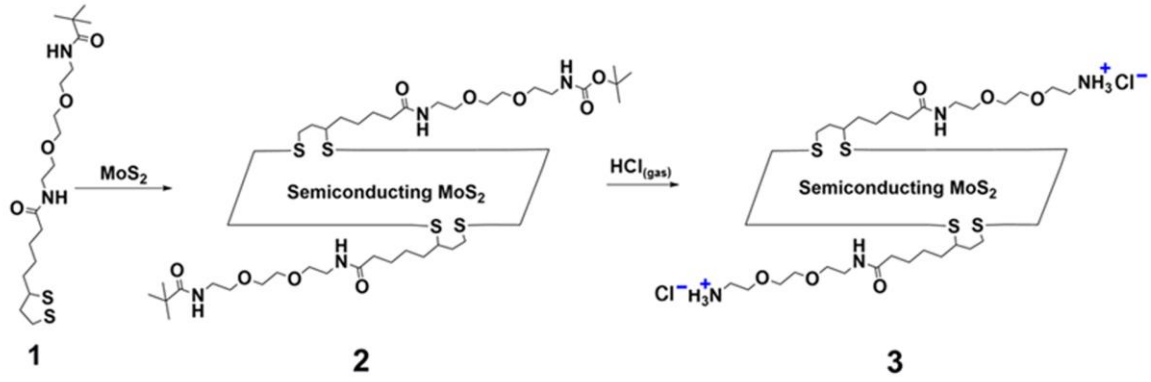

Scheme 4.2. Functionalization of MoS_2 leading to ammonium modified MoS_2-based material 3.

4.3.3.3 Characterization of CDs 4

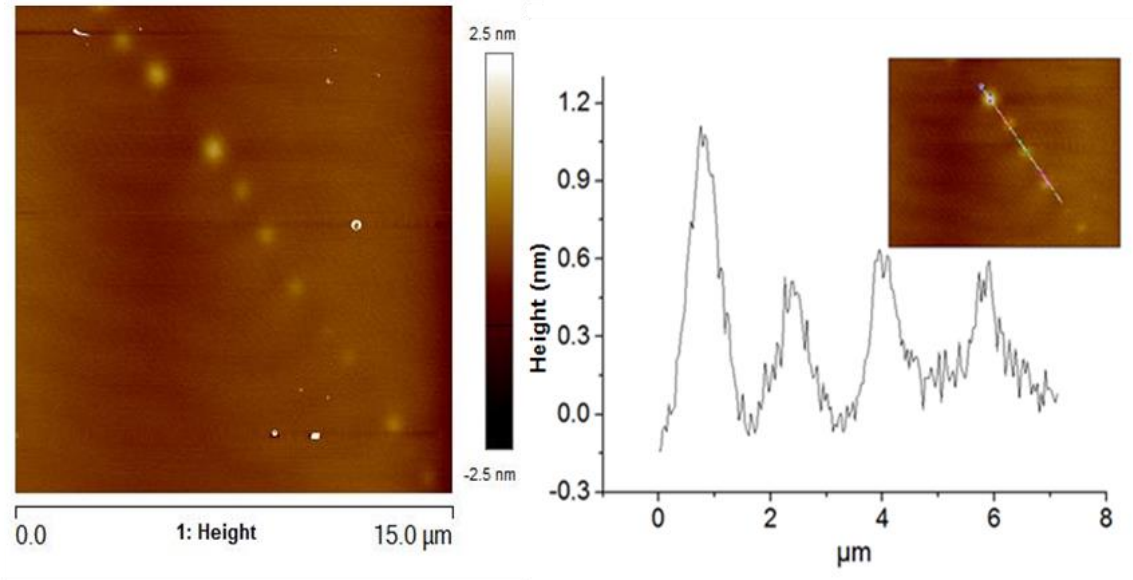

Figure 4.1. AFM picture and height profile of CDs 4.

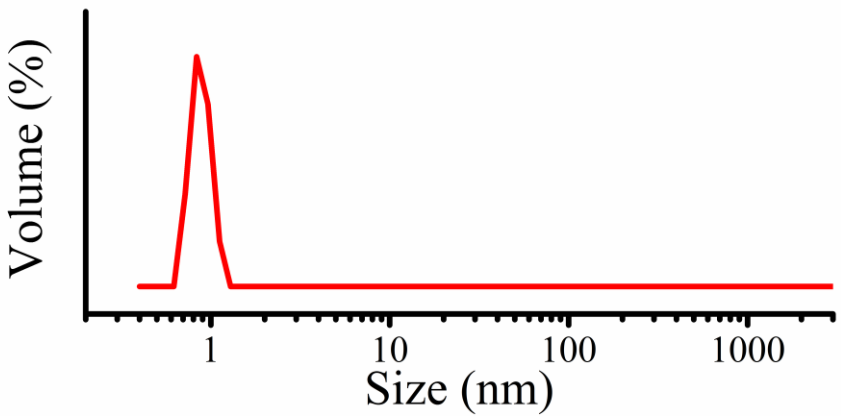

Figure 4.2. DLS size distribution of CDs 4.

The size of CDs **4** was determined by AFM (Figure 4.1) and DLS analysis (Figure 4.2) and found to be of around 1 nm.

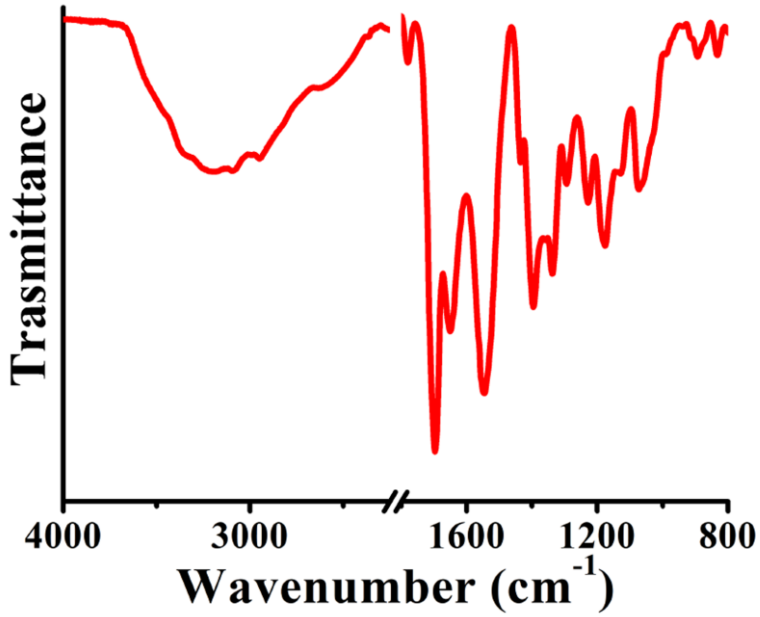

Figure 4.3. ATR-IR spectrum of CDs 4.

The IR spectrum of CDs **4** (Figure 4.3) shows the presence of alcohol and amines (O-H and N-H stretching between 3400-2800 cm^{-1}), carboxylic acids (C=O stretching at 1710 cm^{-1}) and amides (C=O stretching at 1650 and N-H bending at 1560 cm^{-1}).

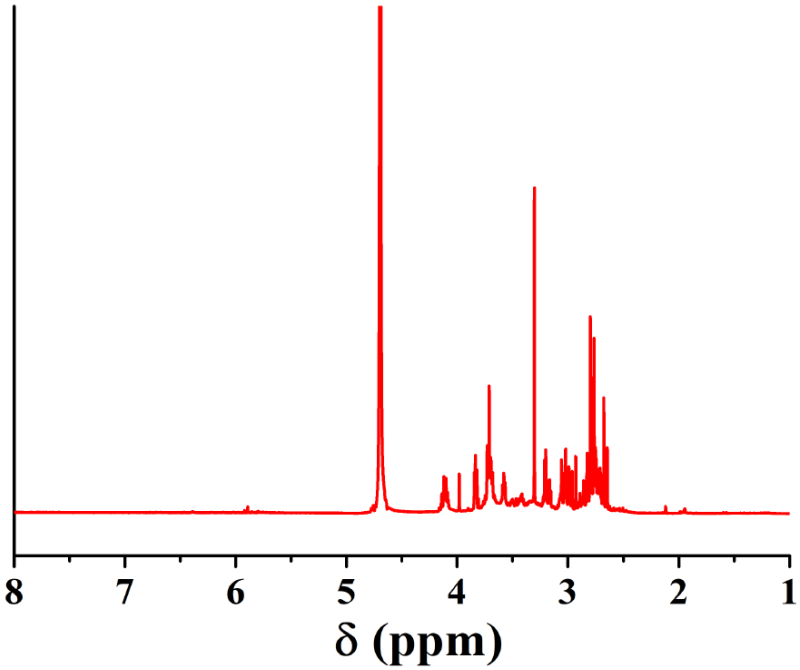

Figure 4.4. H^1 NMR of CDs 4.

The H^1 NMR spectrum of CDs **4** shows one thick set of signals between 4.2 and 2.6 ppm, corresponding to the methylene's protons of the citric acid and ethylenediamine building blocks of the CDs polymer structure (Figure 4.4).

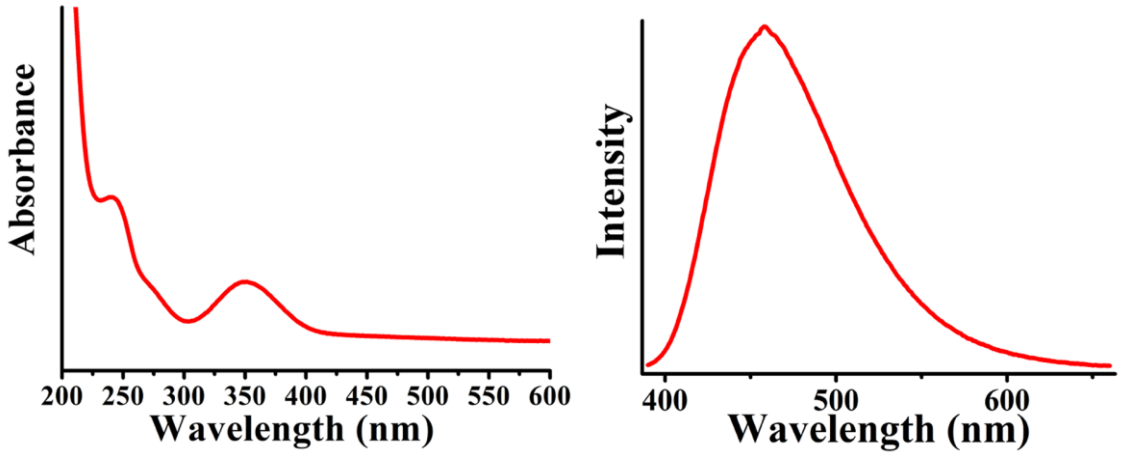

Figure 4.5. UV/Vis. (left) and emission spectra (right, λ_{ex}=370 nm) of CDs 4.

UV/Vis. absorption spectroscopy and photoluminescence spectroscopy shows the typical optical features of this type of CDs: two absorption bands (270 and 350 nm) and fluorescence emission at 460 nm (Figure 4.5).

4.3.3.3 Characterization of MoS_2-based materials 2 and 3

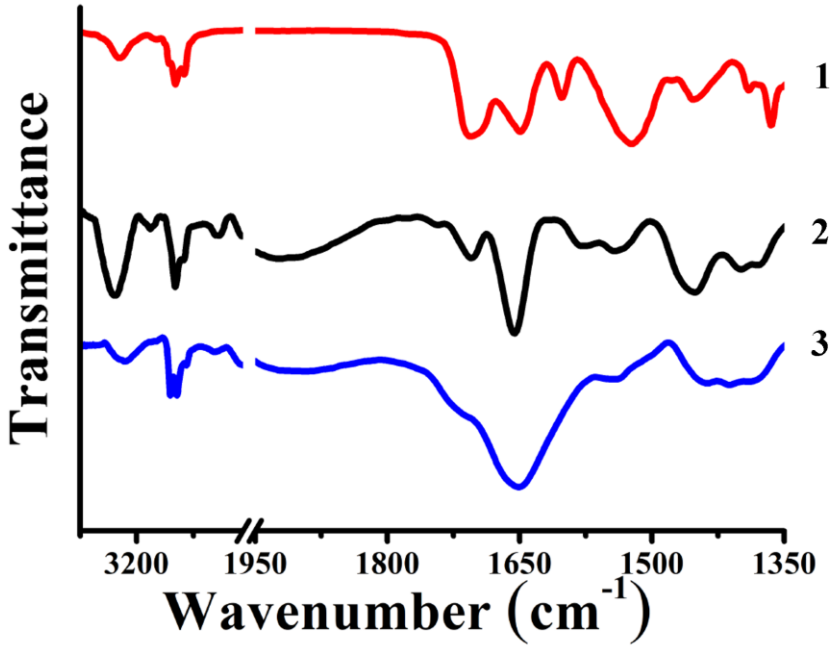

Figure 4.6. ATR-IR spectra for 1,2-dithiolane derivative 1 (red) and MoS_2-based materials 2 (black) and 3 (blue).

ATR-IR spectra comparison of materials **2** and **3** furnish a proof for the deprotection step (figure 4.6). While stretching vibration bands due to C-H units are identified in the region 2800-3000 cm^{-1} for both **2** and **3**, two discrete bands at 1650 and 1710 cm^{-1} owed to carbonyl amide and BOC units, respectively, are present in the IR spectrum of **2**, with the latter band being absent in the spectrum of **3**, thus justifying the effective removal of BOC.

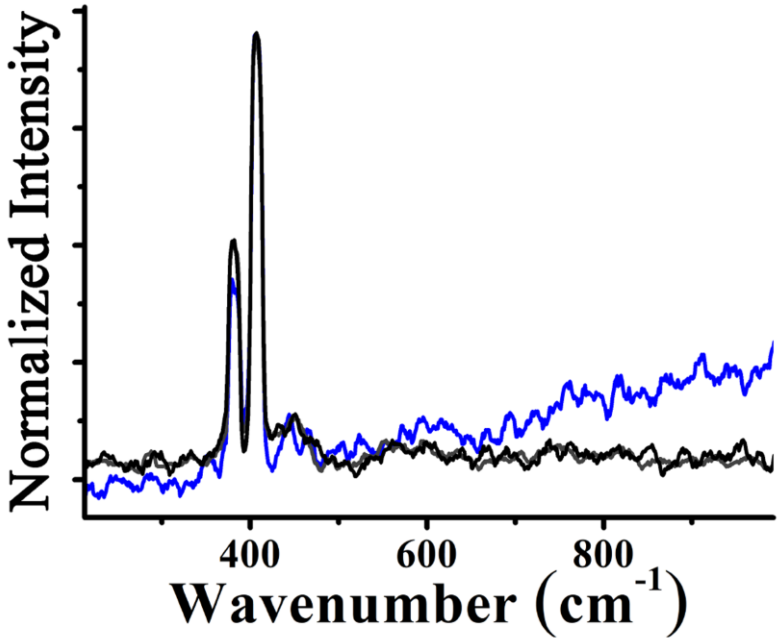

Figure 4.7. Normalized Raman spectra for exfoliated MoS_2 (black) and MoS_2-based materials 2 (gray) and 3 (blue), obtained upon 514 nm excitation.

Raman spectroscopy revealed the presence of the characteristic A_{1g} and E^1_{2g} modes located at 406 and 382 cm^{-1}, respectively, in materials **2** and **3** (Figure 4.7). Moreover, the A_{1g} and E^1_{2g} modes were found unaltered as compared with the ones present in exfoliated MoS_2. Since for exfoliated MoS_2 the calculated frequency difference between A_{1g} and E^1_{2g} is 24 cm^{-1}, corresponding to the presence of 3-4 MoS_2 layers in average[11], it is reasonable to claim that the same number of layers exists in **2** and **3**. Additionally, no other Raman bands were observed in the region 500-1000 cm^{-1}, indicating the absence of oxidation during the exfoliation and functionalization process, hence, proving the preservation of the electronic properties of the semiconducting MoS_2 polytype.

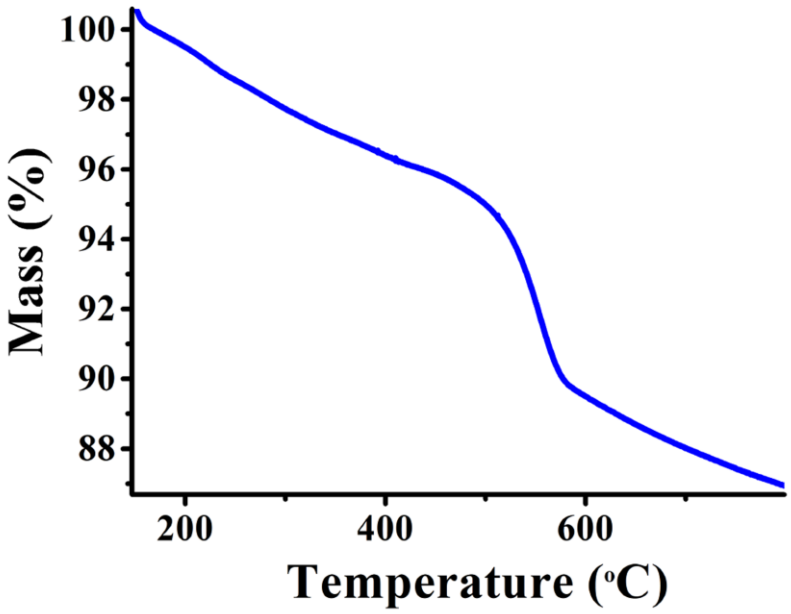

Figure 4.8. Thermographs for MoS_2-based material 3.

The ζ-potential value changed from -24 mV for exfoliated MoS_2 to +2.6 mV for **3**, being consistent with the presence of ammonium functionalities. Moreover, Kaiser test revealed a value of 50 μmol/g for free amine units in **3**. Then, based on TGA analysis, the 4.5% mass loss observed during heating of **3** in the temperature range 200-500 ^oC under nitrogen atmosphere, relate to the decomposition of the organic part incorporated on MoS_2, is consistent with the presence of one functional group for every 49 units of MoS_2 (Figure 4.8).

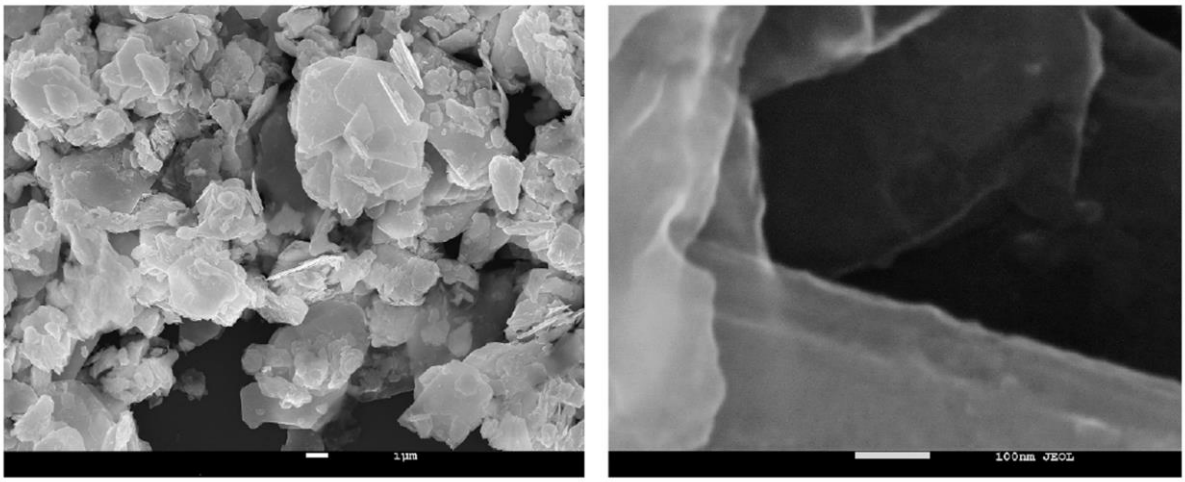

Figure 4.9. SEM images for MoS_2-based material 3.

SEM specimen was prepared by dropcasting a methanol dispersion of MoS_2 onto the sample holder and imaged after the solvent was allowed to slowly evaporate. Polygonal overlapping sheets of MoS_2 with sizes ranging from hundreds of nanometers to several

micrometers in a random distribution were observed (Figure 4.9). Amplification of several areas of the material reveals semi-transparent sheets associated to few layers of MoS_2, with regular and linear edges. It should be pointed out that due to the drying process for imaging, re-staking of the MoS_2 layers occurs explaining not only the observed deviation from the spectroscopically calculated layer size in solution, but also the difficulty of identifying single-layered MoS_2 in the modified material **3**.

4.4. Titration experiment

Once prepared the positively charged modified MoS_2 **3** and the negatively charged CDs^- **4**, electrostatic attractive interactions between the two species were exploited (Scheme 4.3) for the preparation of CDs/MoS_2 complexes.

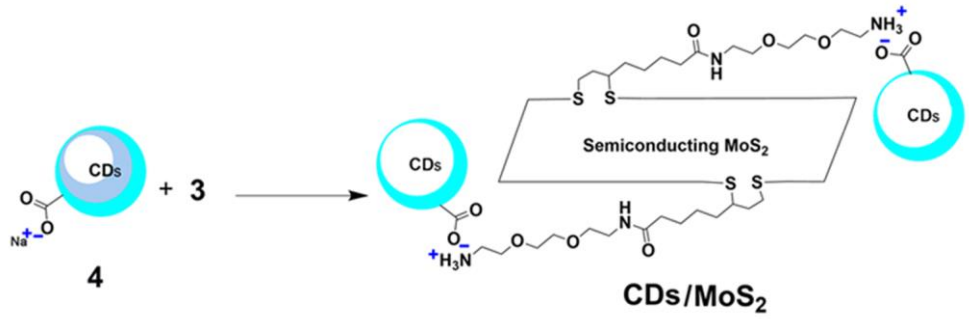

Scheme 4.3. Preparation of the CDs/MoS_2 electrostatic complex.

The experiment consists of a series of aqueous titration assays. In figure 4.10a are shown the absorption spectra of CDs^- **4** (0.35 mg/ml) for several additions of **3**. These spectra are obtained by subtraction of the MoS_2 bands, in order to isolate and easily monitor the changes occurring on the CDs absorption band. A progressive red-shift for the absorption of CDs^- **4** is observed, namely from 350 to 355 nm after the addition of 320 μL of **3**. Moreover, the complex formation between the two species in the ground state is suggested by the presence of a broad isosbestic point at 310 nm. Interestingly, when the neutral MoS_2-based derivative **2** was employed for the titration (Figure 4.10b) neither the red-shift nor the isosbestic point formation were observed, proving that electrostatic attractive forces not only promote the CDs/MoS_2 complex formation, but also play a role for the effective electronic interaction between the two species.

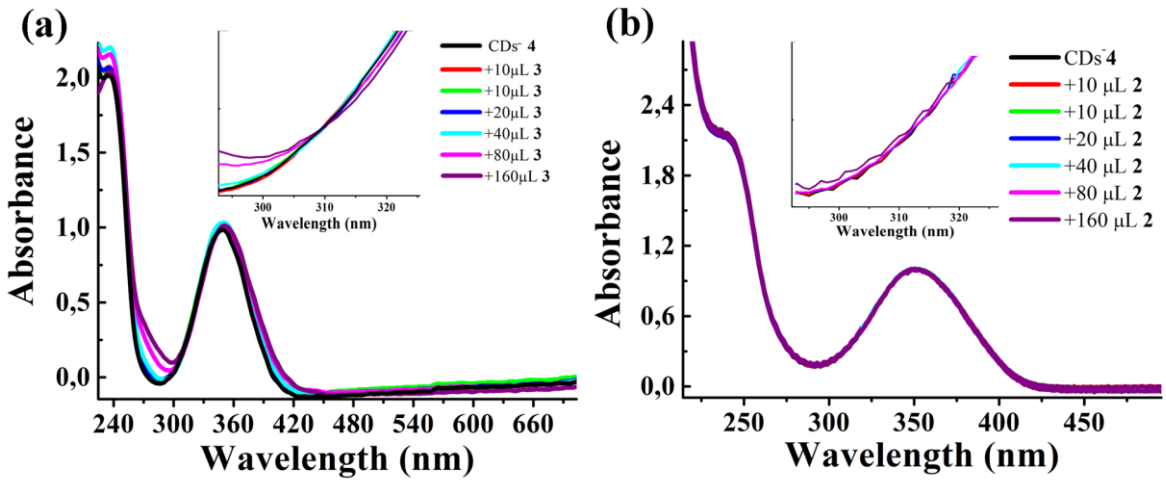

Figure 4.10. UV-Vis absorption spectra of CDs^- 4 upon incremental additions of (a) ammonium modified MoS_2-based material 3. Inset: Enlargement of the 300-320 nm region where the isosbestic point is developed, (b) MoS_2-based material 2.

Additional information on the photoinduced electronic interactions between MoS_2 and CDs were obtained by steady-state and time-resolved fluorescence spectroscopy analysis. Upon incremental addition of ammonium modified MoS_2-based material **3**, the CDs emission at 460 nm (λ_{ex}=370 nm) is progressively quenched (Figure 4.11a). Also when the neutral MoS_2-based derivative **2** is added quenching is observed, but with a much lower extent (Figure 4.11b). Nevertheless Stern-Volmer plots provide a useful hint for better understanding the quenching mechanism in the two systems. In fact, while the intensities ratio I_0/I (where I_0 is the emission intensity of the **CDs^- 4** alone and I upon the addition of quencher) increases linearly with the addition of MoS_2-based derivative **2**, the addition of the ammonium modified MoS_2-based material **3** results in a curved Stern-Volmer plot, implying the ocurring of an additional quenching phenomenon. These results suggest that simple collisions are resulting in the dynamic quenching of CDs for the addition of both MoS_2-based materials **2** and **3**, but only in the case of the latter an additional quenching mechanism is ocurring, which can be reasonably related to the CDs/MoS_2 complex formation.

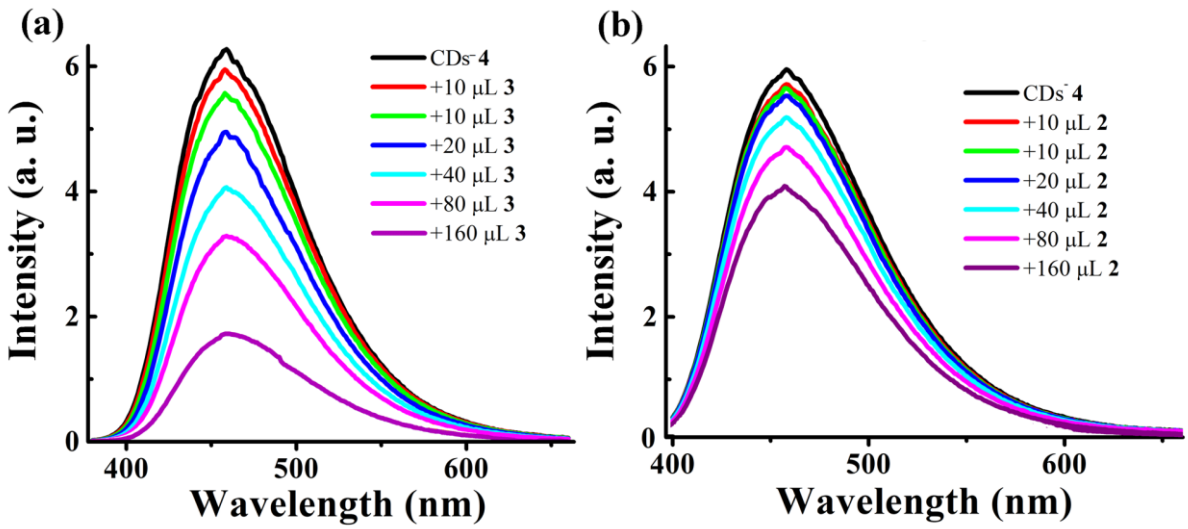

Figure 4.11. Photoluminescence titration assays of CDs^- 4 (20 µg/mL) upon incremental additions of (a) positively charged MoS_2-based material 3, and (b) neutral MoS_2-based material 2. Measurements were conducted in water for samples possessing equal absorbance at the excitation wavelength of 370 nm.

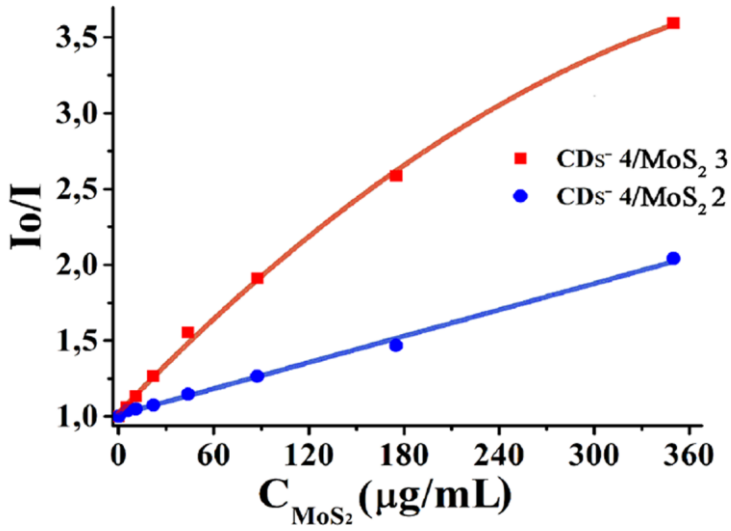

Figure 4.12. Stern-Volmer plot of CDs 4 I_0/I upon incremental additions of (a) positively charged MoS_2-based material 3, and (b) neutral MoS_2-based material 2.

Next, based on the time-correlated-single-photon-counting method, the fluorescence emission decay profiles for CDs^- **4** were acquired (Figure 4.13). The analysis of the decay profiles at 460 nm (excitation at 376 nm) for the singlet excited state of CDs^- **4** was exclusively monoexponentially fitted with a lifetime of 14.0 ns. Addition of the positively charged MoS_2-based material **3** to the negatively charged CDs^- **4** resulted in biexponential fitting, giving rise to the identification of two components, namely, one with the same lifetime, attributed to non-interacting CDs and a faster new one with 3.0

ns lifetime, corresponding to the fluorescence quenching of the emission intensity of the singlet excited state of CDs within the CDs/MoS_2 ensembles. In contrast, the fluorescence decay remained monoexponentially fitted upon addition of neutral MoS_2-based derivative **2**, mantaining the lifetime of intact CDs^- **4** and thus excluding in the blank experiment the occurrence of electronic interactions, which instead are proved for the electrostatic complex.

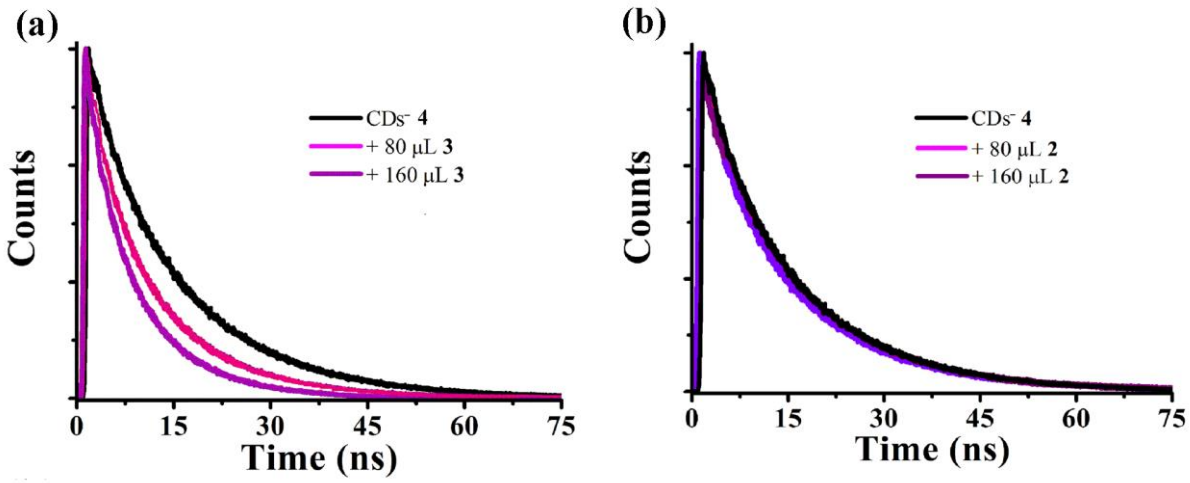

Figure 4.13. (a) Decay profiles for CDs^- 4 upon incremental additions of positively charged MoS_2-based material 3 or (b) neutral MoS_2-based material 2.

Finally, the electrocatalytic activity of CDs/MoS_2 towards the hydrogen evolution reaction (HER) was examined by employing a rotating disc working glassy carbon electrode in a standard three-electrode glass cell at a scan rate of 5 mV/sec in 0.5 M H_2SO_4. In general, MoS_2 are promising materials for HER, based on the overpotential and Tafel slope values they exhibit.[12-14] In addition, the aqueous solubility of CDs together with the presence of surface functional groups contribute to draw hydrated protons, thus enhancing proton adsorption capacity.[15] Based on the above and considering that hydrogen binds too strongly to S, hence leaving as primary active site for MoS_2 the Mo edge, the performance of CDs/MoS_2 towards the HER was probed by linear sweep voltammetry. The polarization curve of CDs/MoS_2 along with those of individual CDs^- **4** and bare glassy carbon electrode for comparison are shown in Figure 4.14a. For a given potential, the cathodic current increased for CDs/MoS_2 as compared to that based on individual CDs^- **4** and the bare carbon glassy electrode. The evolution of gaseous hydrogen for CDs/MoS_2 was visualized as bubbles appearing at currents as small as 0.5 mA/cm^2, with enhanced rate at around -0.7 V vs RHE. Since the cathodic

current density is proportional to the amount of hydrogen evolved, the latter result highlights the better catalytic activity for CDs/MoS_2 and prominent hydrogen evolution behavior exhibiting an onset overpotential near -0.5 V vs RHE, which is lower than the individual CDs^- **4** by around 150 mV. The better electrocatalytic activity of CDs/MoS_2 is mainly attributed to a synergic effect due to enhanced charge-transfer kinetics owed to the intimate contact between the two species CDs and MoS_2 as well as the presence of active sites in MoS_2. Next, the linear regions of the Tafel plots (Figure 4.14b) were fit to the Tafel equation, $\eta = B \log j + a$, where η is the overpotential, j is the current density and B is the Tafel slope, to further characterize the fluent charge transport efficiency and the efficacy of the electrocatalytic reaction. Analysis of the Tafel slope helps to elucidate the possible HER mechanism and define the rate-limiting step. The Tafel slope for CDs/MoS_2 ensemble was found to be 22 mV/dec, smaller than the one owed to CDs^- **4** by 4 mV/dec. Considering that smaller Tafel slope suggests that for the generation of an equivalent current only a lower overpotential is needed to apply, the electrocatalytic activity of individual CDs^- **4** is improved upon realization of the CDs/MoS_2 ensemble. The latter improvement in charge transport is attributed to good electrical contact between the two components in the donor-acceptor CDs/MoS_2 ensemble, in which charge-transfer phenomena prevail. Moreover, the small Tafel slope of CDs/MoS_2 manifests that the electrochemical desorption of adsorbed hydrogen atoms onto the modified electrode to generate hydrogen is the rate-limiting step – see equations 2 and 3 below. Based on the widely applied mechanisms for the HER, initially a proton is adsorbed onto the electrode surface via a reduction process (Volmer adsorption [Eq. (1)]) followed by either direct bonding of the adsorbed hydrogen atom with another proton and electron transfer from the electrode surface (Heyrovsky desorption [Eq. (2)]) or recombination of two hydrogen atoms adsorbed on the electrode surface (Tafel desorption [Eq. (3)]).

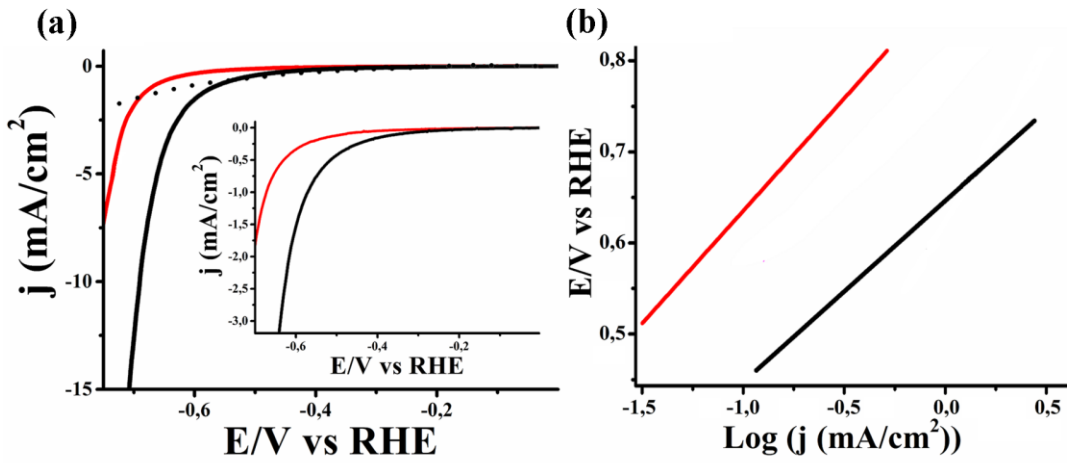

Figure 4.14. (a) Linear sweep voltammograms for the HER of CDs/MoS_2 (black), individual CDs^- 4 (red) and bare glassy carbon electrode (dotted). Inset: enlarged region near the onset. (b) Tafel plots for CDs/MoS_2 (black) and individual CDs^- 4 (red) showing overpotential vs current density.

Volmer adsorption: $H^+ + e^- \rightarrow H^{\bullet}_{(ads)}$ Eq. (1)

Heyrovsky desorption: $H^{\bullet}_{(ads)} + H^+ + e^- \rightarrow H_2$ Eq. (2)

Tafel desorption: $H^{\bullet}_{(ads)} + H^{\bullet}_{(ads)} \rightarrow H_2$ Eq. (3)

4.5. Conclusions

In this study aqueous stable CDs/MoS_2 complexes were developed, profiting of the Coulomb attractive forces for enabling strong electronic interactions between the components. The formation of the complexes was followed by electronic absorption and photoluminescence titration assays, complemented by time-resolved fluorescence emission, proving in this way the occurring of the intra-complex electronic interaction. Significant quenching of the CDs photoluminescence by MoS_2 was revealed, prompting to an additional deactivation channel – electron and/or energy transfer – starting from the singlet excited state of CDs within the CDs/MoS_2 ensembles. Moreover, the electrocatalytic performance of CDs/MoS_2 was evaluated regarding the HER and found improved in comparison with that of the individual CDs species. Without a doubt, such CDs/MoS_2 ensembles performing in electron donor-acceptor schemes can be further exploited for managing charge-transfer processes as well as for electrocatalysis and may be useful for advancing the field of energy conversion in a wide range of technological and environmental applications.

4.6. References

1. Chhowalla, M.; Shin, H. S.; Eda, G.; Li, L.-J.; Loh, K. P.; Zhang, H., The chemistry of two-dimensional layered transition metal dichalcogenide nanosheets. *Nature Chemistry* **2013,** *5*, 263.
2. Wang, Q. H.; Kalantar-Zadeh, K.; Kis, A.; Coleman, J. N.; Strano, M. S., Electronics and optoelectronics of two-dimensional transition metal dichalcogenides. *Nature Nanotechnology* **2012,** *7*, 699.
3. Lee, H. S.; Min, S.-W.; Chang, Y.-G.; Park, M. K.; Nam, T.; Kim, H.; Kim, J. H.; Ryu, S.; Im, S., MoS2 Nanosheet Phototransistors with Thickness-Modulated Optical Energy Gap. *Nano Letters* **2012,** *12* (7), 3695-3700.
4. Jeong, H.; Bang, S.; Oh, H. M.; Jeong, H. J.; An, S.-J.; Han, G. H.; Kim, H.; Kim, K. K.; Park, J. C.; Lee, Y. H.; Lerondel, G.; Jeong, M. S., Semiconductor–Insulator–Semiconductor Diode Consisting of Monolayer MoS2, h-BN, and GaN Heterostructure. *ACS Nano* **2015,** *9* (10), 10032-10038.
5. Perkins, F. K.; Friedman, A. L.; Cobas, E.; Campbell, P. M.; Jernigan, G. G.; Jonker, B. T., Chemical Vapor Sensing with Monolayer MoS2. *Nano Letters* **2013,** *13* (2), 668-673.
6. Ross, J. S.; Klement, P.; Jones, A. M.; Ghimire, N. J.; Yan, J.; Mandrus, D. G.; Taniguchi, T.; Watanabe, K.; Kitamura, K.; Yao, W.; Cobden, D. H.; Xu, X., Electrically tunable excitonic light-emitting diodes based on monolayer WSe2 p–n junctions. *Nature Nanotechnology* **2014,** *9*, 268.
7. Wang, K.; Wang, J.; Fan, J.; Lotya, M.; O'Neill, A.; Fox, D.; Feng, Y.; Zhang, X.; Jiang, B.; Zhao, Q.; Zhang, H.; Coleman, J. N.; Zhang, L.; Blau, W. J., Ultrafast Saturable Absorption of Two-Dimensional MoS2 Nanosheets. *ACS Nano* **2013,** *7* (10), 9260-9267.
8. Huang, X.; Zeng, Z.; Zhang, H., Metal dichalcogenide nanosheets: preparation, properties and applications. *Chemical Society Reviews* **2013,** *42* (5), 1934-1946.
9. Pumera, M.; Sofer, Z.; Ambrosi, A., Layered transition metal dichalcogenides for electrochemical energy generation and storage. *Journal of Materials Chemistry A* **2014,** *2* (24), 8981-8987.
10. Canton-Vitoria, R.; Sayed-Ahmad-Baraza, Y.; Pelaez-Fernandez, M.; Arenal, R.; Bittencourt, C.; Ewels, C. P.; Tagmatarchis, N., Functionalization of MoS2 with 1,2-dithiolanes: toward donor-acceptor nanohybrids for energy conversion. *npj 2D Materials and Applications* **2017,** *1* (1), 13.
11. Li, H.; Zhang, Q.; Yap, C. C. R.; Tay, B. K.; Edwin, T. H. T.; Olivier, A.; Baillargeat, D., From Bulk to Monolayer MoS2: Evolution of Raman Scattering. *Advanced Functional Materials* **2012,** *22* (7), 1385-1390.
12. Wang, D.; Xiao, Y.; Luo, X.; Wu, Z.; Wang, Y.-J.; Fang, B., Swollen Ammoniated MoS2 with 1T/2H Hybrid Phases for High-Rate Electrochemical Energy Storage. *ACS Sustainable Chemistry & Engineering* **2017,** *5* (3), 2509-2515.
13. Chou, S. S.; Sai, N.; Lu, P.; Coker, E. N.; Liu, S.; Artyushkova, K.; Luk, T. S.; Kaehr, B.; Brinker, C. J., Understanding catalysis in a multiphasic two-dimensional transition metal dichalcogenide. *Nature communications* **2015,** *6*, 8311-8311.
14. Li, Y.; Wang, H.; Xie, L.; Liang, Y.; Hong, G.; Dai, H., MoS2 Nanoparticles Grown on Graphene: An Advanced Catalyst for the Hydrogen Evolution Reaction. *Journal of the American Chemical Society* **2011,** *133* (19), 7296-7299.
15. Li, H.; Liu, J.; Guo, S.; Zhang, Y.; Huang, H.; Liu, Y.; Kang, Z., Carbon dots from PEG for highly sensitive detection of levodopa. *Journal of Materials Chemistry B* **2015,** *3* (11), 2378-2387.

5. ELECTRONIC INTERACTIONS IN COVALENT CDs-TMDs HYBRIDS

5.1. Abstract

In this work, novel CD-TMDs hybrid materials were prepared by covalent functionalization of exfoliated semiconducting MoS_2 and WS_2 with 1,2-dithiolane-modified carbon dots (f-CDs). Next, their electronic properties were deeply investigated by a wide set of characterization techniques, including cyclovoltammetry, absorption spectroscopy, steady-state fluorescence spectroscopy, time-resolved fluorescence spectroscopy and transient absorption spectroscopy. These studies revealed the occurring of ultrafast energy transfer from photoexcited f-CDs to both MoS_2 and WS_2. Furthermore, upon MoS_2 photoexcitation charge transfer from an exciton dissociation path of MoS_2 to f-CDs, within CD-MoS_2, was observed. In contrast, CD-WS_2 did not display such behavior due to energetic reasons. These results suggest that CD-MoS_2 hybrids represent suitable donor-acceptor materials for energy applications, laying the basis for further works of optimization and implementation in optoelectronic devices.

5.2. Introduction

Likewise graphene, also monolayer transition metal dichalcogenides (TMDs), such as MoS_2 and WS_2, own their outstanding physical properties to the bidimensional structure, consisting of an atomic plane of a transition metal sandwiched between two atomic planes of chalcogens. The optoelectronic properties of TMDs are governed by excitonic transitions, which can be controlled by modifying the TMDs surface with photo- and/or electro-active species, thus tuning the charge-carrier density.[1] In here, covalent functionalization can be a valuable tool for the improvement of the TMDs properties.[2] Despite its novelty, covalent functionalization of MoS_2 have been already exploited for enhancing solubility,[3-5] improving biocompatibility[6] and even for tailoring the optoelectronic properties.[7-8] Among these approaches, 1,2-dithiolane functionalization, thanks to the high binding affinity of the disulfide group towards molybdenum and tungsten, certainly provides an efficient and reliable strategy for the covalent functionalization of MoS_2 and WS_2 edges, where defects, i.e. sulfur vacant sites, are mostly found.[3] However, covalent functionalization of TMDs with photoactive species for the development of advanced hybrid materials has not been exploited yet. Indeed, the development of such hybrids is timely and surely deserves investigation, especially in the context of their ability to function as donor-acceptor systems upon photoillumination. Valuable characteristics, including photoinduced donor-acceptor

behavior, photostability and opportunity of chemical modifications, certainly makes CDs promising candidates for the tuning of the TMDs properties via covalent functionalization. In the present chapter, the preparation, characterization and photophysical properties of novel CD-TMDs hybrid materials are reported. CDs were prepared by room-temperature coupling agent-mediated condensation of citric acid and ethylenediamine and functionalized *in situ* with n-butyl chains for improving the solubility in organic solvents. Next, lipoic acid was employed for providing CDs of the 1,2-dithiolane groups, consequently exploited for the attachment onto exfoliated MoS_2 and WS_2 and for the formation of the hybrids. Finally, the optical and electrical properties of the hybrids were investigated, indentifying and characterizing the energy and charge transfer phenomena occurring upon photoirradiation.

5.3. Experimental section

5.3.1. Materials

Molybdenum disulfide powder (>99%), chlorosulfonic acid (99%), citric acid anhydrous (≥99.5%), ethylendiamine (99+%), butylamine (99.5%), N,N'-diisopropylcarbodiimide (99%), 1-Ethyl-3-(3-dimethylaminopropyl)carbodiimide (98%) were used without further purifications. Dialysis tubes with molecular weight cut-off (MWCO) 0.5-1 KDa were bought from Spectrum Labs.

5.3.2. Characterization techniques

- Mid-infrared spectra in the region 500−4500 cm^{-1} were obtained on a Fourier transform IR spectrometer (Equinox 55 from Bruker Optics) equipped with a single reflection diamond ATR accessory (DuraSamp1IR II by SensIR Technologies). A drop of the solution was placed on the diamond surface, followed by evaporation of the solvent, in a stream of nitrogen, before recording the spectrum. Typically, 100 scans were acquired at 2 cm^{-1} resolution.
- Micro-Raman scattering measurements were performed at room temperature in the backscattering geometry using a RENISHAW inVia Raman microscope equipped with a CCD camera and a Leica microscope. A 2400 lines mm^{-1} grating was used for all measurements, providing a spectral resolution of ± 1 cm^{-1}. As an excitation source the Ar^{+} laser (514 nm with less than 0,092 mW laser power) was used. Measurements were taken with 15 seconds of exposure

times at varying numbers of accumulations. The laser spot was focused on the sample surface using a long working distance 50x objective. Raman spectra were collected on numerous spots on the sample and recorded with Peltier cooled CCD camera. The data were collected and analyzed with Renishaw Wire and Origin software.

- Thermogravimetric analysis was performed using a TGA Q500 V20.2 Build 27 instrument by TA in a nitrogen (purity >99.999%) inert atmosphere.
- Atomic force microscopy (AFM) images were acquired in air under ambient conditions using a MultiMode AFM with NanoScope V controller (Bruker Nano Surfaces Division, Santa Barbara, CA) operating in tapping mode with Si tips Bruker AFM probe RTESPA PART MPP-11120-10. Samples were prepared on mica substrates. Particle height distribution analysis was carried out by using the Nanoscope Analysis Version 1.5 software (Veeco Ins).
- The DLS measurements were recorded on a Malvern Nano Zetasizer HT, on a 10 mm path-length plastic cuvette.
- ^{1}H spectra were recorded in D_2O solutions at 25 ^{o}C on a Bruker AV500 spectrometer. Electrochemical measurements were carried out at room temperature in N_2-saturated 0.5 M H_2SO_4 in a standard three-compartment electrochemical cell using an EG&G Princeton Applied Research potensiostat/galvanostat (Model PARSTAT^{R} 2273A). As counter electrode, a platinum wire was used and as reference a $Hg/HgSO_4$ (0.5 M K_2SO_4) electrode was placed into Luggin capillary. The working electrode was a glassy carbon disk with geometric surface area of 0.071 cm^2. Linear sweep voltammetry measurements were conducted with a scan rate of 5 mV s^{-1}.
- Electron microscopy imaging: STEM imaging and EELS studies were conducted using an aberration-corrected FEI Titan Low-Base microscope operated at 80 kV. This microscope was equipped with a Cs probe corrector and a Gatan Tridiem ESR 865 electron energy loss spectroscopy (EELS) spectrometer. The energy resolution was ~1 eV. The convergence and collection angles were 25 and 50 mrad, respectively. The EELS studies were conducted in STEM mode, using the spectrum-line scan mode. To increase the signal/noise ratio of the EEL spectra, the datasets were then de-noised with the open-source program Hyperspy by using principal component analysis routines.

- Steady-state UV-Vis electronic absorption spectra were recorded on a PerkinElmer (Lambda 19) UV-Vis-NIR spectrophotometer.
- Steady-state emission spectra were recorded on a Fluorolog-3 JobinYvon-Spex spectrofluorometer (model GL3-21).
- Picosecond time-resolved fluorescence spectra were measured by the time-correlated-single-photon-counting (TCSPC) method on a Nano-Log spectrofluorometer (Horiba JobinYvon), by using a laser diode as an excitation source (NanoLED, 375 nm) and a UV-Vis detector TBX-PMT series (250-850 nm) by Horiba JobinYvon. Lifetimes were evaluated with the DAS6 Fluorescence-Decay Analysis Software.
- Femtosecond transient absorption spectroscopy: Experiments were performed using an Ultrafast Femtosecond Laser Source (Libra series) by Coherent Inc. (Santa Clara, CA) incorporating diode-pumped, mode locked Ti:Sapphire laser (Vitesse) and diode-pumped intra cavity doubled Nd:YLF laser (Evolution) to generate a compressed laser output of 1.45 W. For optical detection, a Helios transient absorption spectrometer from Ultrafast Systems (Sarasota, FL) was used. The source for the pump and probe pulses were derived from the fundamental output of Libra (Compressed output 1.45 W, pulse width 100 fs) at a repetition rate of 1 kHz. About 95% of the fundamental output of the laser was introduced into a TOPAS-Prime-OPA system with 290-2600 nm tuning range from Altos Photonics Inc., (Bozeman, MT), while the rest of the output was used for generation of white light continuum. Kinetic traces at appropriate wavelengths were assembled from the time-resolved spectral data. Data analysis was performed using Surface Xplorer software supplied by Ultrafast Systems. All measurements were conducted in degassed solutions at room temperature.

5.3.3. Synthesis and characterization of modified CDs

5.3.2.2 CDs synthesis

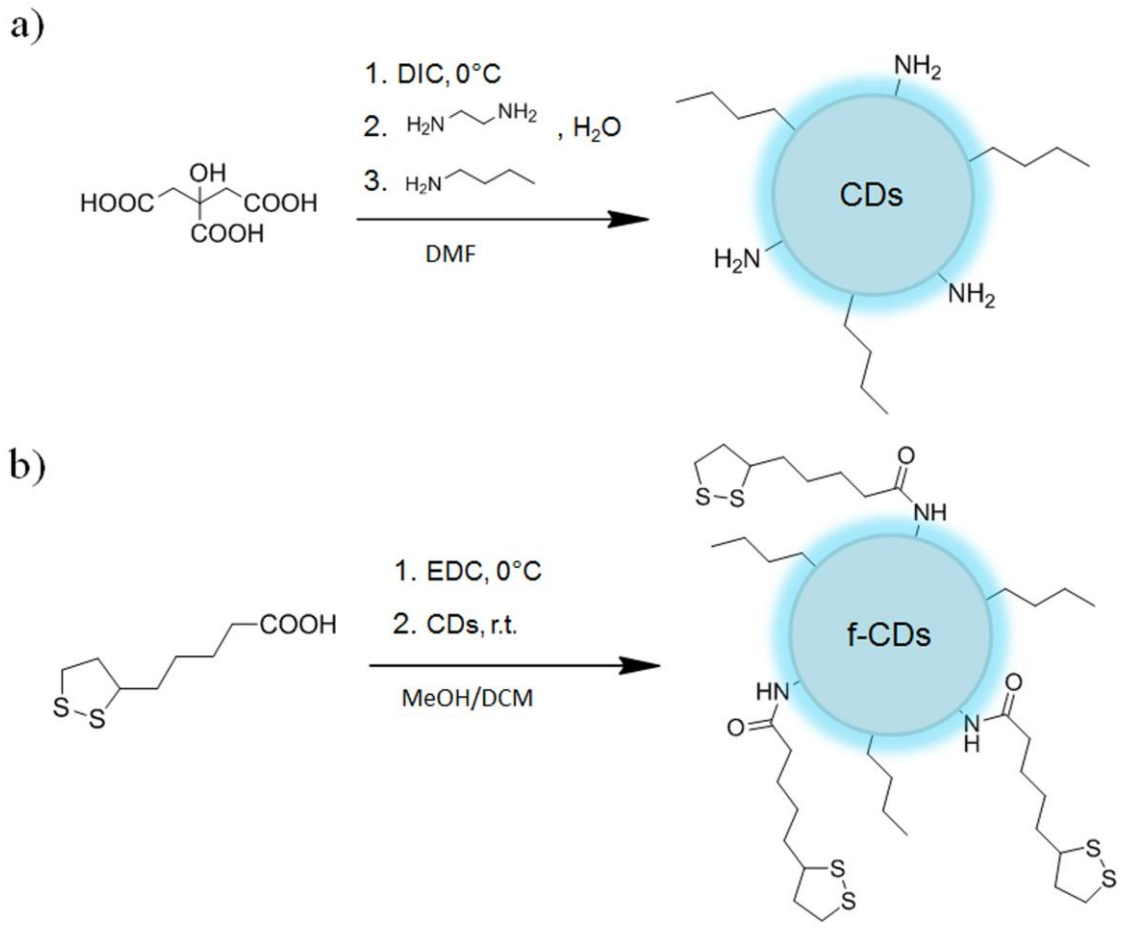

Scheme 5.1. Synthesis of CDs and functionalization with lipoic acid.

The synthesis of functionalized CDs (f-CDs) was carried out in two steps. In the first one, 2g of citric acid (1 eq.) were dissolved in 10 ml of DMF and the solution was cooled in ice bath. 4.4 ml of *N,N'*-Diisopropylcarbodiimide (DIC) coupling agent (3 eq.) were added slowly to the solution while stirring, forming a white dispersion. After around one minute, 1.9 ml of ethylenediamine (EDA) in 10 ml of cold water were poured in the reaction flask. When the color turns to yellow and then orange the fluorescent particles are formed, thus 5 ml of butylamine are added and the reaction is left one day stirring. The addition of butylamine allows the *in situ* introduction of the butyl groups on the CDs surface, which enhance their lipophilicity and, at the same time, consumes all the remaining carboxylic groups, stopping the growth of the nanoparticles. The solution is filtered to remove the white DIC urea byproduct, then the

filtrate is washed three times with Et_2O. The excess of butylamine is removed under vacuum in a rotary evaporator. Finally the water phase is purified by dialysis in ultrapure water (molecular weight cut-off = 0.5-1 kDa, 3 days). The dry product CDs (0.7g), consisting of a yellow powder, is obtained by freeze-drying. Scheme 5.1a.

In the second step 200 mg of CDs were dissolved in 5 ml of MeOH and 25 ml of dichloromethane (DCM) and cooled in ice-bath. In another flask, 300 mg of lipoic acid were dissolved in 5 ml of DCM, cooled in ice-bath and 336 mg of (3-Dimethylaminopropyl)-N′-ethylcarbodiimide hydrochloride (EDC) coupling agent were added. After 20 minutes, the lipoic acid solution was poured to the CDs one. The reaction was left overnight stirring and the day after 100 mg of lipoic acid and 56 mg of EDC were added. After 3h the reaction was washed one time with water, one time with a NaOH water solution (pH=11) and one time with brine. The DCM was partially removed by vacuum and diluited with ethyl acetate, causing the precipitation of the particles (centrifugation at 3200 r.p.m., 5 min.). The redispersion-precipitation was repeated until the lipoic acid spot in TLC disappeared. The precipitate was dissolved again in MeOH/DCM 1:1 and $MgSO_4$ was added to dry the water traces. f-CDs, in the form of a brown solid, were obtained by vacuum removal of the solvent. Scheme 5.1b.

5.3.2.2 CDs characterization

The structure of CDs and f-CDs was determined by ^1H NMR spectroscopy (Figure 5.1). All the signals for the as-synthetized CDs are found in the aliphatic region and correspond to the methylene protons of citric acid and ethylenediamine structural components (4.0-2.3 ppm) and butyl units (1.6-0.7 ppm). Thus, the polymer nature of the structure and the occurring of the butylamine functionalization were confirmed. In the modified f-CDs, multiplets appear between 2.6 and 1.5 ppm, corresponding to the protons of the lipoic amide moiety condensed onto the surface of the nanoparticles.

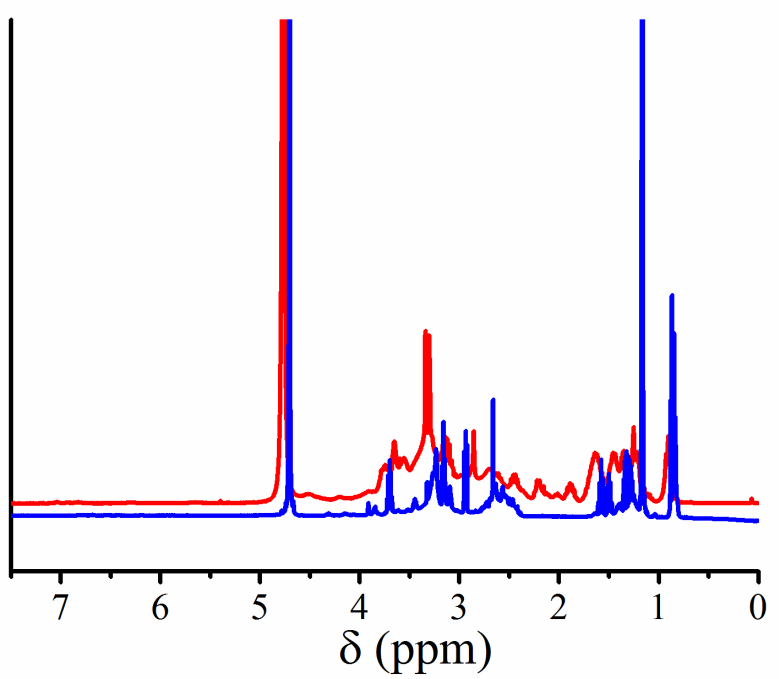

Figure 5.1. H^1 NMR spectra of CDs (blue) and f-CDs (red).

The IR features in the as-produced CDs (Figure 5.2) are assigned as to O-H and N-H stretching vibrations at 3300-3000 cm^{-1}, C-H stretching at 2920 cm^{-1}, C=O stretching of free carboxylic acid units at 1705 cm^{-1}, C=O stretching of amide units at 1640 and 1630 cm^{-1}, and C-O and C-N stretching at 1440-1360 cm^{-1}. In the modified f-CDs, the intensity for the C=O stretching amide band increased.

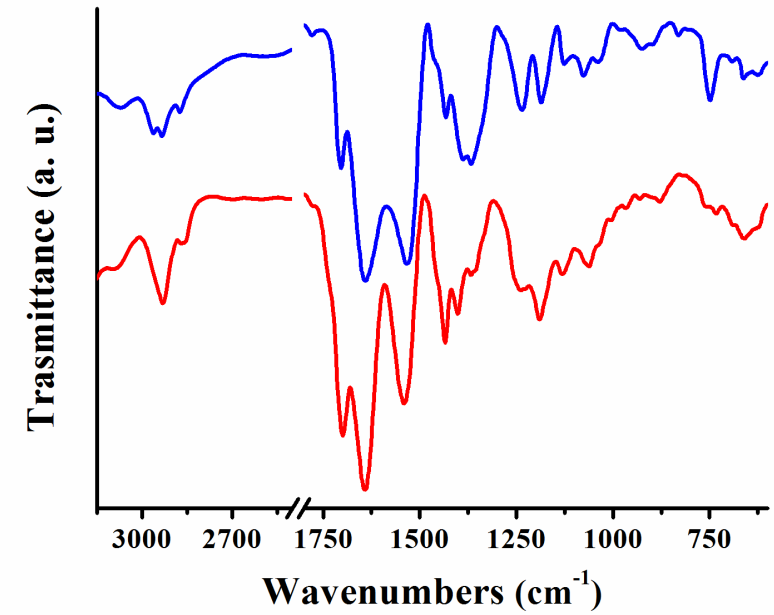

Figure 5.2. ATR-IR spectra of as-produced CDs (blue) and 1,2-dithiolane modified f-CDs (red).

Further proof of the functionalization was given by the Kaiser test, where the amount of free amines on CDs decreased significantly upon condensation with lipoic acid, from 1810 to 72 µmol/g. The 1,2-dithiolane functionalization had an impact on the CDs optical properties, resulting in a red-shift from 345 to 370 nm for the f-CDs absorbance and from 450 to 470 nm for the f-CDs emission (Figure 5.3).

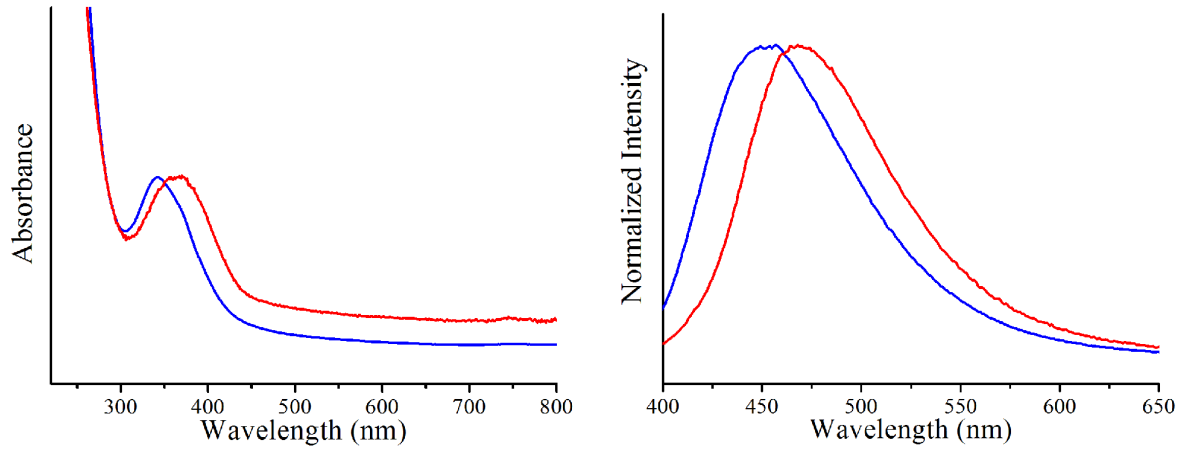

Figure 5.3. UV-Vis (left) and emission (right, λ_{ex}=370 nm) spectra of as-produced CDs (blue) and 1,2-dithiolane modified f-CDs (red), obtained in methanol.

5.3.4. Preparation of exfoliated MoS_2 and WS_2

Bulk TMDs (150-200 mg) were dispersed in chlorosulfonic acid and sonicated for 2 hours at room temperature. The solution was left under stirring during a month, occasionally sonicated for 30 seconds. Afterwards cold water was added to the solution under stirring, drop by drop and extremely carefully. Please notice that the reaction is exothermic and releases gaseous HCl. Next, the mixture was filtrated on a PTFE filter of 0.2 µm pore-size and washed with a good amount of methanol and acetone. The solid compound was added to N-methyl pyrrolidone and sonicated for 1 hour (tip sonication at 30-35% of amplitude (100% of 200 W)). After 3 days the supernatant was taken, filtrated on PTFE filter (0.2 µm pore-size) and washed with a large amount of methanol, acetone and dichloromethane.

5.4. Results and discussion

The f-CDs were conjugated to MoS_2 and WS_2 following the the functionalization methodology for TMDs with 1,2-dithiolanes.[39-41] In here, the f-CDs (50 mg) were dissolved in methanol (1 mL). In another flask, exfoliated TMDs (20 mg) were

dispersed in DMF (10 mL) by sonication (10 min) and dropped in the CNDs solution. The flask was covered with aluminum foil and the reaction mixture was stirred at 70 °C for 4 days. After that period, it was cooled and filtered through a PTFE membrane (0.2 nm pore size). The solid residue was extensively washed with methanol and dichloromethane to obtain the CD-TMDs (Scheme 5.2).

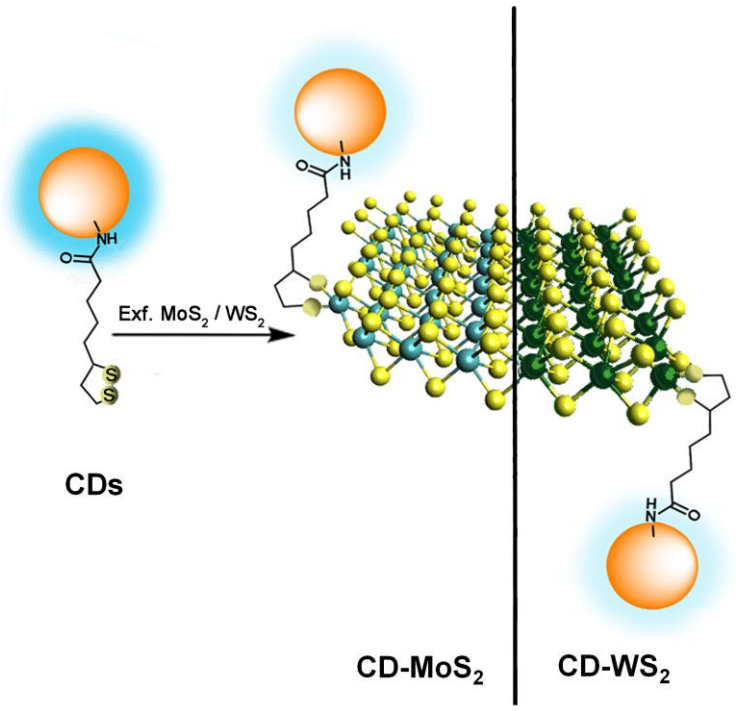

Scheme 5.2. Illustrative preparation of CD-MoS_2 and CD-WS_2 upon covalent 1,2-dithiolane functionalization of exfoliated semiconducting MoS_2 and WS_2 nanosheets.

The as obtained CD-MoS_2 and CD-WS_2 hybrids were furtherly characterized by IR and Raman spectroscopy, thermogravimetric analysis (TGA) and transmission electron microscopy (TEM). In the ATR-IR spectra of CD-MoS_2 and CD-WS_2 (Figure 5.4), the presence of CDs was revealed by the bands at 1640 and 1550 cm^{-1}, corresponding to the amide C=O stretching and N-H bending modes, as well as by the sharp bands at 300-2800 cm cm^{-1}, due to the C-H stretching.

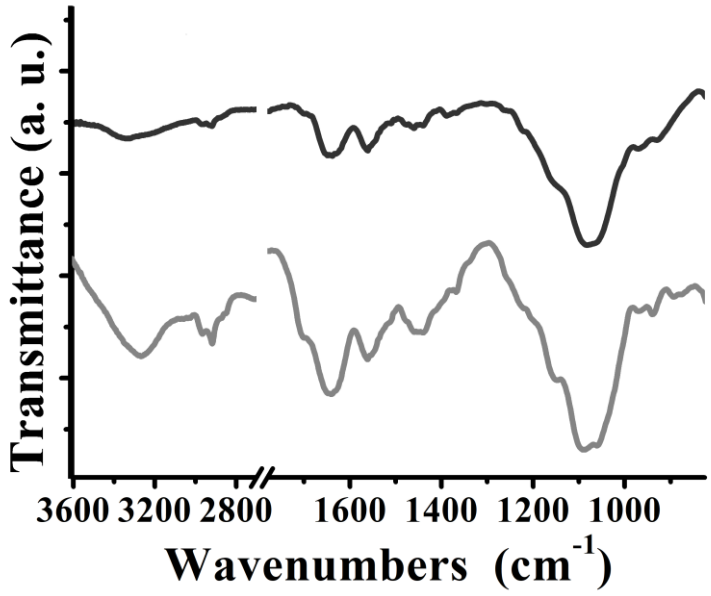

Figure 5.4. ATR-IR spectra of of CD-MoS_2 (black) and CD-WS_2 (grey).

Raman spectroscopy is a useful technique for proving the ocurrence of the covalent functionalization. The spectra of exfoliated MoS_2 and WS_2 were compared with the ones of the respective CD-MoS_2 and CD-WS_2 hybrids, obtained upon excitation under on-resonance conditions at 633 nm and normalized at the A_{1g} mode at 404 cm^{-1} (Figure 5.5). In this way, it was found that the intensity of the 2LA(M) band of MoS_2, located at 447 cm^{-1} and associated to disorder and defects,[9] decreased after the functionalization of MoS_2 with f-CDs, as a consequence of the reduced number of S defects (Figure 5.5a). Moreover, the absence of the characteristic phonon modes of metallic polytype MoS_2 so-called J_1, J_2 and J_3 at 150, 225 and 325 cm^{-1}, respectively,[10-11] ascertained the semiconducting behavior of MoS_2 in the CD-MoS_2 hybrid material. Regarding CD-WS_2, bands due to 2LA(M), E^1_{2g}, and A_{1g}, upon on-resonance excitation at 514 nm, were found at 350, 354 and 419 cm^{-1}, with the intensity of the 2LA(M) mode decreased by 20% as compared to exfoliated WS_2 (Figure 5.5b). Furthermore, for both CD-MoS_2 and CD-WS_2, the A_{1g} and E^1_{2g} modes red-shifted by 1-2 cm^{-1} as compared to the values registered for exfoliated MoS_2 and WS_2, respectively. The latter is attributed to intrahybrid charge-transfer phenomena developed between f-CDs and the TMDs, in accordance with literature reports.[12-13]

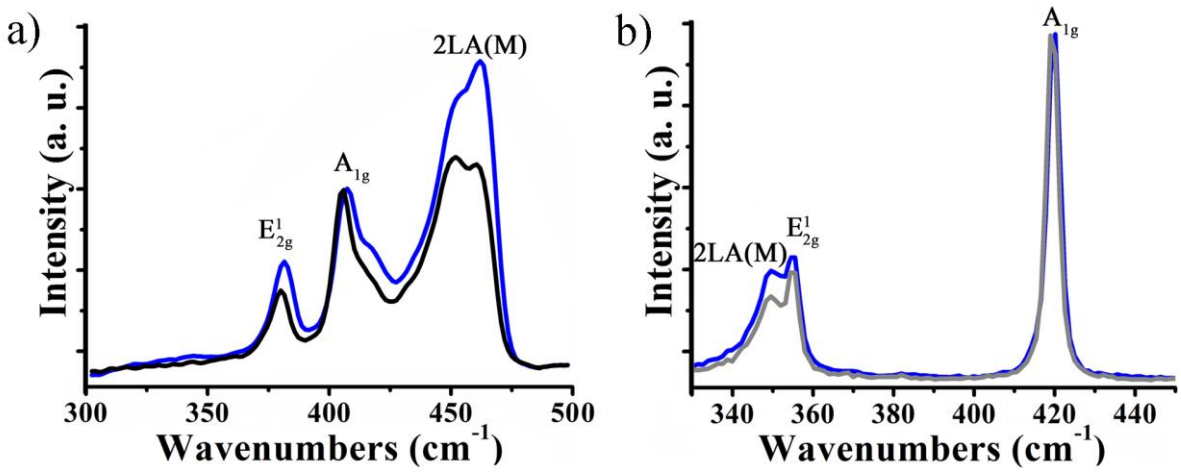

Figure 5.5. Raman spectra normalized at A^1_g mode for (a) exfoliated MoS_2 (blue) and CD-MoS_2 (black) at λ_{exc} 633 nm, and (b) exfoliated WS_2 (blue) and CD-WS_2 (grey) at λ_{exc} 514 nm.

Since CDs are highly fluorescent, weak and broad Raman bands attributed to –NC=O, C=O and C-H units (1700-1200 cm^{-1} and 700-500 cm^{-1}) were observed for both CD-MoS_2 and CD-WS_2 only upon excitation at 1064 nm (Figure 5.6).

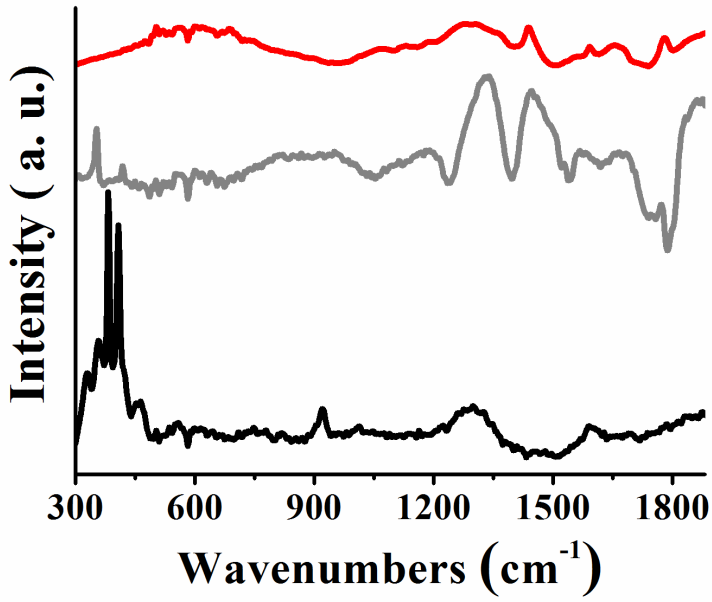

Figure 5.6. Raman spectra (1064 nm) for CDs (red), CD-MoS_2 (black) and CD-WS_2 (grey).

TGA was employed for evaluating the loading of CDs conjugated onto MoS_2 and WS_2 in CD-MoS_2 and CD-WS_2. When heated under nitrogen atmosphere, f-CDs lost the 65% of mass before reaching 500ºC (Figure 5.7). Since MoS_2 and WS_2 are thermally stable in that temperature range, the observed mass loss at 500 ºC for CD-MoS_2 and CD-WS_2, 7.5% and 3.0% respectively, is related to the decomposition of f-CDs present

in the two hybrids. It should be noticed that tungsten atoms are around two times heavier than molybdenum atoms, thus, for an equivalent load of CDs, the WS_2 weight percentage in CD-WS_2 is considerably greater than the MoS_2 weight percentage in CD-MoS_2. Taking this into account, the functionalization rates result similar in the two hybrids. Moreover, although this is a relatively small mass loss, it is consistent with the edge functionalization of the limited S vacant sites of MoS_2 and WS_2.[3]

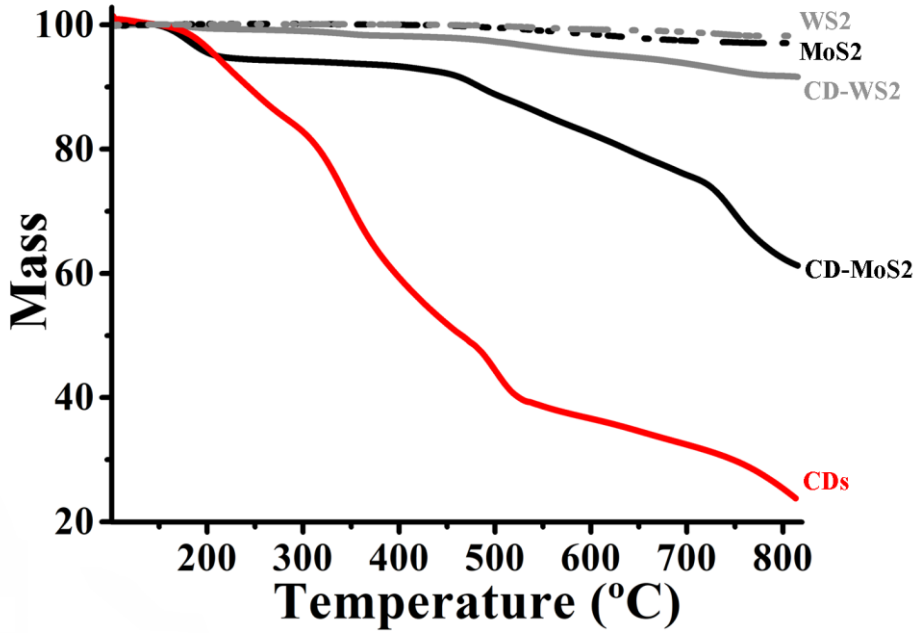

Figure 5.7. Thermographs for CDs (red), exfoliated MoS_2 (dotted black), exfoliated WS_2 (dotted gray), CD-MoS_2 (black), and CD-WS_2 (grey).

The morphology of CD-MoS_2 and CD-WS_2 hybrids were imaged by HR-TEM. A few drops of a dispersion of the materials in hexane were deposited on the TEM grid and imaged after the solvent was evaporated. Extensive imaging of several different areas and flakes of the CD-MoS_2 and CD-WS_2 hybrid materials revealed that the size of MoS_2 and WS_2 is in the order of few hundred nanometres, e.g. around 200-400 nm (Figure 5.8).

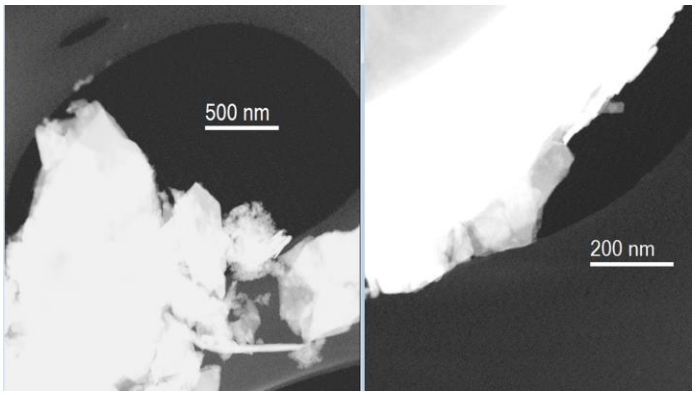

Figure 5.8. Representative low-magnification HR-STEM-ADF images for CD-MoS_2 (left) and CD-WS_2 (right).

Although mostly oligolayered flakes were observed, most likely due to restacking of the TMDs during the drying process of the sample after depositing it on the TEM grid, the presence of some monolayered ones were also identified. In order to get better insight on CD-MoS_2 and CD-WS_2, TEM studies complemented with spatially-resolved electron energy loss spectroscopy (EELS) were performed. Figures 5.9a and 5.10a show high angle annular dark field (HAADF) scanning TEM (STEM) micrographs for CD-MoS_2 and CD-WS_2, respectively. Based on the following spectroscopic/chemical TEM analyses, the bright small objects observed in these images was assigned to f-CDs covalently anchored on TMD flakes. This is confirmed by energy dispersive X-ray spectroscopy (EDS) analyses (Figures 5.9b and 5.10b) and EELS (Figures 5.9c-e and 5.10c-e). Figure 5.9c displays an ADF micrograph of CD-MoS_2 and an EELS spectrum-image (SPIM) was recorded in the red marked rectangular area. Three EEL spectra were extracted in the highlighted square regions (Figure 5.9e(i)-(iii)). Each of these three EEL spectra corresponds to the sum of 9 spectra (3x3 probe positions of the SPIM). The S-$L_{2,3}$ and Mo-M edges are visible in the three spectra and correspond to MoS_2.[14-15] It is worth mentioning that no MoO_x was observed highlighting the high quality and purity of the materials. In addition, C was detected in specific areas, see the presence of the C-K edge (Figure 5.9e(ii)-(iii)). This C-K edge, which is superposed to the Mo-$M_{4,5}$ edge, is associated with the presence of CDs within the CD-MoS_2 hybrid. The chemical C map obtained from the analysis of C-K edge (Figure 5.9d) clearly supports this finding.[14-15] Indeed, f-CDs are observed not only in the ADF-STEM micrograph (Figure 5.9c) but also in this C-map (Figure 5.9d). Similar assays were performed for CD-WS_2 and from TEM analyses (Figures 5.10a-e) the presence of f-CDs attached on WS_2 was confirmed.

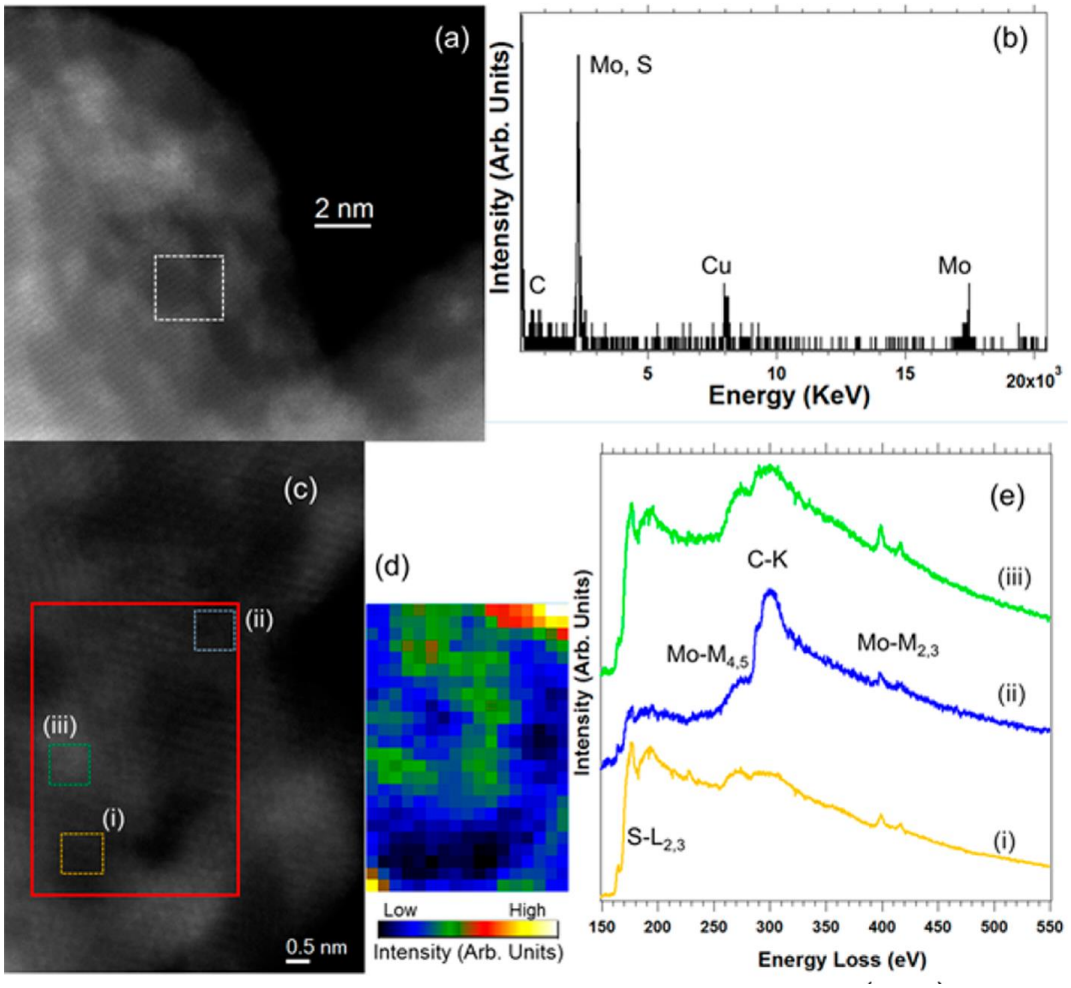

Figure 5.9. Representative HRSTEM-ADF images for (a, d) CD-MoS2. (b) EDS acquired on the squared white area in (a). In the red regions of (c) spectra images of SR-EELS were recorded. (d) Carbon elemental map extracted from the integrated intensity of the C-K edge of the EELS spectrum image recorded in the red area in (c). (e) Three spectra from the sum of nine (3 × 3) EEL spectra extracted from the marked areas of the EELS SPIM of (c). The C-K edge (~284 eV) is observed in (ii) and (iii) superposed with the Mo-M edge. The S-L2,3 and Mo-M edge of MoS2 are visible in the three spectra ((i)−(iii)).

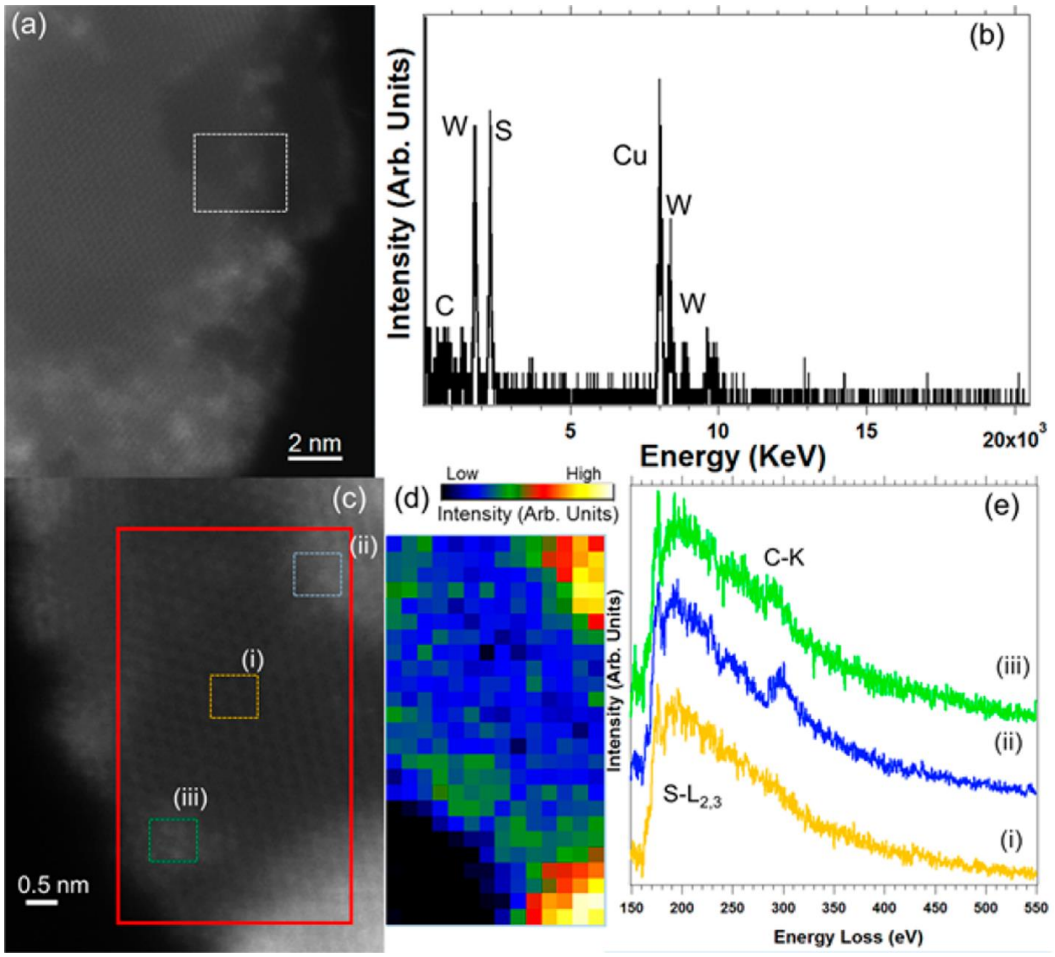

Figure 5.10. Representative HRSTEM-ADF images for (a, d) CD-WS2. (b) EDS acquired on the squared white area in (a). In the red regions of (c) spectra images of SR-EELS were recorded. (d) Carbon elemental maps extracted from the integrated intensity of the C-K edge of the two EELS spectra image recorded in the red area in (c). (e) Three spectra from the sum of 16 (4 × 4) EEL spectra extracted from the EELS SPIM of (c), showing the S-L2,3 and C-K (in this case only in (ii) and (iii)) edges. The C-K edge (~284 eV) is observed in (ii) and (iii). The S-L2,3 edge is visible in the three spectra ((i)−(iii)).

The CD-MoS_2 and CD-WS_2 were analyzed by electronic absorption and fluorescence spectroscopy. The UV-Vis spectra of CD-MoS_2 and CD-WS_2 (Figure 5.11) confirmed the preservation of the semiconducting monolayered form, characterized by the bands centered at 680, 620, 485, 400 nm, and 645, 535, 475, 420 nm, for MoS_2 and WS_2 respectively, in addition to continuous absorption throughout the visible region due to the presence of both TMDs and f-CDs (Figure 5.11a). Unfortunately, the strong absorption features of TMDs masked the broad band of f-CDs, appearing at 370 nm (Figure 5.3a), thus impeeding to investigate the electronic interaction between the two materials in the ground state. Nevertheless, clear changes are observed in the excited state, where the strong emission of f-CDs, centred at 470 nm upon excitation at 370 nm,

was found blue-shifted by 30 nm, at 440 nm, and quantitatively quenched in both CD-MoS_2 and CD-WS_2 (Figure 5.11b).

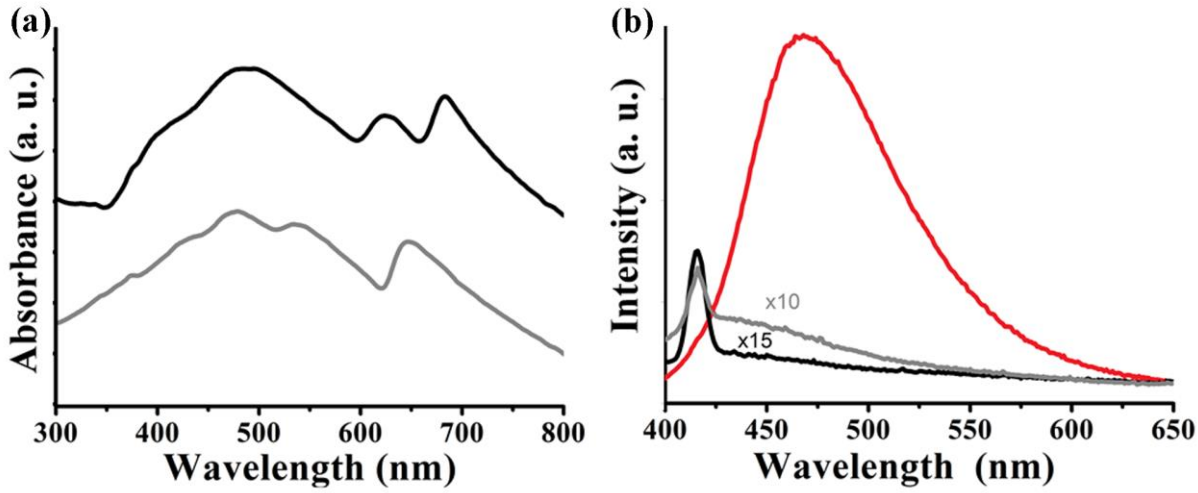

Figure 5.11. (a) Absorption and (b) emission spectra (λ_{ex} = 370 nm) of CD-MoS2 (black), CD-WS2 (gray), and f-CDs (red), in DMF.

Furthermore, time-resolved fluorescence spectroscopy confirmed the existence of an additional deactivation path in the hybrids. In fact, upon excitation at 376 nm, f-CDs decay was found to be monoexponential, with a lifetime of 6.3 ns. In contrast, CD-MoS_2 and CD-WS_2 decays resulted in biexponential curves, with a lifetime for the faster component of 1.2 and 1.1, corresponding to the quenching of singlet excited state of f-CDs in CD-MoS_2 and CD-WS_2, respectively. The electrochemical behavior of CD-MoS_2 and CD-WS_2 was investigated in DMF (Figure 5.12). The cyclic voltammogram (CV) of exfoliated MoS_2 revealed irreversible oxidations at E_{pa} = -0.08 and 0.48 V and reductions at E_{pc} = -1.20 and -1.69 V vs Fc/Fc^+. In CD-MoS_2, the first oxidation wave was too broad to pick the peak potential, while the second one was better defined with an E_{pa} = 0.54 V. The two reductions were located at E_{pc} = -1.48 and -2.20 V as a consequence of the covalent functionalization. The CV of exfoliated WS_2 revealed irreversible oxidations at E_{pa} = 0.23 and 0.44 V and reductions at E_{pc} = -1.40 and -1.98 V. Upon covalent attachment of CDs, the oxidation waves broadened, making it difficult to identify the peak potential, while the reduction was anodically shifted to E_{pc} = -1.37 and -1.63 V. Importantly, both MoS_2 and WS_2 were found to be electroactive and such property persisted upon chemical functionalization with CDs. The facile oxidation of MoS_2 over WS_2 suggests it to be better electron donor. The CV of CDs revealed no measurable electrochemical activity within the potential window.

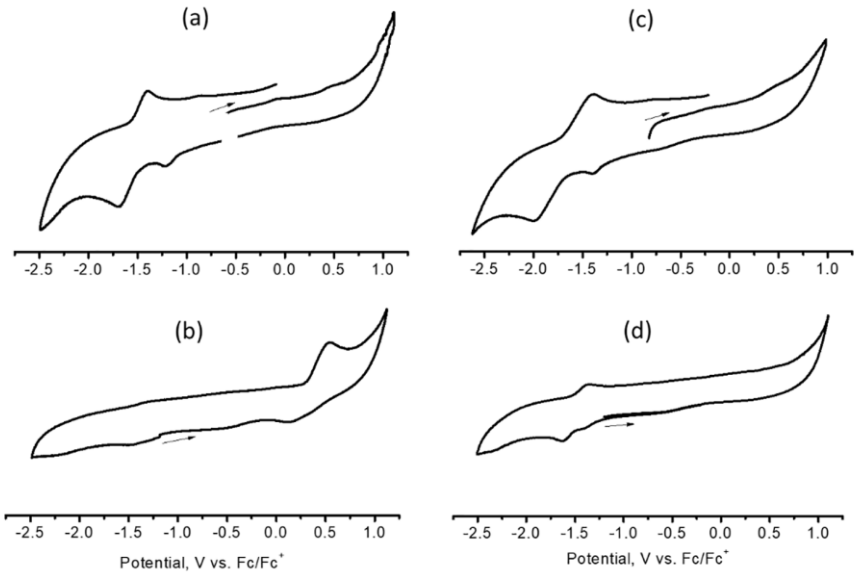

Figure 5.12. Cyclic voltammograms of (a) exfoliated MoS_2, (b) exfoliated WS_2, (c) CD-MoS_2, and (d) CD-WS_2 in DMF containing 0.1 M of n-Bu_4NClO_4 as electrolyte. Scan rate = 100 mV/s.

Differential spectral changes observed during the first oxidation and reduction of MoS_2 and WS_2 are shown in Figure 5.13. In both TMDs, reduction in peak intensity of the neutral species was observed, more so for MoS_2 compared to WS_2. Some positive spectral features in the 300-450 nm range were observed for MoS_2 during oxidation.

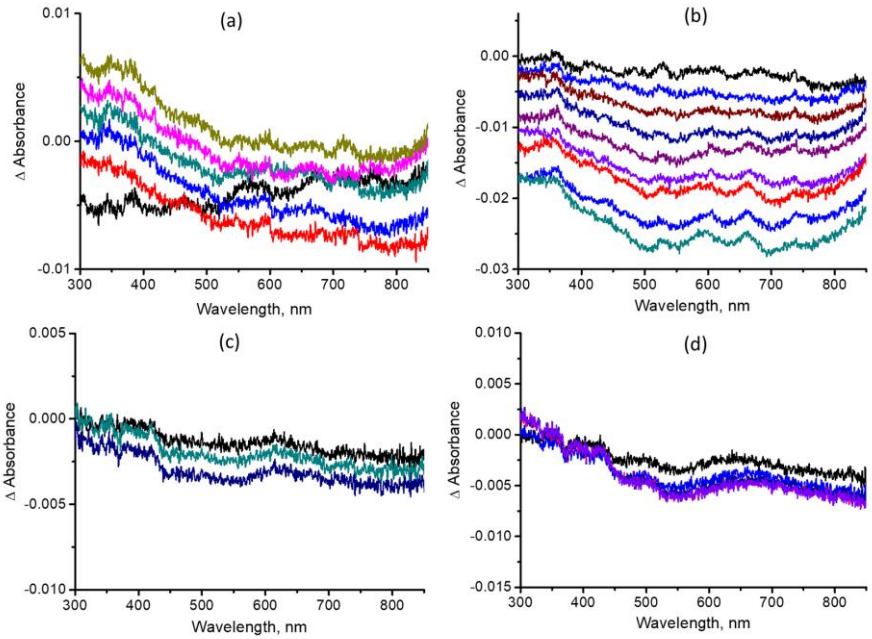

Figure 5.13. Spectral changes observed during (a) first oxidation and (b) first reduction of exfoliated MoS_2, and (c) first oxidation and (d) first reduction of exfoliated WS_2 in DMF containing 0.2 M *n*-BuN_4ClO_4 as electrolyte.

The excited state events were probed by femtosecond pump-probe transient absorption spectroscopy in DMF, where dispersion of the hybrids was appreciable (Figure 5.14). The samples were excited at 370 nm, which corresponds mainly to f-CDs excitation, and at 425 nm, which corresponds mainly to TMDs excitation. In agreement with literature reports,[16-17] immediately after 425 nm excitation of exfoliated MoS_2, three minima at 503, 637 and 696 nm due to excitonic transitions as seen in the absorption spectrum, and two maxima at 595 and 663 nm corresponding to induced absorption of B and A excitons, were observed (Figure 5.14a). During the first 10 ps, all peaks experienced blue shift ascribed to cooling of hot excitons and/or interexcitonic interactions. In the case of exfoliated WS_2, two minima at 545, and 652 nm (B and A excitons, by comparison with the absorption spectrum) and two maxima at 516 and 617 nm were observed (Figure 5.14b). The peak positions also experienced a small blue-shift of 2 nm within the first 10 ps. Also exciting at 370 nm (Figure 5.14c,d), the spectra of exfoliated MoS_2 and WS_2 revealed the above-mentioned features, however, with much diminished peak intensities compared to that at λ_{exc} 425 nm. These observations suggest that at λ_{exc} 370 nm, in addition to f-CDs, both MoS_2 and WS_2 also get excited to some extent.

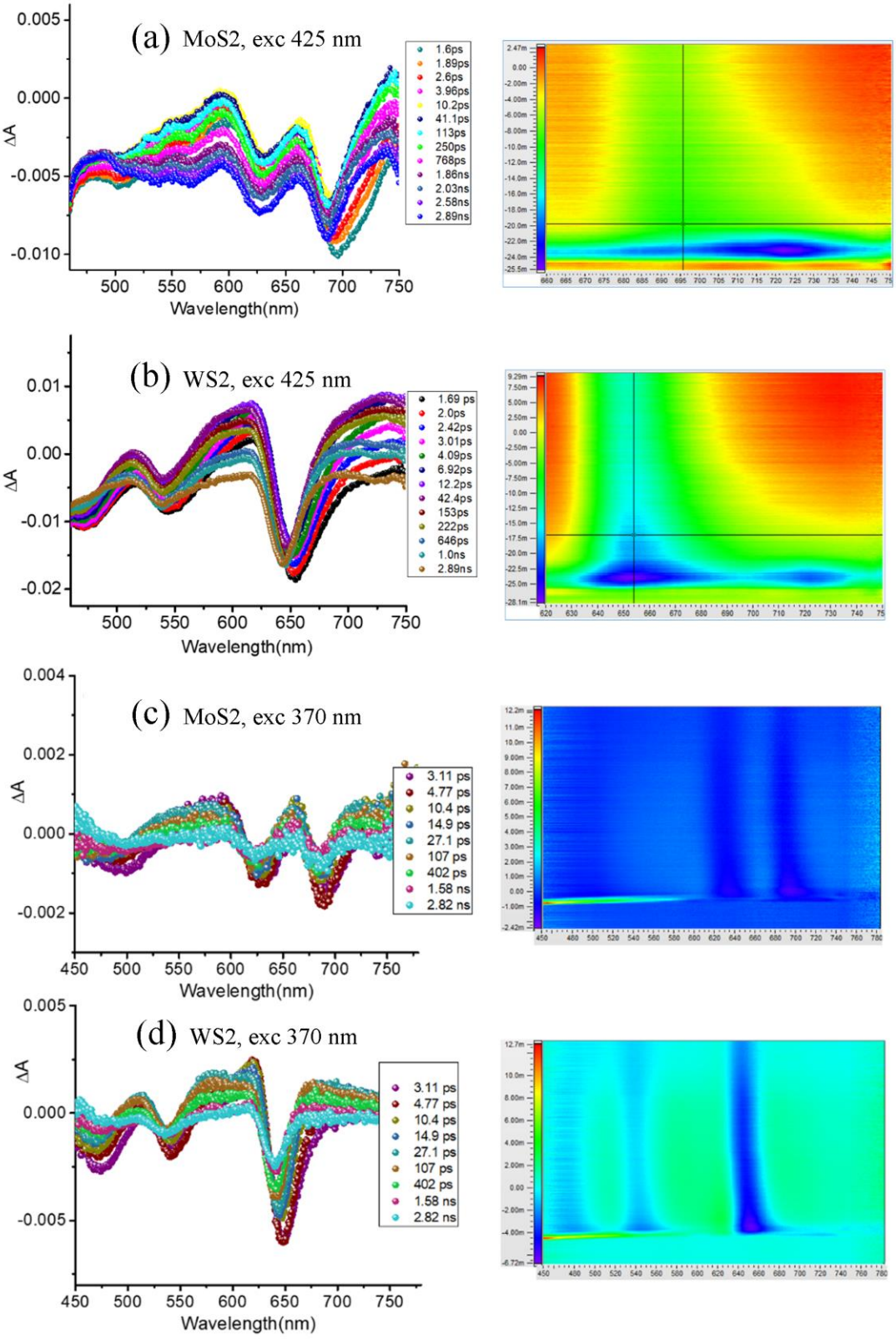

Figure 5.14. Femtosecond transient absorption spectra at the indicated delay times of exfoliated (a, c) MoS_2 and (b, d) WS_2, in DMF at the excitation wavelength of 425 nm (a,b) and 370 nm (c,d). The right-hand panel shows intensity-wavelength maps.

Figure 5.15 shows the transient absorption spectra and intensity-wavelength maps of f-CDs, CD-MoS_2 and CD-WS_2 dispersions in DMF at λ_{exc} 370 nm, mainly exciting the f-CDs. The transient spectra of f-CDs revealed positive peaks at 460 and 590 nm (Figure 5.15a) originating from transitions starting from the excited state of f-CDs. The decay of these peaks was rather slow, reflecting the persistence of the excited state and accordingly with the long fluorescence lifetime of f-CDs (6.3 ns). Interestingly, when CD-MoS_2 and CD-WS_2 were excited at 370 nm, the peaks corresponding to the excited CDs revealed rapid deactivation with simultaneous development of strong excitonic peaks of MoS_2 and WS_2, more for CD-MoS_2 than for CD-WS_2 (Figure 5.15b,c). These results are in agreement with the presence in the hybrids of a new non-radiative deactivation pathway, as observed by steady-state and time-resolved fluorescence spectroscopy, and indicate the occurrence of energy transfer from singlet excited CDs to MoS_2 and WS_2. In both hybrids, the excitation transfer was complete within 4-5 ps, indicating an efficient process.

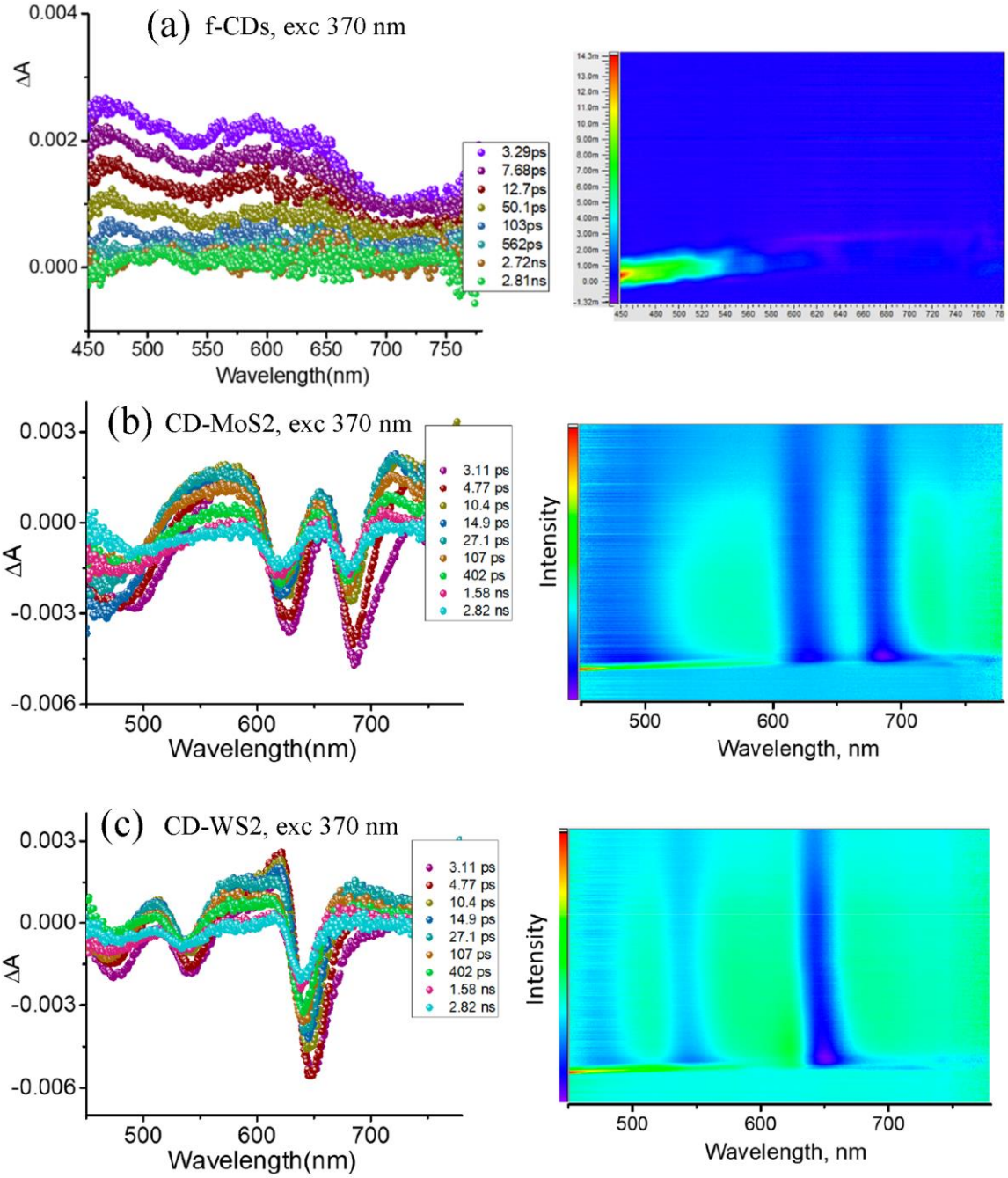

Figure 5.15. Femtosecond transient spectra of (a) f-CDs, (b) CD-MoS_2, and (c) CD-WS_2 in DMF (λ_{exc} 370 nm). The right-hand panel shows intensity-wavelength maps.

Next, the hybrids were excited at 425 nm, where majority of MoS_2 and WS_2 have absorbance. The transient spectral features of CD-MoS_2 (Figure 5.16a) were distinctly different from that of exfoliated MoS_2 (Figure 5.14a), especially with respect to the peak time profiles (see intensity-wavelength maps). Figure 5.16a (iii) shows the time profile of the 688 nm peak of exfoliated MoS_2 and CD-MoS_2 corresponding to the excitonic peak at 688 nm. The recovery of the exciton peak was slow for CD-MoS_2 suggesting occurrence of excited state events from the excited MoS_2 to the covalently

linked CDs. Earlier, a facile oxidation was observed for MoS_2 (E_{pa} = -0.08 V) suggesting that it could act as an electron donor generating charge separated state.[18-21] In such an event, charge transfer from a dissociated excitonic state would be promoted to f-CDs LUMO, generating a charge separated state. The hole in MoS_2 layer would recover slowly due to a charge recombination process.

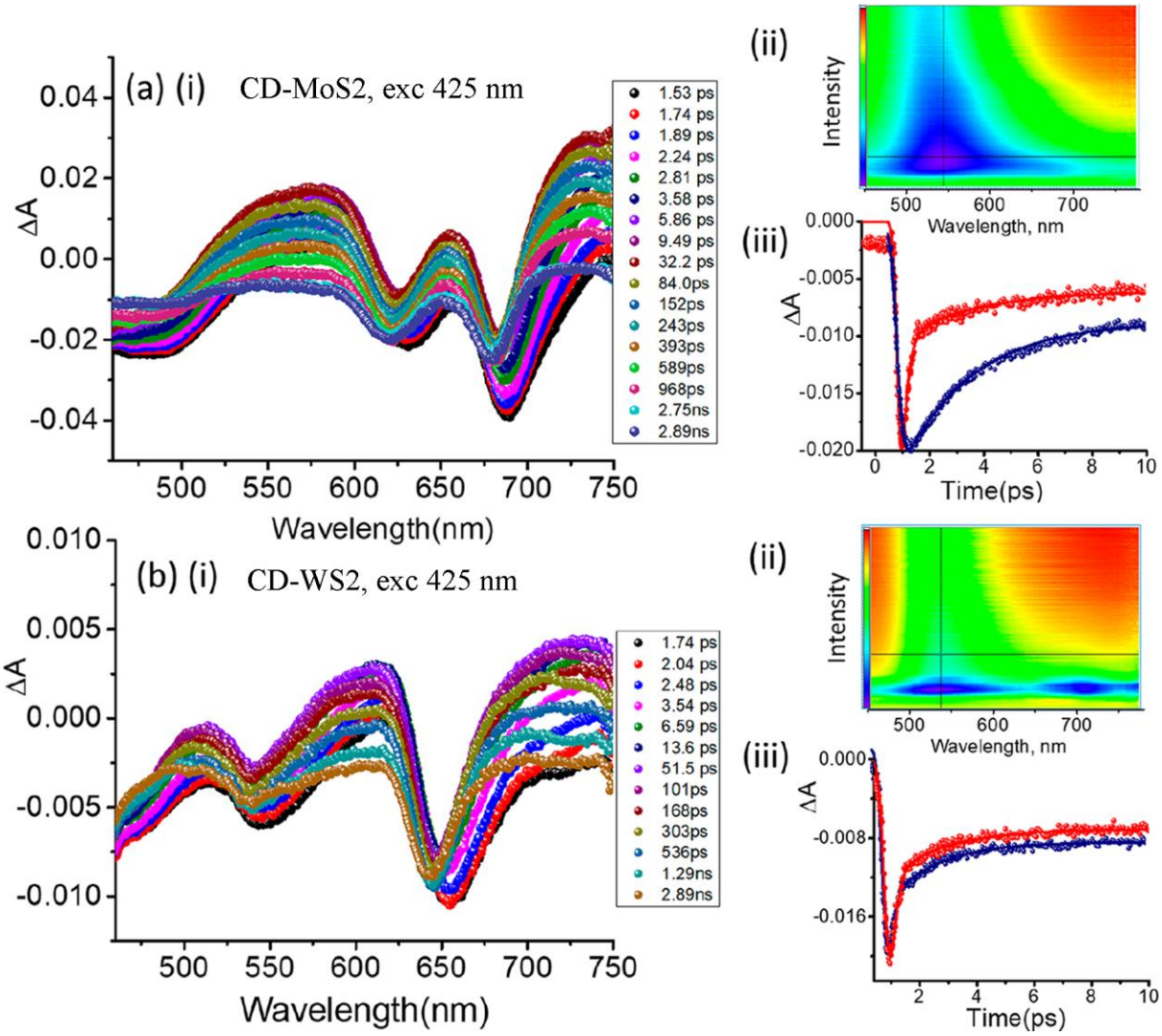

Figure 5.16. Femtosecond transient spectra of (a) CD-MoS_2, and (b) CD-WS_2, in DMF (λ_{exc} 425 nm). The right-hand panels show (ii) intensity-wavelength map and (iii) an overlap time profile of the 688 nm of CD-MoS_2 (blue) and exfoliated MoS_2 (red) and 652 nm of CD-WS_2 (blue) and exfoliated WS_2 (red).

Further, the transient data of exfoliated MoS_2 and CD-MoS_2 were subjected to global analysis for kinetic evaluations (Figure 5.17). Decay associated spectra of exfoliated MoS_2 revealed three major components; the spectrum at 2.3 ps consists of positive peaks at the spectral range, where excitonic peaks are expected. The spectrum at 1.1 ns had decay of positive transients. The final component with over 3 ns related to only the

excitonic signals with positive shift relative to A exciton. Earlier, for the ultimate decay of the excitons, a lifetime of around 30 ns was established.[16] Interestingly, for CD-MoS_2, at least 5 components were needed for satisfactory fit. The component at 1 ps was too fast to be assigned to any excited state process as several ultrafast processes such as vibrational cooling, solvent relaxation, etc. occur. The 4.2 and 1.3 ps components had features of excitons in the growth and decay, respectively. The 246 ps component had features in the 450-550 nm range, ascribed to trionic state that revealed faster decay. The long-lived decay component had only the excitonic features similar to that observed for unmodified MoS_2. These results suggest that the charge separation occurs with a time constant of about 250 ps in the CD-MoS_2 hybrid.

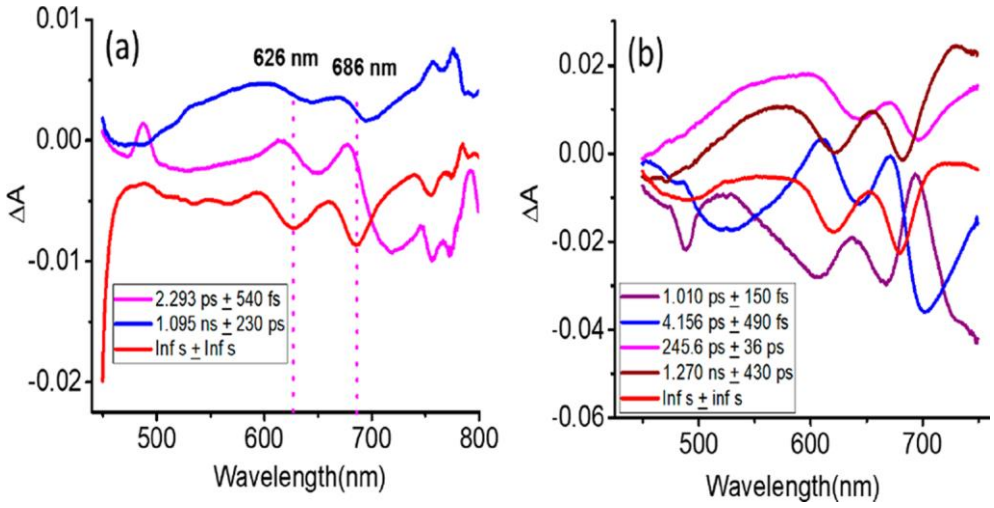

Figure 5.17. Decay associated spectra of (a) exfoliated MoS_2, and (b) CND-MoS_2 for the transient data shown in Figure 5.14a and Figure 5.16a.

Transient spectra recorded for CD-WS_2 (Figure 5.16b) were close to that of unmodified WS_2 (Figure 5.14b). The time profiles of the 652 nm peak (Figure 5.16b (iii)) were superimposable suggesting lack of major excited state events such as charge transfer from excited WS_2 to f-CDs. This could be rationalized to the harder oxidation of WS_2 (E_{pa} = 0.23) that would dampen any charge transfer events due to energy considerations. Hence, no further analysis was performed on this hybrid material.

5.5. Conclusions

In summary, modified CDs bearing 1,2-dithiolane groups were employed for the covalent functionalization of exfoliated MoS_2 and WS_2. The formation of the covalent CD-MoS_2 and CD-WS_2 hybrids was proved by complementary spectroscopic, thermal

and electron microscopy imaging techniques. Furthermore, cyclovoltammetry experiments showed that MoS_2 was a better electron donor compared to WS_2. The excited state of the hybrids was investigated by steady-state fluorescence spectroscopy, time-resolved fluorescence spectroscopy and transient absorption spectroscopy, and compared with the one of f-CDs and the exfoliated TMDs. In this way it was demonstrated the ocurrence of ultrafast energy transfer from the excited f-CDs to MoS_2 or WS_2 upon irradiation of the hybrids at 370 nm. Additionally, exciting the TMDs within the hybrid materials at 425 nm, charge transfer in CD-MoS_2 but not in CD-WS_2 was seen. The electron transfer processes discovered in this novel material certainly can be of interest for the development of donor-acceptor components in energy harvesting devices and further studies for the optimization of this system are recommended.

5.6. References

1. Ryder, C. R.; Wood, J. D.; Wells, S. A.; Hersam, M. C., Chemically Tailoring Semiconducting Two-Dimensional Transition Metal Dichalcogenides and Black Phosphorus. *ACS Nano* **2016,** *10* (4), 3900-3917.
2. Bertolazzi, S.; Gobbi, M.; Zhao, Y.; Backes, C.; Samorì, P., Molecular chemistry approaches for tuning the properties of two-dimensional transition metal dichalcogenides. *Chemical Society Reviews* **2018,** *47* (17), 6845-6888.
3. Canton-Vitoria, R.; Sayed-Ahmad-Baraza, Y.; Pelaez-Fernandez, M.; Arenal, R.; Bittencourt, C.; Ewels, C. P.; Tagmatarchis, N., Functionalization of MoS2 with 1,2-dithiolanes: toward donor-acceptor nanohybrids for energy conversion. *npj 2D Materials and Applications* **2017,** *1* (1), 13.
4. Knirsch, K. C.; Berner, N. C.; Nerl, H. C.; Cucinotta, C. S.; Gholamvand, Z.; McEvoy, N.; Wang, Z.; Abramovic, I.; Vecera, P.; Halik, M.; Sanvito, S.; Duesberg, G. S.; Nicolosi, V.; Hauke, F.; Hirsch, A.; Coleman, J. N.; Backes, C., Basal-Plane Functionalization of Chemically Exfoliated Molybdenum Disulfide by Diazonium Salts. *ACS Nano* **2015,** *9* (6), 6018-6030.
5. Backes, C.; Berner, N. C.; Chen, X.; Lafargue, P.; LaPlace, P.; Freeley, M.; Duesberg, G. S.; Coleman, J. N.; McDonald, A. R., Functionalization of Liquid-Exfoliated Two-Dimensional 2H-MoS2. *Angewandte Chemie International Edition* **2015,** *54* (9), 2638-2642.
6. Liu, T.; Wang, C.; Cui, W.; Gong, H.; Liang, C.; Shi, X.; Li, Z.; Sun, B.; Liu, Z., Combined photothermal and photodynamic therapy delivered by PEGylated MoS2 nanosheets. *Nanoscale* **2014,** *6* (19), 11219-11225.
7. Cheng, H.; Dong, N.; Bai, T.; Song, Y.; Wang, J.; Qin, Y.; Zhang, B.; Chen, Y., Covalent Modification of MoS2 with Poly(N-vinylcarbazole) for Solid-State Broadband Optical Limiters. *Chemistry – A European Journal* **2016,** *22* (13), 4500-4507.
8. McAdams, S. G.; Lewis, E. A.; Brent, J. R.; Haigh, S. J.; Thomas, A. G.; O'Brien, P.; Tuna, F.; Lewis, D. J., Dual Functionalization of Liquid-Exfoliated Semiconducting 2H-MoS2 with Lanthanide Complexes Bearing Magnetic and Luminescence Properties. *Advanced Functional Materials* **2017,** *27* (42), 1703646.

9. Li, H.; Zhang, Q.; Yap, C. C. R.; Tay, B. K.; Edwin, T. H. T.; Olivier, A.; Baillargeat, D., From Bulk to Monolayer MoS2: Evolution of Raman Scattering. *Advanced Functional Materials* **2012,** *22* (7), 1385-1390.
10. Nayak, A. P.; Pandey, T.; Voiry, D.; Liu, J.; Moran, S. T.; Sharma, A.; Tan, C.; Chen, C.-H.; Li, L.-J.; Chhowalla, M.; Lin, J.-F.; Singh, A. K.; Akinwande, D., Pressure-Dependent Optical and Vibrational Properties of Monolayer Molybdenum Disulfide. *Nano Letters* **2015,** *15* (1), 346-353.
11. Jiménez Sandoval, S.; Yang, D.; Frindt, R. F.; Irwin, J. C., Raman study and lattice dynamics of single molecular layers of ${\mathrm{MoS}}_{2}$. *Physical Review B* **1991,** *44* (8), 3955-3962.
12. Chakraborty, B.; Bera, A.; Muthu, D. V. S.; Bhowmick, S.; Waghmare, U. V.; Sood, A. K., Symmetry-dependent phonon renormalization in monolayer MoS${}_{2}$ transistor. *Physical Review B* **2012,** *85* (16), 161403.
13. Shi, Y.; Huang, J.-K.; Jin, L.; Hsu, Y.-T.; Yu, S. F.; Li, L.-J.; Yang, H. Y., Selective Decoration of Au Nanoparticles on Monolayer MoS2 Single Crystals. *Scientific Reports* **2013,** *3*, 1839.
14. Arenal, R.; De Matteis, L.; Custardoy, L.; Mayoral, A.; Tence, M.; Grazu, V.; De La Fuente, J. M.; Marquina, C.; Ibarra, M. R., Spatially-Resolved EELS Analysis of Antibody Distribution on Biofunctionalized Magnetic Nanoparticles. *ACS Nano* **2013,** *7* (5), 4006-4013.
15. Arenal, R.; March, K.; Ewels, C. P.; Rocquefelte, X.; Kociak, M.; Loiseau, A.; Stéphan, O., Atomic Configuration of Nitrogen-Doped Single-Walled Carbon Nanotubes. *Nano Letters* **2014,** *14* (10), 5509-5516.
16. Wibmer, L.; Lages, S.; Unruh, T.; Guldi, D. M., Excitons and Trions in One-Photon- and Two-Photon-Excited MoS2: A Study in Dispersions. *Advanced Materials* **2018,** *30* (12), 1706702.
17. Jiang, T.; Chen, R.; Zheng, X.; Xu, Z.; Tang, Y., Photo-induced excitonic structure renormalization and broadband absorption in monolayer tungsten disulphide. *Opt. Express* **2018,** *26* (2), 859-869.
18. Bettis Homan, S.; Sangwan, V. K.; Balla, I.; Bergeron, H.; Weiss, E. A.; Hersam, M. C., Ultrafast Exciton Dissociation and Long-Lived Charge Separation in a Photovoltaic Pentacene–MoS2 van der Waals Heterojunction. *Nano Letters* **2017,** *17* (1), 164-169.
19. Kafle, T. R.; Kattel, B.; Lane, S. D.; Wang, T.; Zhao, H.; Chan, W.-L., Charge Transfer Exciton and Spin Flipping at Organic–Transition-Metal Dichalcogenide Interfaces. *ACS Nano* **2017,** *11* (10), 10184-10192.
20. Nguyen, E. P.; Carey, B. J.; Harrison, C. J.; Atkin, P.; Berean, K. J.; Della Gaspera, E.; Ou, J. Z.; Kaner, R. B.; Kalantar-zadeh, K.; Daeneke, T., Excitation dependent bidirectional electron transfer in phthalocyanine-functionalised MoS2 nanosheets. *Nanoscale* **2016,** *8* (36), 16276-16283.
21. Choi, J.; Zhang, H.; Choi, J. H., Modulating Optoelectronic Properties of Two-Dimensional Transition Metal Dichalcogenide Semiconductors by Photoinduced Charge Transfer. *ACS Nano* **2016,** *10* (1), 1671-1680.

6. GENERAL CONCLUSION AND OUTLOOK

6.1. General conclusions

This thesis covers three main aspects of CDs' investigation. The initial one addresses to the fundamental nature and fluorescent behavior of CDs. The origin of the fluorescence, i.e. how chemical structure is related to CDs optical properties, is an interesting issue that at the state of the art has not been satisfactorily established, being the current theories shallow or incomplete. Through detailed structural studies, optical characterization and DFT calculations, the first part of the thesis accomplishes to identify the organic structures and the forces originating the blue fluorescence, thus providing an important contribution to the debate. Exploiting the knowledge gained by these studies, the second aspect addressed by this work is the improvement of the control on the CDs chemical structure and functionalities during the synthesis. Thus, in here a new method for controlling the structure and the chemical properties of the polymer nanoparticles is provided, furnishing an extremely versatile tool for the design of CDs based material such as sensors and drug nanocarriers. The third and final part of the work focuses on the preparation of CDs hybrid materials in view of photocatalysis and energy conversion-related applications. For the preparation of the hybrids, transition metal dichalcogenides (MoS_2 and WS_2) were chosen because of their well-known donor-acceptor properties and coupled with CDs by non-covalent and covalent strategies. In this way, photoactive materials were successfully obtained, whose electronic properties can be of interest for potential applications.

The specific conclusions for each different work, described in chapters two to five are summarized in the following:

- ***Chapter two: Elucidation of the relationship between polymer structure and blue fluorescence of carbon dots.***

With the purpose to identify the CDs structural elements involved in the fluorescence emission, three model samples were prepared, by varying the reagents or the synthetic method. The chemical structure and the size of the samples were deeply characterized by means of a wide set of techniques, including AFM, DLS, elemental analysis, IR, XPS and NMR. In this way, it was proved that the formed CDs are produced by polycondensation and consists of polyamide particles of about 1-2 nm size. Moreover, by comparing the optical properties of each sample, it was proved that the bright blue

fluorescence emission should be related unambiguously to the determined polyamide structure, excluding thus the role of other minor synthesis by-products. The understanding of the fluorescence mechanism was achieved by DFT and TDDFT calculations. The modelled CDs, whose structure was based on the experimental results, showed that strong intra-molecular H-bonds are responsible for the rigid and compact entanglement of the polymer structure. The rigidity hinders the vibrational and rotational motions, promoting the radiative relaxation. Amide and carboxylic acids were found to participate to the fluorescence mechanism respectively as the major contribution to the HOMO and the LUMO involved in the transition. Due to the spatial separation of these orbitals, the process was therefore recognized as a photo-induced charge transfer. These findings may certainly be of interest for the development of the CDs studies, increasing the comprehension of their chemical and optical properties as well as providing the basis for the tailoring and enhancement of those.

- ***Chapter three: A versatile method for the controllable room-temperature synthesis and in-situ functionalization of fluorescent carbon dots.***

CDs synthesis procedures commonly involve harsh conditions and they aim to achieve the partial carbonization of the nanoparticles' structure. Based on the studies reported in Chapter 2, a simple and mild method for the preparation of fluorescent polymeric CDs was explored. In here, carbodiimide chemistry is exploited for the catalytic polycondensation at room temperature of citric acid with a set of different polyamines, obtaining blue fluorescent nanoparticles. This method offers the clear advantage of controlling the final CDs structure by choosing opportunely the precursors. Additionally, it was demonstrated that the *in-situ* functionalization of the nanoparticles can be easily achieved by quenching the polymerization with the addition of any primary amine. In this way, several types of CDs functionalization were performed, supplying an additional level of control on the final structure.

- ***Chapter four: Electronic interactions in CDs/MoS_2 electrostatic complex.***

In this study, the titration essay of a dispersion of exfoliated functionalized MoS_2 was performed by adding aliquots of a CDs solution and studying ongoing the optical properties of the forming complex by absorption and fluorescence spectroscopies. Negative charges on the CDs surface and positive charges on the MoS_2 functional groups provided the basis for the electronic interaction between the two materials. The

formation of the electrostatic complex was reflected in the strong quenching of the CDs fluorescence, prompting to an additional deactivation channel – electron and/or energy transfer – starting from the singlet excited state of CDs within the CDs/MoS_2 ensembles. Finally, the electrocatalytic performance of CDs/MoS_2 was evaluated regarding the HER and found improved in comparison with that of the individual CDs species.

- ***Chapter five: Electronic interactions in covalent CDs/TMDs hybrids.***

Covalent CDs/TMDs hybrids were prepared by functionalizing exfoliated MoS_2 and WS_2 with modified CDs bearing 1,2-dithiolane groups. Characterization by complementary spectroscopic, thermal and electron microscopy imaging techniques ascertained the success of the functionalization. Steady-state and time-resolved fluorescence spectroscopy showed the ocurrence of charge and/or energy transfer in both the hybrids. Further studies performed by transient absorption spectroscopy demonstrated that ultrafast energy transfer from the excited CDs to MoS_2 or WS_2 takes place upon irradiation at 370 nm. In addition, exciting the TMDs at 425 nm, charge transfer from the MoS_2 to the CDs is observed in CD-MoS_2, but not in CD-WS_2. The reason should be ascribed to the better electron-donor ability of MoS_2 with respect to WS_2. The electron transfer processes discovered in this novel material certainly can be of interest for the development of donor-acceptor components in energy harvesting devices and further studies for the optimization of this system are recommended.

6.2. Outlook

The results reported in this thesis have an impact on the current knowledge in the field of CDs and CDs-based materials on three levels: theory, preparation and applications.

- *Theory: comprehension of the organic structures and intra-molecular forces that originates the blue fluorescence emission.* This information provides new arguments for the interpretation of the CDs sensing and energy/charge transfer abilities that have been widely reported in literature. Besides, the understanding of the fluorescence mechanism in CDs provides the basis for the development of strategies aiming on achieving CDs with tailored optival properties as well on the rational design of new fluorescent structures, as demonstrated in Chapter 3.

- *Preparation: development of a new, versatile method for the synthesis of CDs with defined chemical structures.* The advantages of this method are multiple. On one side it allows the exploration of a large number of possibilities for building the CDs polymeric structure, playing with the choice of the precursors and functional groups. For example, this approach could be promising for investigating the tailoring of the fluorescence emission or even the generation of different types of photoluminescence, such as phosphorescence. On the other side, the suitability for analytical and medical applications can be greatly improved by this method. In fact, the control on the CDs structure and functional groups can enhance the sensitivity and specificity towards the desired analyte or pharmacological target, but also change CDs solubility or improve biocompatibility.
- *Application: development of hybrid CDs-based materials for energy applications.* Thanks to their semi-conducting nature and charge transfer ability, layered TMDs are intensively studied for the preparation of donor-acceptor components in energy conversion devices. Matching TMDs with CDs by covalent and non-covalent approaches surely add a new contribution to this field. The resulting hybrids exhibited interesting photo-induced electronic properties, which strongly encourage further investigation on these promising materials. For example, modification of the CDs structure and functional groups could open the way to the improvement of the photocatalytic or donor-acceptor ability of the hybrids.

6.3. Conclusiones generales

En este trabajo se cubren tres aspectos fundamentales de la investigación en el campo de los CDs. El primero se dirige a la naturaleza y al comportamiento fluorescente de los CDs. El origen de la fluorescencia, i.e. cómo la estructura química está relacionada con las propiedades ópticas de los CDs, es un problema interesante para el que el estado del arte no tiene todavía una solución clara, siendo las teorías actuales superficiales o incompletas. A través de detallados estudios estructurales, caracterización óptica y cálculos teóricos, la primera parte de la tesis consigue identificar las estructuras orgánicas y las fuerzas que producen la fluorescencia azul, aportando así una contribución importante al debate. Aprovechando el conocimiento ganado por estos estudios, el segundo aspecto considerado en este trabajo ha sido la mejora del control sobre la estructura química y los grupos funcionales de los CDs durante la síntesis. En este sentido, se ha presentado un nuevo método para controlar la estructura y las propiedades químicas de nanopartículas poliméricas, ofreciendo una herramienta muy versátil para el diseño de materiales basados en CDs como sensores y vectores de fármacos. La tercera y ultima parte de la tesis se focaliza en la preparación de materiales híbridos con vistas a su posible uso en aplicaciones de fotocatálisis y conversión de energía. Para la preparación de los híbridos, se han elegido dicalcogenuros de metales de transición (MoS_2 y WS_2) por sus eficaces propiedades donor-aceptor, acoplándolos a los CDs por medio de estrategias covalentes y non-covalentes. De esta manera, se han obtenido con éxito materiales fotoactivos, cuyas propiedades electrónicas pueden ser de interés para potenciales aplicaciones.

Las conclusiones específicas por cada diferente trabajo, descritas del Capítulo 2 al Capítulo 5, están resumida en los siguientes párrafos:

- ***Capítulo 2: Esclarecimiento de la relación entre estructura polimérica y fluorescencia azul en los CDs.***

Con el propósito de identificar los elementos estructurales de los CDs involucrados en la emisión de fluorescencia, se han preparado tres muestras modelo, diferentes en cuanto a reactivos o método sintético utilizados. La estructura química y el tamaño de las muestras han sido caracterizados por medio de un amplio grupo de técnicas, como son AFM, DLS, análisis elemental, IR, XPS y NMR. De esta manera, se ha probado que

los CDs formados se han producido por policondensación y consisten en nanopartículas de poliamida de aproximadamente 1-2 nm de tamaño. Además, comparando las propiedades ópticas de cada muestra, se ha probado que la emisión de fluorescencia azul está relacionada únicamente con la estructura de poliamida encontrada, excluyendo entonces el papel de otros subproductos menores de síntesis. Calculos de DFT y TDDFT han permitido lograr la comprensión del mecanismo de la fluorescencia. Los CDs modelizados, cuya estructura se ha basado en los resultados experimentales, muestran que fuertes enlaces hidrogeno intra-moleculares son los responsables del rígido y compacto entrelazamiento de la estructura polimérica. La rigidez dificulta la movilidad vibracional y rotacional, favoreciendo el mecanismo de relajación radiativo. Se ha visto además que amida y ácidos carboxílicos participan en el mecanismo de fluorescencia como la mayor contribución al HOMO y al LUMO, respectivamente, involucrados en la transición. A causa de la separación espacial de estos orbitales, el proceso ha sido reconocido como una trasferencia de carga foto-inducida. Estos descubrimientos pueden ciertamente ser de interés para el desarrollo de los estudios en el campo de los CDs, aumentando la comprensión de sus propiedades químicas y ópticas así como aportando las bases para la modificación y la mejora de las mismas.

- ***Capítulo 3: un método versátil para la síntesis controlable y a temperatura ambiente de CDs fluorescentes y su funcionalización in-situ***

Los procedimientos de síntesis de los CDs suponen a menudo unas condiciones de alta temperatura que apuntan a la parcial carbonización de la estructura de las nanopartículas. Utilizando el conocimiento conseguido en los estudios reportados en el Capítulo 2, se ha explorado aquí un método simple y suave para la síntesis de CDs poliméricos. La química de las carbodiimidas ha sido explotada para la policondensación catalizada a temperatura ambiente entre ácido cítrico y una colección de diferentes aminas, obteniendo nanopartículas con fluorescencia azul. Este método ofrece la clara ventaja de poder controlar la estructura final de los CDs con la oportuna elección de los precursores. Asimismo, se ha demostrado que la funcionalización *in-situ* de las nanoparticulas puede ser fácilmente conseguida con la incorporación de una amina primaria durante la reacción, la cual actúa como "quencher" de la polimerización. De esta manera, se han obtenido distintos tipos de funcionalización, aportando un nivel adicional de control de la estructura final.

- ***Capítulo 4: Interacciones electrónicas en complejos electroestaticos CDs/MoS_2***

En este estudio, el ensayo de valoración de una dispersión de MoS_2 exfoliado y funcionalizado se ha realizado añadiendo alícuotas de una disolución de CDs y estudiando paralelamente las propiedades ópticas del complejo que se forma por medio de espectroscopias de absorción y fluorescencia. Las cargas negativas situadas en la superficie de los CDs y las cargas positivas de los grupos funcionales en MoS_2 han creado las condiciones adecuadas para la interacción entre los dos materiales. La formación del complejo electroestático se ha ido reflejando en el fuerte "quenching" observado en la fluorescencia de los CDs, sugiriendo la presencia de un canal de desactivación adicional – transferencia de energía y/o de carga – que parte del estado excitado de los CDs en el complejo. Finalmente, el rendimiento electrocatalitico de CDs/MoS_2 ha sido evaluado en relación a la reacción de desarrollo de hidrogeno (HER), mostrándose superior comparado al rendimiento de los CDs solos.

- ***Capítulo 5: interacciones electrónicas en híbridos covalentes CDs/TMDs***

En este trabajo, se han preparado unos híbridos covalentes CDs/TMDs a través de la funcionalización de MoS_2 y WS_2 exfoliados con CDs modificados con grupos 1,2-ditiolanos. El éxito de la funcionalización ha sido confirmado por medio de técnicas espectroscópicas, termales y de microscopía complementarias. Las espectroscopías de fluorescencia han mostrado la presencia de trasferencia de carga y/o de energía foto-inducida en ambos híbridos. Estudios adicionales hechos por espectroscopia de absorción transitoria han verificado que se trata de una trasferencia de energía ultra-rápida desde el estado excitado de los CDs hasta MoS_2 y WS_2 bajo irradiación a 370 nm. Además, excitando a 425 nm, se observa una trasferencia de carga desde MoS_2 hasta los CDs en CD-MoS_2, pero no en CD-WS_2. La razón está relacionada con la mejor habilidad de MoS_2 con respecto a la de WS_2 para formar compuestos donor-aceptor. Los procesos de transferencia electrónica descubiertos en este nuevo material podrían ciertamente ser de interés para el desarrollo de compuestos donor-aceptor en sistemas para la recolección de energía y se aconsejan estudios adicionales sobre el sistema.

6.4. Perspectiva

Los resultados reportados en esta tesis tienen un fuerte impacto en el actual conocimiento en el campo de los CDs en tres niveles: teoría, preparación y aplicaciones.

- *Teoría: comprensión de las estructuras orgánicas y fuerzas intra-moleculares que generan la fluorescencia azul.* Esta información aporta nuevas argumentaciones para la interpretación de las capacidades de sensorización y trasferencia de energía/carga abundantemente reportadas en la literatura. Además, la comprensión del mecanismo de fluorescencia en los CDs sienta las bases para el desarrollo de estrategias dirigidas a la alteración de las propiedades ópticas así como al diseño racional de nuevas estructuras fluorescentes, como demostrado en el Capítulo 3.
- *Preparación: desarrollo de un nuevo y versátil método para la síntesis de CDs con estructuras químicas definidas.* Las ventajas de este método son múltiples. Por un lado permite la exploración de un gran número de posibilidades para construir la estructura polimérica de los CDs, jugando con la elección de los precursores y de los grupos funcionales. Por ejemplo, este método puede ser prometedor para la investigación y la modificación de la emisión de fluorescencia o también para la generación de diferentes tipos de fotoluminiscencia, como la fosforescencia. Por otro lado, la idoneidad de los CDs para aplicaciones analíticas y médicas podría mejorar mucho con este método. De hecho, el control sobre la estructura y los grupos funcionales puede aumentar la sensibilidad y la especifidad hacia el analito o el objetivo farmacológico deseado, así como poder cambiar la solubilidad o mejorar la biocompatibilidad de los CDs.
- *Aplicaciones: desarrollo de materiales híbridos basados en los CDs para aplicaciones energéticas.* Gracias a su naturaleza de semi-conductores y a su habilidad de trasferencia de carga, los TMDs en capas están siendo estudiado intensamente para la preparación de compuestos donor-aceptor en sistemas para la conversión de energía. La combinación de TMDs con los CDs por medio de estrategias covalentes y non-covalentes aporta seguramente una nueva contribución en este campo. Los híbridos obtenidos muestran propiedades electrónicas foto-inducidas interesantes, que incentivan investigaciones adicionales de estos materiales prometedores. Por ejemplo, modificaciones en la estructura de los CDs y de sus grupos funcionales podrían abrir el camino hacia la mejora de las capacidades fotocatalíticas y de donor-aceptor de los híbridos.

7. ANNEX A

7.1. Calculation of the hydrodynamic radius

The diffusion coefficients (D) found from the DOSY experiments were related to the hydrodynamic radius (rH) through the Stokes-Einstein equation (Eq. 7.1), assuming the particles spherical.

$$rH = \frac{kT}{6\pi\eta D} \quad \text{Eq. 7.1.}$$

k = Boltzmann constant = $1.3806*10^{-23}$ $m^2kg\ s^{-2}K^{-1}$

T = temperature (K) = 298K

η = dynamic viscosity. For water at 298 K = $0.89*10^{-3}$ kg $m^{-1}s^{-1}$

D = diffusion coefficient (m^2s^{-1})

7.2. Calculation of the Quantum Yield

The quantum yield (QY) measurements were performed with quinine sulphate in 0.10 M H_2SO_4 (literature quantum yield 0.54 at 350 nm) as the standard. The quantum yields were calculated from Eq. 7.2, where Φ is the quantum yield, *Grad* is the slope from the plot of integrated intensity vs absorbance and η the refractive index of the solvent. The indices *x* and *st* denote the sample and the standard, respectively.

$$\Phi_x = \Phi_{st}\left(\frac{Grad_x}{Grad_{st}}\right)\left(\frac{\eta_x^2}{\eta_{st}^2}\right) \quad \text{Eq. 7.2}$$

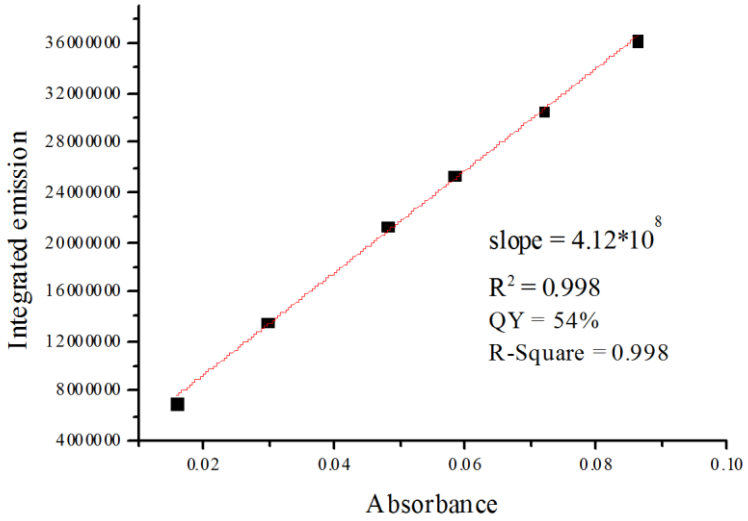

Figure 7.1. Absorption (λ 350 nm) vs integrated emission plot for different concentrations of quinine sulfate.

8. ANNEX B

8.1. Abstract

In the following study **CDs1** are obtained from citric acid and ethylenediamine under microwave irradiation at 140°C, respectively for 1, 2 and 3 minutes. The resulting materials are labeled **CDsA**, **CDsB**, **CDsC**. The characterization of the three samples allowed to investigate the influence of the reaction time on the CDs features, i.e. their size, structure and optical properties. Finally **CDsC** was chosen for the experiments described in Chapter 2, renamed **CDs1**.

8.2. Synthesis of CDsA, CDsB and CDsC

2.0 g of citric acid monohydrate (9.5 mmol, 1 eq.) were dissolved in 15 ml of ultrapure water. Upon addition of 0.64 ml of EDA (1 eq.) the solution was heated up to 140°C through microwave irradiation (stirring, open batch), causing the evaporation of the water. The temperature was kept constant for 1 minute, after that the irradiation was stopped and the mixture cooled down. This yields in a yellow, transparent solid product **CDsA**, insoluble in most common organic solvents but highly soluble in water. In the case of **CDsB**, after the first minute of heating, the mixture was redissolved in 10 ml of water and put one additional minute at 140°C under microwave irradiation, for a total of 2 minutes. **CDsC** was prepared as **CDsB**, but one additional step of redissolution and heating at 140°C for 1 minute was effectuated, for a total of 3 minutes. The redissolution step is an important adjustment that allows the reagents to reorganize randomly in the liquid phase before increasing the time of the reaction, that instead takes place in the solid phase. The solid products were diluted with ultrapure water, filtrated on 0.45 µm PTFE membrane and dialyzed against ultrapure water (MWCO = 0.5-1.0 KDa, 3 days, twice a day). The dry products were obtained by freeze-drying.

8.3. Size determination of CDsA-C

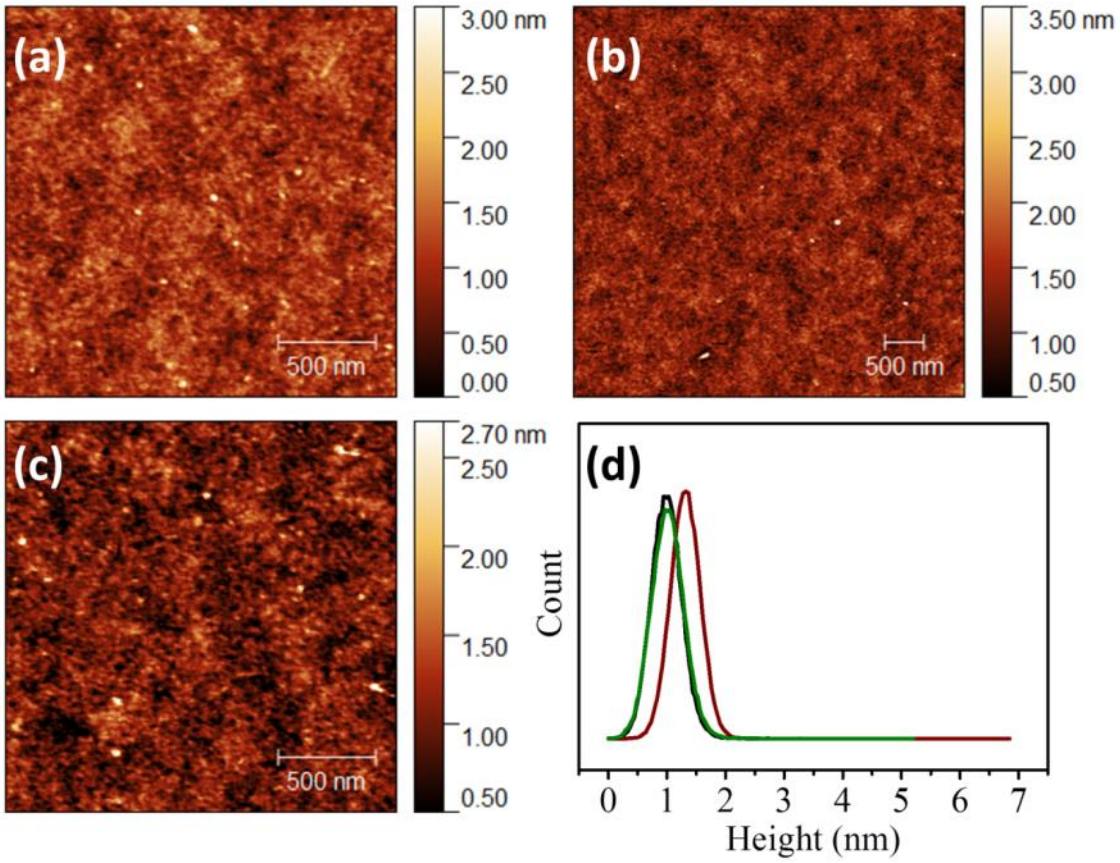

Figure 8.1. AFM images of CDs1 samples obtained at different reaction times: CDsA (a), CDsB (b), CDsC (c) and their respective height distribution (d) in green, brown and black.

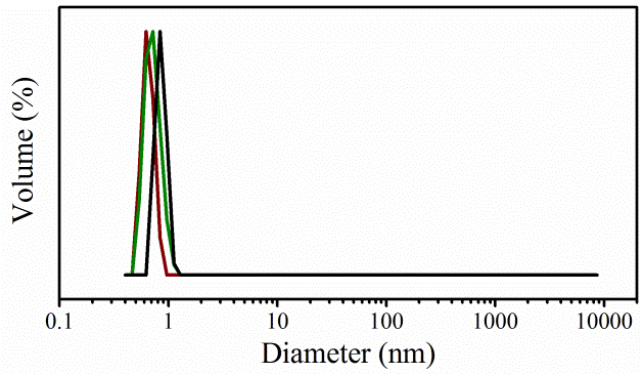

Figure 8.2. DLS size distribution of CDs1 samples obtained at different reaction times: CDsA (green), CDsB (brown) and CDsC (black).

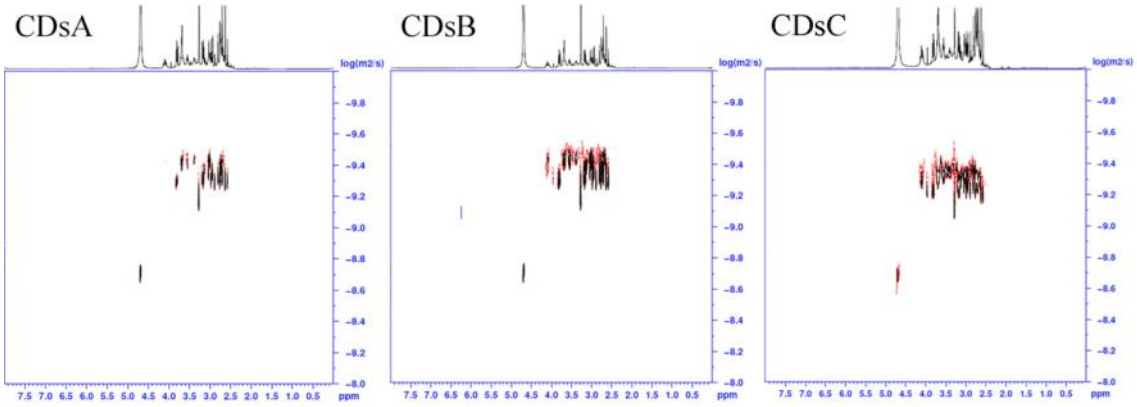

Figure 8.3. DOSY spectra of CDs1 samples obtained at different reaction times: CDsA, CDsB, CDsC.

Table 8.1. Measured diffusion coefficient (D) and the calculated hydrodynamic radius (rH) and diameter of CDs1 samples obtained at different reaction times: CDsA, CDsB, CDsC.

	D (m^2/s)	rH (nm)	Diameter (nm)
CDsA	$10^{-9.4}$	0.6	1.2
CDsB	$10^{-9.4}$	0.6	1.2
CDsC	$10^{-9.4}$	0.6	1.2

By the AFM, DLS and DOSY analysis, all the samples show a size between 1.0-1.5 nm.

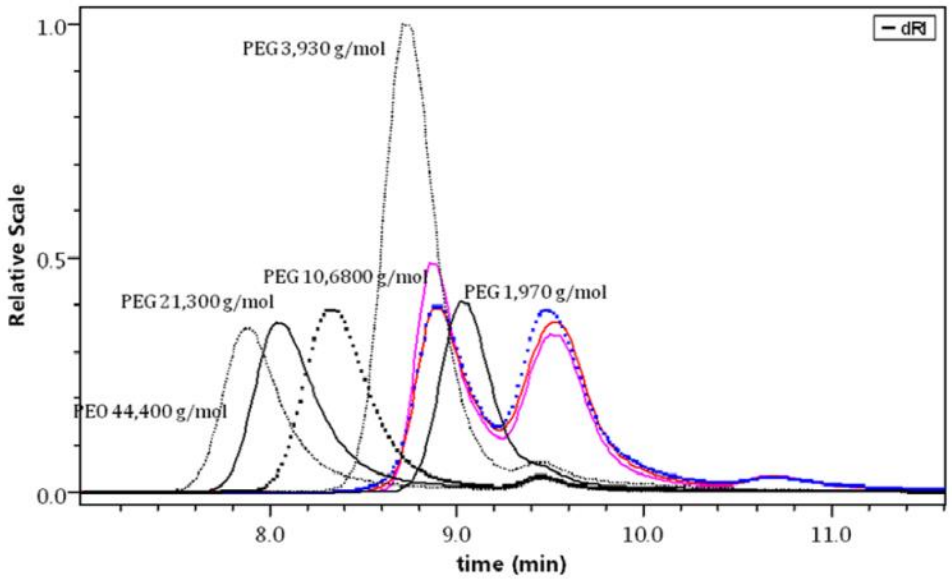

Figure 8.4. SEC/RI chromatograms of CDs1 samples obtained at different reaction times: CDsA (pink), CDsB (red), CDsC (blue).

The Size exclusion chromatography (SEC/RI) profiles are identical. The first eluition peak at 8.9 min, in the same position for all the samples, appear between the peaks of PEG 3930 g/mol and PEG 1970 g/mol. A second peak of much smaller molecular mass (out of calibration) at 9.6 min could be due to the salt employed in the mobile phase (0.1 M sodium acetate) or to the CDs' counter ions.

Table 8.2. Average molecular weight in number ($\overline{M_n}$), in weight ($\overline{M_w}$) and polydispersity (Đ) of CDs1 samples obtained at different reaction times: CDsA, CDsB and CDsC.

	$\overline{M_n}$ (g/mol)	$\overline{M_w}$ (g/mol)	Đ
CDsA	2300	2500	1.07
CDsB	2300	2500	1.08
CDsC	2300	2600	1.09

8.4. Optical properties of CDsA-C

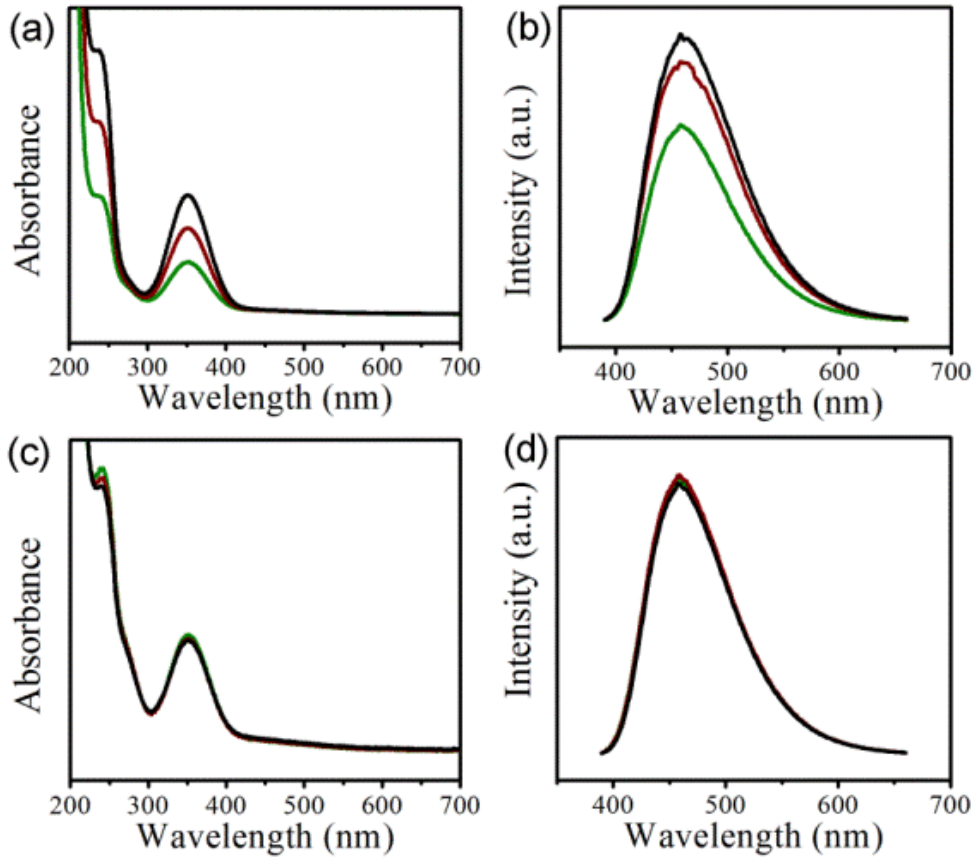

Figure 8.5. (a) UV/vis and (b) emission spectra of CDs1 samples obtained at different reaction times: CDsA (green), CDsB (brown), CDsC (black) at the same mass concentration of 0.05 mg/mL. (c) UV/Vis and (d) emission spectra of CDsA (green), CDsB (brown), CDsC (black) at the same optical concentration.

While, for solution with the same mass concentration, absorption and emission increase from **CDsA** to **CDsC**, when the solution are prepared with the same absorption (optical concentration) the emission intensity is the same for all the samples. This means that increasing the reaction time the same fluorophore is forming in larger amounts, without changing its nature.

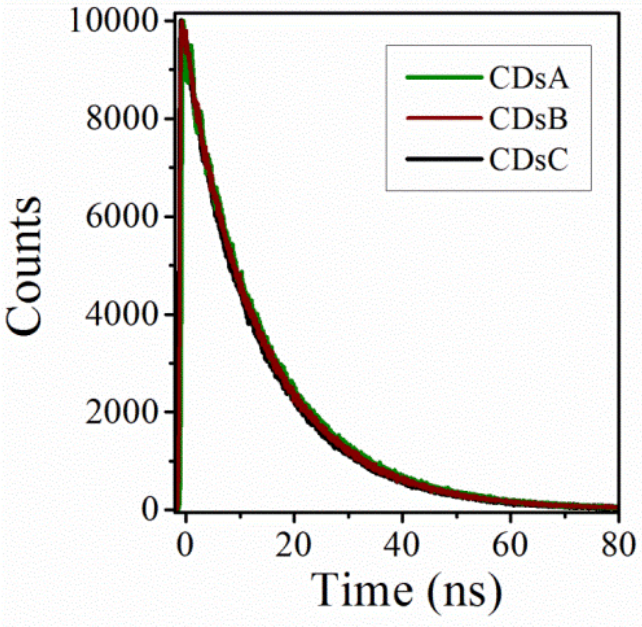

Figure 8.6. Fluorescence decay of CDs1 samples obtained at different reaction times: CDsA (green), CDsB (brown) and CDsC (black).

8.5. Structure characterization of CDsA-C

Table 8.3. Elemental Analysis of CDs1 samples obtained at different reaction times: CDsA, CDsB, and CDsC.

	C (mol%)	H (mol%)	N (mol%)	O (mol%)
CDsA	26,3	47,0	6,9	20,0
CDsB	27,9	45,8	7,2	19,2
CDsC	30,0	44,3	8,0	17,7
$C_8H_{12}N_2O_5$	29,6	44,4	7,4	18,5

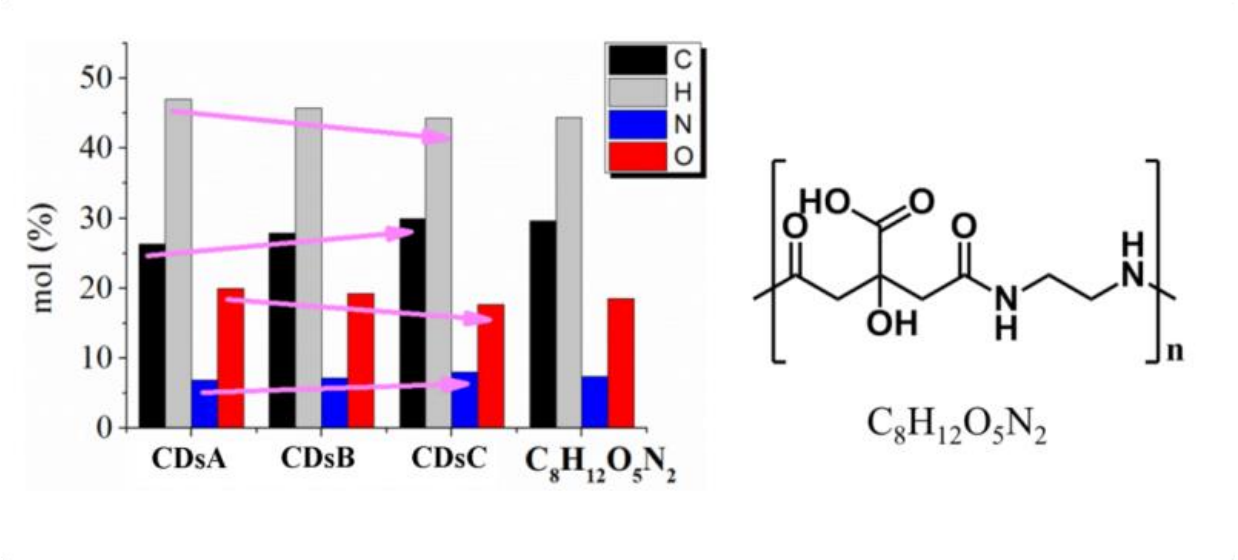

Figure 8.7. Mole percentages of C, H, N, O of CDs1 samples obtained at different reaction times, i.e. CDsA, CDsB and CDsC, and the calculated values of the polymeric repetitive unit $C_8H_{12}O_5N_2$.

From **CDsA** to **CDsC** it can be observed the relative increase of C and N and decrease of H and O. These changes are due to the loss of water happening during the condensation of the reagents that forms the CDs. In fact the amount of unreacted material (CA and EDA retained on the CDs as counter ions) diminuishes from **CDsA** to **CDsC** forming new particles.

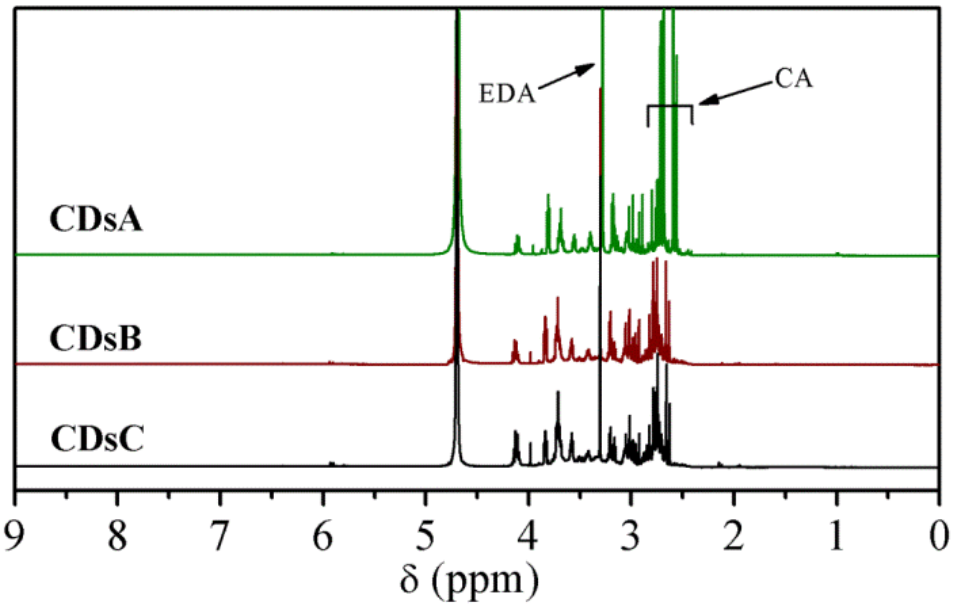

Figure 8.8. ^{1}H NMR of CDs1 samples obtained at different reaction times: CDsA, CDsB and CDsC.

In the ^{1}H NMR spectra the nanoparticles have the same profile in the three cases, but the presence of unreacted EDA and CA decreases considerably from **CDsA** to **CDsC**. These reagents could be present in the samples in the form of CDs counter ions, in the way that dialysis cannot remove them completely. Increasing the reaction time, the consumption of the reagent towards the formation of the CDs removes the most part.

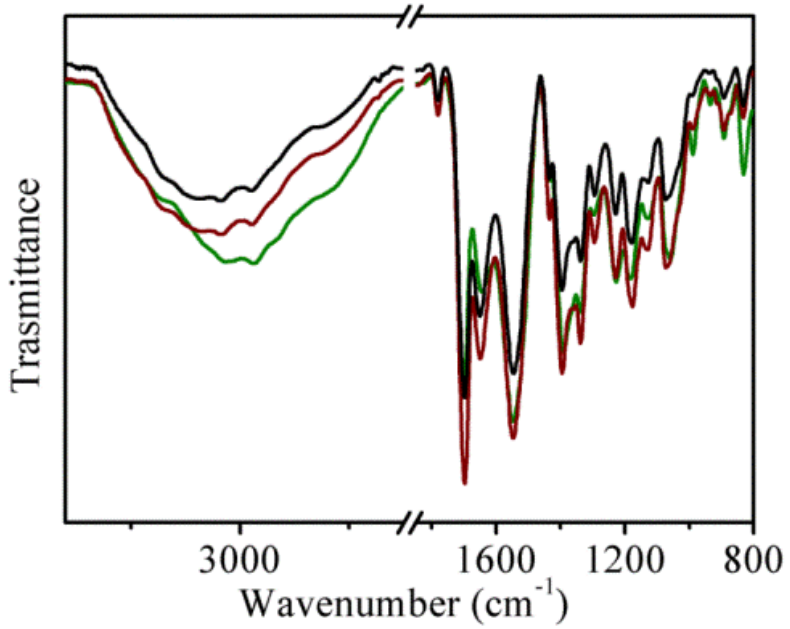

Figure 8.9. IR spectra of CDs1 samples obtained at different reaction times: CDsA (green), CDsB (brown), CDsC (black). The profile is the same for all the samples.

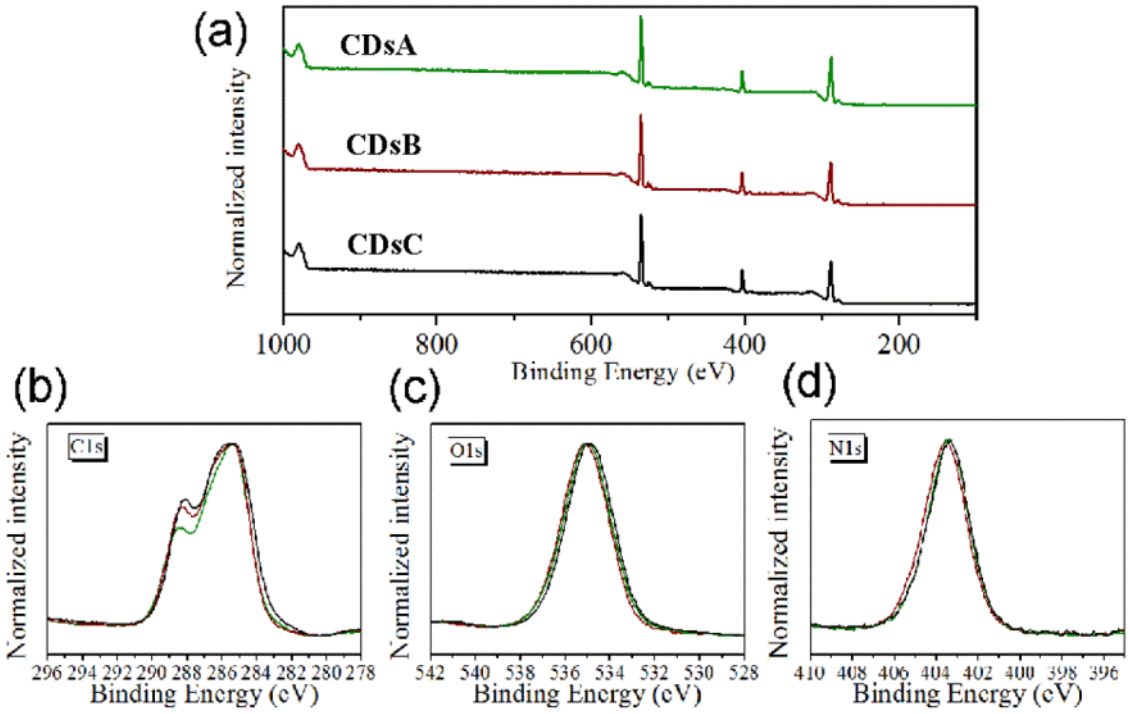

Figure 8.1. XPS spectra of CDs1 samples obtained at different reaction times: CDsA (green), CDsB (brown), CDsC (black). The profile is the same for all the samples.

8.6. Conclusion

The analysis of the size, structure and optical properties of CDsA, CDsB and CDsC shows that the three samples are equivalent, differing only for their content of unreacted precursors, namely citric acid and ethylenediamine. In fact, increasing the reaction time the reagents content decreases. Finally, it is suggested that citric acid and ethylenediamine in the samples are found in the salt form, as CDs counter ions.

8.7. Details of the DFT and TDDFT calculations

Geometry optimizations in the ground state were carried out within density functional theory (DFT)[1-2] using the ωB97XD functional[3] combined with the 6-31G(d) basis set.[4] Besides, time-dependent density functional theory (TDDFT)[5] has been used to compute the vertical absorption energy as well as to optimize the first excited electronic state, using the B3LYP functional[6-8] and the 6-31G(d) basis set. All the calculations were performed with the Gaussian 09 suite of programs.[9]

Cartesian coordinates:

Dimer one chain:

C	5.968405	0.322405	-0.827510
N	6.843575	1.473131	-0.864602
C	4.481529	0.711942	-0.785889
N	3.618649	-0.421448	-0.535721
C	3.502202	-0.932500	0.717350
O	4.085460	-0.464568	1.686040
C	2.587093	-2.146359	0.868575
C	1.463278	-2.274275	-0.165167
C	0.611373	-0.992307	-0.155927
O	0.308054	-0.531419	-1.342719
O	2.039487	-2.514505	-1.419500
C	0.503333	-3.435409	0.222520
C	-0.624499	-3.527213	-0.798361
O	-0.355143	-3.497677	-2.003011
N	-1.902274	-3.576892	-0.377255
C	-2.445680	-3.728856	0.958912
C	-2.660111	-2.435780	1.745846
N	-3.548963	-1.445260	1.156347
C	-4.192726	-1.461653	-0.035019
C	-4.724915	-0.103447	-0.504117
C	-4.067970	1.151603	0.099541
C	-2.535585	0.999144	0.001112
O	-1.984534	0.859926	-1.084223
O	0.210830	-0.514135	0.901208
O	-4.352269	-2.447546	-0.746840
C	-4.485088	2.398643	-0.705574
C	-3.894464	3.670186	-0.110471
O	-3.693879	3.778728	1.099355
O	-4.493941	1.238300	1.433113
O	-1.917736	1.011318	1.157084
N	-3.626343	4.660027	-0.988441
H	6.976903	1.945205	-1.748607
C	7.238183	2.228116	0.214208
H	6.196420	-0.279248	0.055169
H	6.169884	-0.303259	-1.703557
H	4.330943	1.444974	0.012194
H	4.180681	1.177504	-1.729487
H	3.210129	-0.942948	-1.303974
H	3.202529	-3.050844	0.805769
H	2.172331	-2.087594	1.876237
H	-0.422810	0.138570	-1.265827
H	1.086398	-4.361592	0.185770
H	0.146015	-3.287137	1.243163
H	1.304619	-2.812823	-2.001647
H	-2.602582	-3.466693	-1.103603
H	-3.392970	-4.259235	0.852366
H	-1.785108	-4.365032	1.556405
H	-3.049045	-2.718630	2.732195
H	-1.691471	-1.944230	1.904468
H	-3.621888	-0.578727	1.680793
H	-4.602055	-0.109591	-1.589213
H	-5.797134	-0.049360	-0.287063
H	-4.190615	2.274925	-1.751887
H	-5.577756	2.475727	-0.662241
H	-0.994608	0.652272	1.044148
H	-4.174143	2.104142	1.760444
C	-3.084831	5.943652	-0.586867
H	-3.773208	4.484883	-1.970248
H	-3.740044	6.757249	-0.912188
H	-3.016839	5.948341	0.501084
H	-2.086010	6.093689	-1.008277
O	7.787514	3.304939	0.051335
C	7.006373	1.625910	1.586955
H	7.673767	0.768470	1.733434
H	7.246475	2.386876	2.329751
H	5.982535	1.267509	1.736686

Dimer two chains intramolecular HB:

C	1.197417	-4.909136	-1.081842
N	2.551711	-4.643312	-0.637664
C	0.200434	-4.773460	0.074708
N	-1.170801	-4.826780	-0.369314
C	-2.149499	-5.309533	0.447848
O	-1.920451	-5.882510	1.500279
C	-3.583896	-5.094916	-0.036637
C	-3.839536	-3.776091	-0.777942
C	-3.394211	-2.588387	0.095103
O	-2.523201	-1.776850	-0.466624
O	-3.151829	-3.817861	-1.998447
C	-5.359030	-3.570517	-1.016268
C	-5.597585	-2.243859	-1.727355
O	-4.825578	-1.884521	-2.626040
N	-6.631264	-1.467559	-1.365290
C	-7.619450	-1.628063	-0.314935
C	-7.193058	-1.133842	1.072134
N	-6.658316	0.218023	1.142151
C	-6.623632	1.169386	0.181527
C	-5.678093	2.341847	0.434030
C	-4.599398	2.224456	1.527618
C	-3.832486	0.895365	1.365845
O	-3.129268	0.660889	0.387296
O	-3.880977	-2.395374	1.201684
O	-7.250784	1.129007	-0.874052
C	-3.628410	3.409348	1.375135
C	-2.504836	3.340511	2.395090
O	-2.658804	2.729957	3.460582
O	-5.250677	2.255596	2.769619
O	-4.031762	0.033569	2.336204
N	-1.377393	3.988099	2.073675
H	2.872568	-3.675248	-0.690987
C	3.350271	-5.491171	0.060428
H	1.121665	-5.903973	-1.531260
H	0.971766	-4.186976	-1.875330
H	0.341205	-5.573755	0.804949
H	0.394351	-3.831039	0.605466
H	-1.459421	-4.321027	-1.201220
H	-3.857635	-5.910373	-0.715462
H	-4.214742	-5.159650	0.851453
H	-2.564774	-0.901883	0.009727
H	-5.703020	-4.381329	-1.667893
H	-5.890809	-3.638772	-0.065906
H	-3.495321	-3.054925	-2.516943
H	-6.661353	-0.558327	-1.817319
H	-8.506114	-1.086257	-0.644370
H	-7.898085	-2.681803	-0.217933
H	-8.065213	-1.225750	1.732110
H	-6.411173	-1.795660	1.464729
H	-6.211248	0.456830	2.020814
H	-5.203486	2.530472	-0.532181
H	-6.281030	3.223685	0.674898
H	-3.230695	3.488644	0.360814
H	-4.207248	4.321084	1.563940
H	-3.737139	-0.867719	2.048195
H	-4.525072	2.296240	3.427664
C	-0.260485	4.068942	2.995101
H	-1.300645	4.427270	1.161038
H	0.442584	4.806716	2.611002
H	-0.614045	4.363581	3.986643
H	0.248904	3.103728	3.083927
O	4.360843	-5.083417	0.633337
C	2.970091	-6.956627	0.084263
H	2.902743	-7.359685	-0.931646
H	3.738715	-7.496036	0.637213
H	2.003312	-7.115953	0.572259
C	6.443244	-2.321253	0.587371
N	7.885197	-2.429165	0.633813
C	5.793982	-2.413948	1.976820
N	4.348290	-2.447835	1.866010
C	3.660939	-1.316565	1.598636
O	4.146338	-0.191870	1.665535
C	2.212590	-1.494868	1.146701
C	2.137640	-0.985967	-0.297984
C	2.435833	0.522100	-0.275536
O	3.300452	0.943924	-1.160138
O	3.078603	-1.730553	-1.024838
C	0.714789	-1.109666	-0.920710
C	0.764092	-0.699372	-2.387505
O	1.578969	-1.236360	-3.142920
N	-0.033185	0.293044	-2.850611
C	-1.237553	0.864789	-2.250416
C	-0.979057	1.982674	-1.248481
N	-0.246930	3.088375	-1.834489
C	-0.519258	4.378032	-1.498879
C	0.505539	5.399874	-1.972282
C	1.609942	5.649916	-0.915760
C	2.175085	4.268934	-0.543614
O	2.868338	3.634377	-1.339045
O	1.767380	1.250315	0.452114
O	-1.507225	4.702630	-0.848928
C	2.737067	6.504503	-1.527324
C	3.849129	6.735996	-0.512561
O	3.613976	6.768761	0.695723
O	1.012372	6.286315	0.170365
O	1.774894	3.827760	0.613465
N	5.085554	6.914971	-1.022356
H	8.413616	-1.619759	0.929946
C	8.624964	-3.582532	0.615545
H	6.034629	-3.114422	-0.043171
H	6.166550	-1.368806	0.125865
H	6.119573	-3.328543	2.480510
H	6.081269	-1.558296	2.592458
H	3.989745	-3.338814	1.534656
H	1.893924	-2.539303	1.184221
H	1.562063	-0.897684	1.789104
H	3.298170	1.937573	-1.157815
H	0.402519	-2.156479	-0.882315
H	0.004854	-0.528470	-0.332298
H	2.872928	-1.613155	-1.977466
H	0.104979	0.448006	-3.841030
H	-1.835167	1.257800	-3.076633
H	-1.833847	0.079930	-1.783332
H	-1.941683	2.361675	-0.912584
H	-0.447156	1.614233	-0.364643
H	0.655262	2.880667	-2.242179
H	0.969412	5.076832	-2.909337
H	-0.012993	6.347693	-2.130561
H	3.125968	6.027999	-2.431565
H	2.310189	7.475777	-1.802807
H	1.944147	2.841408	0.667642
H	1.751393	6.532616	0.761268
C	6.251572	7.149647	-0.192857
H	5.215651	6.807679	-2.016152
H	6.780110	8.049066	-0.521753
H	5.906858	7.286864	0.832133
H	6.934833	6.295176	-0.227344
O	9.823126	-3.564012	0.848857
C	7.890840	-4.857633	0.241365
H	6.999614	-5.035881	0.850998
H	7.560873	-4.812542	-0.802778
H	8.588331	-5.687617	0.356610

Dimer two chains intermolecular HB:

C	5.396229	4.102622	-1.964853
N	5.809927	3.056787	-1.050008
C	5.076049	2.750012	0.041086
O	4.078424	3.393216	0.365684
C	5.519250	1.513949	0.809887
C	4.813422	0.275172	0.208195
C	4.996416	-0.966079	1.112389
C	4.128345	-2.112367	0.594553
O	4.248859	-2.512703	-0.560019
O	3.453219	0.559338	0.026400
C	5.437097	-0.024561	-1.160913
O	4.538310	-0.073100	-2.152956
O	6.624932	-0.157093	-1.332120
N	3.257446	-2.636334	1.487383
C	2.185715	-3.581344	1.178133
C	2.509115	-4.745135	0.220089
N	1.978732	-4.505131	-1.111169
C	0.638119	-4.512658	-1.317469
C	0.136682	-3.826582	-2.579513
C	0.255429	-2.304556	-2.403271
C	1.733825	-1.901205	-2.495476
O	2.530219	-2.376769	-3.273310
O	-0.146456	-4.985009	-0.492767
C	-0.493771	-1.526974	-3.516467
C	-0.071773	-0.059304	-3.491723
N	-0.715739	0.711964	-2.578084
C	-0.190119	2.000525	-2.181000
C	0.477264	1.881105	-0.804029
N	1.139187	3.094728	-0.341729
C	0.463966	4.235417	-0.062220
C	1.317816	5.426703	0.318725
O	-0.256726	-1.979091	-1.120481

O	1.992714	-0.951672	-1.615256
O	0.854498	0.342119	-4.185617
O	-0.766226	4.306836	-0.090288
O	-2.603023	1.746683	-0.031841
C	-3.806898	1.752753	0.159508
O	-4.374949	1.513218	1.323397
C	-4.754534	2.048196	-0.993543
C	-4.648209	3.546391	-1.405184
N	-3.448317	4.134704	-1.381322
C	-3.292796	5.529885	-1.748881
C	-4.333797	1.153481	-2.192345
C	-4.130572	-0.281946	-1.725366
O	-3.028250	-0.830247	-1.800378
N	-5.192106	-0.882393	-1.154049
C	-4.995780	-2.075540	-0.330836
C	-4.714020	-3.340161	-1.145924
C	-4.200617	-4.488494	-0.266578
N	-2.922205	-4.185144	0.350564
C	-2.841940	-3.665299	1.596980
O	-3.815743	-3.469296	2.318038
C	-1.437004	-3.262160	2.016784
C	-1.340254	-1.719837	2.113542
O	-1.930513	-1.083344	1.004383
C	0.145995	-1.373543	2.255208
O	0.813193	-1.702916	3.213482
O	0.641619	-0.679757	1.226597
C	-2.054113	-1.189136	3.372765
C	-1.820963	0.279424	3.707436
O	-1.723389	0.668887	4.862931
N	-1.774018	1.145607	2.645979
C	-1.456071	2.554409	2.809989
C	-0.093966	2.839376	3.454971
N	0.999461	2.167767	2.775642
C	1.843656	1.264868	3.289870
O	2.687379	0.701310	2.558510
C	1.760764	0.923011	4.753756
O	-5.692072	4.091567	-1.756154
H	2.580236	-4.013176	-1.760645
H	3.581850	-4.918247	0.140488
H	2.036803	-5.651155	0.604422
H	1.347218	-3.034332	0.738020
H	1.851152	-3.973873	2.140329
H	3.134137	-2.146392	2.364311
H	4.730424	-0.682500	2.134470
H	6.043712	-1.283695	1.094207
H	4.958151	-0.445775	-2.945870
H	5.185226	1.633046	1.843431
H	6.603441	1.372570	0.792713
H	3.110362	0.852563	0.899758
H	6.581220	2.456221	-1.302621
H	6.203389	4.293442	-2.673590
H	4.494642	3.812277	-2.515618
H	5.183148	5.017908	-1.407772
H	0.705567	-4.124412	-3.464314
H	-0.912344	-4.100628	-2.711970
H	-2.059573	-4.390166	-0.149979
H	-4.910297	-4.706119	0.536924
H	-4.085004	-5.393750	-0.870663
H	-0.706437	-3.637808	1.294928
H	-1.206992	-3.697250	2.992430
H	1.569711	-0.451655	1.446083
H	-1.662350	-1.488825	0.156668
H	-3.124350	-1.380113	3.241685
H	-1.724916	-1.752856	4.245945
H	-1.678531	0.747023	1.712766
H	-1.503131	3.005777	1.814989
H	-2.216430	3.031754	3.437606
H	0.075554	3.922309	3.433757
H	-0.117322	2.518814	4.494767
H	1.139952	2.385345	1.790667
H	1.966577	1.804498	5.369803
H	0.767108	0.547009	5.015910
H	2.499769	0.150757	4.961381
H	-5.622048	-3.662042	-1.670703
H	-3.957598	-3.108972	-1.901741
H	-5.891520	-2.205701	0.281339
H	-4.163234	-1.877639	0.347861
H	-5.998648	-0.294502	-0.978143
H	0.280176	-1.260223	-0.748257
H	2.921867	-0.646095	-1.683447
H	-0.212118	-1.932413	-4.491014
H	-1.564655	-1.653188	-3.341147
H	-3.397393	1.496773	-2.634172
H	-5.129204	1.228348	-2.940008
O	-6.084766	1.808019	-0.648496
H	-3.648289	1.310715	1.956111
H	-1.484819	0.292283	-2.057439
H	0.539960	2.300436	-2.935474
H	-0.990919	2.742306	-2.151120
H	-0.278969	1.577785	-0.075452
H	1.239779	1.104248	-0.852485
H	2.156521	3.122899	-0.340564
H	2.378972	5.181484	0.405061
H	1.184113	6.206896	-0.437068
H	0.953215	5.830387	1.267495
H	-2.646796	3.663491	-0.969771
H	-2.316521	5.855939	-1.390041
H	-3.351908	5.658515	-2.834370
H	-4.079999	6.132456	-1.287657
H	-6.565996	2.575280	-1.023207

Octamer:

C	-2.468978	2.945278	-2.989126
N	-3.103272	1.630085	-2.933293
C	-3.323100	0.928556	-1.803088
C	-3.679410	-0.531388	-1.975255
C	-3.168809	-1.350336	-0.773112
C	-1.682082	-1.039714	-0.503371
O	-0.831507	-1.200237	-1.370015
O	-3.216874	1.421917	-0.672311
O	-3.940080	-1.102191	0.378479
C	-3.272410	-2.841331	-1.124006
C	-2.637069	-3.860588	-0.183031
N	-2.349608	-3.414258	1.054116
C	-1.518396	-3.989085	2.102027
C	-0.846655	-5.325699	1.791599
N	0.004996	-5.353397	0.617506
C	1.295885	-5.004394	0.460436
C	2.052477	-4.362197	1.616122
C	2.797256	-3.091436	1.115469
C	1.716585	-2.128830	0.589434
O	1.651578	-2.041976	-0.714597
O	-2.387327	-4.991361	-0.612114
O	1.862031	-5.156687	-0.626379
O	3.729472	-3.428084	0.125564
C	3.545051	-2.426408	2.276057
C	4.176434	-1.066298	1.981238
N	4.492428	-0.819866	0.682640
C	5.110171	0.430314	0.298577
C	6.595098	0.475472	0.678798
N	7.203767	1.748736	0.336415
C	7.591758	2.041091	-0.919705
O	7.446089	1.245217	-1.852693
O	4.375659	-0.260313	2.879002
C	8.196064	3.416074	-1.142362
C	9.249296	3.373023	-2.259239
C	10.378344	2.404273	-1.858830
O	11.207780	2.133713	-2.843969
O	8.685408	3.015410	-3.487282
C	9.904087	4.761623	-2.471279
C	10.784319	5.142014	-1.292205
O	10.336934	5.667281	-0.285449
O	0.956832	-1.557403	1.365882
O	-1.427003	-0.654048	0.725329
N	12.100641	4.777721	-1.413952
C	12.914818	4.618532	-0.226984
C	14.409957	4.691697	-0.547035
N	15.189895	4.301422	0.616242
C	15.615137	3.043778	0.927276
O	15.767999	2.711068	2.103067
C	15.980951	2.068902	-0.173877
C	15.152314	0.762165	-0.082680
C	13.726681	1.103305	-0.552836
O	13.526423	1.477784	-1.707481
O	10.526755	2.001211	-0.710738
C	15.675585	-0.317411	-1.056347
C	17.079275	-0.782772	-0.694518
N	17.263125	-2.086552	-0.352029
C	16.279937	-3.107587	-0.038346
C	15.745988	-2.984884	1.395037
N	14.756334	-4.002285	1.690770
C	15.113238	-5.299207	1.909249
C	13.988880	-6.237556	2.306106
O	15.162985	0.219904	1.202074
O	12.788620	0.983423	0.351055
O	18.028992	-0.011395	-0.761396
O	16.269926	-5.679537	1.805027
H	7.378865	2.419752	1.067703
H	6.692749	0.326808	1.755864
H	7.135484	-0.321237	0.159692
H	4.584721	1.248598	0.799760
H	5.005100	0.553959	-0.781806
H	4.435045	-1.586736	0.021076
H	4.338905	-3.110843	2.595709
H	2.872981	-2.269120	3.121369
H	0.817760	-1.570995	-0.984172
H	2.816162	-5.064301	1.967197
H	1.406465	-4.101331	2.456464
H	3.263574	-4.038487	-0.488772
H	-0.480032	-5.591507	-0.241332
H	-1.606402	-6.095047	1.642676
H	-0.268780	-5.611551	2.676212
H	-2.131355	-4.126851	3.001379
H	-0.750416	-3.241752	2.338813
H	-2.765745	-2.520486	1.295720
H	-2.777451	-2.988602	-2.085118
H	-4.326274	-3.093357	-1.266455
H	-3.275928	-0.932138	-2.907741
H	-4.768141	-0.655425	-2.023042
H	-0.454490	-0.758849	0.912588
H	-3.859394	-0.147311	0.549302
H	-3.175327	1.119153	-3.800297
C	-3.273292	4.106362	-2.402323
H	-1.492199	2.900135	-2.492805
H	-2.292871	3.146008	-4.048364
H	7.398337	4.087616	-1.480034
H	8.619456	3.835244	-0.226710
H	12.017460	1.698395	-2.464600
H	8.146449	2.221339	-3.296374
H	10.465140	4.712015	-3.408947
H	9.108776	5.502411	-2.576360
H	12.338444	4.190146	-2.202506
H	12.628161	5.404815	0.475341
H	12.698628	3.657183	0.259774
H	14.646863	4.020532	-1.375612
H	14.689740	5.703654	-0.855177
H	15.016881	4.844884	1.455177
H	15.899146	2.478979	-1.180220
H	17.028098	1.794917	-0.017154
H	11.921146	1.280258	-0.043453
H	15.369668	0.936742	1.835749
H	14.954945	-1.138927	-1.058300
H	15.712363	0.094333	-2.067995
H	18.225143	-2.286524	-0.110903
H	15.453635	-3.072614	-0.754385
H	16.759504	-4.081977	-0.154618
H	16.584310	-3.084762	2.092990
H	15.298360	-1.999072	1.539757
H	13.798059	-3.721914	1.821776
H	12.990875	-5.806975	2.181695
H	14.065119	-7.148021	1.707359
H	14.121906	-6.520313	3.354852
N	-3.120449	4.201427	-0.965804
H	-2.913042	5.047081	-2.825788
H	-4.331608	4.005125	-2.674921
C	-3.129864	5.384726	-0.325541
H	-3.129440	3.318724	-0.460884
O	-3.196886	6.471151	-0.905658
C	-3.162302	5.321738	1.192667
H	-3.001013	4.308338	1.571135
H	-2.389939	5.983249	1.595264
C	-4.538326	5.854484	1.667641
C	-4.679066	5.782250	3.190901
O	-4.712633	7.193759	1.284962
C	-5.609066	4.986092	0.990112
H	-4.377801	7.278770	0.369710
C	-6.105675	5.911746	3.724351
H	-4.306173	4.829798	3.571228
H	-4.064620	6.582036	3.618228
O	-5.790194	3.822729	1.569032
O	-6.181655	5.363746	-0.023591
H	-6.631723	3.408166	1.227040
O	-6.425358	5.417890	4.792404
N	-6.990904	6.581711	2.930521
H	-6.616472	7.165933	2.190637
C	-8.352591	6.767069	3.396711
C	-9.248968	7.455642	2.372753
H	-8.775388	5.794164	3.656885
H	-8.358336	7.370838	4.314292
N	-9.608348	6.663398	1.205234
H	-10.176509	7.730074	2.884289
H	-8.785646	8.380316	2.012196
H	-9.182370	6.870505	0.315336
C	-10.547304	5.689258	1.270450
O	-11.032673	5.316743	2.339103
C	-10.953961	5.024783	-0.032805

H	-10.592750	5.564135	-0.910183
C	-10.427191	3.568826	-0.053307
H	-12.045538	4.986199	-0.074170
C	-10.786727	2.841296	-1.363472
C	-8.897950	3.637409	0.024798
O	-10.946472	2.829192	1.010036
O	-8.384535	4.366852	-0.949629
O	-8.247665	3.100029	0.904773
H	-7.442280	4.604536	-0.716901
H	-11.019368	3.422088	1.781373
H	-10.174675	1.941586	-1.454462
C	-12.267121	2.516294	-1.425535
H	-10.563780	3.492044	-2.211176
O	-13.080515	3.338594	-1.817562
N	-12.658189	1.247468	-1.083841
H	-13.666166	1.147243	-1.106990
C	-11.973434	0.318844	-0.199602
C	-12.076805	-1.082071	-0.761949
H	-12.455634	0.299776	0.780516
H	-10.940130	0.620325	-0.057949
H	-12.997072	-2.762991	-0.773351
N	-12.988271	-1.847669	-0.316991
N	-11.221245	-1.464121	-1.825556
C	-9.965525	-1.018603	-2.146327
H	-11.510662	-2.305034	-2.306584
O	-9.380047	-0.109643	-1.572011
C	-9.298725	-1.767529	-3.286175
C	-7.775684	-1.910625	-3.037211
H	-9.757508	-2.747594	-3.437584
H	-9.423792	-1.185355	-4.206155
C	-7.529538	-2.449415	-1.622065
C	-7.208745	-2.917203	-4.058370
O	-7.123913	-0.686613	-3.201081
H	-7.519176	-0.087932	-2.544472
O	-8.371627	-3.411448	-1.297551
O	-6.636099	-2.030176	-0.909126
H	-8.151483	-3.751909	-0.388690
C	-5.772734	-3.390165	-3.826439
H	-7.878336	-3.781125	-4.102576
H	-7.222171	-2.417908	-5.031331
O	-4.803805	-2.722741	-4.164488
N	-5.656986	-4.625729	-3.276908
H	-6.471714	-5.165069	-2.999517
C	-4.375724	-5.313888	-3.266734
C	-4.464151	-6.656213	-2.556548
H	-4.039868	-5.478876	-4.299218
H	-3.620712	-4.704880	-2.775914
H	-3.479332	-7.127533	-2.611735
N	-4.842882	-6.589960	-1.157585
H	-5.183675	-7.308369	-3.061170
C	-6.130724	-6.713160	-0.771748
H	-4.126181	-6.388117	-0.466475
O	-7.070689	-6.707819	-1.567005
C	-6.374142	-6.935376	0.724433
C	-5.781240	-5.856671	1.644847
H	-7.455224	-6.980821	0.856708
H	-5.932709	-7.894398	1.016785
C	-6.233687	-6.060868	3.109814
O	-4.389062	-5.928399	1.548097
C	-6.352780	-4.512109	1.171582
O	-5.459565	-3.592420	0.923998
O	-7.564266	-4.366092	1.049465
H	-5.884665	-2.813139	0.479695
C	-5.637013	-4.974571	3.995838
H	-7.325547	-6.082032	3.162306
H	-5.846536	-7.028596	3.445862
H	-4.029285	-5.365316	2.261681
O	-4.436041	-4.697264	3.933873
N	-6.492383	-4.337349	4.818455
H	-7.469372	-4.583189	4.779734
C	-6.087953	-3.252784	5.693334
H	-6.349423	-3.479700	6.730773
H	-5.007026	-3.142833	5.608546
H	-6.568224	-2.316051	5.395225

Decamer:

C	-6.422482	-4.441779	4.254137
C	-7.605044	-3.524629	4.568558
O	-7.832555	-3.175959	5.716782
N	-8.411655	-3.165932	3.529676
C	-9.699604	-2.548209	3.798421
C	-9.572152	-1.132543	4.410163
N	-10.320822	-0.115145	3.685682
C	-10.042306	0.407467	2.463677
O	-10.782188	1.225794	1.930540
C	-8.744215	-0.037082	1.804807
C	-8.989154	-0.648045	0.410773
O	-9.917448	-1.681869	0.530663
C	-9.424146	0.427803	-0.619681
C	-9.758908	-0.187606	-1.964099
O	-10.670059	-1.010636	-2.039016
N	-9.100385	0.230224	-3.085908
C	-7.712668	0.662334	-3.183830
C	-6.843031	-0.484673	-3.712636
N	-5.428501	-0.172700	-3.598330
C	-4.506282	-1.031867	-4.120209
O	-4.778659	-1.874021	-4.960641
C	-3.110201	-0.962766	-3.498710
C	-2.974960	-2.020923	-2.378043
O	-1.886087	-1.632580	-1.561865
C	-2.764960	-3.436656	-2.904656
C	-2.777077	-4.426656	-1.751340
O	-2.629283	-4.038611	-0.575824
N	-2.947327	-5.704456	-2.087821
C	-2.792581	-6.832968	-1.186194
C	-1.423751	-6.939372	-0.511736
N	-0.278163	-6.766099	-1.385893
C	-0.228985	-6.804251	-2.737382
O	-1.148065	-7.160739	-3.470890
C	1.095628	-6.354766	-3.353456
C	2.023759	-5.460472	-2.507056
O	2.433730	-6.228688	-1.409775
C	3.198482	-5.010173	-3.444267
C	4.513363	-4.694519	-2.743300
O	5.115777	-5.627411	-2.185935
N	5.015332	-3.453321	-2.759773
C	4.639206	-2.305867	-3.567368
C	3.421777	-1.479925	-3.146742
N	3.526116	-0.619606	-1.969001
C	3.858234	-1.018463	-0.704556
O	4.642151	-1.931090	-0.491773
C	3.232746	-0.261402	0.456657
C	1.899064	0.437842	0.190428
O	2.101145	1.481522	-0.728496
C	1.330307	0.992650	1.528954
C	-0.095959	1.395288	1.241508
O	-0.314079	2.217007	0.336308
N	-1.068081	0.731278	1.900444
C	-2.427626	0.465178	1.415694
C	-3.217741	1.657134	0.874341
N	-2.864933	1.982214	-0.492256
C	-3.741280	2.100372	-1.494751
C	-3.166758	2.624876	-2.802616
C	-3.263117	4.170940	-2.835996
C	-2.413231	4.709620	-1.678862
O	-2.922712	5.157742	-0.660862
C	0.897114	-0.589315	-0.379873
O	0.448867	-0.315352	-1.580340
O	0.534398	-1.576161	0.260826
C	1.223989	-4.214776	-2.050651
O	0.683051	-3.453213	-2.831239
O	1.181670	-4.070036	-0.735775
C	-4.273235	-1.955417	-1.569631
O	-5.215471	-2.704716	-1.777004
O	-4.290209	-0.963334	-0.703447
C	-7.635169	-1.158923	-0.080389
O	-7.623129	-2.350319	-0.619491
O	-6.650487	-0.422468	-0.005802
O	-4.955666	1.876958	-1.388880
C	-2.744456	4.712559	-4.172479
C	-2.390378	6.199307	-4.206694
N	-3.045059	7.003447	-3.319661
C	-2.817095	8.436757	-3.369594
C	-3.462883	9.194025	-2.212965
N	-2.850622	9.004052	-0.906524
C	-1.669418	9.582118	-0.582292
C	-1.189766	9.433916	0.850649
C	0.002439	8.447730	0.886838
O	1.053422	8.897732	0.086095
O	-4.592505	4.607673	-2.699708
O	-1.127313	4.582042	-1.896482
O	-1.553198	6.619645	-4.986174
O	-0.975810	10.165428	-1.416198
C	0.550300	8.234620	2.311139
C	1.188805	9.497031	2.863215
N	2.551877	9.614381	2.794497
C	3.452522	8.987937	1.840300
C	4.744007	8.618713	2.540060
N	4.841199	7.382472	3.222300
C	4.072388	6.249863	3.125185
C	4.575963	5.075388	3.947994
C	4.152561	3.723567	3.324703
O	2.769563	3.551158	3.396626
C	-0.505982	7.084362	0.396430
O	0.045173	6.442030	-0.480201
O	-1.608402	6.702835	1.021079
O	0.512015	10.359091	3.403215
N	5.687859	9.470214	2.540011
O	3.065502	6.153252	2.437378
C	4.617818	3.654254	1.865622
O	3.883024	3.272347	0.970988
C	4.833690	2.585613	4.109558
C	4.669312	1.171655	3.539053
N	5.749875	0.688831	2.877765
C	5.884647	-0.733539	2.580786
C	7.296241	-1.065206	2.109892
N	7.620675	-0.602045	0.769491
C	8.013696	0.660508	0.521630
C	8.351716	0.986883	-0.935418
C	7.077352	1.164417	-1.779083
C	6.200224	2.223492	-1.099321
O	6.629834	3.326588	-0.783226
O	5.875474	4.015764	1.713586
O	3.652078	0.518765	3.727084
O	8.090786	1.530261	1.394980
C	7.372379	1.673156	-3.214805
C	6.041231	1.838496	-3.937389
N	5.549929	3.102484	-3.972989
C	4.179960	3.353718	-4.378195
O	6.464733	-0.086100	-1.822700
O	4.962746	1.831219	-0.940757
O	5.414229	0.880025	-4.376822
H	-2.830680	-5.944686	-3.065169
H	-2.991532	-7.721383	-1.783249
H	-3.546580	-6.774401	-0.394157
H	-1.350029	-6.168224	0.260047
H	-1.383179	-7.912809	-0.005121
H	0.611543	-6.579814	-0.931011
H	1.664569	-7.253195	-3.617266
H	0.833353	-5.845518	-4.283407
H	0.771326	-3.205424	-0.500509
H	3.423497	-5.858297	-4.097707
H	2.835377	-4.191890	-4.070726
H	2.935809	-5.651857	-0.789480
H	5.806250	-3.299316	-2.129059
H	5.514882	-1.655401	-3.622100
H	4.440562	-2.640316	-4.592151
H	3.233264	-0.795763	-3.978359
H	2.542861	-2.125143	-3.050087
H	2.952566	0.216589	-2.011700
H	3.111699	-0.991730	1.262277
H	3.937135	0.495234	0.811218
H	1.430380	0.254136	2.326776
H	1.935220	1.861348	1.805309
H	-0.280796	-0.951655	-1.796947
H	1.303251	2.042808	-0.691775
H	-0.737408	0.065074	2.583484
H	-2.379776	-0.293527	0.627869
H	-2.977295	0.043346	2.262510
H	-1.780059	-3.479710	-3.384800
H	-3.528846	-3.682018	-3.647132
H	-5.251795	-0.741118	-0.453033
H	-1.798339	-2.345394	-0.897356
H	-2.906032	0.007128	-3.038317
H	-2.360757	-1.156462	-4.269845
H	-5.172958	0.445658	-2.831049
H	-7.077095	-0.698938	-4.759560
H	-7.063750	-1.396838	-3.142057
H	-7.359581	0.975795	-2.199283
H	-7.633235	1.532705	-3.843556
H	-9.473164	-0.218905	-3.915774
H	-8.668866	1.212941	-0.669738
H	-10.343500	0.872738	-0.227213
H	-6.717604	-2.535764	-0.990310
H	-10.422818	-1.729043	-0.305330
H	-8.203765	-0.772193	2.405749
H	-8.098428	0.839298	1.705543
H	-11.198497	0.207042	4.068783
H	-8.517743	-0.853197	4.475438
H	-9.940973	-1.130780	5.436681
H	-10.283986	-3.189548	4.468995
H	-10.223437	-2.477132	2.843183
H	-8.292390	-3.669350	2.659142
C	-5.858918	-4.428620	2.837466
H	-5.624970	-4.206008	4.961582
H	-6.750617	-5.465796	4.469352

H	-4.279048	1.401930	0.881218
H	-3.072648	2.537279	1.510217
H	-1.881203	2.208567	-0.619410
H	-2.121373	2.328738	-2.933748
H	-3.763609	2.233079	-3.630758
H	-4.973664	4.213781	-1.900700
H	-1.835871	4.187244	-4.470209
H	-3.511745	4.513493	-4.928866
H	-0.608499	5.135626	-1.241347
H	-3.887611	6.639506	-2.889203
H	-1.741132	8.618896	-3.372690
H	-3.212910	8.850897	-4.307111
H	-3.410344	10.259877	-2.456262
H	-4.521998	8.930941	-2.119373
H	-3.339281	8.473592	-0.202350
H	-1.976371	9.095724	1.526831
H	-0.833493	10.407780	1.194491
H	-2.027458	5.951297	0.522486
H	0.673532	9.363837	-0.681915
H	1.256053	7.400975	2.297874
H	-0.275117	7.979769	2.979435
H	2.869557	10.508865	3.149509
H	3.717994	9.694320	1.049941
H	2.977795	8.128657	1.379087
H	6.511253	9.157591	3.059744
H	5.682939	7.280971	3.773993
H	5.662240	5.119540	4.064834
H	4.121780	5.130217	4.944458
H	2.386596	4.277468	2.875644
H	6.170674	3.868553	0.774663
H	5.895027	2.826240	4.220350
H	4.373190	2.569802	5.101484
H	6.565163	1.268347	2.694580
H	5.650953	-1.312471	3.480972
H	5.174721	-1.057812	1.821847
H	7.393468	-2.152934	2.107403
H	8.038135	-0.659167	2.806240
H	7.441823	-1.237177	-0.009297
H	8.932262	1.910124	-0.931676
H	8.933533	0.180985	-1.393872
H	4.436873	2.489305	-0.407919
H	7.940866	2.607429	-3.176768
H	7.959869	0.907415	-3.725943
H	5.543765	-0.002788	-2.124519
H	6.044703	3.827685	-3.475499
H	4.039927	4.426200	-4.522078
H	3.978688	2.834876	-5.317165
H	3.471541	2.994206	-3.622240
C	-4.659182	-5.410454	2.684867
O	-6.883149	-4.838601	1.941443
C	-5.343313	-3.035435	2.459732
H	-4.556911	-5.630885	1.616794
C	-3.360149	-4.844480	3.242423
H	-4.902806	-6.338129	3.207660
H	-6.609632	-4.606870	1.042337
O	-5.176231	-2.967826	1.126941
O	-5.038606	-2.145283	3.210679
H	-4.711629	-2.138054	0.920009
O	-3.104388	-4.842134	4.435551
N	-2.555334	-4.287081	2.294700
H	-2.808205	-4.333595	1.312374
C	-1.390442	-3.508755	2.636172
C	-0.087466	-4.277967	2.420766
H	-1.380754	-2.608473	2.006350
H	-1.476747	-3.205396	3.682489
N	1.027827	-3.371651	2.609797
H	-0.036466	-5.096144	3.145361
H	-0.084989	-4.712266	1.409708
C	2.348680	-3.706493	2.605223
H	0.889208	-2.428565	2.263193
O	3.211382	-2.844578	2.524827
C	2.690823	-5.187148	2.678562
H	2.022032	-5.733011	2.005683
C	4.155268	-5.492934	2.300779
H	2.521873	-5.562138	3.693721
C	4.231902	-6.943817	1.754322
C	4.529865	-4.570861	1.132721
O	4.965293	-5.334532	3.423465
O	5.610497	-3.838529	1.267851
O	3.862132	-4.588303	0.111402
H	5.599977	-3.203389	0.512128
H	5.762529	-5.877413	3.288276
C	5.651427	-7.265309	1.332547
H	3.959812	-7.623233	2.567478
H	3.527731	-7.080138	0.930680
O	6.546115	-7.366227	2.175624
N	5.869150	-7.390806	0.005716
C	7.199771	-7.627167	-0.523577
H	5.168408	-7.056126	-0.649567
H	7.087841	-7.817016	-1.594448
C	8.175324	-6.472356	-0.290918
H	7.614182	-8.525849	-0.057614
H	9.135724	-6.733188	-0.756084
N	7.639713	-5.246669	-0.852813
H	8.334096	-6.366888	0.785149
C	8.002101	-4.002631	-0.511263
H	6.782571	-5.318329	-1.413631
O	7.392902	-3.013623	-0.952791
C	9.161972	-3.843418	0.444007
H	8.855715	-4.160859	1.447550
H	10.020868	-4.453793	0.148893
H	9.452466	-2.792696	0.478773

8.8. References

[1] P. Hohenberg and W. Kohn, *Phys. Rev.*, **1964**, *B* 136, B864

[2] W. Kohn and L. Sham, *Phys. Rev.*, **1965**, 140, A1133

[3] J.-D. Chai and M. Head-Gordon, *Phys. Chem. Chem. Phys.*, **2008**, 10, 6615

[4] W. J. Hehre, R. Ditchfield and J. A. Pople, *J. Chem. Phys.*, **1972**, 56, 2257

[5] E. Runge and E. K. U. Gross, *Phys. Rev. Lett.*, **1984**, 52, 997

[6] A. D. Becke, *Phys. Rev. A*, **1988**, 38, 3098

[7] C. T. Lee, W. T. Yang and R. G. Parr, *Phys. Rev.*, **1988**, *B* 37, 785

[8] S. H. Vosko, L. Wilk and M. Nusair, *Can. J. Phys.*, **1980**, 58, 1200

[9] Gaussian 09, Revision A.1, M. J. Frisch, G. W. Trucks, H. B. Schlegel, G. E. Scuseria, M. A. Robb, J. R. Cheeseman, G. Scalmani, V. Barone, B. Mennucci, G. A. Petersson, H. Nakatsuji, M. Caricato, X. Li, H. P. Hratchian, A. F. Izmaylov, J. Bloino, G. Zheng, J. L. Sonnenberg, M. Hada, M. Ehara, K. Toyota, R. Fukuda, J. Hasegawa, M. Ishida, T. Nakajima, Y. Honda, O. Kitao, H. Nakai, T. Vreven, J. A. Montgomery Jr., J. E. Peralta, F. Ogliaro, M. Bearpark, J. J. Heyd, E. Brothers, K. N. Kudin, V. N. Staroverov, R. Kobayashi, J. Normand, K. Raghavachari, A. Rendell, J. C. Burant, S. S. Iyengar, J. Tomasi, M. Cossi, N. Rega, J. M. Millam, M. Klene, J. E. Knox, J. B. Cross, V. Bakken, C. Adamo, J. Jaramillo, R. Gomperts, R. E. Stratmann, O. Yazyev, A. J. Austin, R. Cammi, C. Pomelli, J. W. Ochterski, R. L. Martin, K. Morokuma, V. G. Zakrzewski, G. A. Voth, P. Salvador, J. J. Dannenberg, S. Dapprich, A. D. Daniels, Ö. Farkas, J. B. Foresman, J. V. Ortiz, J. Cioslowski, D. J. Fox, Gaussian Inc., Wallingford CT, **2009**.

9. ANNEX C

9.1. Abstract

In this chapter the complete structural and optical characterization of **CDs 1a-d**, **CDs 2a-f** and **CDs 3a-e** (with regard to Chapter 3) is reported.

9.2.Experimental section

9.2.1. Materials

N,N′-Diisopropylcarbodiimide (≥98%), N-(3-Dimethylaminopropyl)-N'-ethylcarbodiimide hydrochloride (≥99%), O-(7-Azabenzotriazol-1-yl)-N,N,N',N'-tetramethyluronium hexafluorophosphate (99%), Thionyl chloride (97%), Citric acid anhydrous (≥99.5%), ethylendiamine (99+%), diethylenetriamine (≥99%), triethylenetetramine (≥97%), tris(2-aminoethyl)amine (96%), *o*-phenylenediamine, *m*-phenylenediamine, *p*-phenylenediamine, n-butylamine (≥99%), N,N-Diethylethylenediamine (≥99%), aniline (≥99.5%), cysteamine (95%), N-Boc-ethylenediamine(≥98%), were used without further purifications. Dialysis tubes with molecular weight cut-off (MWCO) 0.5-1 KDa were bought from Spectrum Labs.

9.2.2. Instruments

- Atomic force microscopy (AFM) images were acquired in air under ambient conditions using a NT-MDT Aura NTEGRA instrument operating in tapping mode at 110 kHz resonance with Au tips HA_NC ETALON (10nm curvature radius). Samples were prepared on silica substrates by drop casting of diluite water solutions and dried at 50 ^{o}C. Particle height distribution analysis was carried out by using the Gwyddion software.
- Elemental analyses were performed in a Thermo Flash EA 1112 instrument with ∼3 mg of powder samples.
- Infrared absorption measurements were performed on powder samples pressed with KBr into pellets with a Bruker Vertex 70 spectrometer.
- ^{1}H and ^{13}C NMR spectra were recorded in D_2O solutions at 25 ^{o}C on a Bruker AV500 spectrometer (δ in ppm and J in Hz) at a ^{1}H NMR operating frequency of 500.13 MHz. ^{1}H and ^{13}C NMR spectra were referenced using the solvent signal as an internal standard. The assignment of the ^{1}H NMR signals and the corresponding ^{13}C NMR peaks was carried out using standard ^{1}H–^{13}C edited-HSQC and ^{1}H–^{13}C HMBC (J_{HC} = 8 Hz) 2D-experiments. The determination of the diffusion coefficients D (m^2/s) was

performed at controlled temperature (300 K) in spinning solutions of the corresponding compounds in D_2O (concentrations about 2 mM). The values of delta (δ) and delta (Δ) were optimized for each sample. In the case of δ the values found were in the range 1.7-2.0 ms, while for Δ the optimized values ranged from 0.17-0.20 s.

- UV/Vis absorption spectra were recorded on a Shimadzu UV-2401 PC spectrophotometer.
- Photoluminescence excitation and emission spectra were recorded on a Horiba Jobin Yvon Fluoromax-P, slits of excitation and emission at 1 mm. All the spectra were recorded at room temperature using 10 mm path-length quartz cuvette.

9.2.3. Procedures

CDs 1a

500 mg of anhydrous citric acid (2.6 mmol, 1 eq.) was dissolved in 5.0 ml of DMF. The solution was cooled in an ice bath and 1.21 ml of diisopropyl carbodiimide (DIC, 3 eq.) were added. Subsequently, 175 µl of ethylenediamine (1 eq.) in 5 ml of water were added and the reaction was stirred for 10 minutes at room temperature, during which the mixture turns its color from slightly yellow to orange. Afterwards the reaction was filtrated on paper filter and stopped by adding a NaOH solution until the pH is around 10. The reaction was stirred for 1 hour. The crude was diluted in ultrapure water, filtrated on paper filter and washed with ethyl acetate 3 times. During these operations the coupling agent urea byproduct, in the form of a white precipitate, was removed. Finally the water phase was adjusted to pH=7 with a diluited HCl solution and dialyzed against ultrapure water (MWCO = 0.5-1.0 KDa, 4 days, twice a day). After filtration on a 0.22 µm pore-size filter, the water was removed by freeze-drying, obtaining 310 mg of product (yield in mass of 45 wt. %).

CDs 1b

520 mg of anhydrous citric acid (2.7 mmol, 1 eq.) was dissolved in 6.0 ml of water with 180 µl of EDA (1 eq.) and the solution was cooled in an ice bath. Subsequently, 1.55 g of N-(3-Dimethylaminopropyl)-N′-ethylcarbodiimide hydrochloride (EDC, 3 eq.) were added under stirring and the reaction was removed from the ice bath. In 30 minutes the solution becomes intense yellow, at this point a NaOH solution was added until reaching pH=10. The reaction was stirred for 1 hour. Afterwards the crude was washed with ethyl acetate 3 times. Finally

the water phase was adjusted to pH=7 with a diluited HCl solution and dialyzed against ultrapure water (MWCO = 0.5-1.0 KDa, 4 days, twice a day). After filtration on a 0.22 μm pore-size filter, the water was removed by freeze-drying, obtaining 270 mg of product (yield in mass of 40 wt. %).

CDs 1c

520 mg of anhydrous citric acid (2.7 mmol, 1 eq.) was dissolved in 5 ml of water with 180 μl of EDA (1 eq.). Subsequently, 3.08 g of N-methylmethanaminium hexafluorophosphate N-oxide (HATU, 3 eq.) dissolved in 5 ml of water. In 20 minutes the solution becomes dark yellow, at this point a NaOH solution was added until reaching pH=10. The reaction was stirred for 1 hour. Afterwards the crude was washed with ethyl acetate two times and dichloromethane one time. Finally the water solution was adjusted to pH=7 with a diluited HCl solution and dialyzed against ultrapure water (MWCO = 0.5-1.0 KDa, 4 days, twice a day). After filtration on a 0.22 μm pore-size filter, the water was removed by freeze-drying, then acetonitrile was added to the solid in order to clean the traces of HATU, and the product was recovered by centrifugation and dried under vacum. 130 mg of product were obtained (yield in mass of 19 wt. %).

CDs 1d

520 mg of anhydrous citric acid (2.7 mmol, 1 eq.) was dissolved in 2 ml of anhydrous THF in a round bottom flask. The solution was heated up to 60°C, then 2.4 ml of thyonil chloride were added under stirring. After 3 hours the flask was cooled and the thyonyl chloride was carefully removed by rotavapor equipped with a trap containing a cold NaOH solution. Next, 5 ml of cold THF containing 180 μl of EDA (1 eq.) and 400 μl of N,N-diisopropylethylamine were added slowly to the flask while stirring. The solution turned quickly to dark brown. After two minutes a NaOH solution was added until reaching pH=10. After one hour the crude was filtrated on a 0.45 μm pore-size filter and washed two times with dichloromethane. The pH of the dispersion was adjusted to 7 with a diluited HCl solution, then the product was concentrated in rotavapor and ethanol was added. The solid was recovered by centrifugation and redissolved in water. The solution was dialyzed against ultrapure water (MWCO = 0.5-1.0 KDa, 4 days, twice a day), filtrated on a 0.22 μm pore-size filter and the dry solid was obtained by freeze-drying with a mass of 400 mg (yield in mass of 59 wt. %).

CDs 2a

500 mg of anhydrous citric acid (2.6 mmol, 1 eq.) was dissolved in 5.0 ml of DMF. The solution was cooled in an ice bath and 1.21 ml of diisopropyl carbodiimide (DIC, 3 eq.) were added. Subsequently, 280 µl of diethylenetriamine (1 eq.) in 5 ml of water were added and the reaction was stirred for 10 minutes at room temperature, during which the mixture turned to yellow. Afterwards the reaction was filtrated on paper filter and stopped by adding a NaOH solution until the pH is around 10. The reaction was stirred for 1 hour. The crude was diluted in ultrapure water, filtrated on paper filter and washed with ethyl acetate 3 times. Finally the water phase was adjusted to pH=7 with a diluited HCl solution and dialyzed against ultrapure water (MWCO = 0.5-1.0 KDa, 4 days, twice a day). After filtration on a 0.22 µm pore-size filter, the water was removed by freeze-drying, obtaining 280 mg of product (yield in mass of 32 wt. %).

CDs 2b

500 mg of anhydrous citric acid (2.6 mmol, 1 eq.) was dissolved in 5.0 ml of DMF. The solution was cooled in an ice bath and 1.21 ml of diisopropyl carbodiimide (DIC, 3 eq.) were added. Subsequently, 390 µl of triethylenetetramine (1 eq.) in 5 ml of water were added and the reaction was stirred for 10 minutes at room temperature, during which the mixture turned to yellow. Afterwards the reaction was filtrated on paper filter and stopped by adding a NaOH solution until the pH is around 10. The reaction was stirred for 1 hour. The crude was diluted in ultrapure water, filtrated on paper filter and washed with ethyl acetate 3 times. Finally the water phase was adjusted to pH=7 with a diluited HCl solution and dialyzed against ultrapure water (MWCO = 0.5-1.0 KDa, 4 days, twice a day). After filtration on a 0.22 µm pore-size filter, the water was removed by freeze-drying, obtaining 280 mg of product (yield in mass of 32 wt. %).

CDs 2c

0.650 mg of anhydrous citric acid (3.4 mmol, 1 eq.) and 0.510 ml of tris(2-aminoethyl)amine (1 eq.) were dissolved in 10 ml of water and the solution was cooled in an ice bath. Subsequently, 1.95 g of N-(3-Dimethylaminopropyl)-N′-ethylcarbodiimide hydrochloride (EDC, 3 eq.) were added under stirring and the reaction was removed from the ice bath. In 20 minutes the solution becomes intense yellow, at this point a NaOH solution was added until reaching pH=10. The reaction was stirred for 1 hour. Afterwards the crude was washed with

ethyl acetate 3 times. Finally the water phase was adjusted to pH=7 with a diluited HCl solution and dialyzed against ultrapure water (MWCO = 0.5-1.0 KDa, 4 days, twice a day). After filtration on a 0.22 μm pore-size filter, the water was removed by freeze-drying, obtaining 785 mg of product (yield in mass of 68 wt. %).

CDs 2d, 2e, 2f

300 mg of anhydrous citric acid (1.6 mmol, 1 eq.) was dissolved in 4.0 ml of DMF. The solution was cooled in an ice bath and 0.73 ml of diisopropyl carbodiimide (DIC, 3 eq.) were added. Subsequently, 169 mg of *o*-, *m*- or *p*-phenylenediamine (1 eq.) in 4 ml of water were added and the reaction was stirred for 10 minutes at room temperature, during which the mixture turns into yellow. at this point a NaOH solution was added until reaching pH=10. The reaction was stirred for 1 hour. Afterwards the crude was washed with ethyl acetate 2 times and dichloromethane 2 times. Finally the water phase was adjusted to pH=7 with a diluited HCl solution and dialyzed against ultrapure water (MWCO = 0.5-1.0 KDa, 4 days, twice a day). After filtration on a 0.22 μm pore-size filter, the water was removed by freeze-drying, obtaining 60 mg (2d), 140 mg (2e) and 130 mg (2f) of product.

CDs 3a

300 mg of anhydrous citric acid (1.6 mmol, 1 eq.) was dissolved in 4.0 ml of DMF. The solution was cooled in an ice bath and 0.73 ml of diisopropyl carbodiimide (DIC, 3 eq.) were added. Subsequently, 105 μl of ethylenediamine (1 eq.) in 4 ml of water were added and the reaction was stirred for 10 minutes at room temperature, during which the mixture turns its color from slightly yellow to orange. Afterwards 0.62 ml of n-butylamine (4 eq.) dissolved in 4 ml of water were poured into the reaction. The reaction was stirred for 1 hour. The crude was diluted in ultrapure water, filtrated on paper filter and washed with ethyl acetate 2 times and dichloromethane 2 times. Finally the water phase was adjusted to pH=7 with a diluited HCl solution and dialyzed against ultrapure water (MWCO = 0.5-1.0 KDa, 4 days, twice a day). After filtration on a 0.22 μm pore-size filter, the water was removed by freeze-drying, obtaining 250 mg of product.

CDs 3b

600 mg of anhydrous citric acid (3.1 mmol, 1 eq.) was dissolved in 6.0 ml of DMF. The solution was cooled in an ice bath and 1.45 ml of diisopropyl carbodiimide (DIC, 3 eq.) were added. Subsequently, 210 μl of ethylenediamine (1 eq.) in 6 ml of water were added and the

reaction was stirred for 10 minutes at room temperature, during which the mixture turns its color from slightly yellow to orange. Afterwards 2.64 ml of *N*,*N*-Diethylethylenediamine (6 eq.) dissolved in 4 ml of water were poured into the reaction. The reaction was stirred for 1 hour. The crude was diluted in ultrapure water, filtrated on paper filter and washed with ethyl acetate 2 times and dichloromethane 2 times. Finally the water phase was adjusted to pH=7 with a diluited HCl solution and dialyzed against ultrapure water (MWCO = 0.5-1.0 KDa, 4 days, twice a day). After filtration on a 0.22 μm pore-size filter, the water was removed by freeze-drying, obtaining 250 mg of product.

CDs 3c

300 mg of anhydrous citric acid (1.6 mmol, 1 eq.) was dissolved in 4.0 ml of DMF. The solution was cooled in an ice bath and 0.73 ml of diisopropyl carbodiimide (DIC, 3 eq.) were added. Subsequently, 105 μl of ethylenediamine (1 eq.) in 4 ml of water were added and the reaction was stirred for 10 minutes at room temperature, during which the mixture turns its color from slightly yellow to orange. Afterwards 0.58 ml of aniline (4 eq.) dissolved in 4 ml of water were poured into the reaction. The reaction was stirred for 1 hour. The crude was diluted in ultrapure water, filtrated on paper filter and washed with ethyl acetate 2 times and dichloromethane 2 times. Finally the water phase was adjusted to pH=7 with a diluited HCl solution and dialyzed against ultrapure water (MWCO = 0.5-1.0 KDa, 4 days, twice a day). After filtration on a 0.22 μm pore-size filter, the water was removed by freeze-drying, obtaining 170 mg of product.

CDs 3d

300 mg of anhydrous citric acid (1.5 mmol, 1 eq.) was dissolved in 4.0 ml of DMF. The solution was cooled in an ice bath and 0.73 ml of diisopropyl carbodiimide (DIC, 3 eq.) were added. Subsequently, 105 μl of ethylenediamine (1 eq.) in 4 ml of water were added and the reaction was stirred for 10 minutes at room temperature, during which the mixture turns its color from slightly yellow to orange. Afterwards 480 mg of cysteamine (4 eq.) dissolved in 4 ml of water were poured into the reaction. The reaction was stirred for 1 hour. The crude was diluted in ultrapure water, filtrated on paper filter and washed with ethyl acetate 3 times. Finally the water phase was adjusted to pH=7 with a diluited HCl solution and dialyzed against ultrapure water (MWCO = 0.5-1.0 KDa, 4 days, twice a day). After filtration on a 0.22 μm pore-size filter, the water was removed by freeze-drying, obtaining 160 mg of product.

CDs 3e

300 mg of anhydrous citric acid (1.6 mmol, 1 eq.) was dissolved in 4.0 ml of DMF. The solution was cooled in an ice bath and 0.73 ml of diisopropyl carbodiimide (DIC, 3 eq.) were added. Subsequently, 105 µl of ethylenediamine (1 eq.) in 4 ml of water were added and the reaction was stirred for 10 minutes at room temperature, during which the mixture turns its color from slightly yellow to orange. Afterwards 1.01 ml of N-Boc-ethylenediamine (4 eq.) dissolved in 4 ml of water were poured into the reaction. The reaction was stirred for 1 hour. The crude was diluted in ultrapure water, filtrated on paper filter and washed with ethyl acetate 3 times. Finally the water phase was adjusted to pH=7 with a diluited HCl solution and dialyzed against ultrapure water (MWCO = 0.5-1.0 KDa, 4 days, twice a day). After filtration on a 0.22 µm pore-size filter, the water was removed by freeze-drying, obtaining 220 mg of product.

9.2.4. Pictures of the reaction

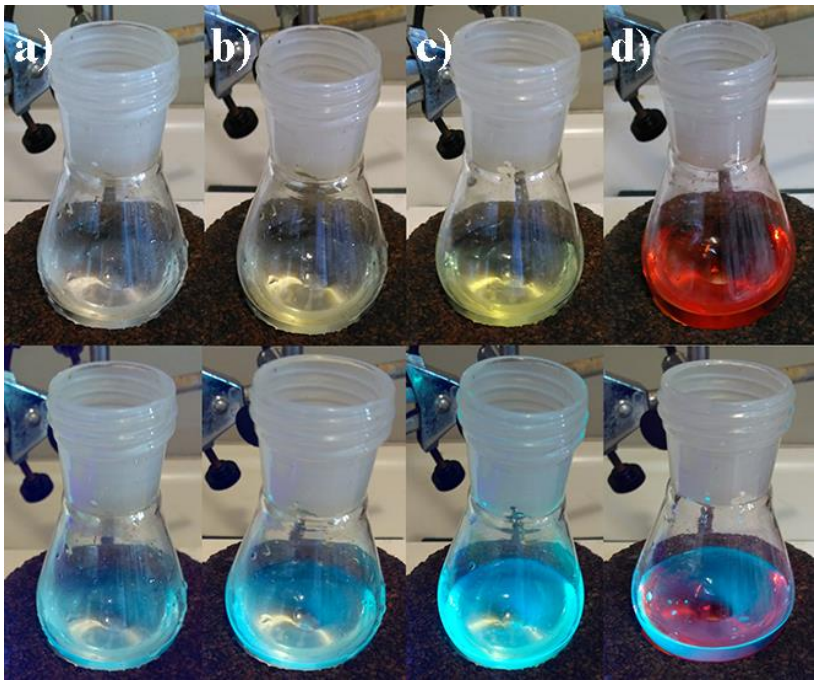

Figure 9.2. Pictures taken at different times during the synthesis of **CDs 1b**, with the UV lamp off (top) and on (bottom): a) after the addition of EDC, b) after 5 minutes, c) after 20 minutes, d) after 30 minutes and addition of NaOH solution.

9.3. Characterization

9.3.1. Atomic force microscopy of CDs 1a-d

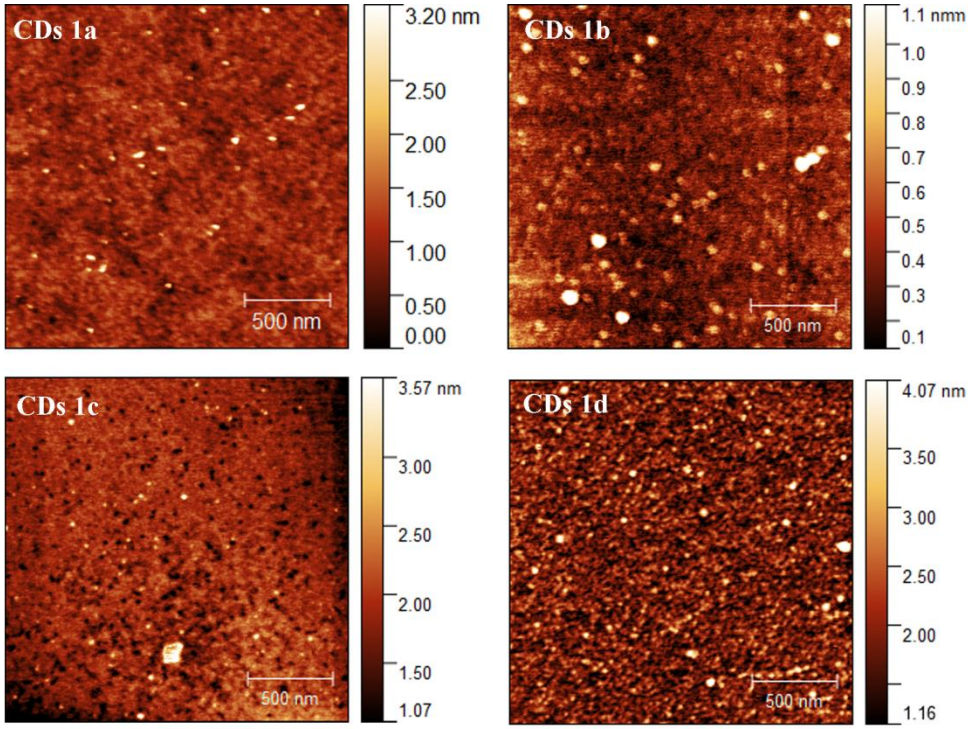

Figure 9.3. AFM pictures of CDs 1a-d. In all the samples, the height of the nanoparticles is comprised between 1-2 nm.

9.3.2. Diffusion ordered spectroscopy (DOSY) of CDs 1a-d

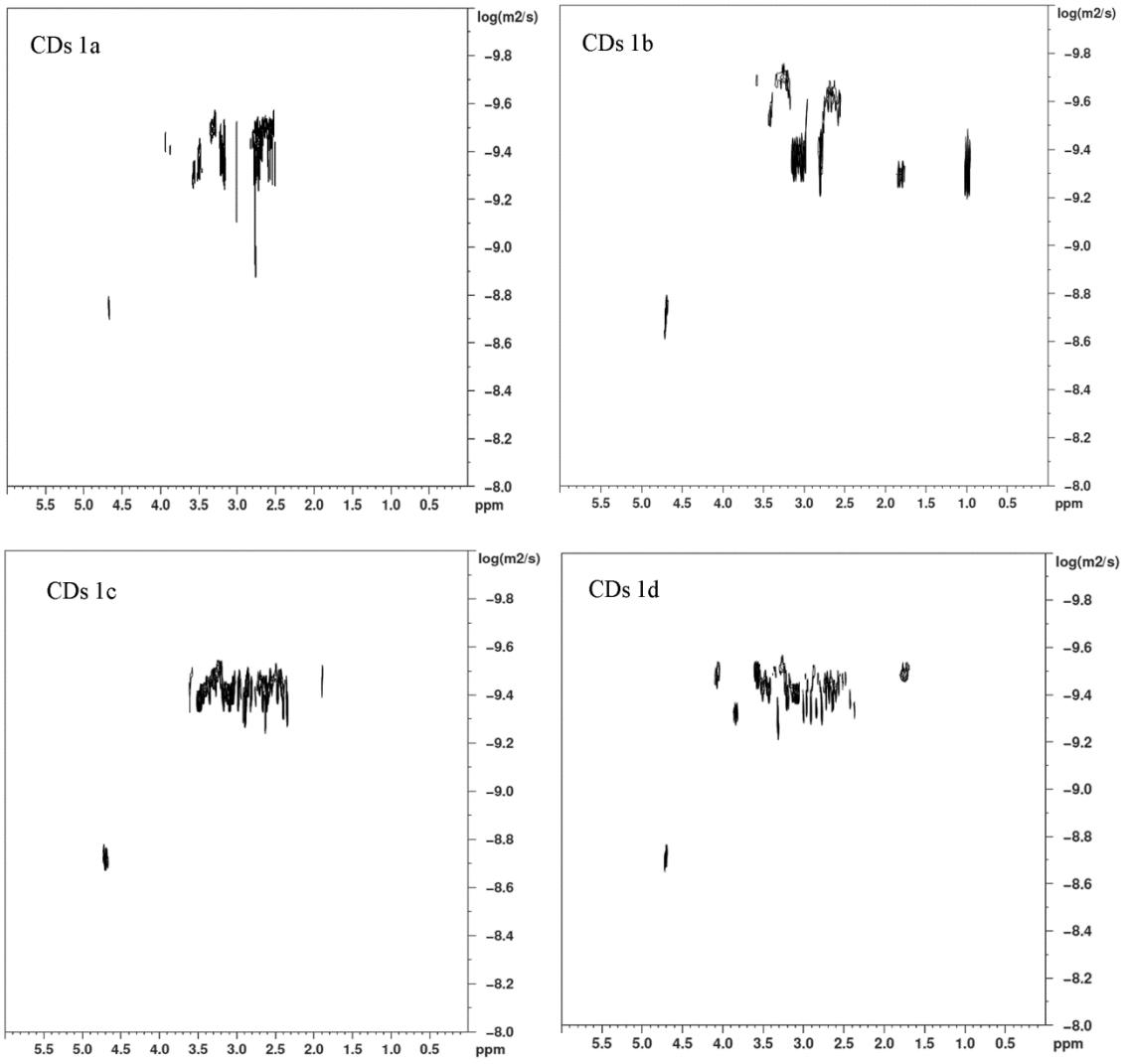

Figure 9.4. DOSY spectra of CDs 1a-d.

Table 9.4. The measured diffusion coefficients (D) and the calculated hydrodynamic rays (rH) and diameters of CDs 1a-d. Assuming a globular shape, the calculated size of the nanoparticles is comprised between 1.2-2.0 nm.

	D (m^2/s)	rH (nm)	Diameter (nm)
CDs 1a	$10^{-9.4}$	0.6	1.2
CDs 1b	$10^{-9.6}$	1.0	2.0
CDs 1c	$10^{-9.4}$	0.6	1.2
CDs 1d	$10^{-9.5}$	0.8	1.6

9.3.3. Elemental analysis of CDs 1a-d

Table 9.5. C, H, N, O and S mole percentages of CDs 1a-d, obtained by elemental analysis. Additionally, the calculated elemental composition of the expected polymer repetitive unit is reported for comparison.

	C (mol%)	H (mol%)	N (mol%)	O (mol%)	S (mol%)
$C_8H_{12}N_2O_5$	29.6	44.4	7.4	18.5	--
CDs 1a	26.5	48	7	18.5	--
CDs 1b	27.3	50	8.1	14.6	--
CDs 1c	27.1	48	8.6	16.4	--
CDs 1d	26.2	45.8	6.6	21.4	1.2

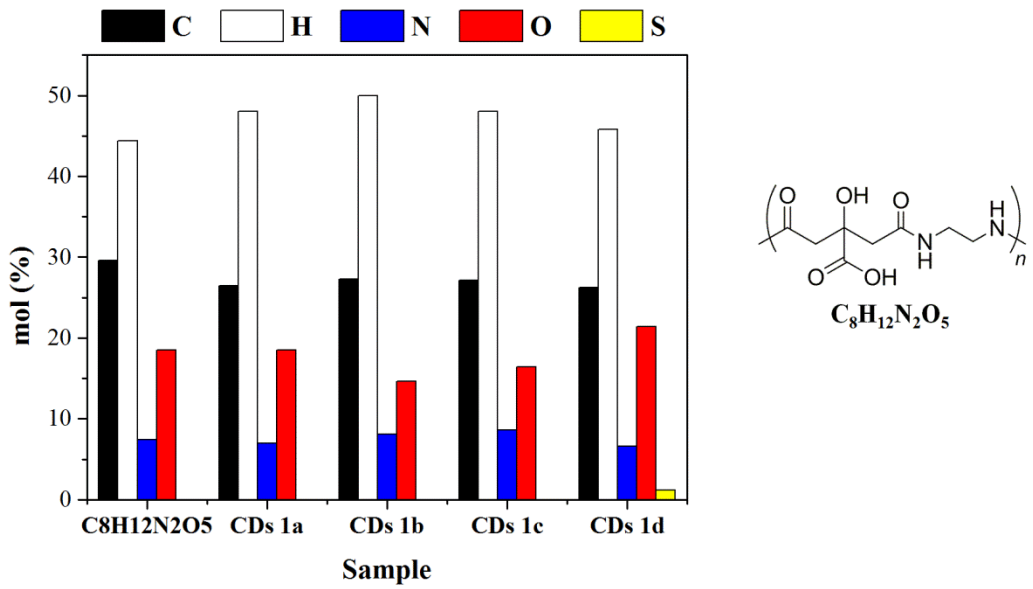

Figure 9.5. Visual comparison between the measured elemental composition of CDs 1a-d and the calculated elemental composition of the expected polymer structure.

9.3.4. IR spectra of CDs 1a-d

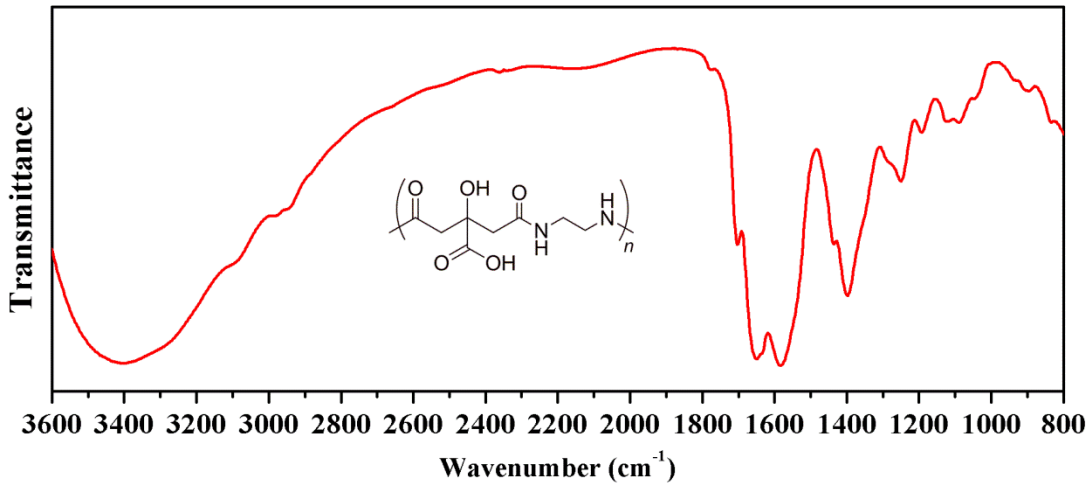

Figure 9.6. IR spectrum of CDs 1a. 3400-2800 cm^{-1}: O-H and N-H stretching, 1704 cm^{-1}: C=O stretching (carboxylic acid), 1650 and 1583 cm^{-1}: C=O stretching (amide), 1440-1350 cm^{-1}: C-O and C-N stretching.

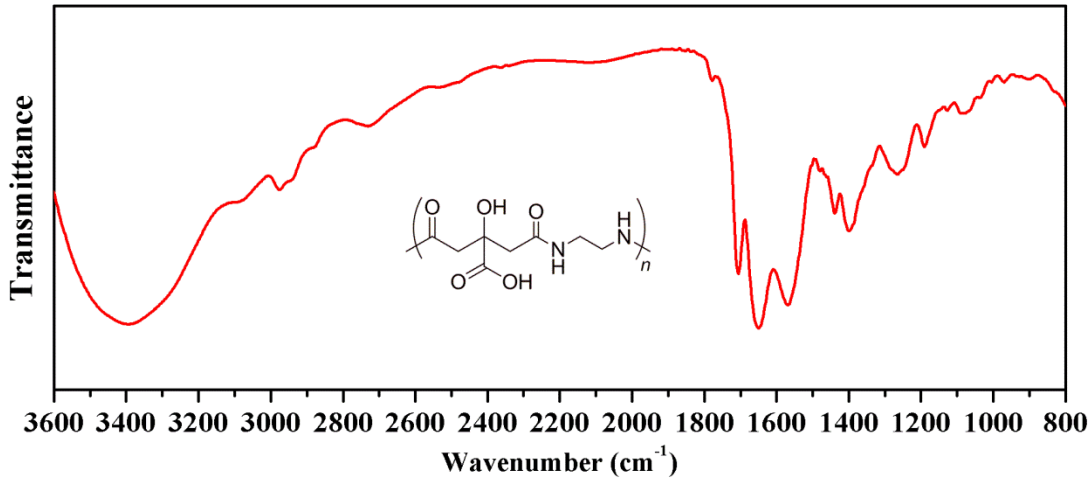

Figure 9.7. IR spectrum of CDs 1b. 3400-2800 cm^{-1}: O-H and N-H stretching, 1704 cm^{-1}: C=O stretching (carboxylic acid), 1650 and 1567 cm^{-1}: C=O stretching (amide), 1440-1350 cm^{-1}: C-O and C-N stretching.

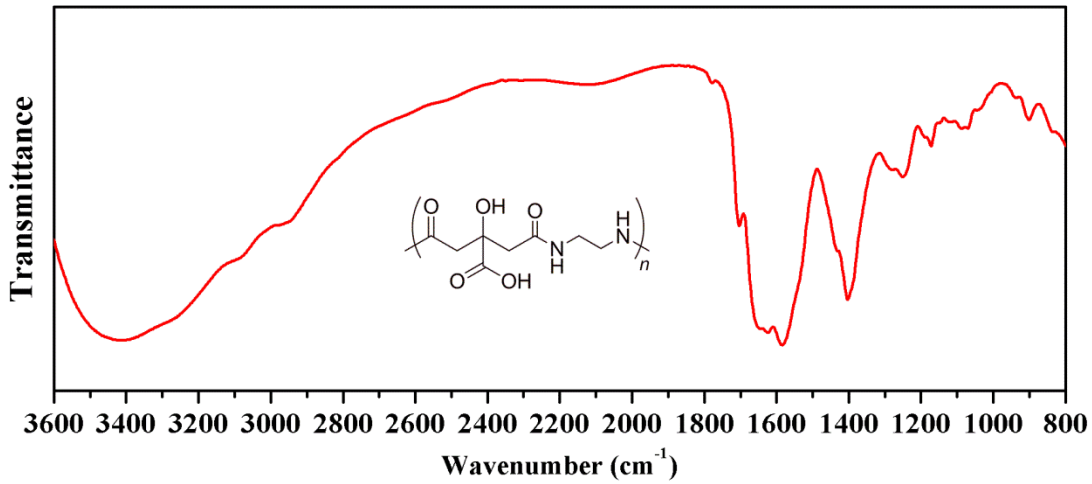

Figure 9.8. IR spectrum of CDs 1c. 3400-2800 cm^{-1}: O-H and N-H stretching, 1702 cm^{-1}: C=O stretching (carboxylic acid), 1650 and 1582 cm^{-1}: C=O stretching (amide), 1440-1350 cm^{-1}: C-O and C-N stretching.

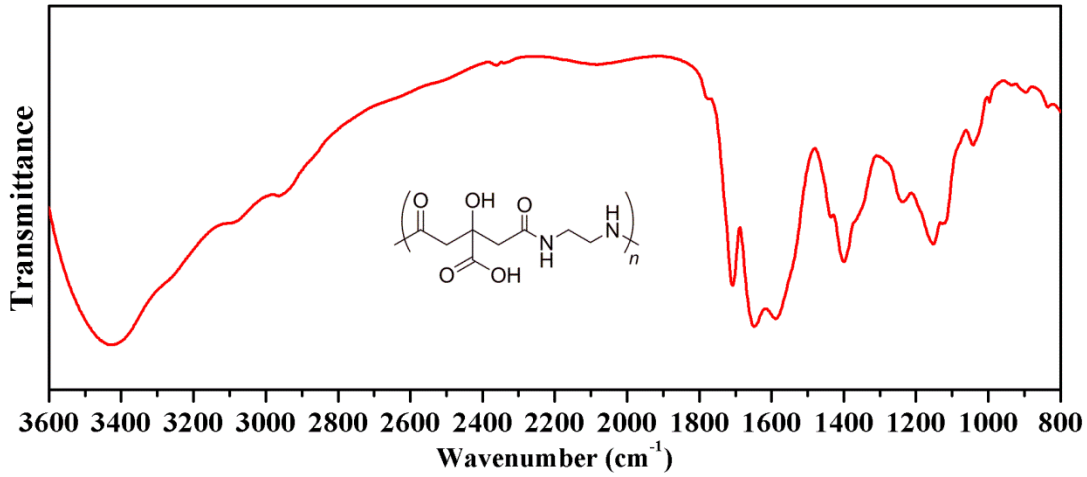

Figure 9.9. IR spectrum of CDs 1d. 3400-2800 cm^{-1}: O-H and N-H stretching, 1708 cm^{-1}: C=O stretching (carboxylic acid), 1650 and 1588 cm^{-1}: C=O stretching (amide), 1440-1350 cm^{-1}: C-O and C-N stretching.

9.3.5. NMR spectra of CDs 1a-d

CDs 1a

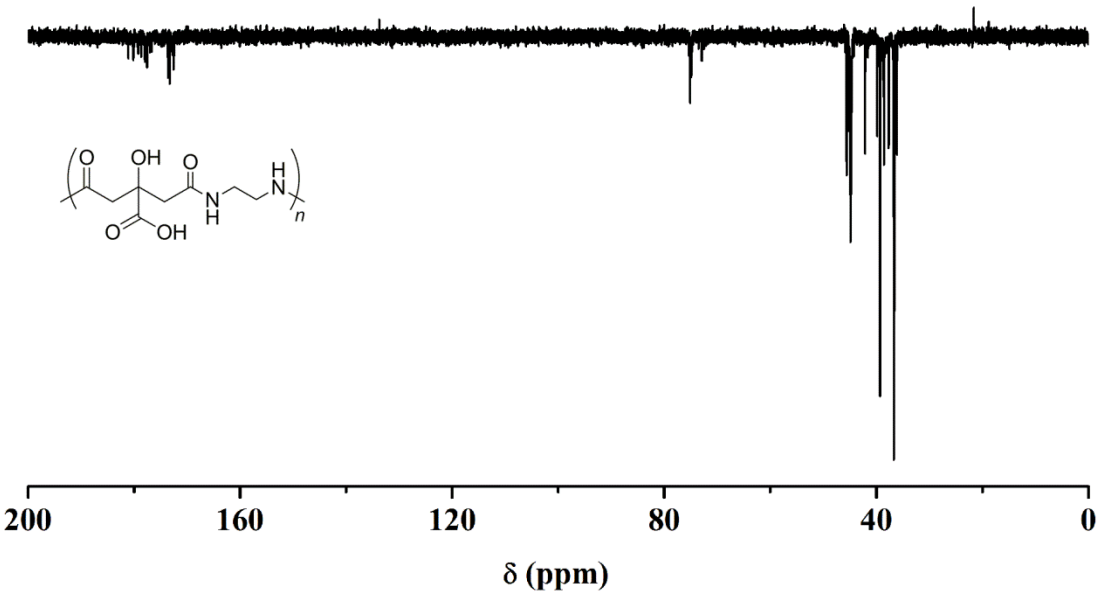

Figure 9.10. APT ^{13}C NMR spectrum of CDs 1a. Carboxylic acid and amide C: 182-171 ppm, quaternary C: 75-72 ppm, methylene C: 45-36 ppm. The positive signal at 21 ppm is due to DIC impurities.

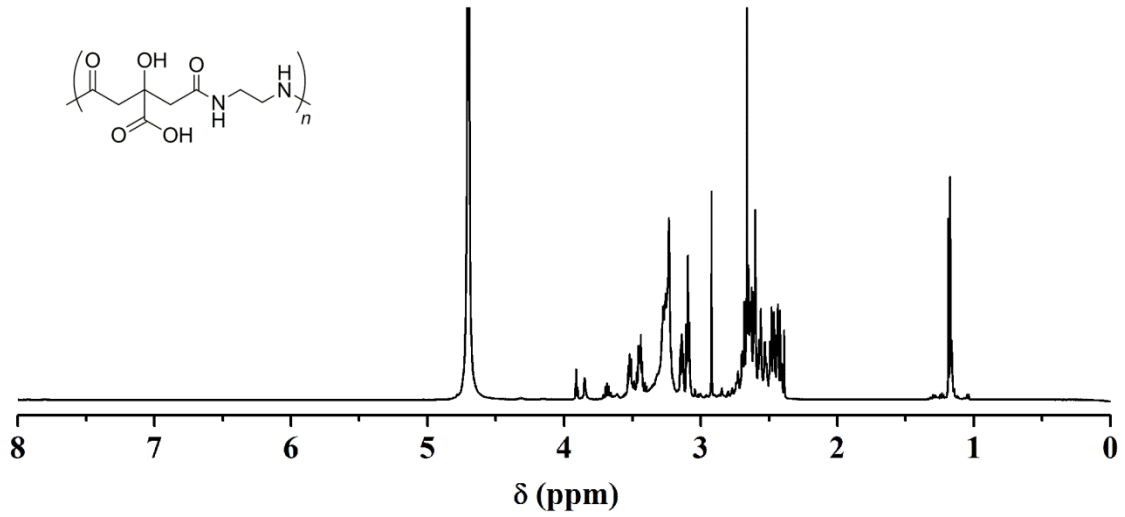

Figure 9.11. ^{1}H NMR spectrum of CDs 1a. methylene H: 3.9-2.3 ppm. The signal at 1.2 ppm is due to DIC impurities.

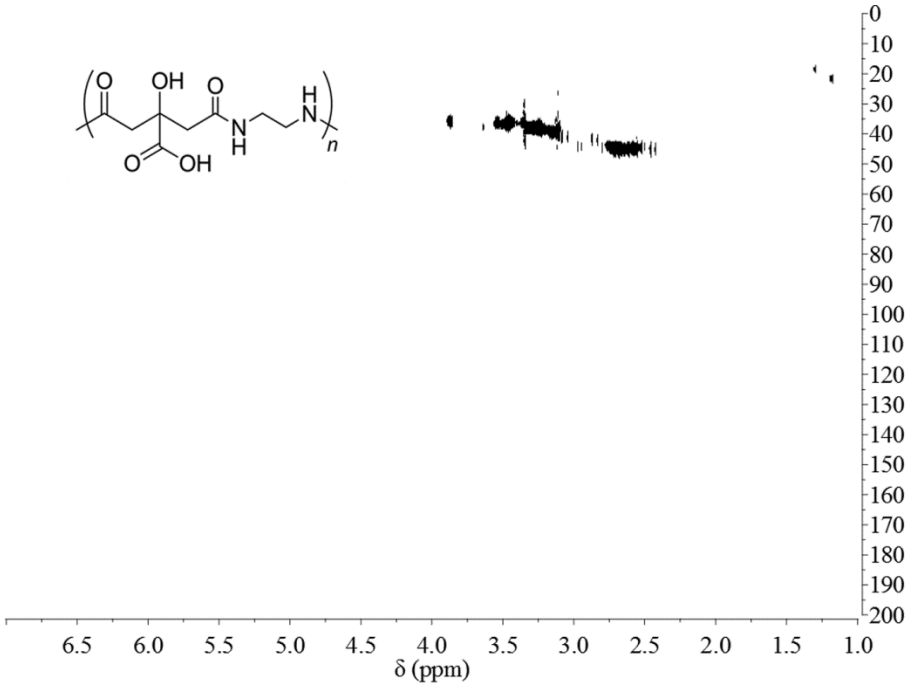

Figure 9.12. ^{1}H-^{13}C HSQC spectrum of CDs 1a.

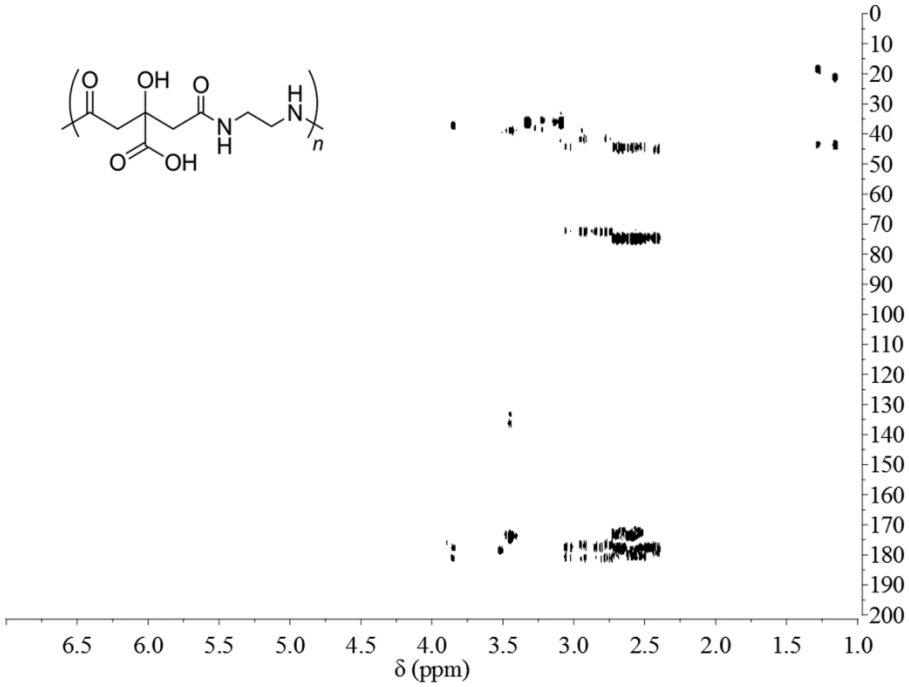

Figure 9.13. ^{1}H-^{13}C HMBC spectrum of CDs 1a.

CDs 1b

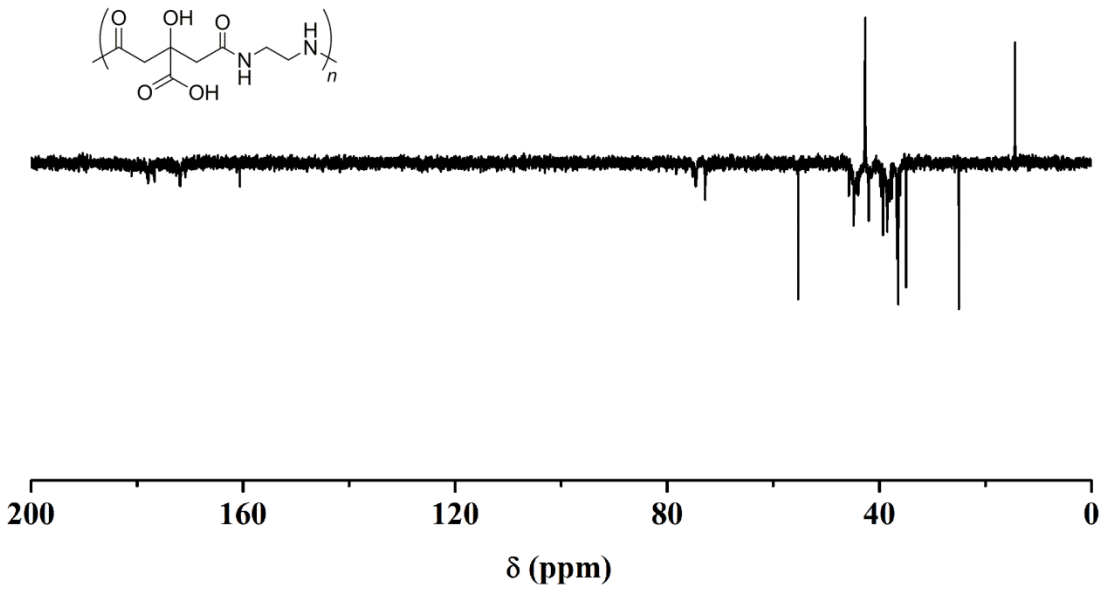

Figure 9.14. APT ^{13}C NMR spectrum of CDs 1b. Carboxylic acid and amide C: 180-170 ppm, quaternary C: 75-72 ppm, methylene C: 46-35 ppm. The signals at 160, 55, 42, 24, 14 ppm are due to EDC impurities.

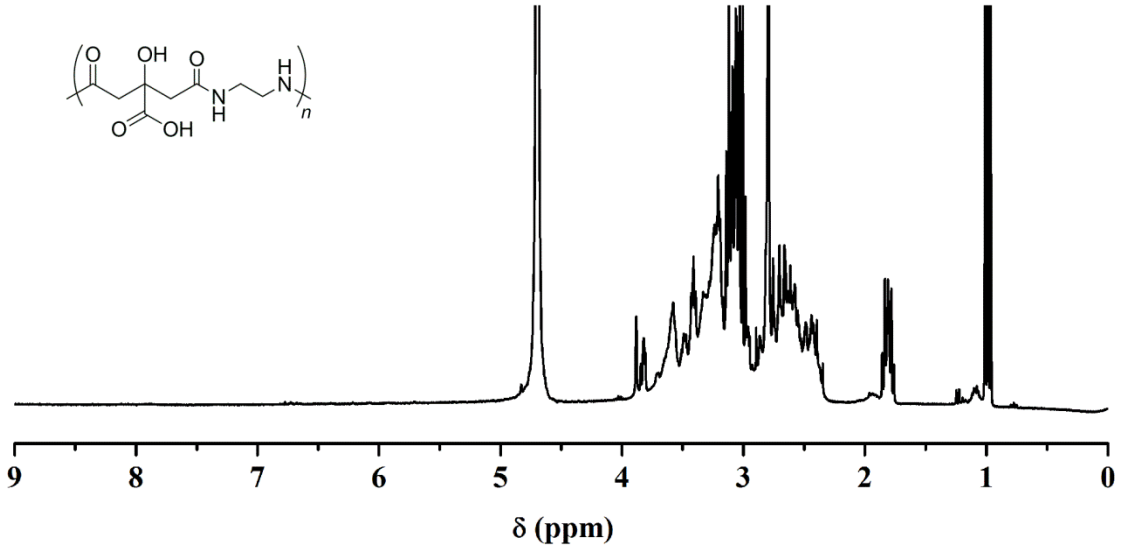

Figure 9.15. ^{1}H NMR spectrum of CDs 1b. methylene H: 3.9-2.3 ppm. The signals at 3.0, 2.8, 1.8, 1.0 ppm are due to EDC impurities.

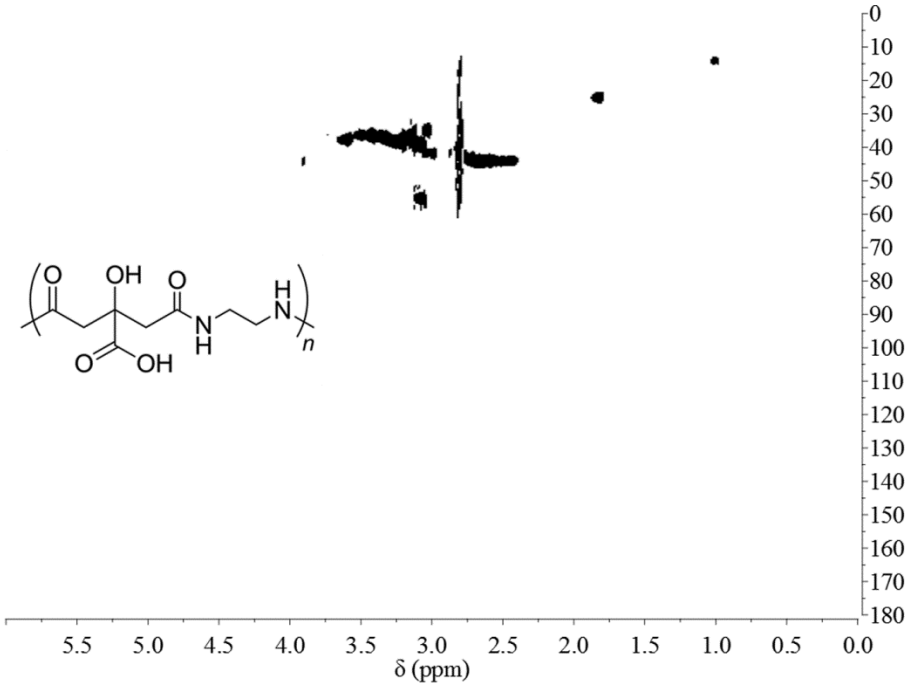

Figure 9.16. ^{1}H-^{13}C HSQC spectrum of CDs 1b.

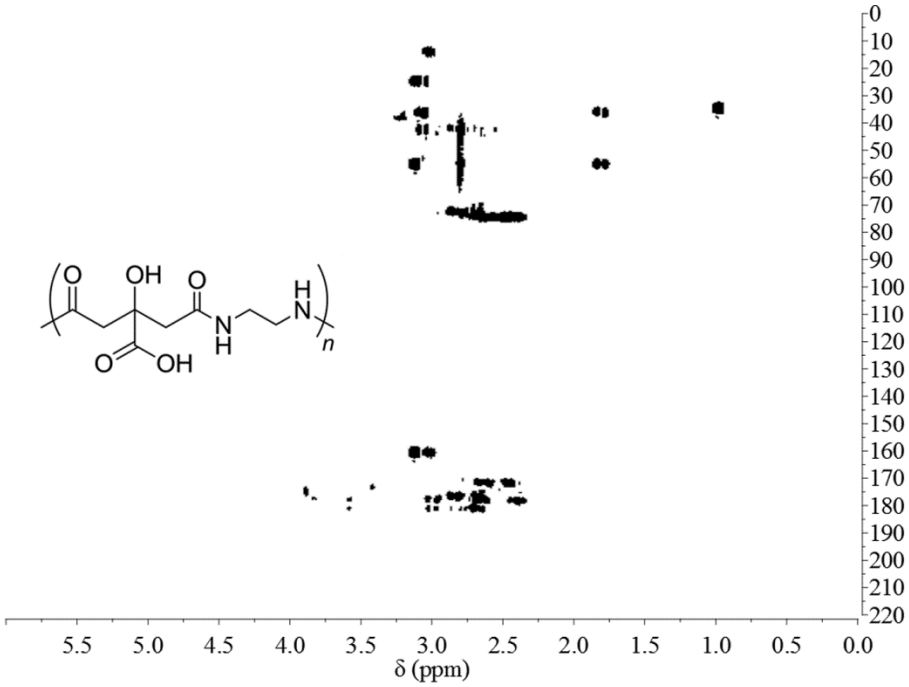

Figure 9.17. ^{1}H-^{13}C HMBC spectrum of CDs 1b.

CDs 1c

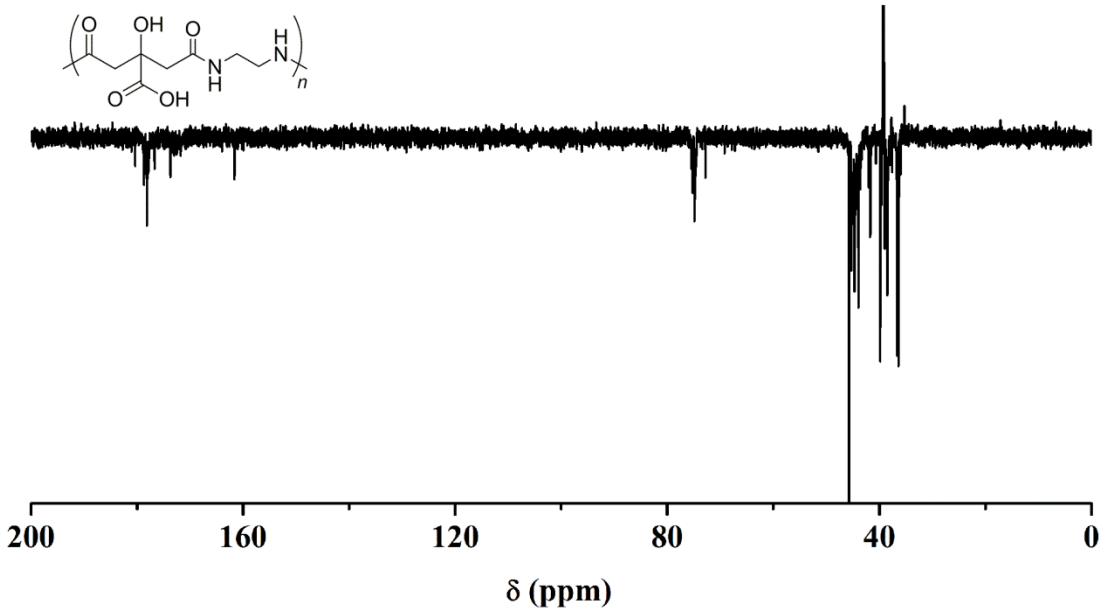

Figure 9.18. APT ^{13}C NMR spectrum of CDs 1c. Carboxylic acid and amide C: 180-172 ppm, quaternary C: 76-72 ppm, methylene C: 46-35 ppm. The signals at 161, 39, ppm are due to DMF traces.

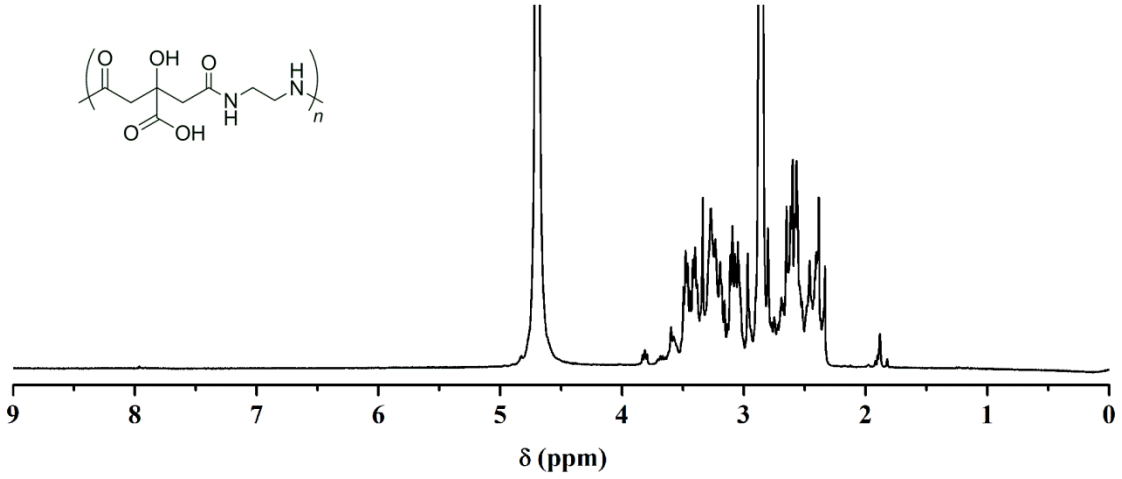

Figure 9.19. ^{1}H NMR spectrum of CDs 1b. methylene H: 3.8-2.3 ppm. The signals at 2.8 ppm is due to DMF traces.

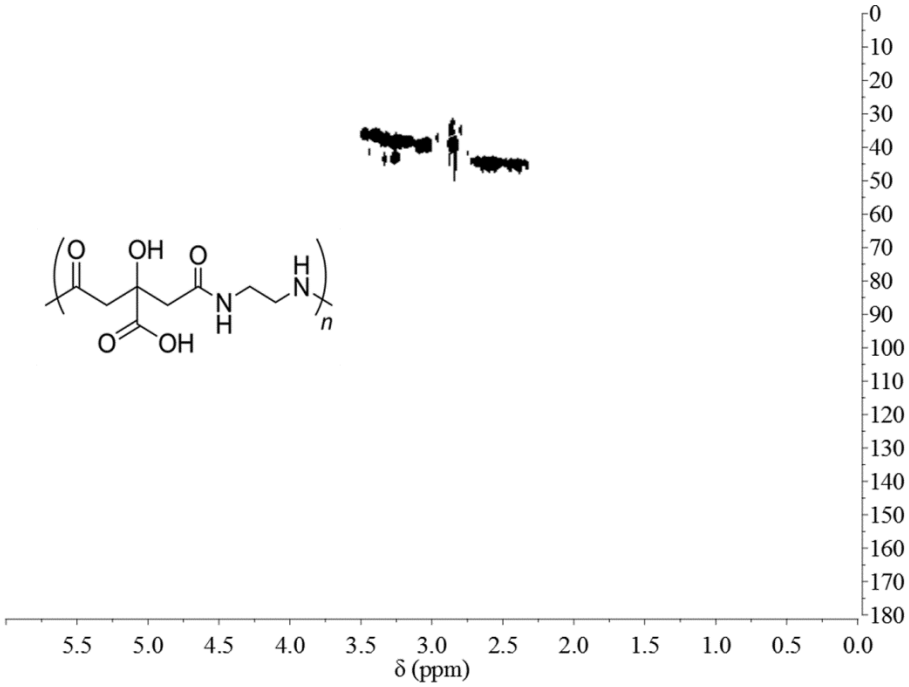

Figure 9.20. ^{1}H-^{13}C HSQC spectrum of CDs 1c.

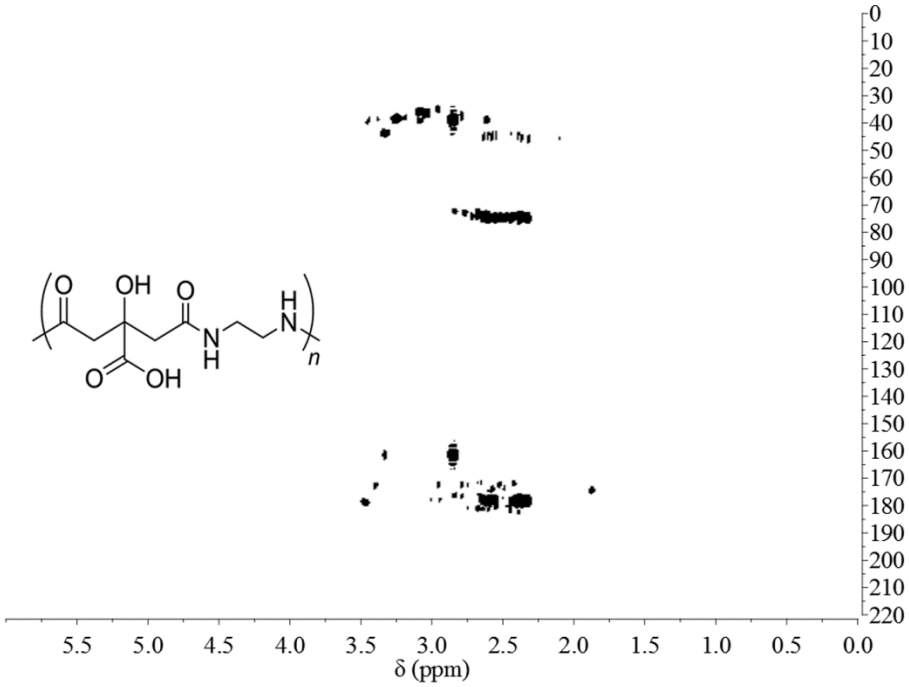

Figure 9.21. ^{1}H-^{13}C HMBC spectrum of CDs 1c.

CDs 1d

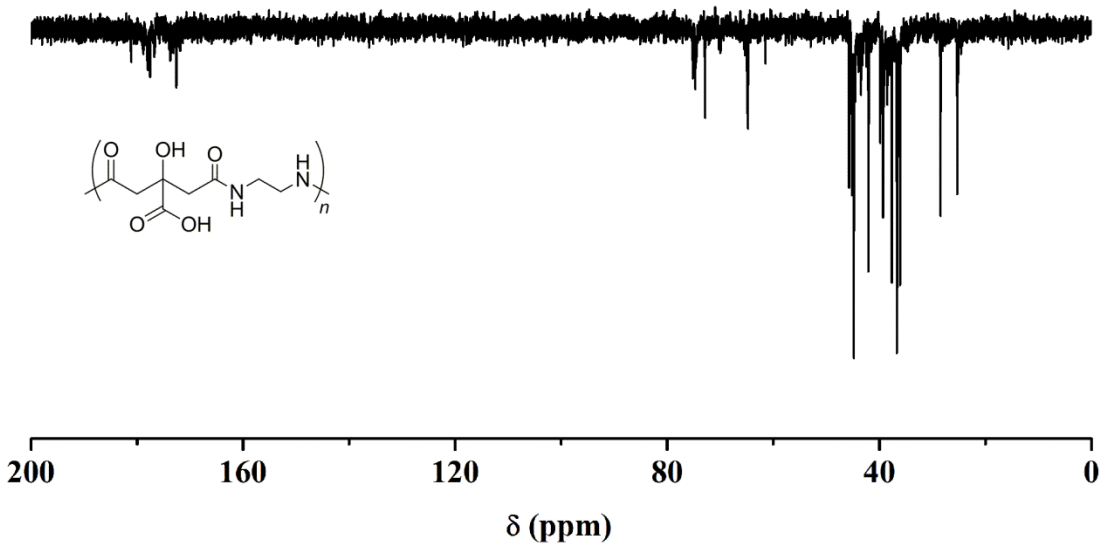

Figure 9.22. APT ^{13}C NMR spectrum of CDs 1d. Carboxylic acid and amide C: 181-172 ppm, quaternary C: 75-72 ppm, methylene C: 46-35 ppm. The signals at 65, 29, 25 ppm are due to the THF and its cleavage product by means of HCl.

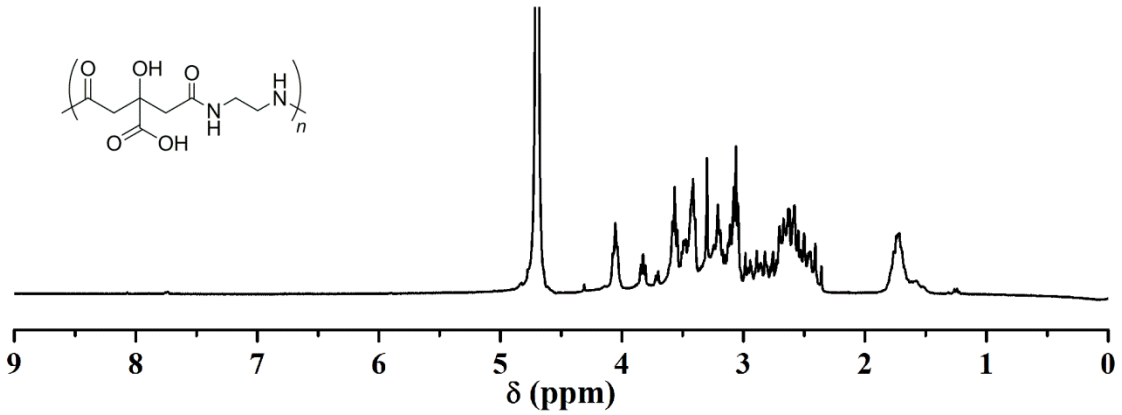

Figure 9.23. ^{1}H NMR spectrum of CDs 1d. methylene H: 3.8-2.3 ppm. The signals at 4.0, 1.7 ppm are due to the THF and its cleavage product by means of HCl.

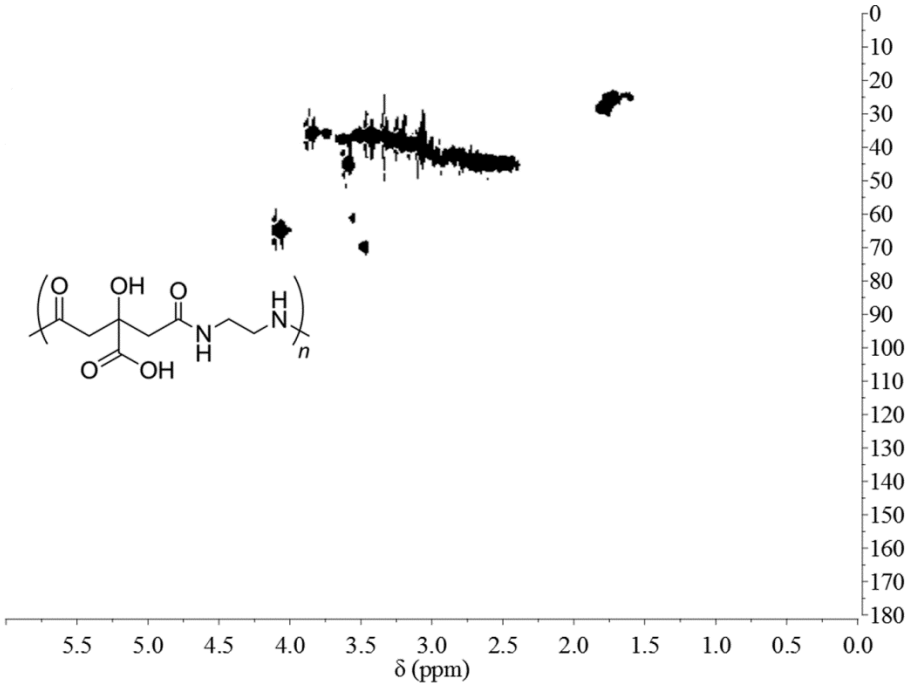

Figure 9.24. ^{1}H-^{13}C HSQC spectrum of CDs 1d.

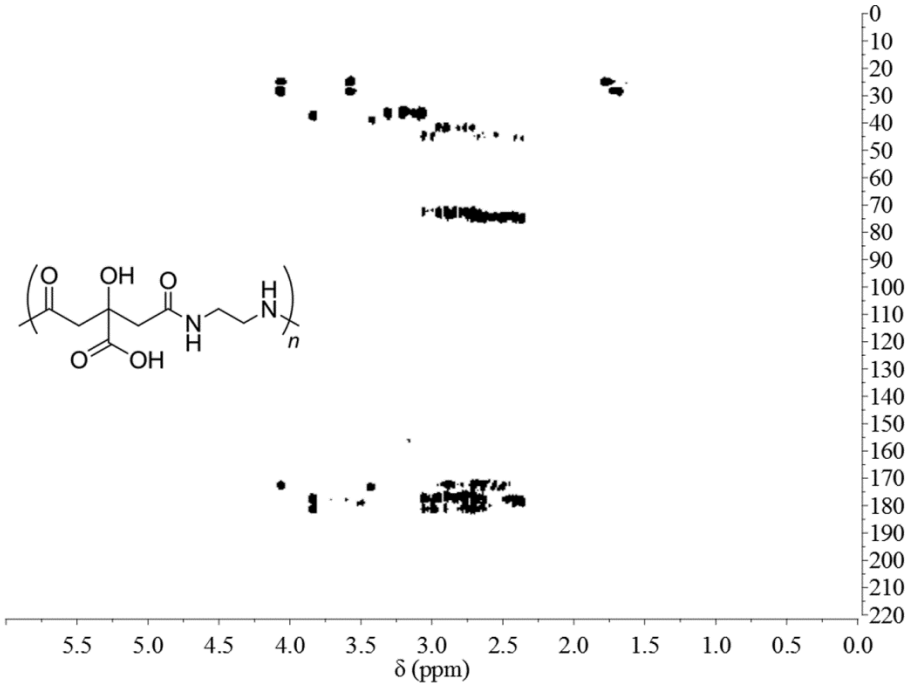

Figure 9.25. ^{1}H-^{13}C HMBC spectrum of CDs 1d.

9.3.6. UV/vis spectra of CDs 1a-d

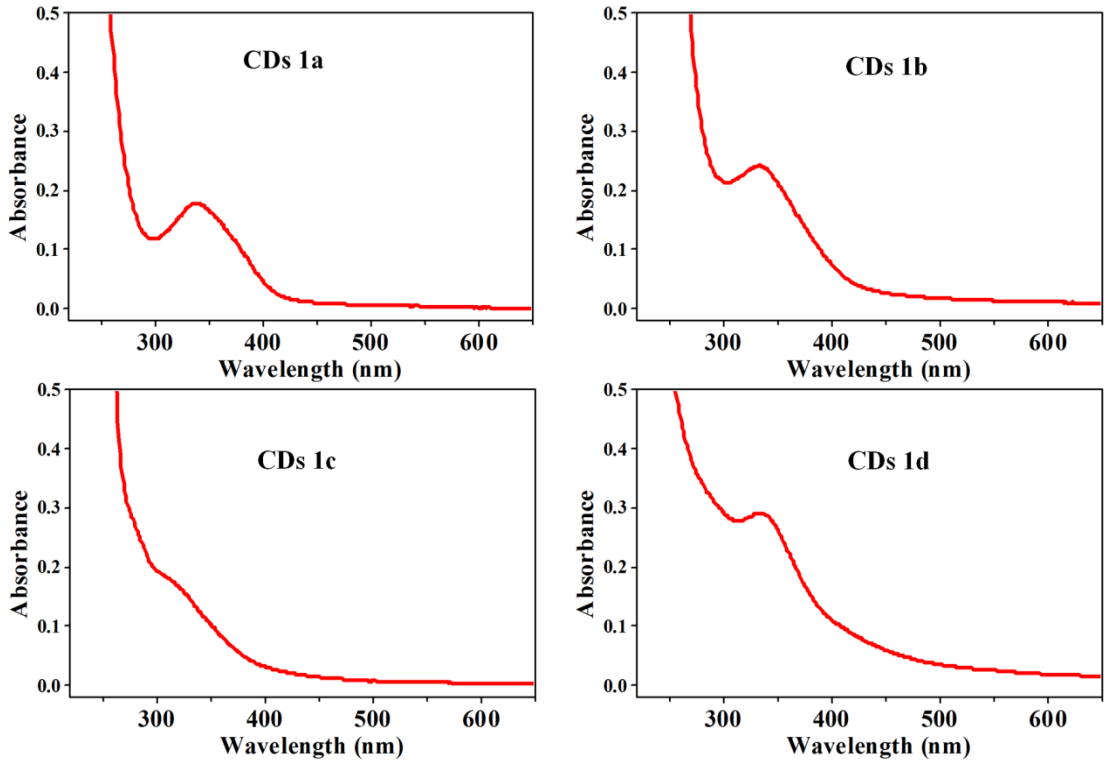

Figure 9.26. UV/vis spectra of CDs 1a-d.

9.3.7. Excitation and emission spectra of CDs 1a-d

CDs 1a

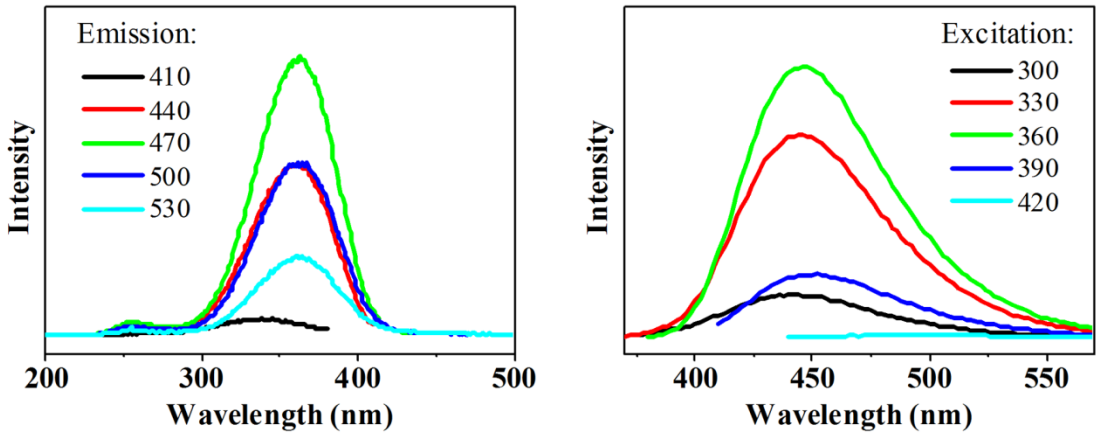

Figure 9.27. (left) excitation spectra for different emissions and (right) emission spectra for different excitations of CDs 1a.

CDs 1b

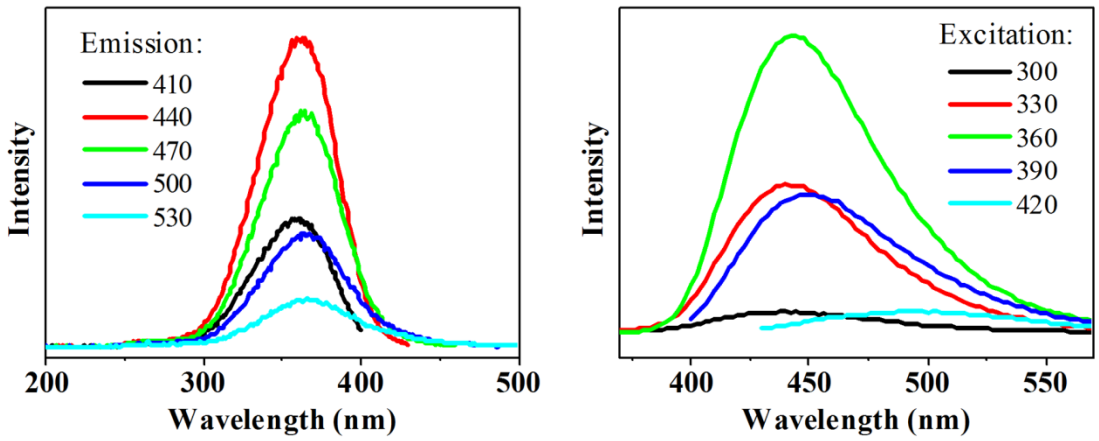

Figure 9.28. (left) excitation spectra for different emissions and (right) emission spectra for different excitations of CDs 1b.

CDs 1c

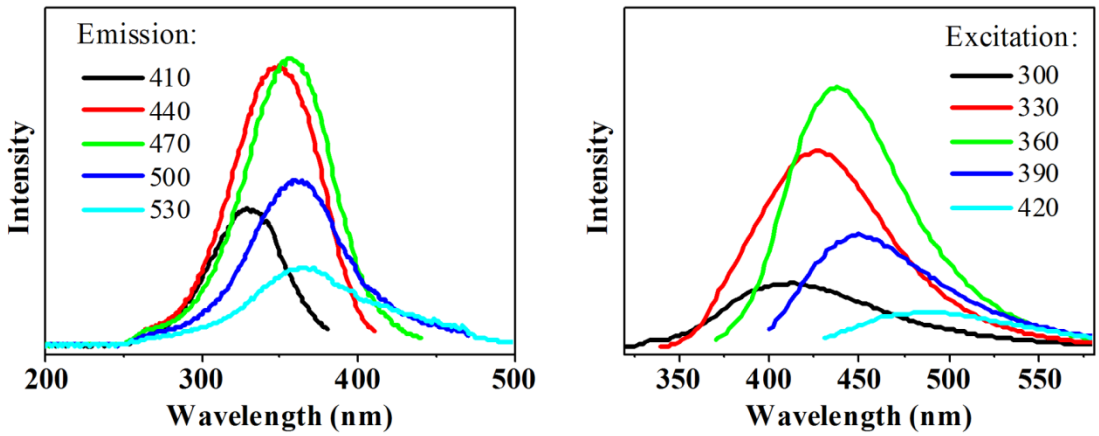

Figure 9.29. (left) excitation spectra for different emissions and (right) emission spectra for different excitations of CDs 1c.

CDs 1d

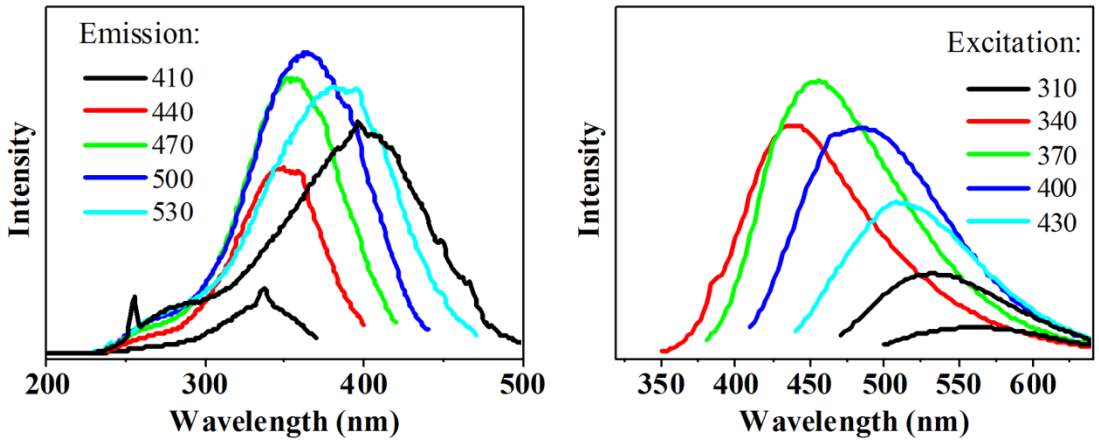

Figure 9.30. (left) excitation spectra for different emissions and (right) emission spectra for different excitations of CDs 1d.

9.3.8. Quantum yield measurements of CDs 1a-d

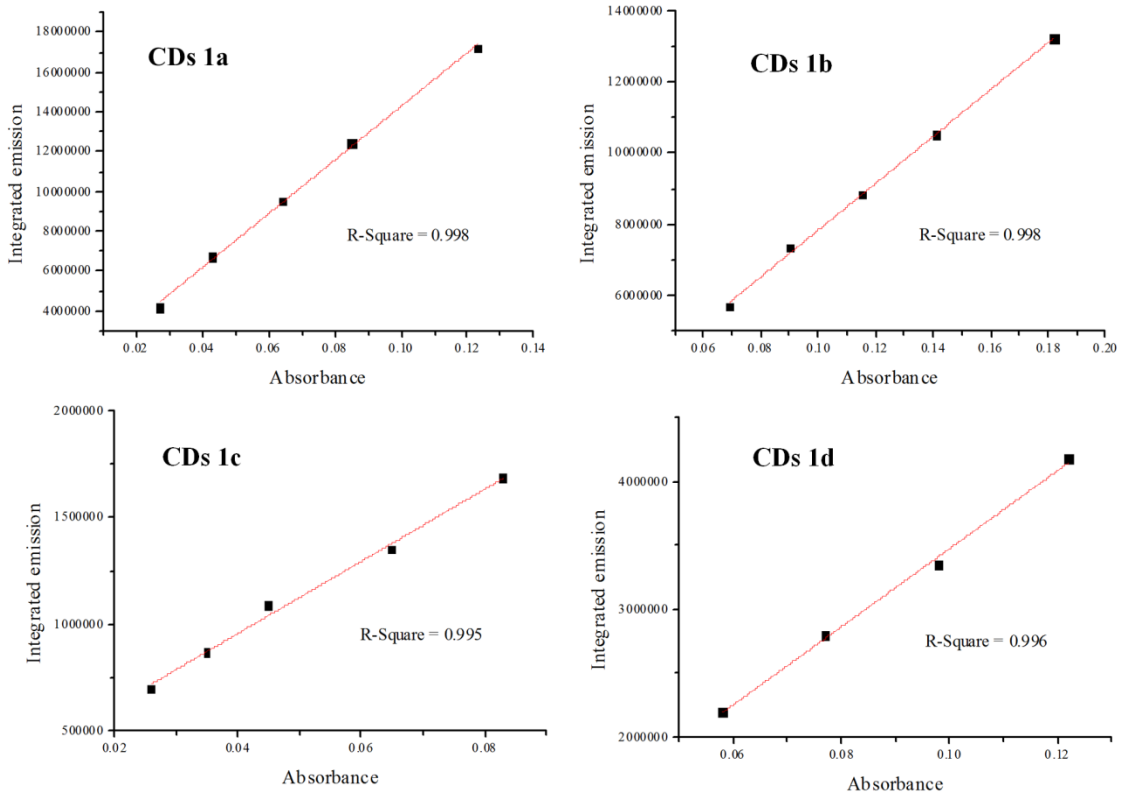

Figure 9.31. absorbance vs integrated fluorescence intensity of CDs 1a-d at different concentrations. The slope of the linear fitting was used for calculating the QY.

9.3.9. Atomic force microscopy of CDs 2a-f

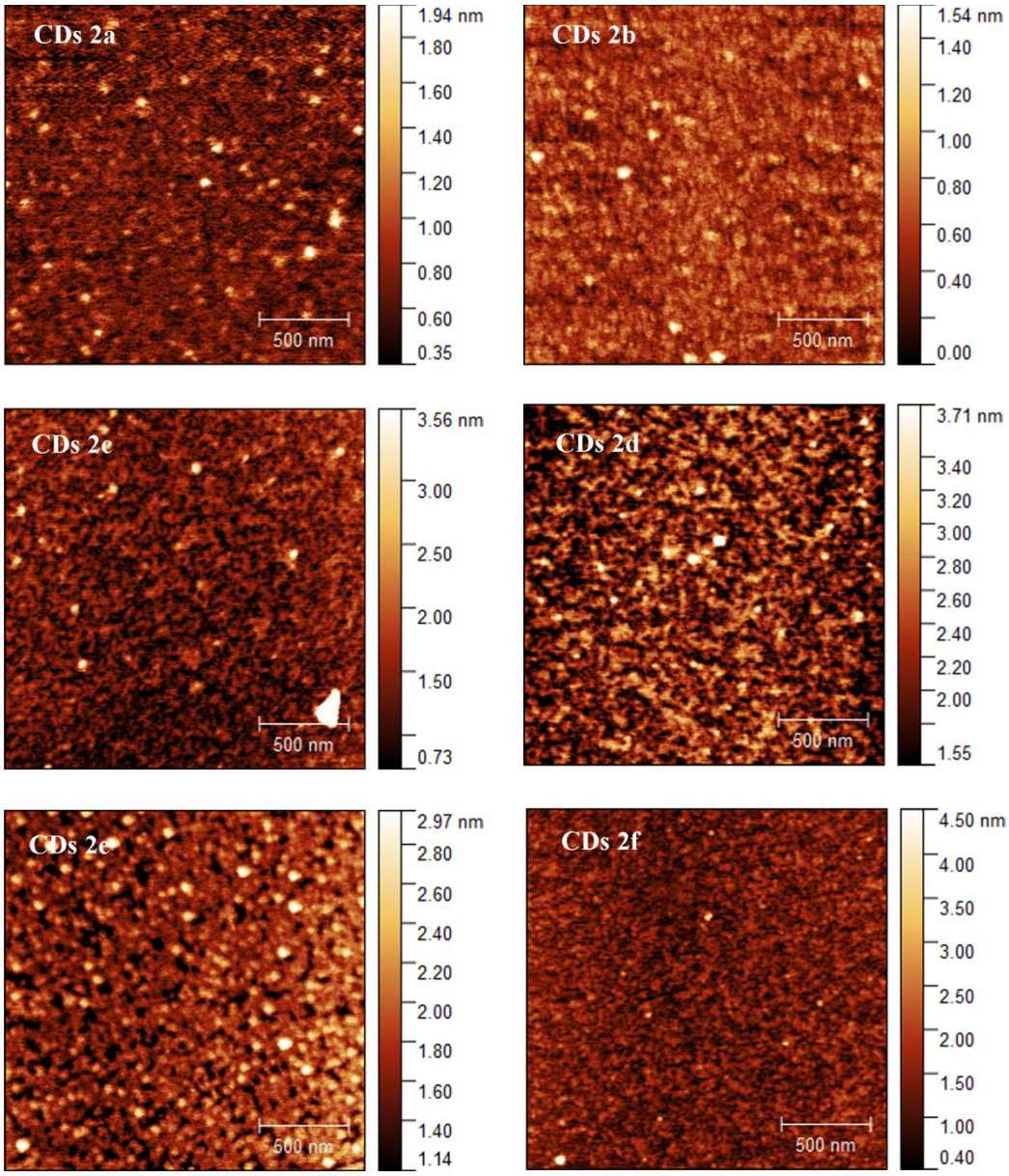

Figure 9.32. AFM pictures of CDs 2a-f. In all the samples, the height of the nanoparticles is comprised between 1.0-2.5 nm.

1. DOSY of CDs 2a-f

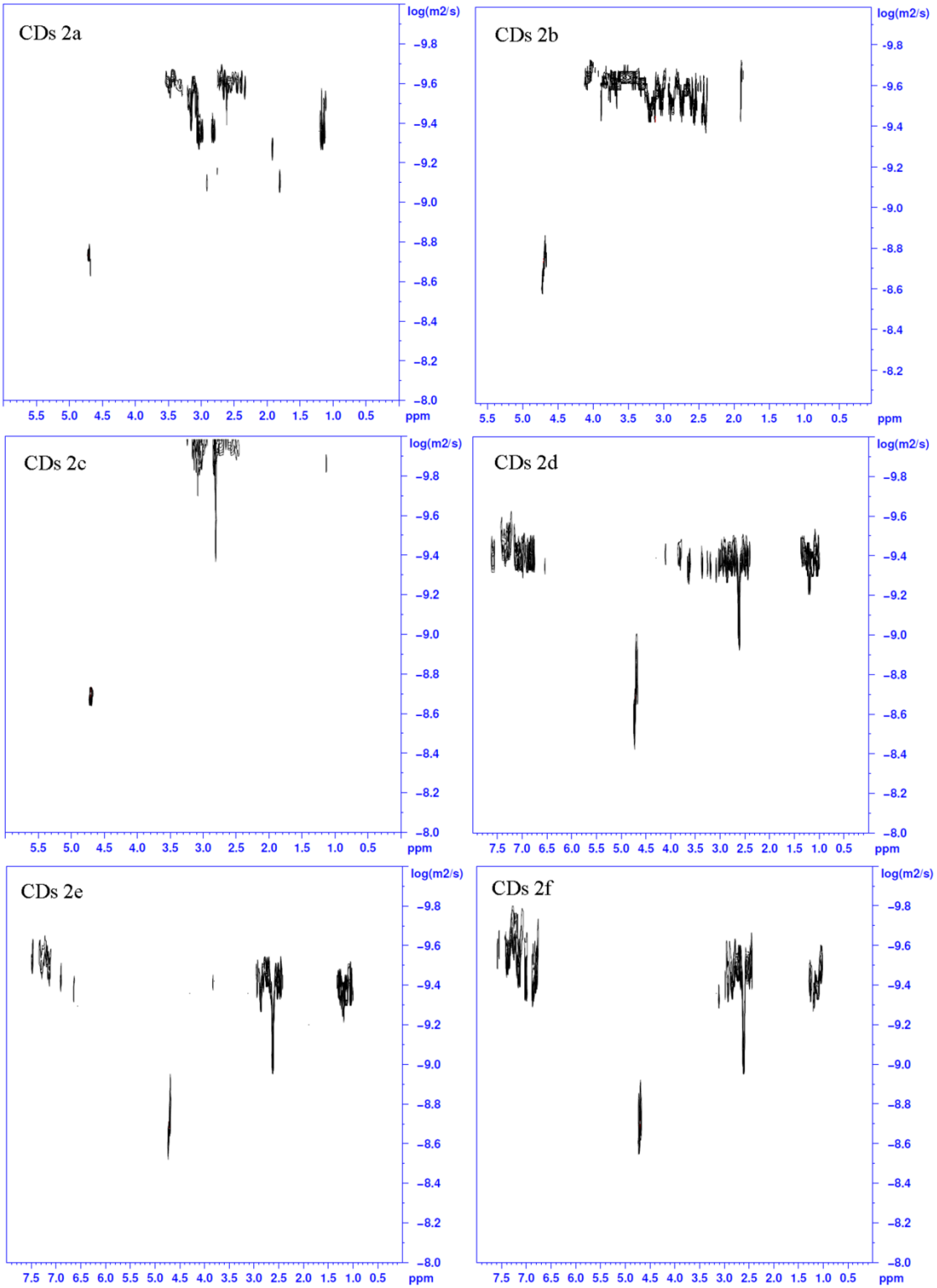

Figure 9.33. DOSY spectra of CDs 2a-f.

Table 9.6. The measured diffusion coefficients (D) and the calculated hydrodynamic rays (rH) and diameters of CDs 2a-f. Assuming a globular shape, the calculated size of the nanoparticles is comprised between 1.2-2.0 nm, with the exception of CDs 2c, which show a size of 4.8 nm.

	D (m^2/s)	rH (nm)	Diameter (nm)
CDs 2a	$10^{-9.6}$	1.0	2.0
CDs 2b	$10^{-9.6}$	1.0	2.0
CDs 2c	$10^{-10.0}$	2.4	4.8
CDs 2d	$10^{-9.4}$	0.6	1.2
CDs 2e	$10^{-9.4}$	0.6	1.2
CDs 2f	$10^{-9.5}$	0.8	1.6

9.3.10. Elemental analysis of CDs 2a-f

Table 9.7. C, H, N, O and S mole percentages of CDs 2a, obtained by elemental analysis. Additionally, the calculated elemental composition of the expected polymer repetitive unit is reported for comparison.

	C (mol%)	H (mol%)	N (mol%)	O (mol%)
$C_{10}H_{17}N_3O_5$	28.6	48.6	8.6	14.3
CDs 2a	25.3	51.4	7.3	16

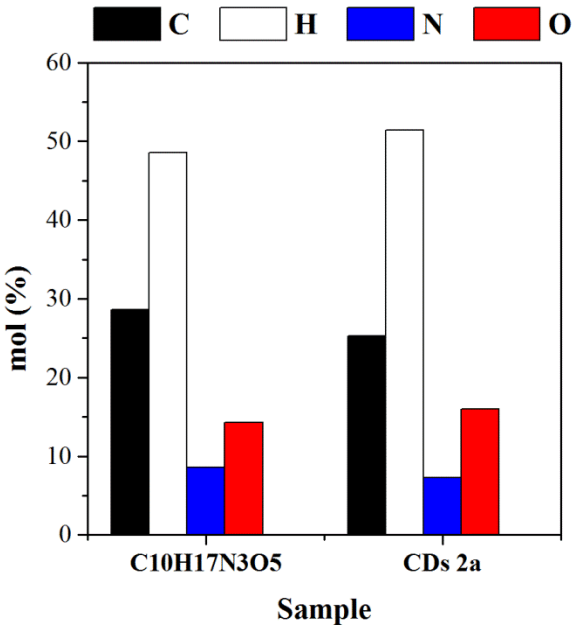

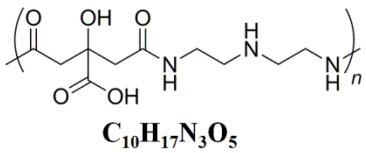

$C_{10}H_{17}N_3O_5$

Figure 9.34. Visual comparison between the measured elemental composition of CDs 2a and the calculated elemental composition of the expected polymer structure.

Table 9.8. C, H, N, O and S mole percentages of CDs 2b, obtained by elemental analysis. Additionally, the calculated elemental composition of the expected polymer repetitive unit is reported for comparison.

	C (mol%)	H (mol%)	N (mol%)	O (mol%)
$C_{12}H_{22}N_4O_5$	27.9	51.2	9.3	11.6
CDs 2b	24.8	52.6	9.4	13.8

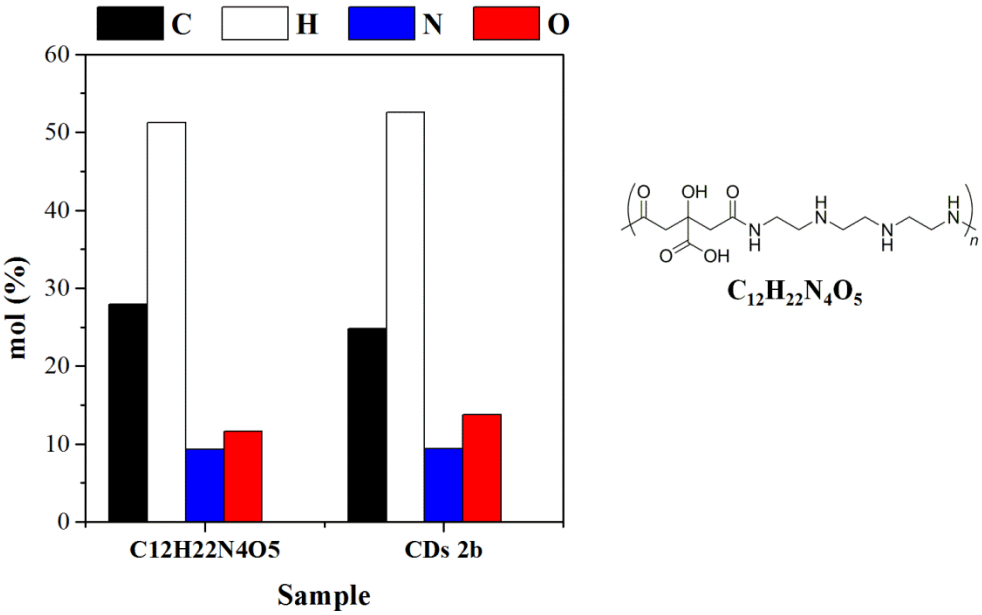

Figure 9.35. Visual comparison between the measured elemental composition of CDs 2b and the calculated elemental composition of the expected polymer structure.

Table 9.9. C, H, N, O and S mole percentages of CDs 2c, obtained by elemental analysis. Additionally, the calculated elemental composition of the expected polymer repetitive unit is reported for comparison.

	C (mol%)	H (mol%)	N (mol%)	O (mol%)
$C_{12}H_{18}N_2O_7$	30.8	46.2	5.1	17.9
CDs 2c	29	48.3	5.6	16.9

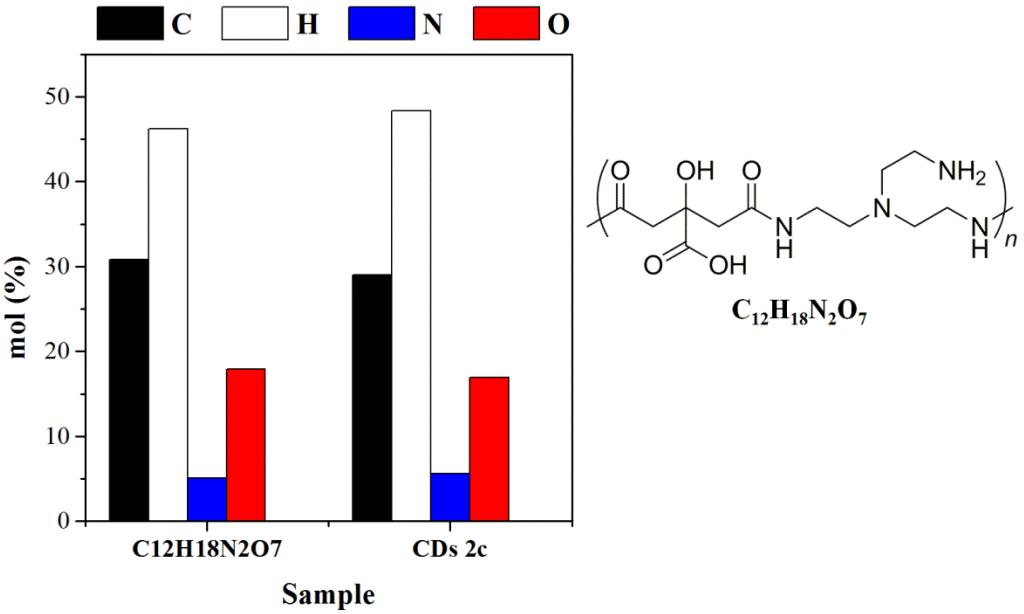

Figure 9.36. Visual comparison between the measured elemental composition of CDs 2c and the calculated elemental composition of the expected polymer structure.

Table 9.10. C, H, N, O and S mole percentages of CDs 2d-f, obtained by elemental analysis. Additionally, the calculated elemental composition of the expected polymer repetitive unit is reported for comparison.

	C (mol%)	H (mol%)	N (mol%)	O (mol%)
$C_{12}H_{12}N_2O_5$	38.7	38.7	6.4	16.1
CDs 2d	31.2	45.2	5.2	18.3
CDs 2e	32.7	44.5	5.5	17.2
CDs 2f	34.5	44	6.9	14.7

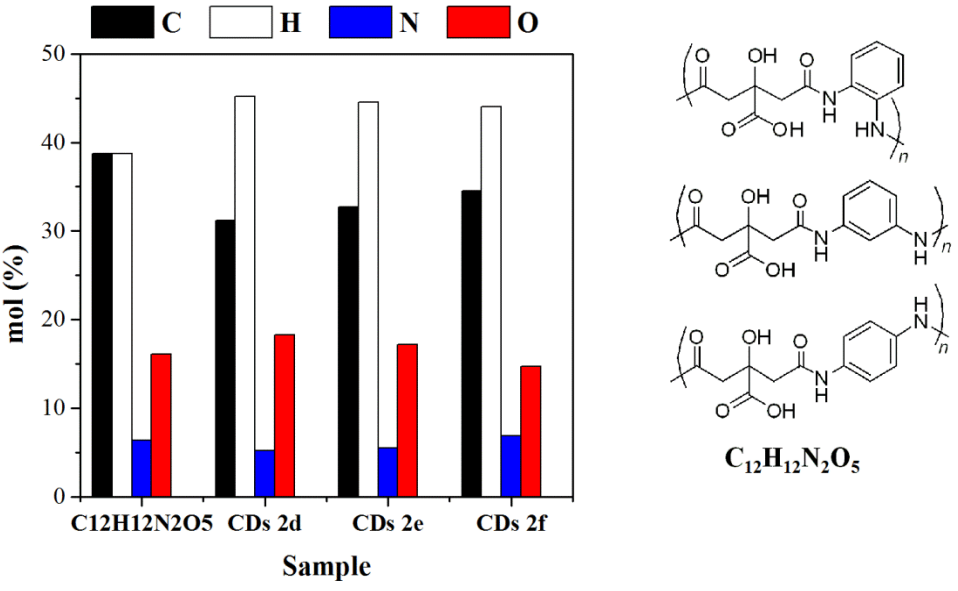

Figure 9.37. Visual comparison between the measured elemental composition of CDs 2d-f and the calculated elemental composition of the expected polymer structure.

9.3.11. IR spectra of CDs 2a-f

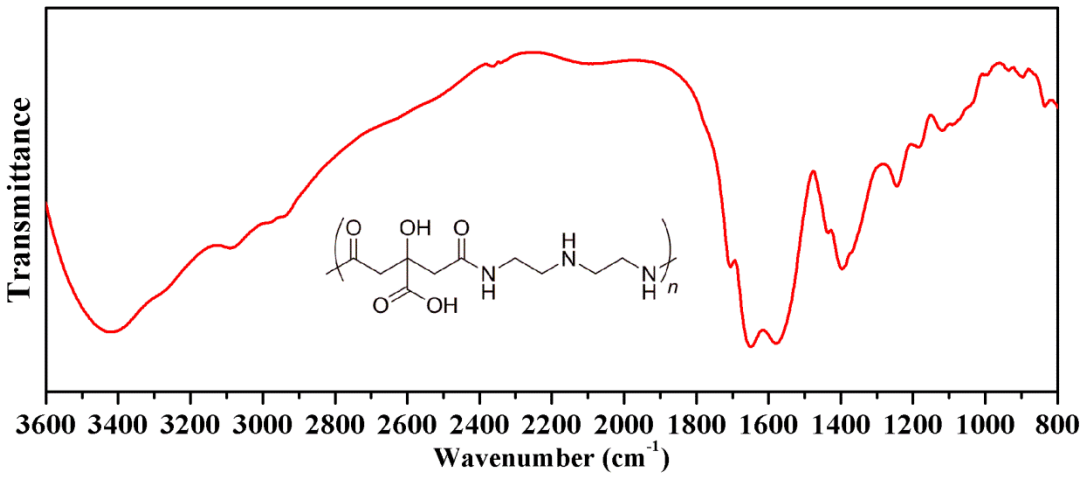

Figure 9.38. IR spectrum of CDs 2a. 3400-2800 cm^{-1}: O-H and N-H stretching, 1702 cm^{-1}: C=O stretching (carboxylic acid), 1653 and 1580 cm^{-1}: C=O stretching (amide), 1440-1350 cm^{-1}: C-O and C-N stretching.

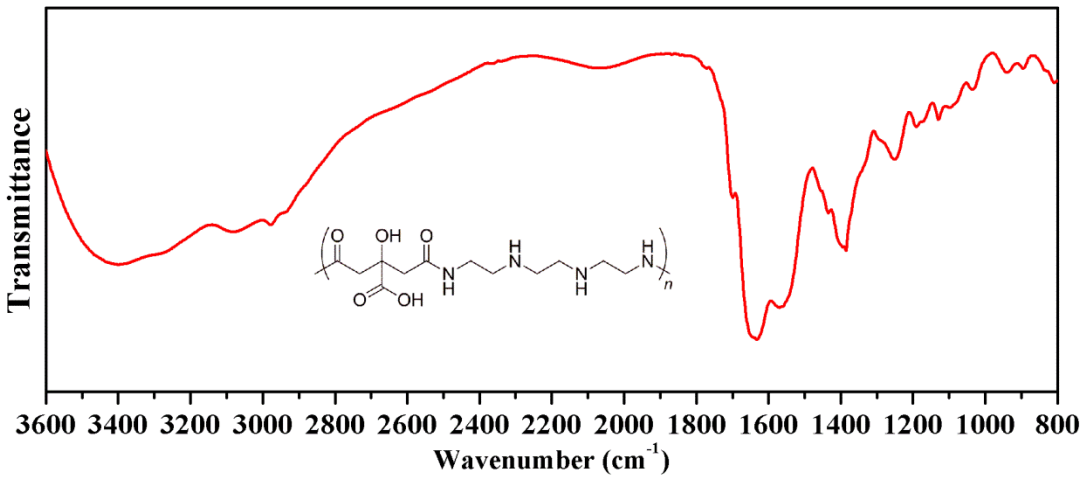

Figure 9.39. IR spectrum of CDs 2b. 3400-2800 cm^{-1}: O-H and N-H stretching, 1704 cm^{-1}: C=O stretching (carboxylic acid), 1638 and 1566 cm^{-1}: C=O stretching (amide), 1440-1350 cm^{-1}: C-O and C-N stretching.

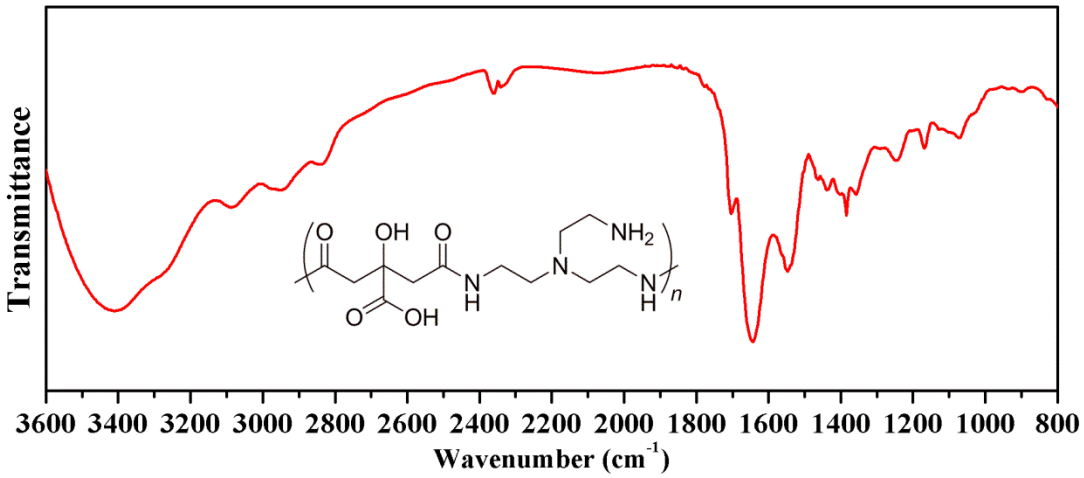

Figure 9.40. IR spectrum of CDs 2c. 3400-2800 cm^{-1}: O-H and N-H stretching, 1704 cm^{-1}: C=O stretching (carboxylic acid), 1643 and 1545 cm^{-1}: C=O stretching (amide), 1440-1350 cm^{-1}: C-O and C-N stretching.

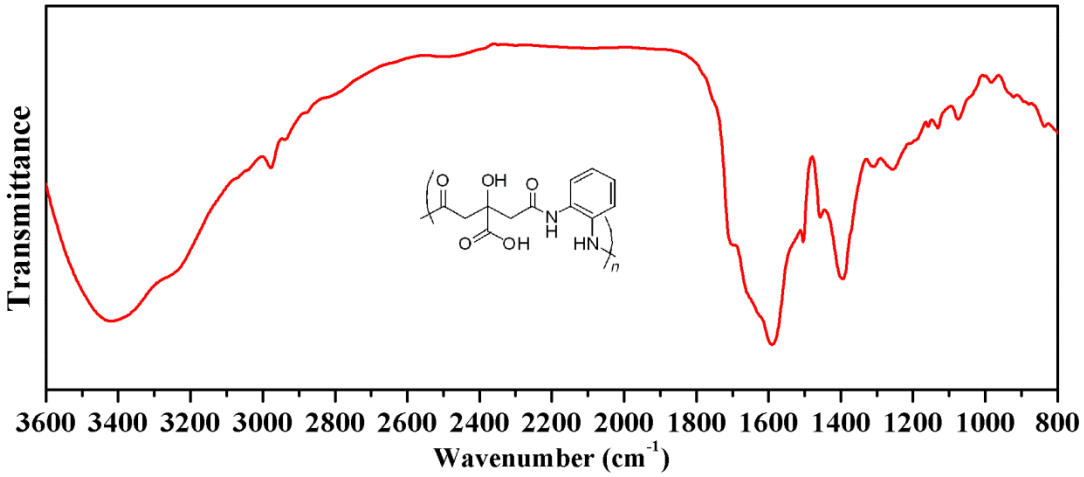

Figure 9.41. IR spectrum of CDs 2d. 3400-2800 cm^{-1}: O-H and N-H stretching, 1707 cm^{-1}: C=O stretching (carboxylic acid), 1664 and 1590 cm^{-1}: C=O stretching (amide), 1502 cm^{-1}: C-C stretching (aromatic ring), 1440-1350 cm^{-1}: C-O and C-N stretching.

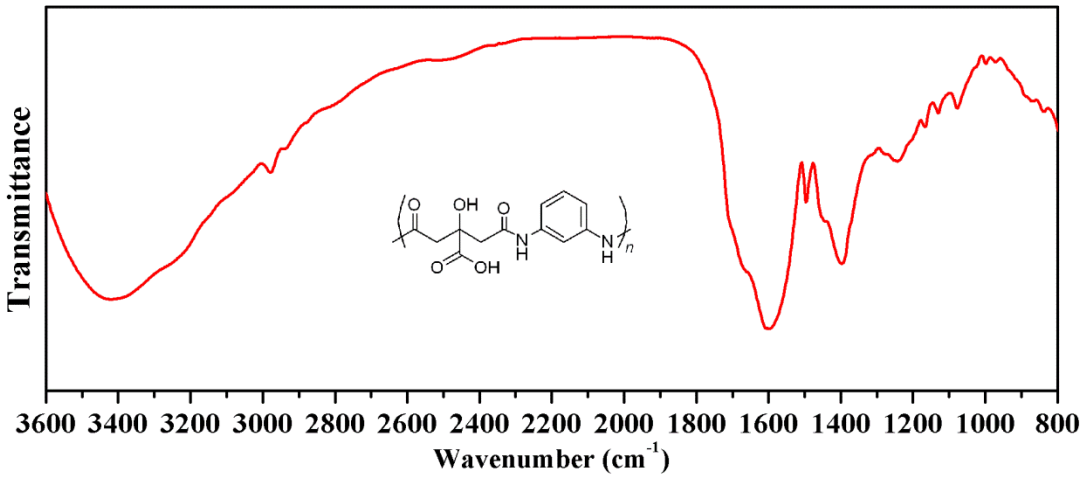

Figure 9.42. IR spectrum of CDs 2e. 3400-2800 cm^{-1}: O-H and N-H stretching, 1715 cm^{-1}: C=O stretching (carboxylic acid), 1670 and 1590 cm^{-1}: C=O stretching (amide), 1497 cm^{-1}: C-C stretching (aromatic ring), 1440-1350 cm^{-1}: C-O and C-N stretching.

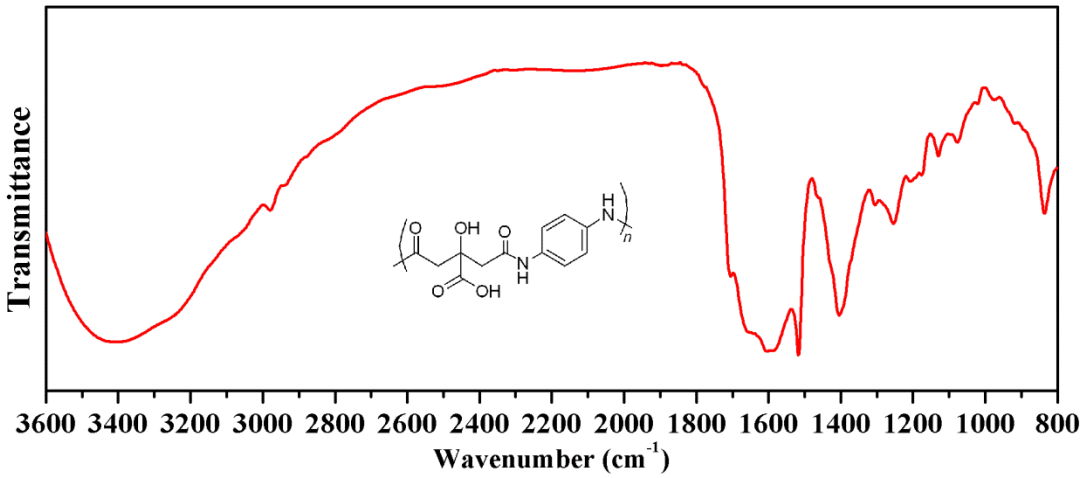

Figure 9.43. IR spectrum of CDs 2f. 3400-2800 cm^{-1}: O-H and N-H stretching, 1707 cm^{-1}: C=O stretching (carboxylic acid), 1660 and 1605 cm^{-1}: C=O stretching (amide), 1516 cm^{-1}: C-C stretching (aromatic ring), 1440-1350 cm^{-1}: C-O and C-N stretching.

9.3.12. NMR spectra of CDs 2a-f

CDs 2a

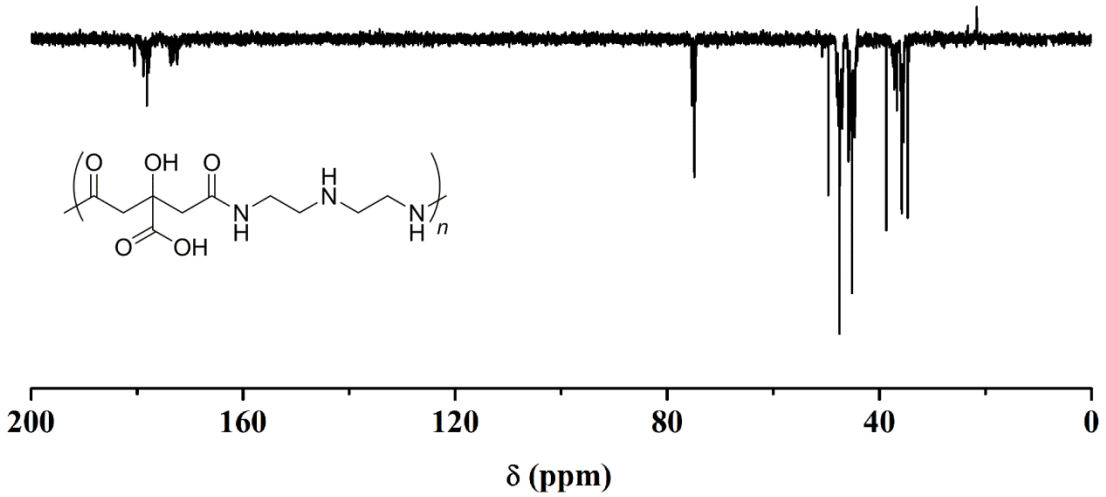

Figure 9.44. APT ^{13}C NMR spectrum of CDs 2a. Carboxylic acid and amide C: 182-171 ppm, quaternary C: 75-72 ppm, methylene C: 45-36 ppm. The positive signal at 21 ppm is due to DIC impurities.

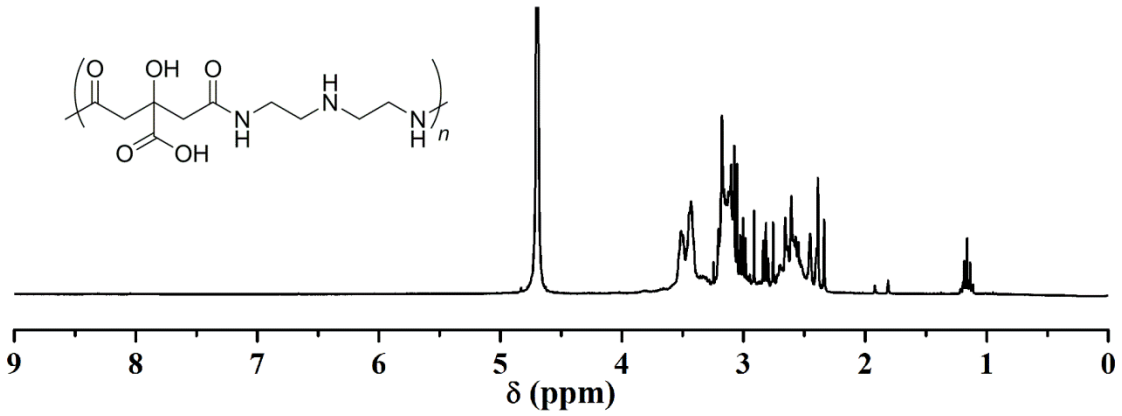

Figure 9.45. ^{1}H NMR spectrum of CDs 2a. methylene H: 3.6-2.3 ppm. The signal at 1.2 ppm is due to DIC impurities.

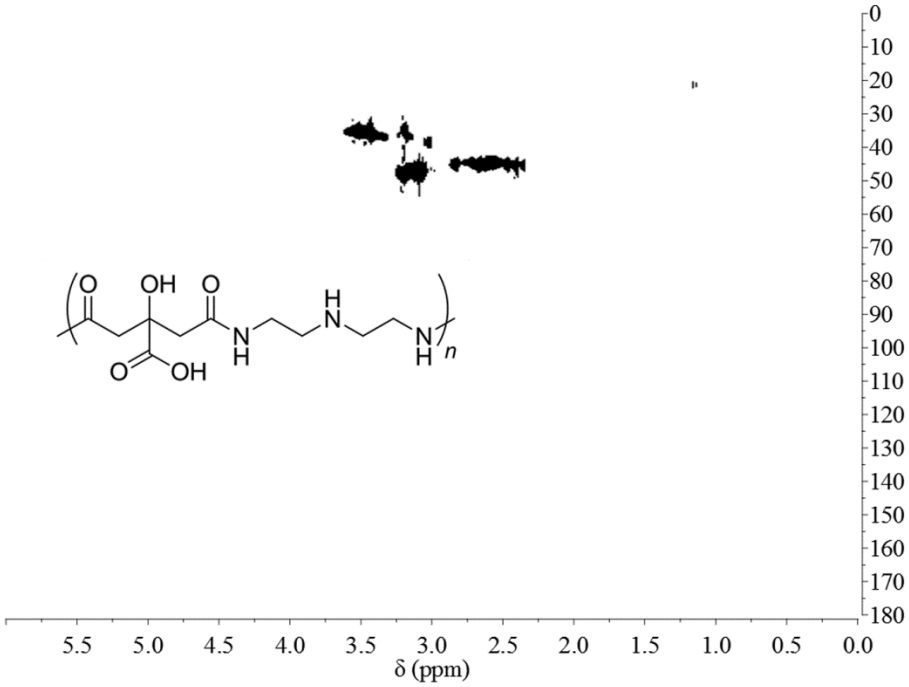

Figure 9.46. ^{1}H-^{13}C HSQC spectrum of CDs 2a.

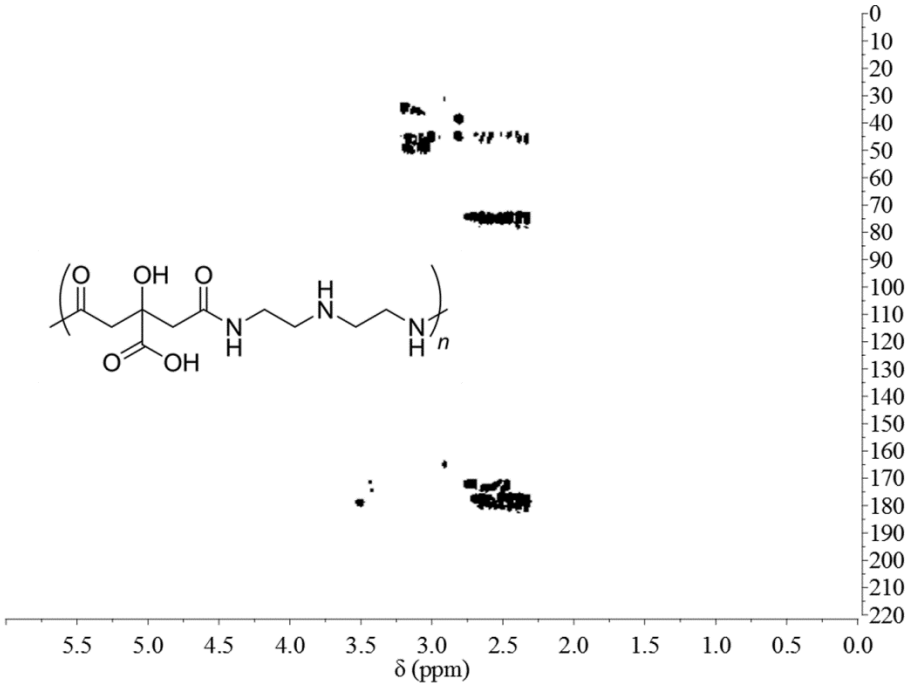

Figure 9.47. ^{1}H-^{13}C HMBC spectrum of CDs 2a.

CDs 2b

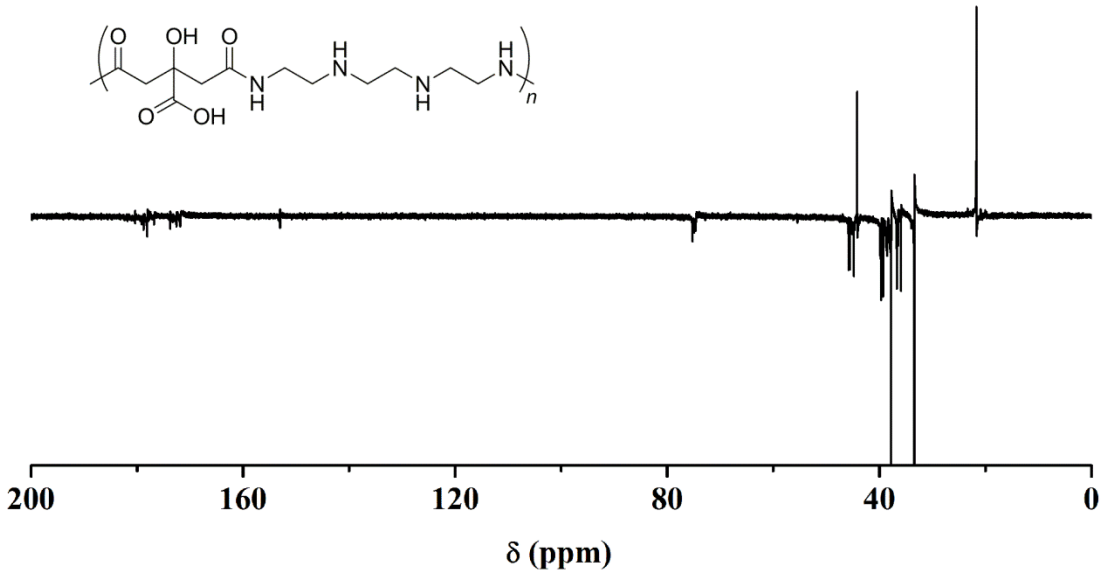

Figure 9.48. APT ^{13}C NMR spectrum of CDs 2b. Carboxylic acid and amide C: 181-171 ppm, quaternary C: 76-74 ppm, methylene C: 46-32 ppm. The positive signal at 153, 44, 21 ppm are due to DIC impurities.

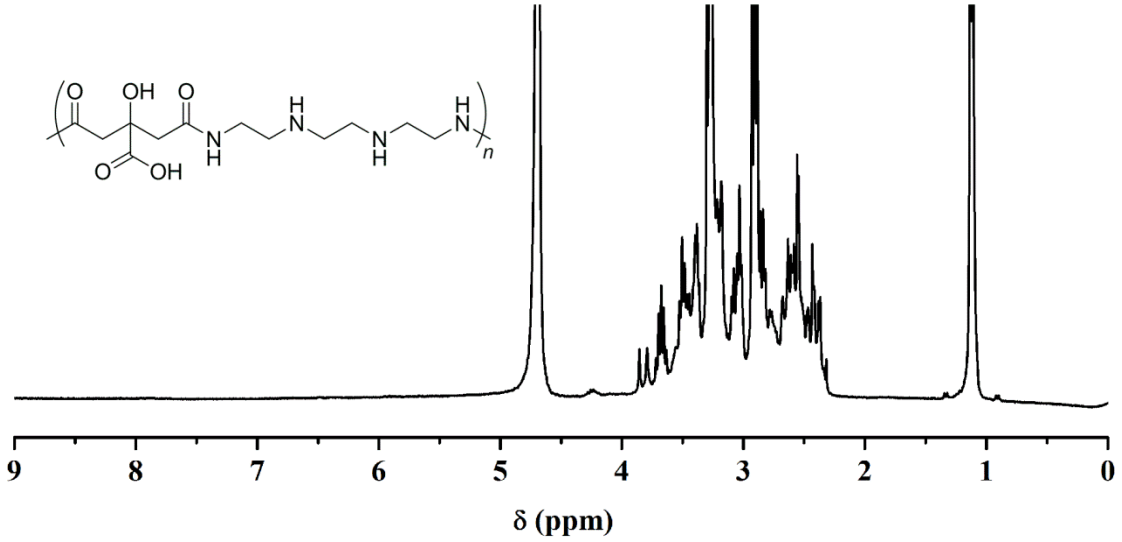

Figure 9.49. ^{1}H NMR spectrum of CDs 2b. methylene H: 3.8-2.3 ppm. The signals at 3.5, 1.2 ppm are due to DIC impurities.

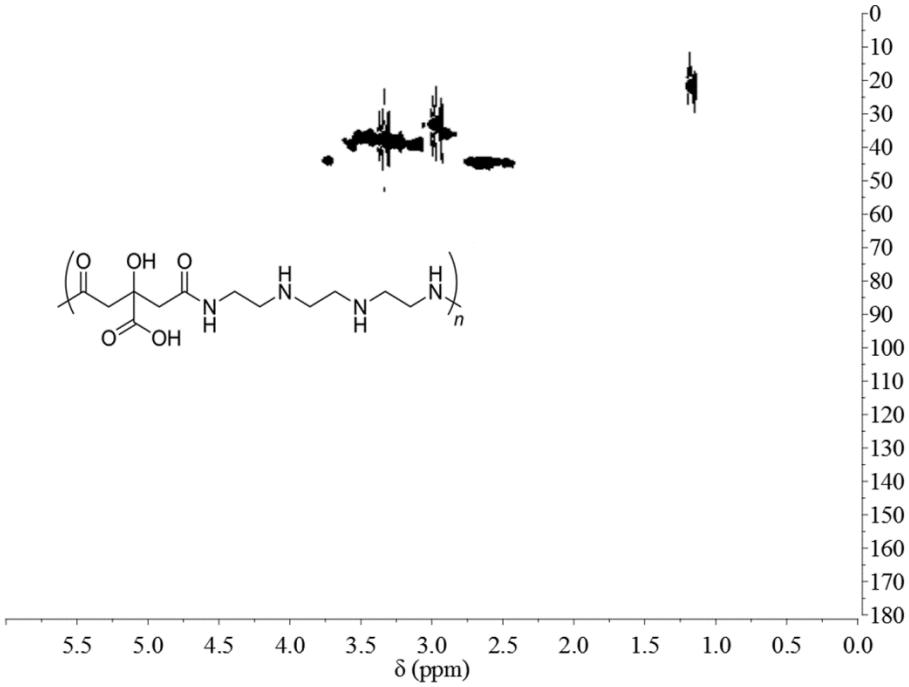

Figure 9.50. ^{1}H-^{13}C HSQC spectrum of CDs 2b.

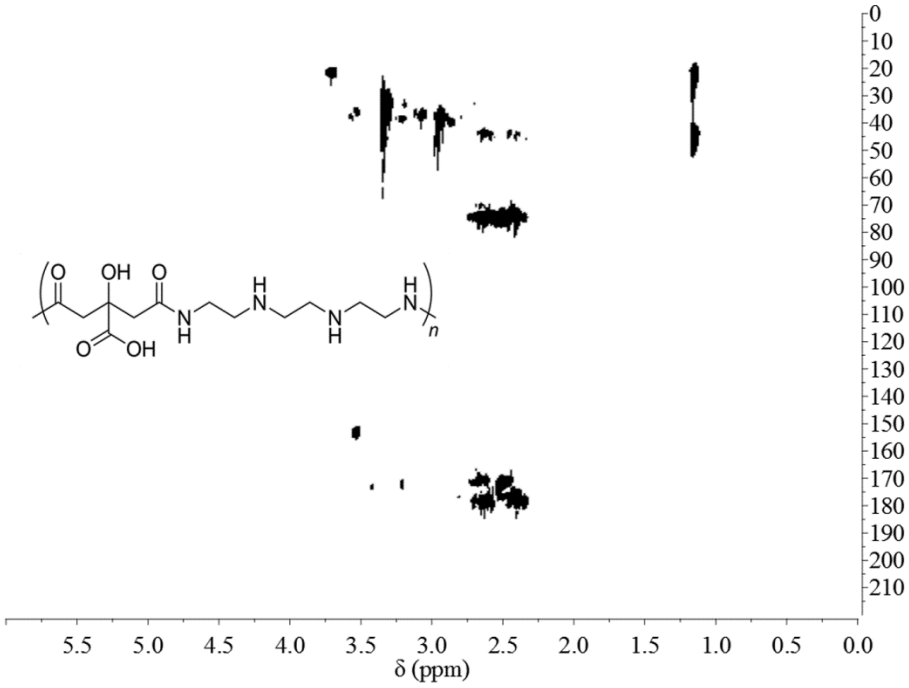

Figure 9.51. ^{1}H-^{13}C HMBC spectrum of CDs 2b.

CDs 2c

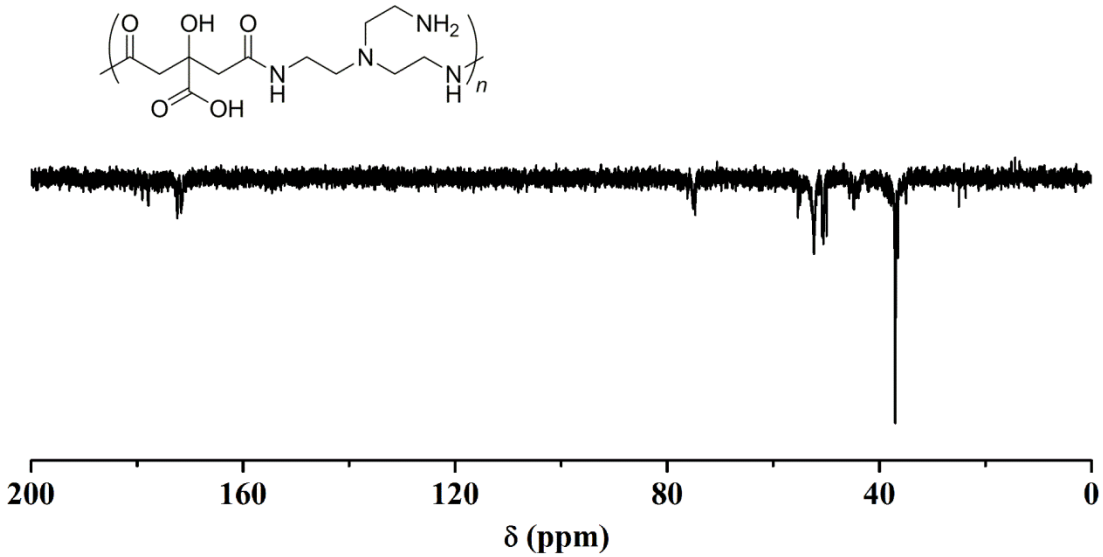

Figure 9.52. APT ^{13}C NMR spectrum of CDs 2c. Carboxylic acid and amide C: 180-171 ppm, quaternary C: 76-74 ppm, methylene C: 55-35 ppm.

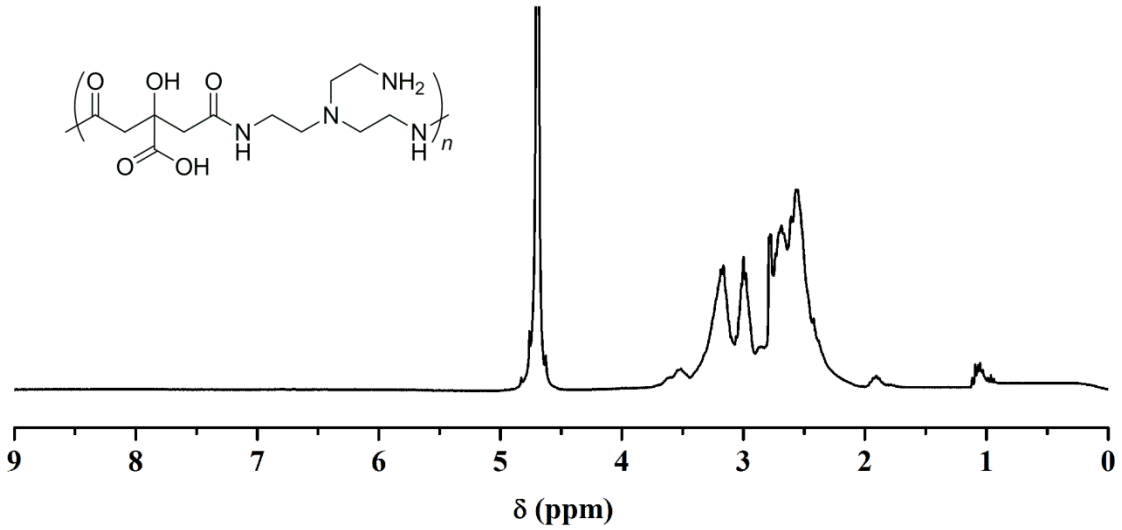

Figure 9.53. ^{1}H NMR spectrum of CDs 2c. methylene H: 3.7-2.3 ppm.

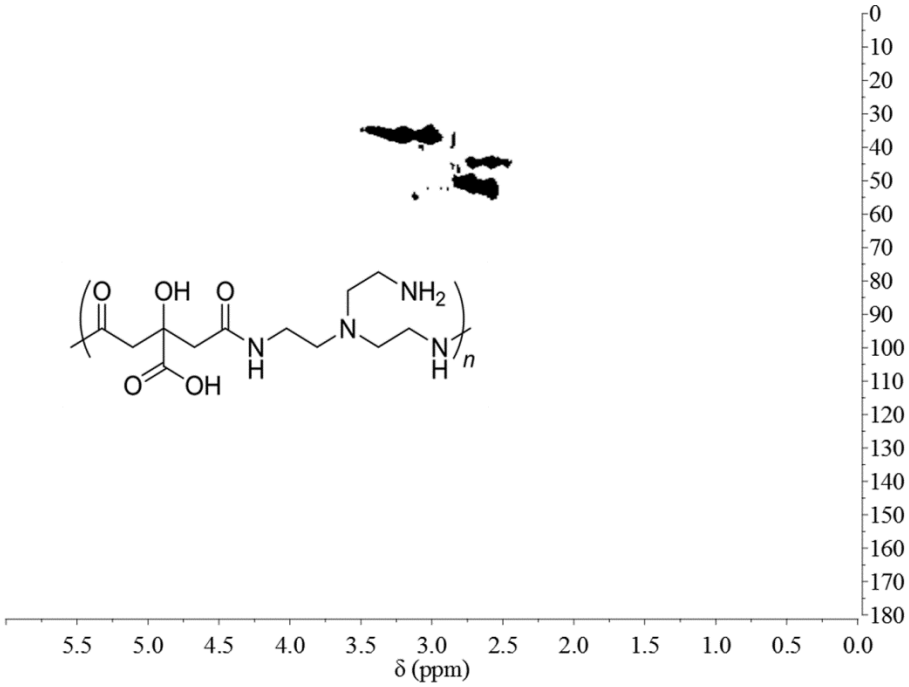

Figure 9.54. ^{1}H-^{13}C HSQC spectrum of CDs 2c.

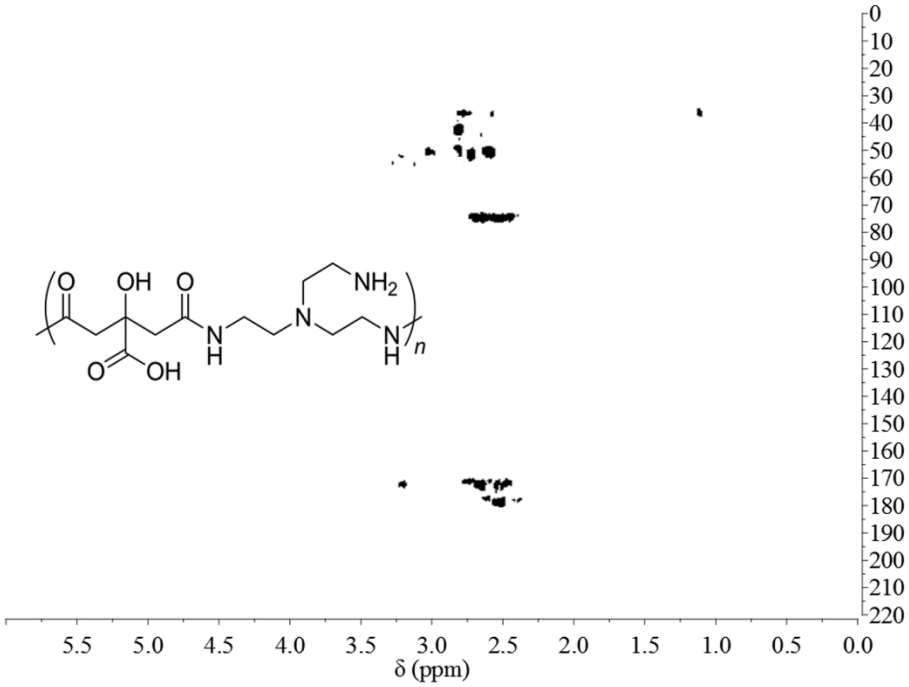

Figure 9.55. ^{1}H-^{13}C HMBC spectrum of CDs 2c.

CDs 2d

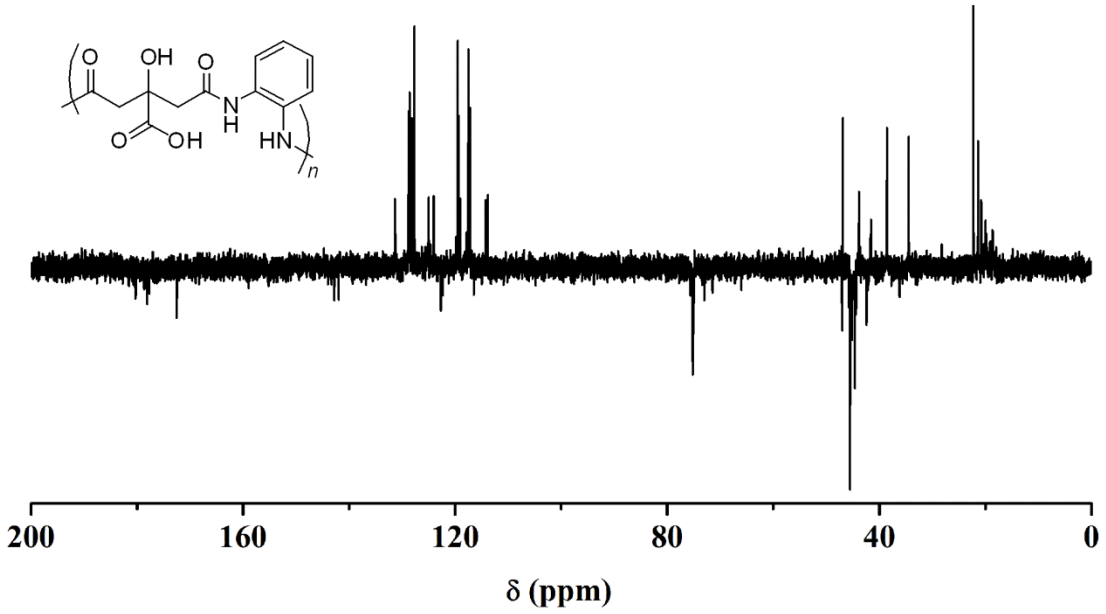

Figure 9.56. APT ^{13}C NMR spectrum of CDs 2d. Carboxylic acid and amide C: 180-170 ppm, aromatic quaternary C bonded to amine N: 147 ppm, aromatic quaternary C bonded to amide N: 134 ppm, aromatic C-H: 131-113 ppm, quaternary C in citric acid: 76-74 ppm, methylene C: 46-41 ppm. The signals at 153, 44, 21 ppm are due to DIC impurities. The positive signals at 43, 41, 39, 34 ppm are due to molecular impurities.

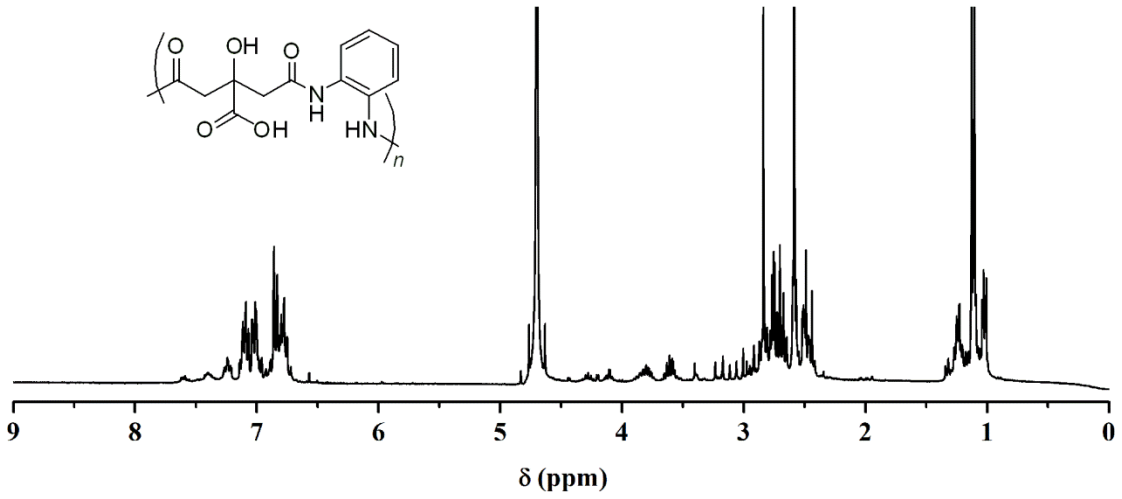

Figure 9.57. ^{1}H NMR spectrum of CDs 2d. Aromatic H: 7.6-6.7 ppm. methylene H: 4.3-2.3 ppm. The signals at 3.5, 1.2 ppm are due to DIC impurities. The singlets at 2.8 and 2.6 ppm are due to molecular impurities.

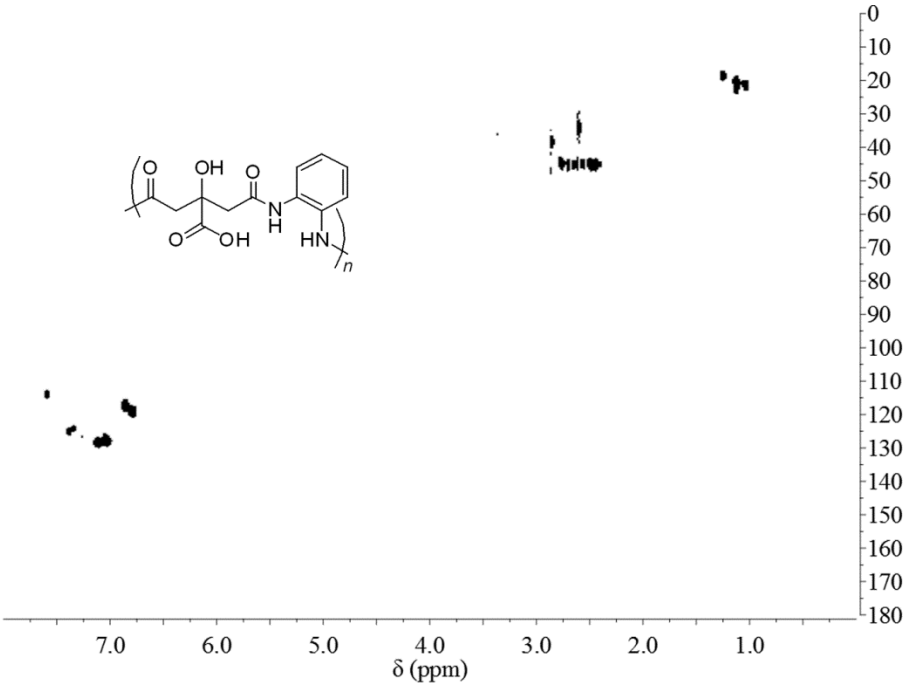

Figure 9.58. ^{1}H-^{13}C HSQC spectrum of CDs 2d.

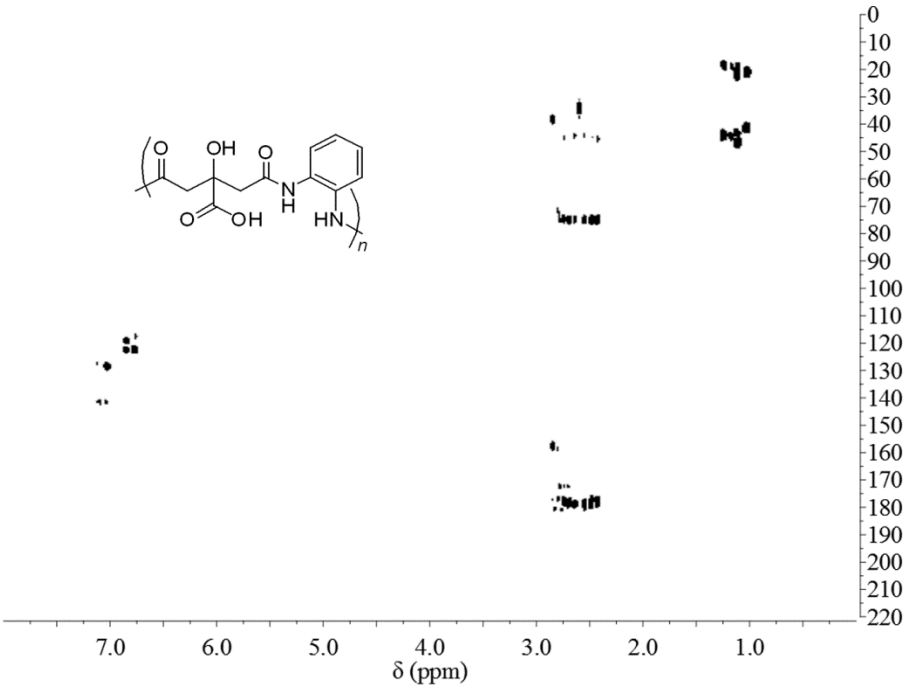

Figure 9.59. ^{1}H-^{13}C HMBC spectrum of CDs 2d.

CDs 2e

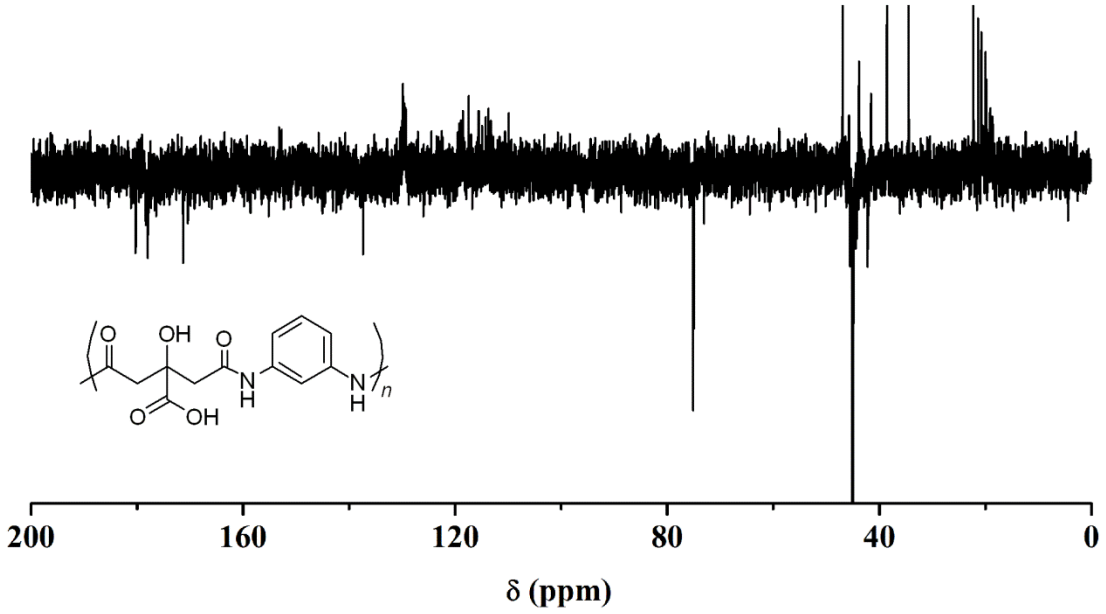

Figure 9.60. APT ^{13}C NMR spectrum of CDs 2e. Carboxylic acid and amide C: 180-170 ppm, aromatic quaternary C bonded to amide N: 137 ppm, aromatic C-H: 131-109 ppm, quaternary C in citric acid: 76-74 ppm, methylene C: 46-41 ppm. The signals at 153, 44, 21 ppm are due to DIC impurities. The positive signals at 43, 41, 39, 34 ppm are due to molecular impurities.

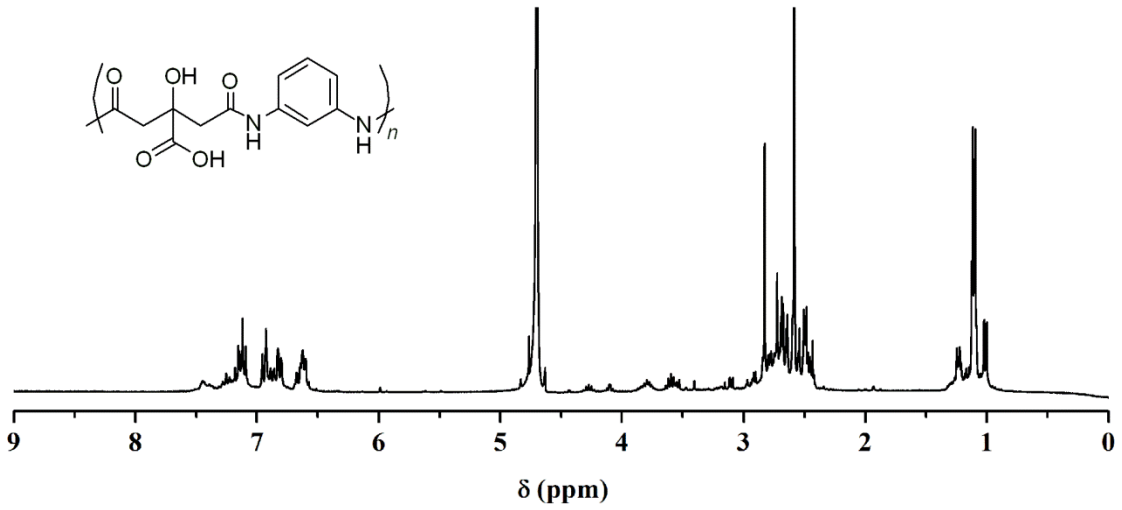

Figure 9.61. ^{1}H NMR spectrum of CDs 2e. Aromatic H: 7.5-6.5 ppm. Methylene H: 4.3-2.3 ppm. The signals at 3.5, 1.2 ppm are due to DIC impurities. The singlets at 2.8 and 2.6 ppm are due to molecular impurities.

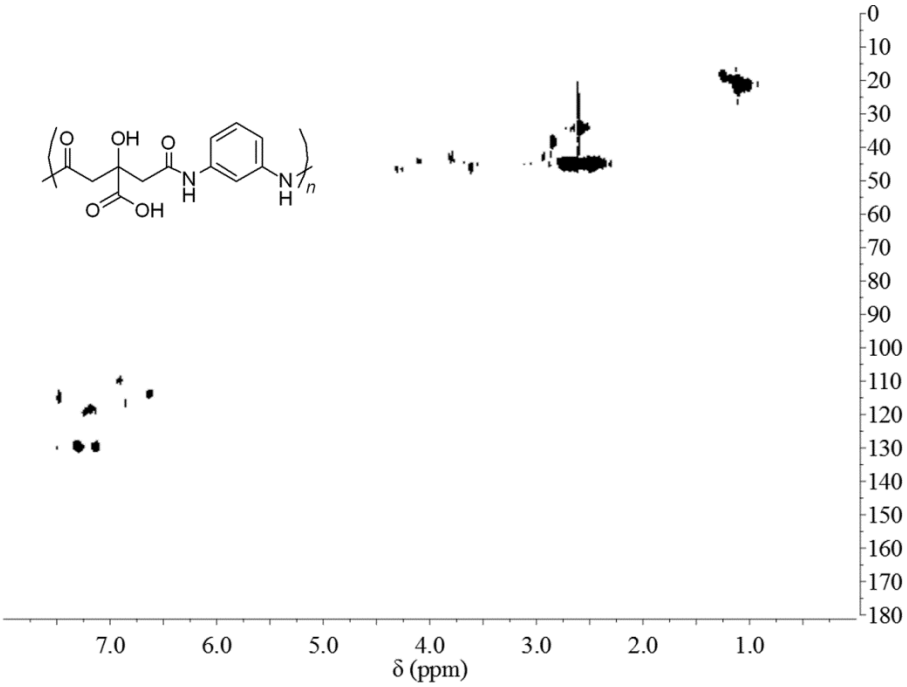

Figure 9.62. ^{1}H-^{13}C HSQC spectrum of CDs 2e.

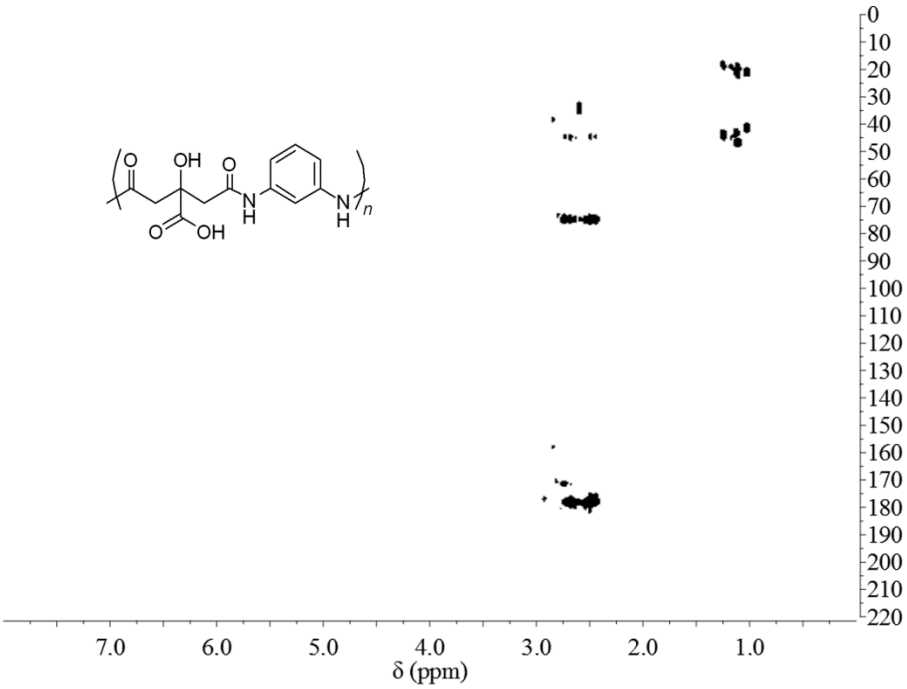

Figure 9.63. ^{1}H-^{13}C HMBC spectrum of CDs 2e.

CDs 2f

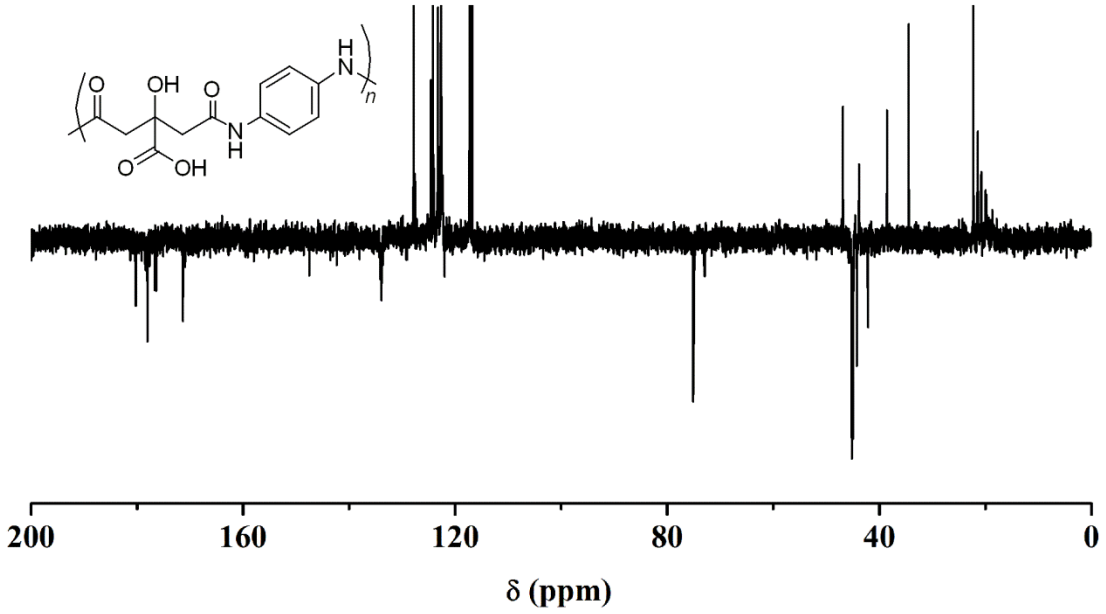

Figure 9.64. APT ^{13}C NMR spectrum of CDs 2f. Carboxylic acid and amide C: 180-170 ppm, aromatic quaternary C bonded to amine N: 148 ppm, aromatic quaternary C bonded to amide N: 134 ppm, aromatic C-H: 128-117 ppm, quaternary C in citric acid: 76-74 ppm, methylene C: 46-41 ppm. The signals at 153, 44, 21 ppm are due to DIC impurities. The positive signals at 43, 41, 39, 34 ppm are due to molecular impurities.

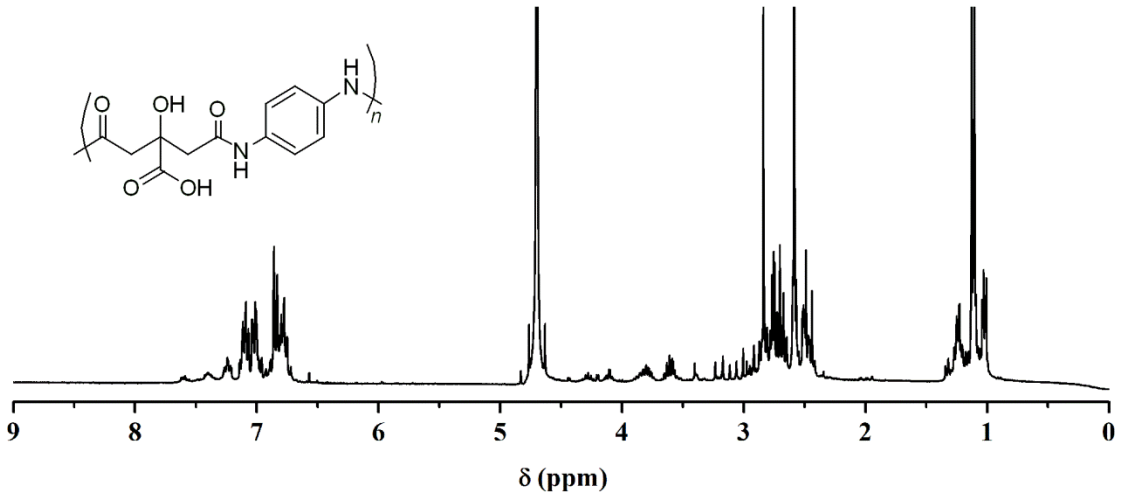

Figure 9.65. ^{1}H NMR spectrum of CDs 2f. Aromatic H: 7.6-6.6 ppm. Methylene H: 4.3-2.3 ppm. The signals at 3.5, 1.2 ppm are due to DIC impurities. The singlets at 2.8 and 2.6 ppm are due to molecular impurities.

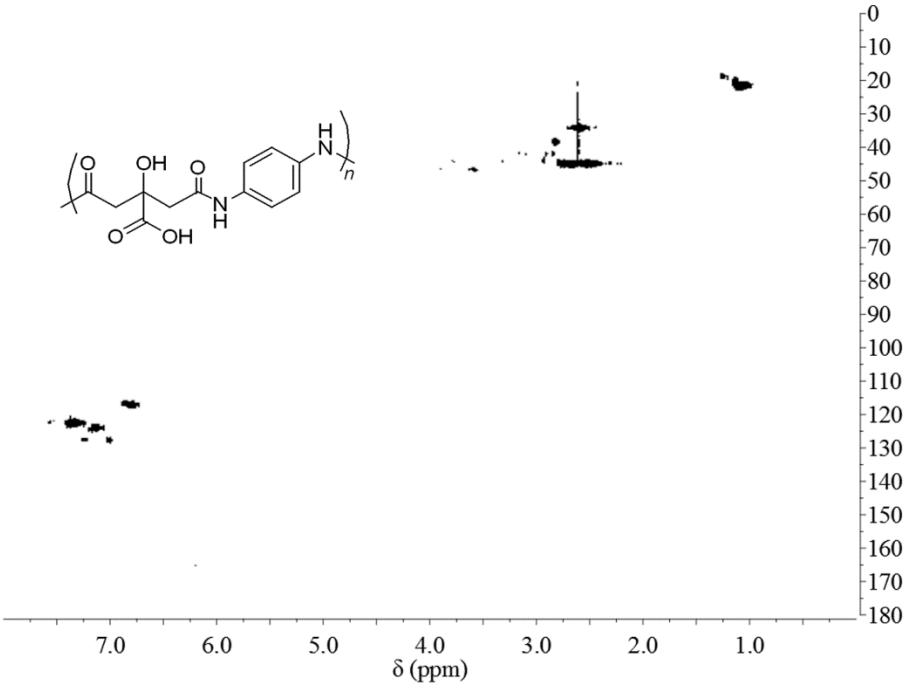

Figure 9.66. ^{1}H-^{13}C HSQC spectrum of CDs 2f.

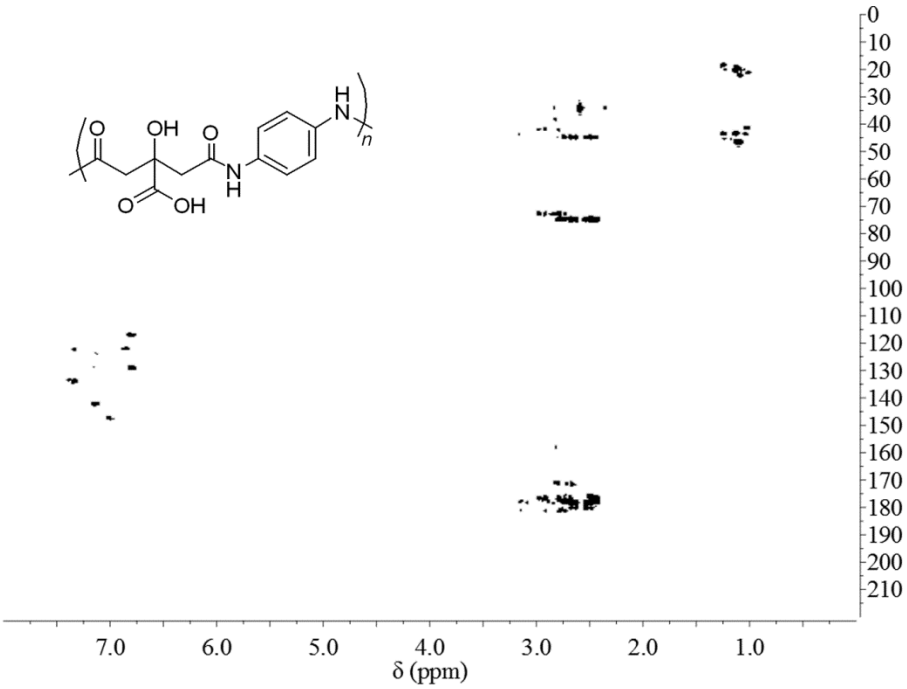

Figure 9.67. ^{1}H-^{13}C HMBC spectrum of CDs 2f.

9.3.13. UV/vis spectra of CDs 2a-f

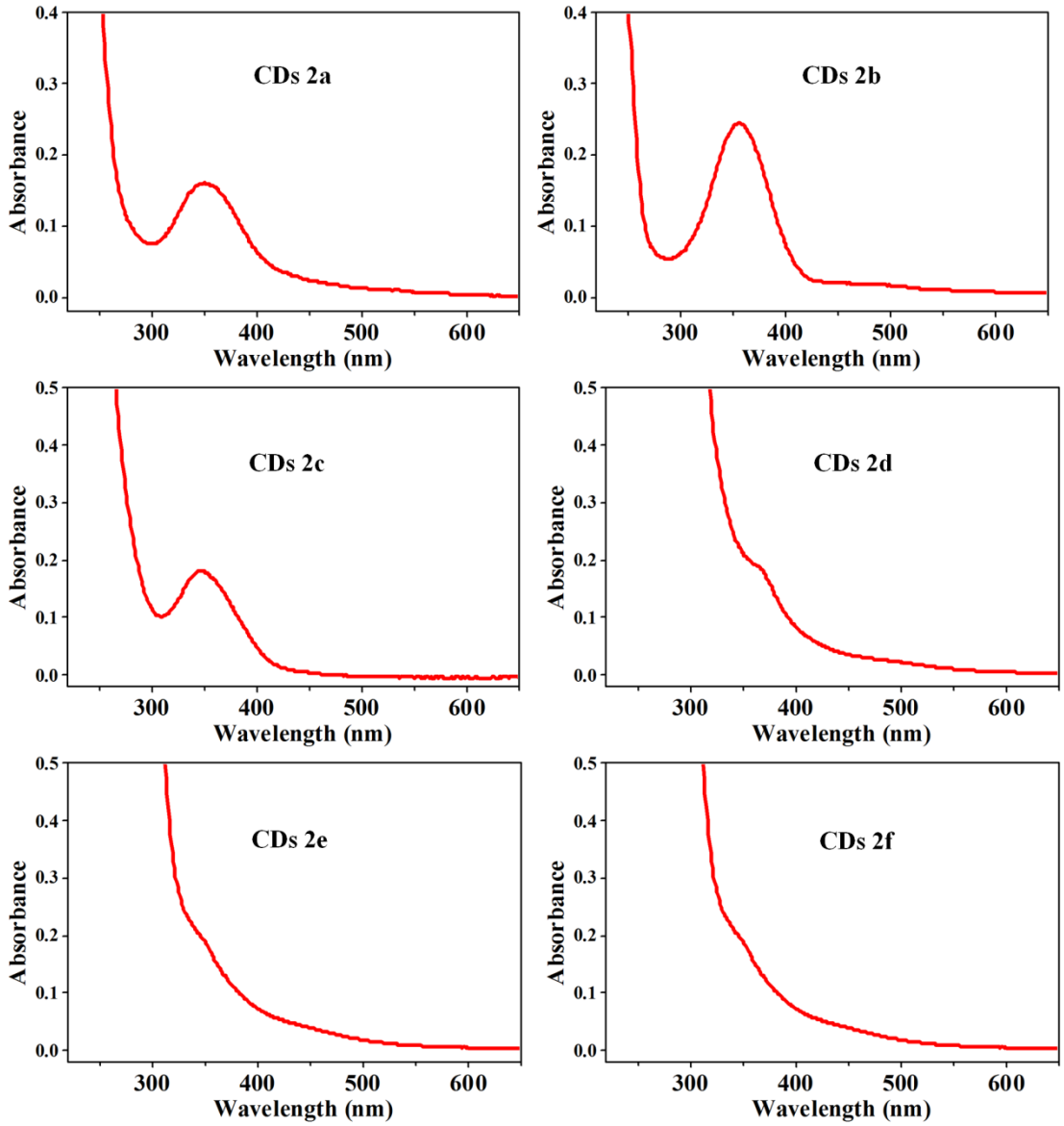

Figure 9.68. UV/vis spectra of CDs 2a-f.

9.3.14. Excitation and emission spectra of CDs 2a-f

CDs 2a

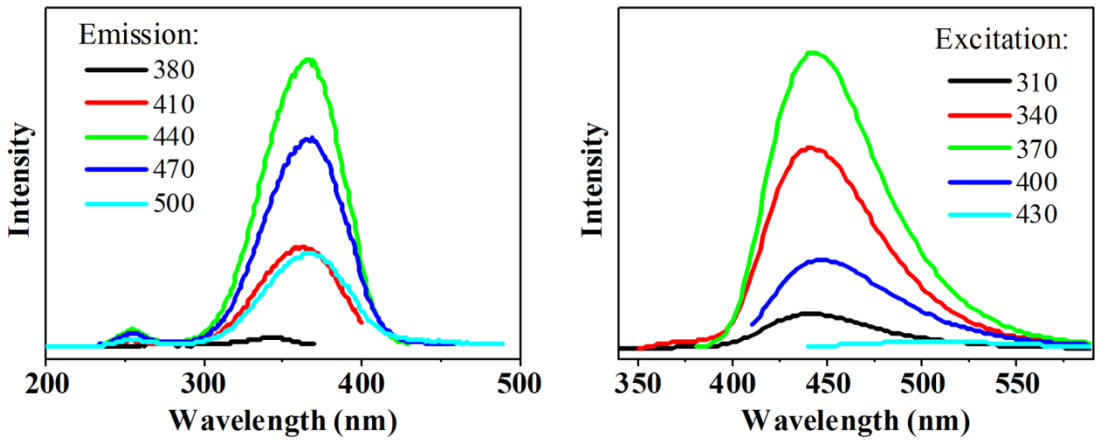

Figure 9.69. (left) excitation spectra for different emissions and (right) emission spectra for different excitations of CDs 2a.

CDs 2b

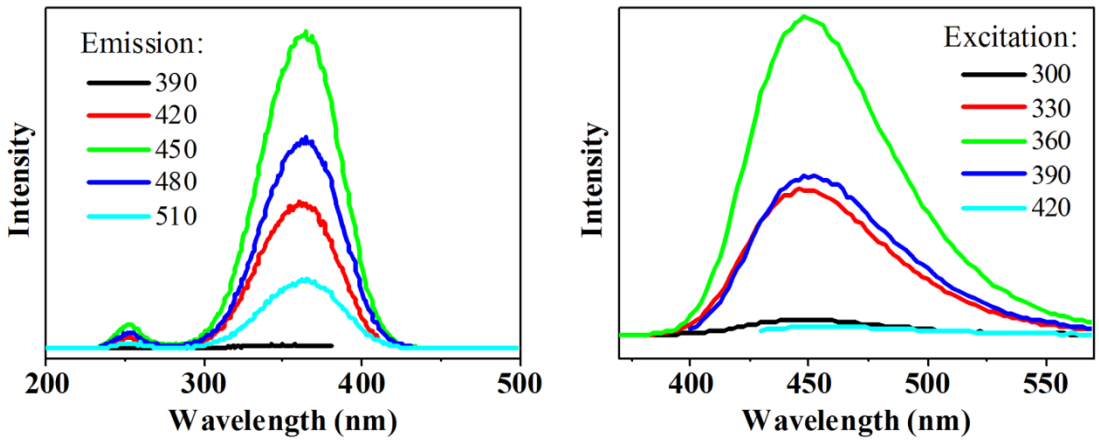

Figure 9.70. (left) excitation spectra for different emissions and (right) emission spectra for different excitations of CDs 2b.

CDs 2c

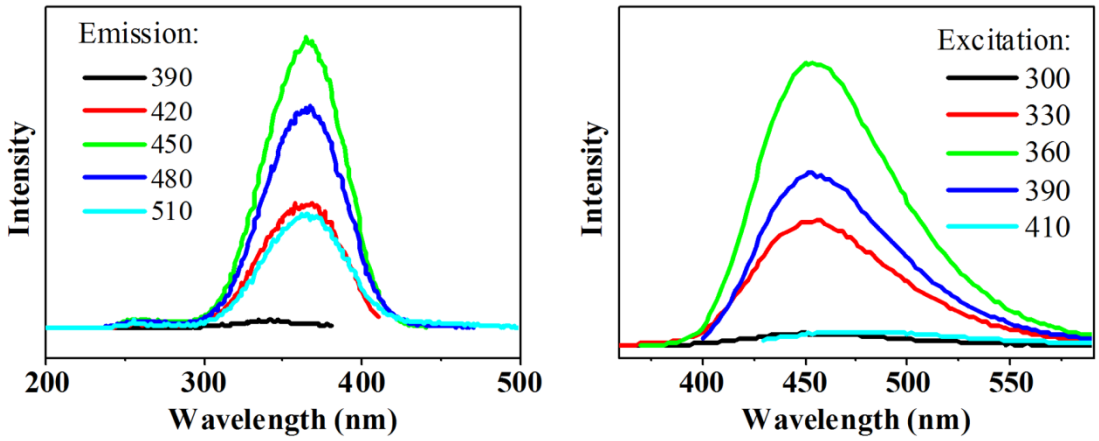

Figure 9.71. (left) excitation spectra for different emissions and (right) emission spectra for different excitations of CDs 2c.

CDs 2d

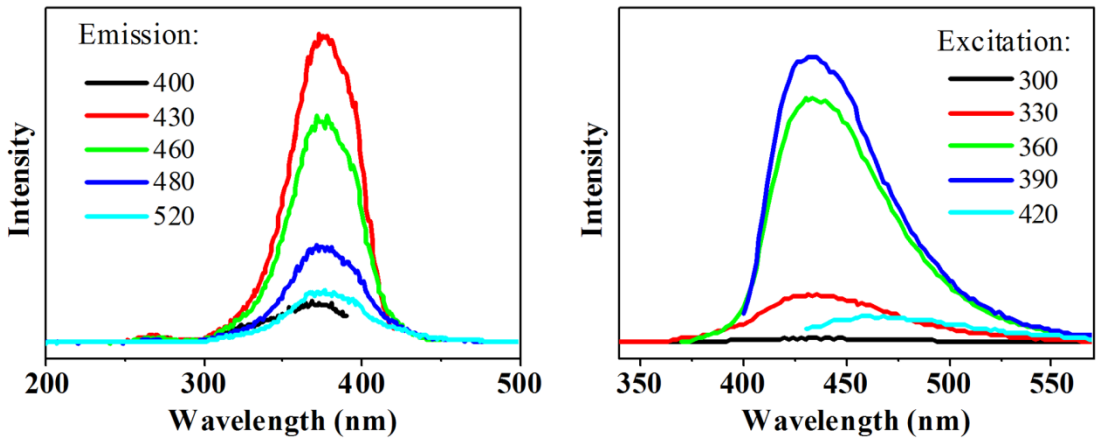

Figure 9.72. (left) excitation spectra for different emissions and (right) emission spectra for different excitations of CDs 2d.

CDs 2e

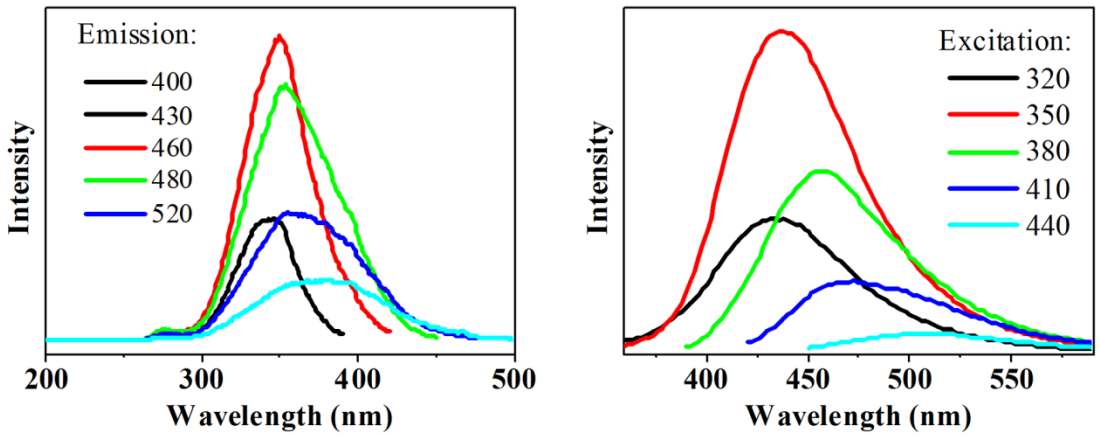

Figure 9.73. (left) excitation spectra for different emissions and (right) emission spectra for different excitations of CDs 2e.

CDs 2f

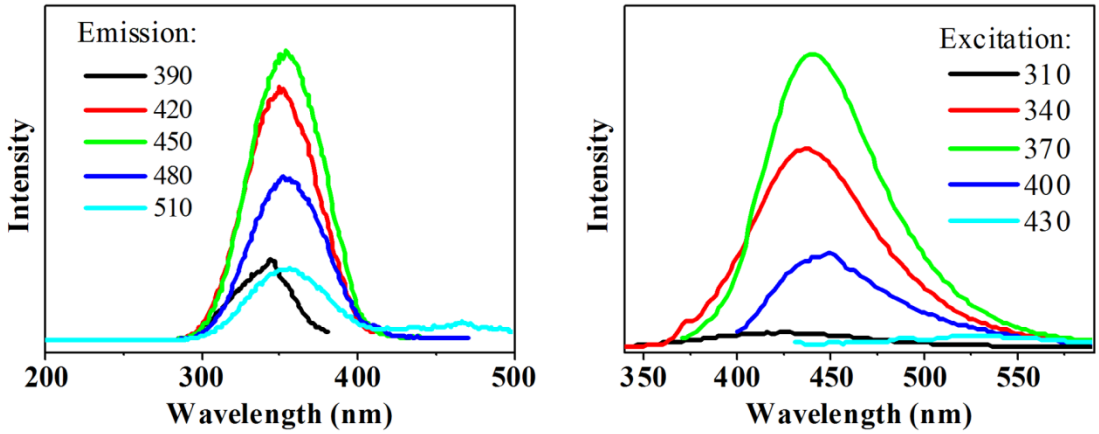

Figure 9.74. (left) excitation spectra for different emissions and (right) emission spectra for different excitations of CDs2f.

9.3.15. Quantum yield measurements of CDs 2a-f

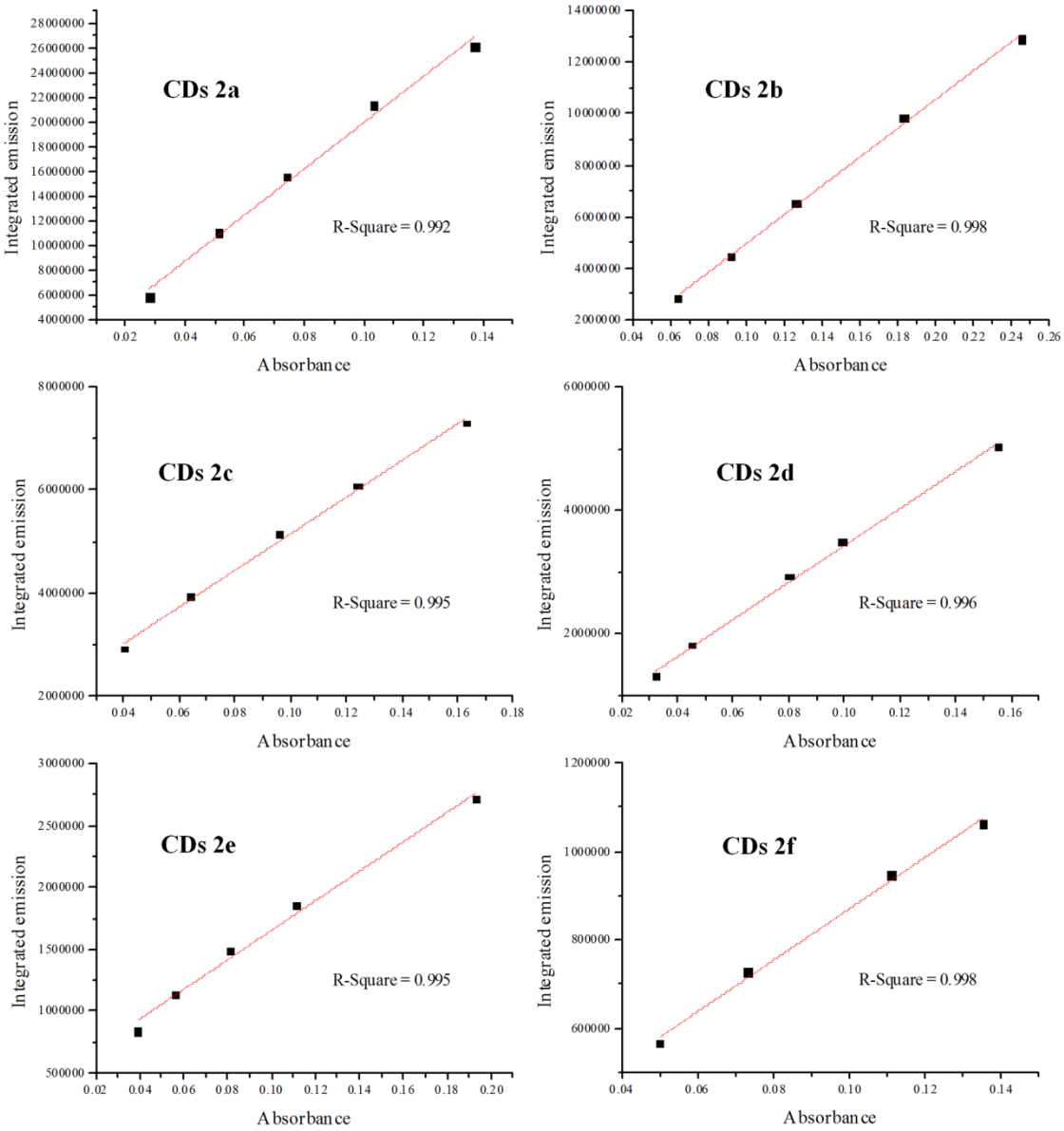

Figure 9.75. absorbance vs integrated fluorescence intensity of CDs 2a-f at different concentrations. The slope of the linear fitting was used for calculating the QY.

9.3.16. Atomic force microscopy of CDs 1a-d

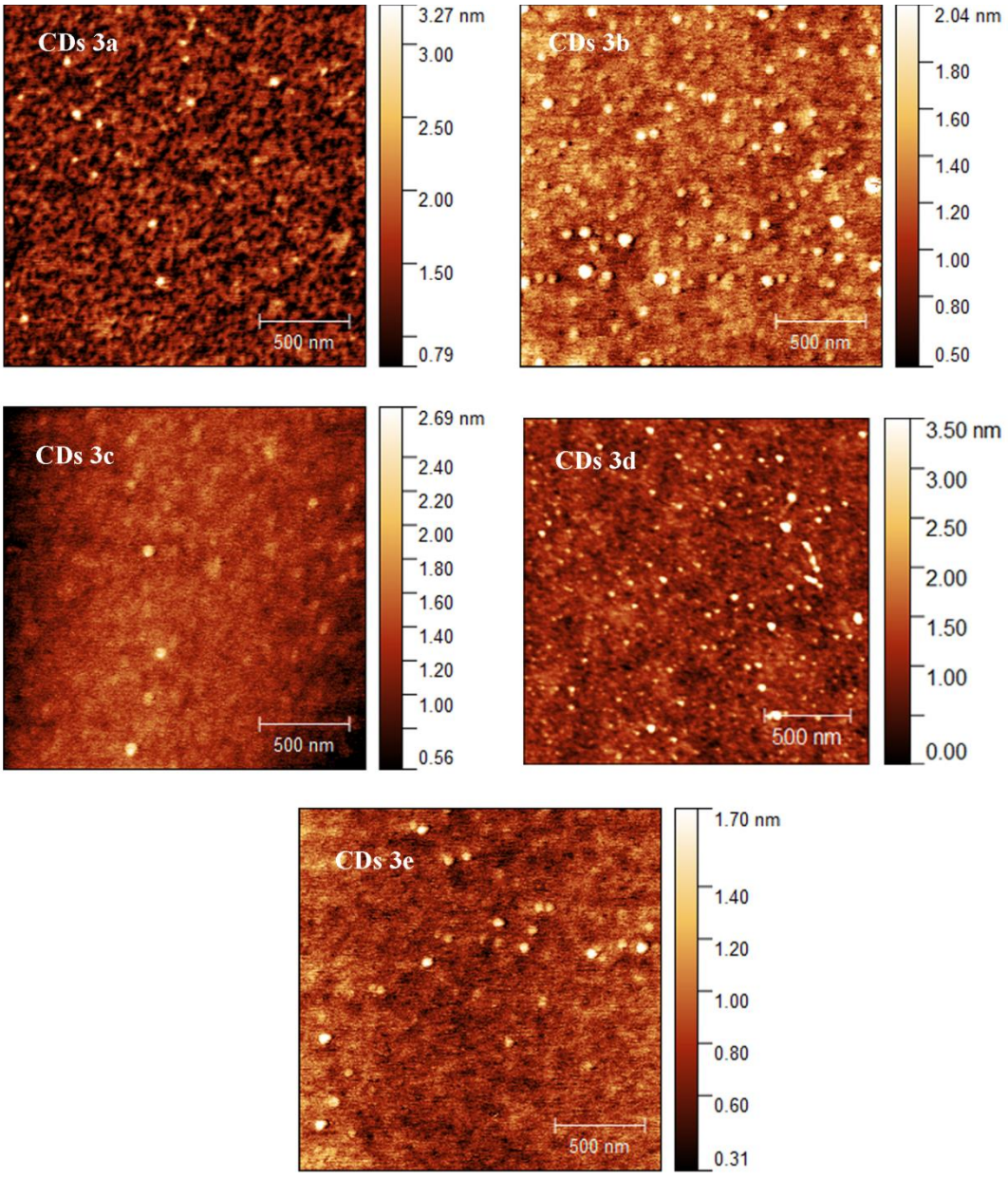

Figure 9.76. AFM pictures of CDs 3a-e. In all the samples, the height of the nanoparticles is comprised between 1.0-2.5 nm.

9.3.17. DOSY of CDs 3a-e

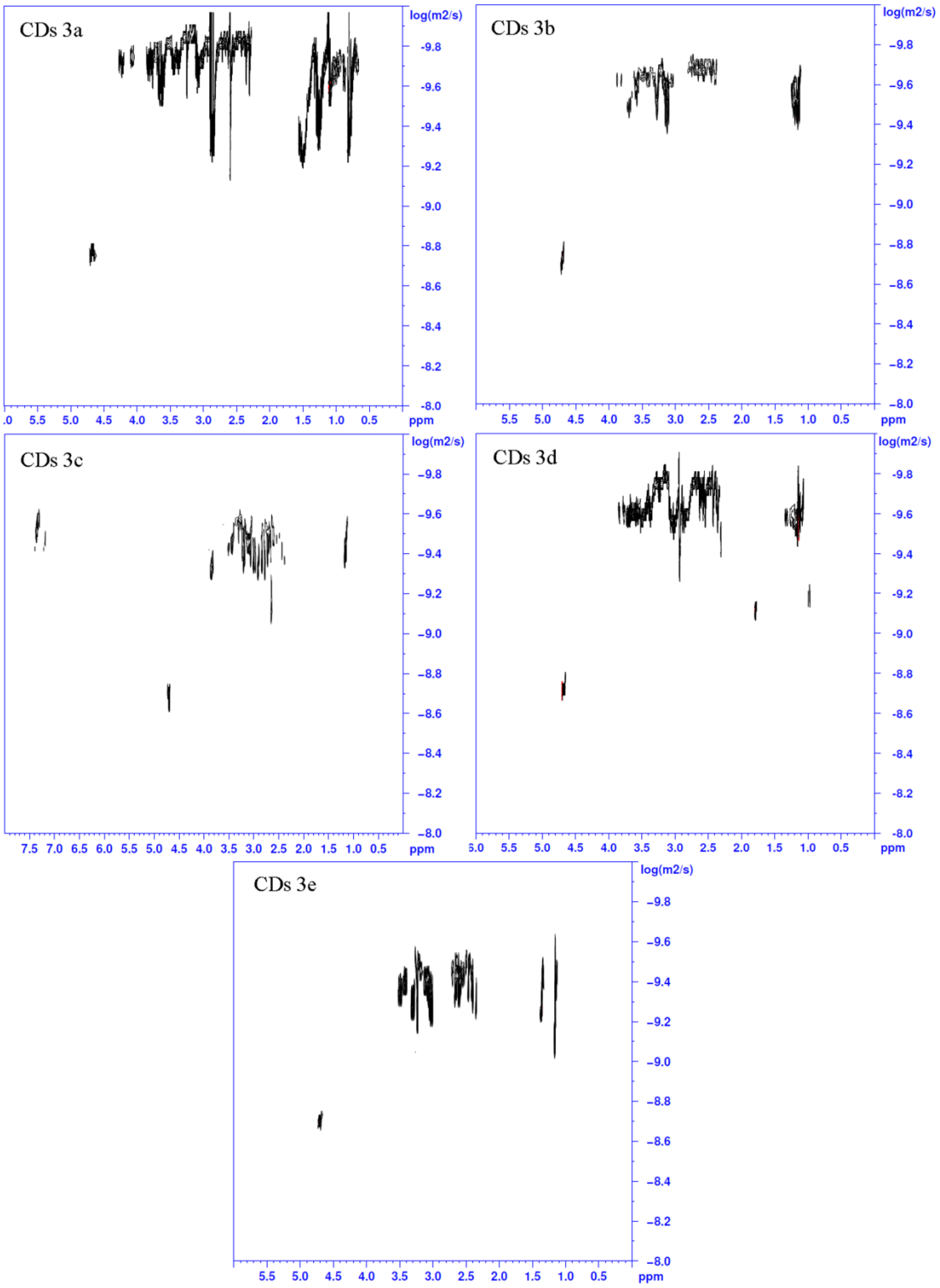

Figure 9.77. DOSY spectra of CDs 3a-e.

Table 9.11. The measured diffusion coefficients (D) and the calculated hydrodynamic rays (rH) and diameters of CDs 3a-e. Assuming a globular shape, the calculated size of the nanoparticles is comprised between 1.2-2.4 nm.

	D (m^2/s)	rH (nm)	Diameter (nm)
CDs 3a	$10^{-9.7}$	1.2	2.4
CDs 3b	$10^{-9.7}$	1.2	2.4
CDs 3c	$10^{-9.5}$	0.8	1.6
CDs 3d	$10^{-9.7}$	1.2	2.4
CDs 3e	$10^{-9.4}$	0.6	1.2

9.3.18. Elemental analysis of CDs 3a-e

Table 9.12. C, H, N, O and S mole percentages of CDs 3a-e, obtained by elemental analysis.

	C (mol%)	H (mol%)	N (mol%)	O (mol%)	S (mol%)
$C_8H_{12}N_2O_5$	29.6	44.4	7.4	18.5	--
CDs 1a	26.5	48	7	18.5	--
CDs 3a	28.8	52.7	7.5	11	--
CDs 3b	27.5	52	7.8	12.7	--
CDs 3c	30.4	46.4	7.2	16	--
CDs 3d	24.2	52.3	7.8	12.7	3.0
CDs 3e	27	51.2	7.1	14.2	--

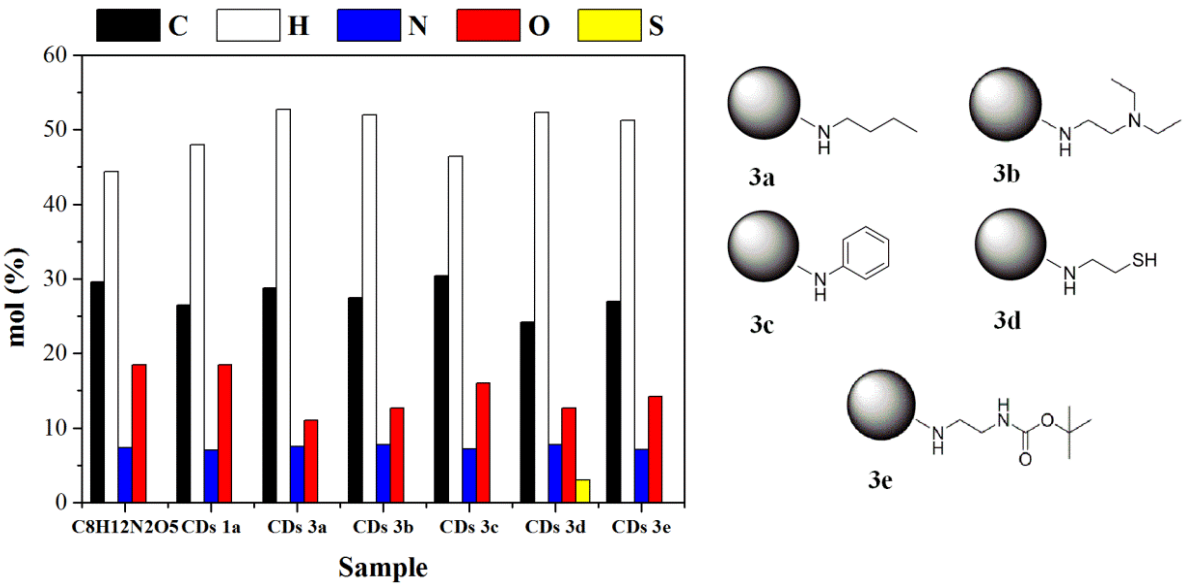

Figure 9.78. Visual comparison between the measured elemental composition of CDs 3a-e and the calculated elemental composition of the expected polymer structure.

9.3.19. IR spectra of CDs 3a-e

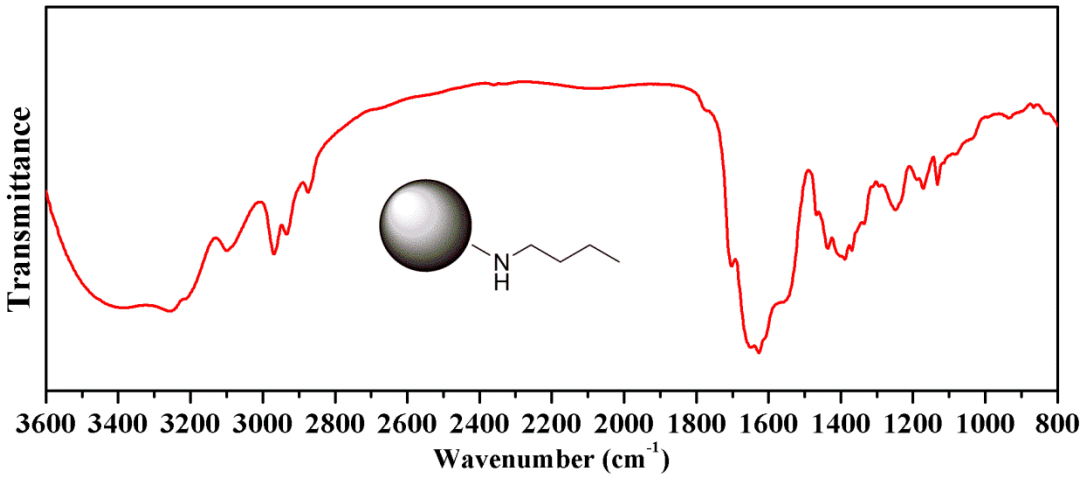

Figure 9.79. IR spectrum of CDs 3a. 3400-2800 cm^{-1}: O-H and N-H stretching, 2970, 2933, 2872 cm^{-1}: C-H stretching (butyl), 1704 cm^{-1}: C=O stretching (carboxylic acid), 1646 and 1552 cm^{-1}: C=O stretching (amide), 1440-1350 cm^{-1}: C-O and C-N stretching.

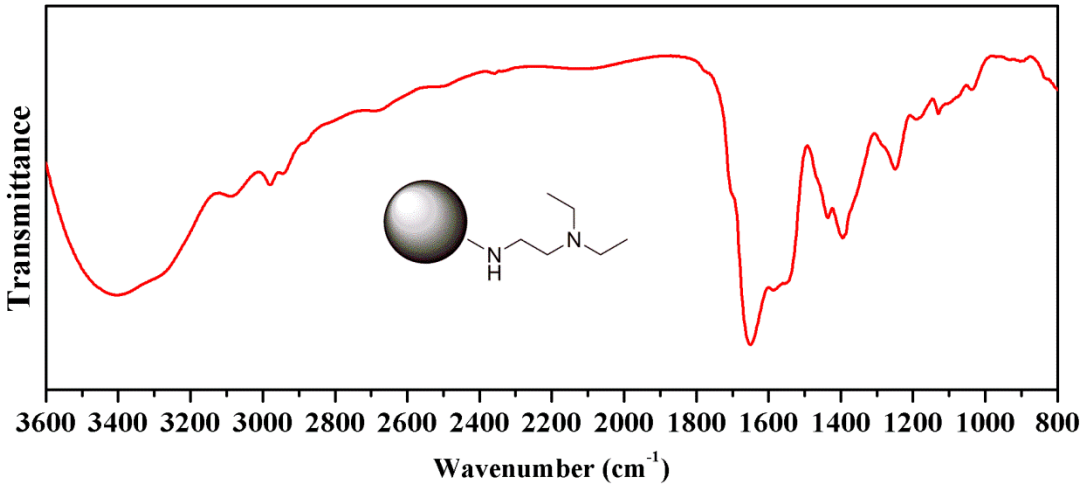

Figure 9.80. IR spectrum of CDs 3b. 3400-2800 cm^{-1}: O-H and N-H stretching, 2978, 2936 cm^{-1}: C-H stretching (N-ethyl), 1700 cm^{-1}: C=O stretching (carboxylic acid), 1651 and 1547 cm^{-1}: C=O stretching (amide), 1440-1350 cm^{-1}: C-O and C-N stretching.

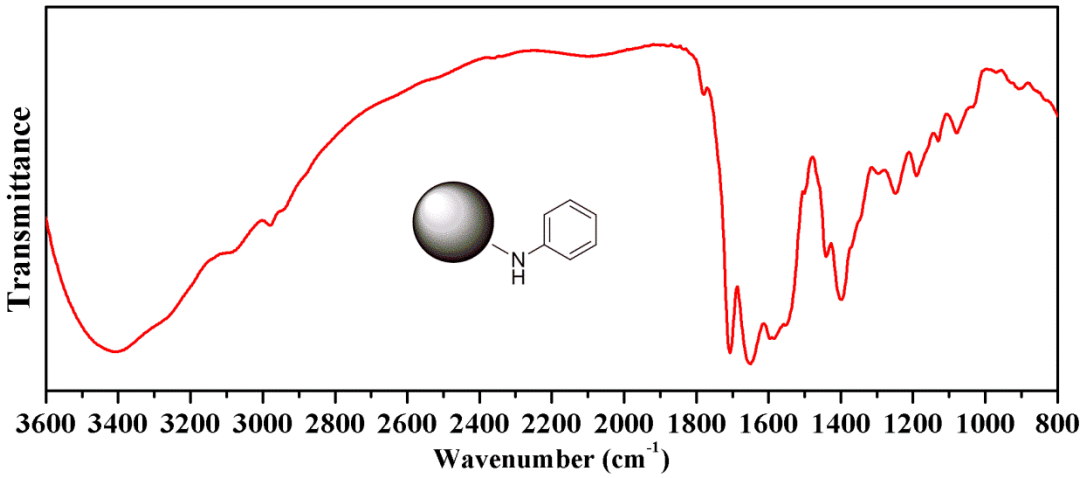

Figure 9.81. IR spectrum of CDs 3c. 3400-2800 cm^{-1}: O-H and N-H stretching, C=O stretching (carboxylic acid), 1648 and 1590 cm^{-1}: C=O stretching (amide), 1545 cm^{-1}: C-C stretching (aromatic ring), 1440-1350 cm^{-1}: C-O and C-N stretching.

CDs 3d

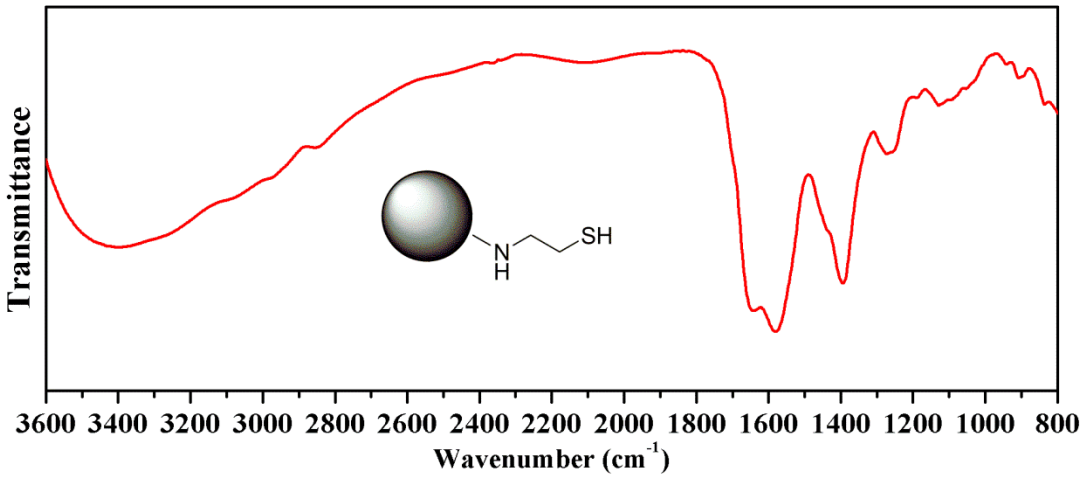

Figure 9.82. IR spectrum of CDs 3d. 3400-2800 cm^{-1}: O-H and N-H stretching, 1700 cm^{-1}: C=O stretching (carboxylic acid), 1646 and 1579 cm^{-1}: C=O stretching (amide), 1440-1350 cm^{-1}: C-O and C-N stretching.

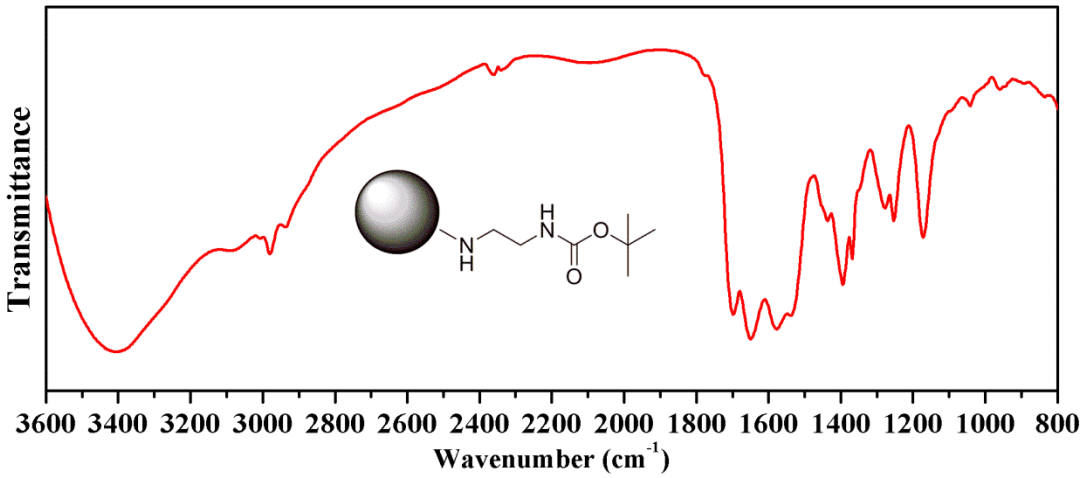

Figure 9.83. IR spectrum of CDs 3e. 3400-2800 cm^{-1}: O-H and N-H stretching, 1700 cm^{-1}: C=O stretching (carbamate, carboxylic acid), 1650, 1575 and 1536 cm^{-1}: C=O stretching (amide), 1440-1350 cm^{-1}: C-O and C-N stretching.

9.3.20. NMR spectra of CDs 3a-e

CDs 3a

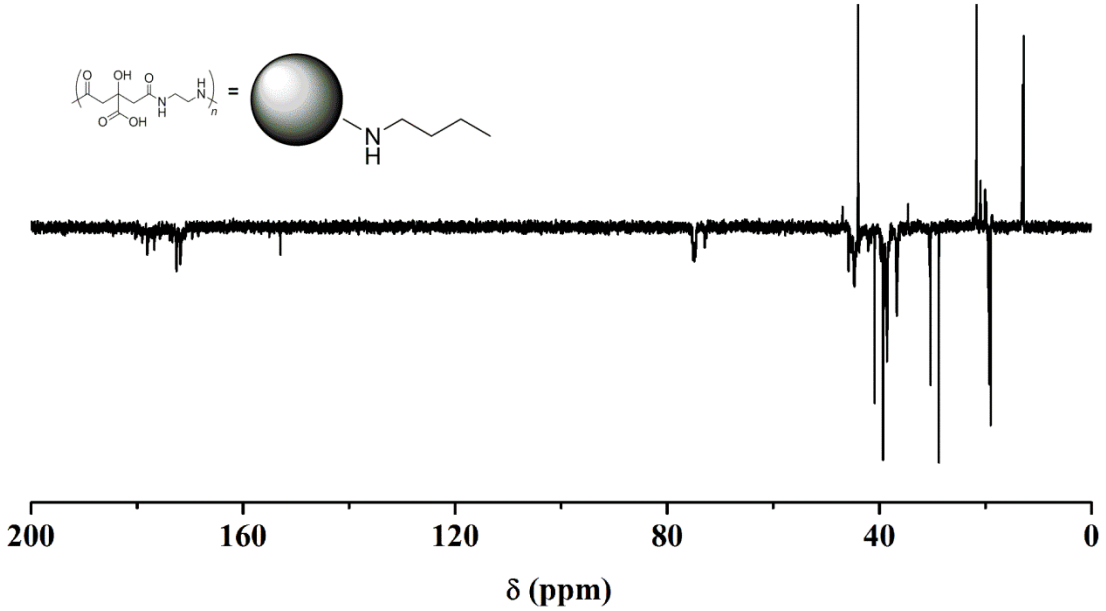

Figure 9.84. APT ^{13}C NMR spectrum of CDs 3a. Carboxylic acid and amide C: 180-171 ppm, quaternary C: 75-73 ppm, methylene C: 45-36 ppm, N-butyl C: 39, 30, 19, 13 ppm. The signals at 153, 44 , 21 ppm are due to DIC impurities.

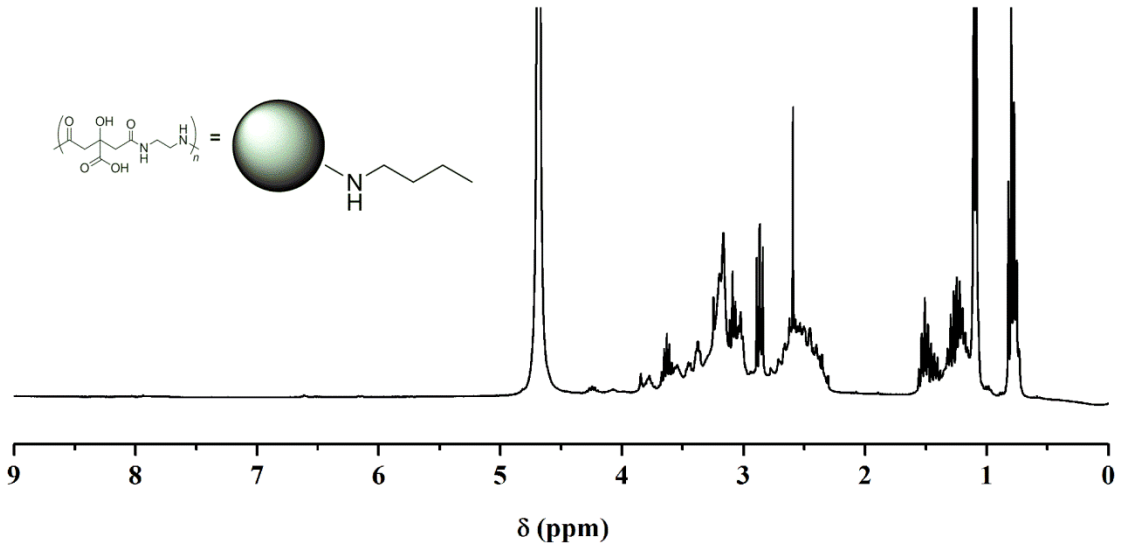

Figure 9.85. ^{1}H NMR spectrum of CDs 3a. methylene H: 3.9-2.2 ppm, N-butyl H: 2.9, 1.5, 1.3, 0.8 ppm. The signal at 1.2 ppm is due to DIC impurities.

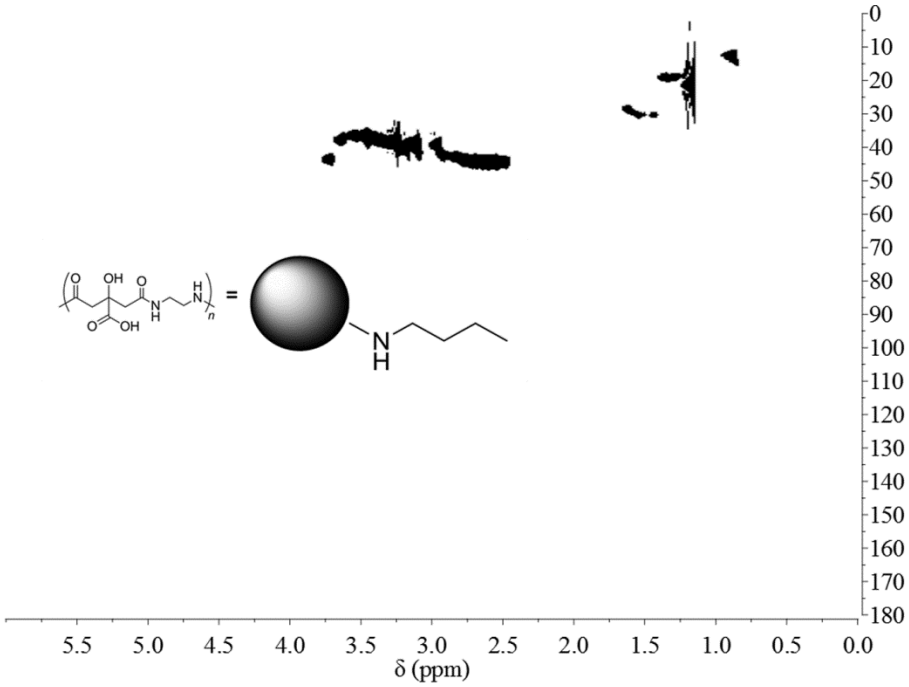

Figure 9.86. ^{1}H-^{13}C HSQC spectrum of CDs 3a.

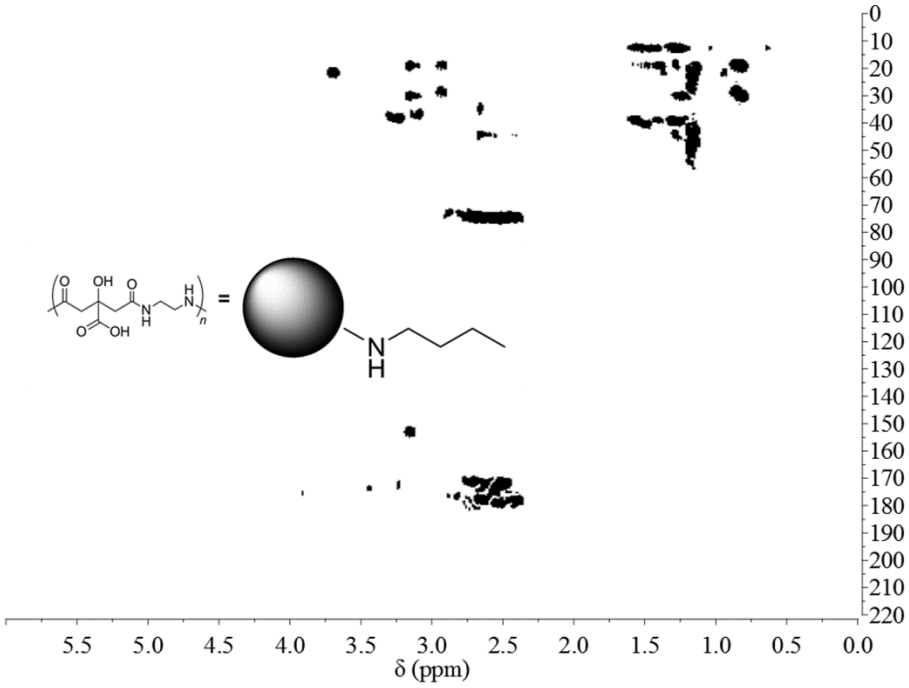

Figure 9.87. ^{1}H-^{13}C HMBC spectrum of CDs 3a.

CDs 3b

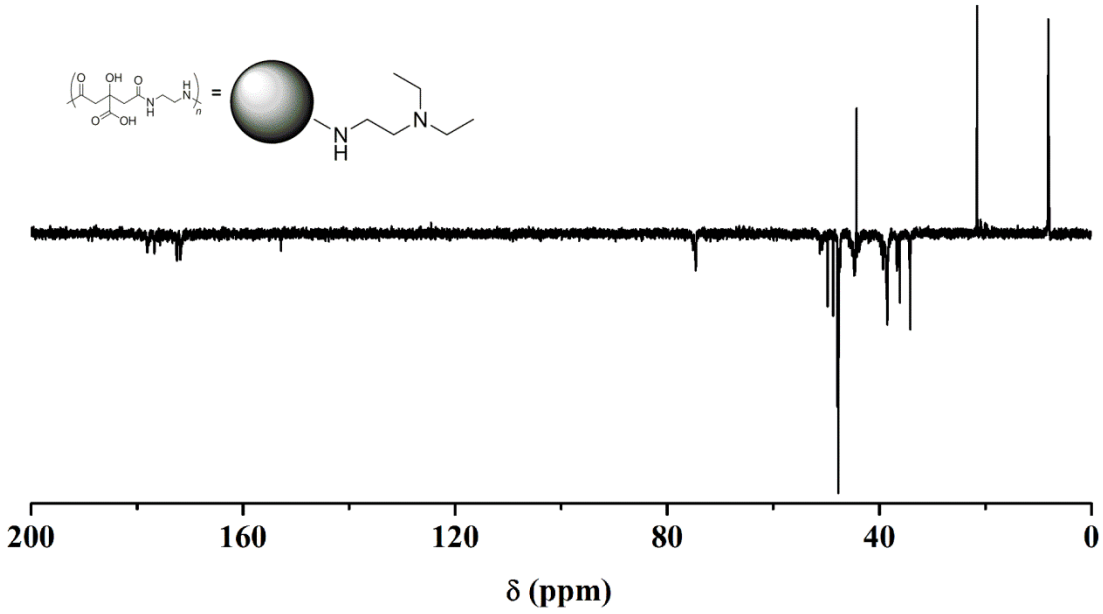

Figure 9.88. APT ^{13}C NMR spectrum of CDs 3b. Carboxylic acid and amide C: 178-171 ppm, quaternary C: 76-74 ppm, methylene C: 50-34 ppm, N-ethyl C: 48, 8 ppm. The signals at 153, 44, 21 ppm are due to DIC impurities.

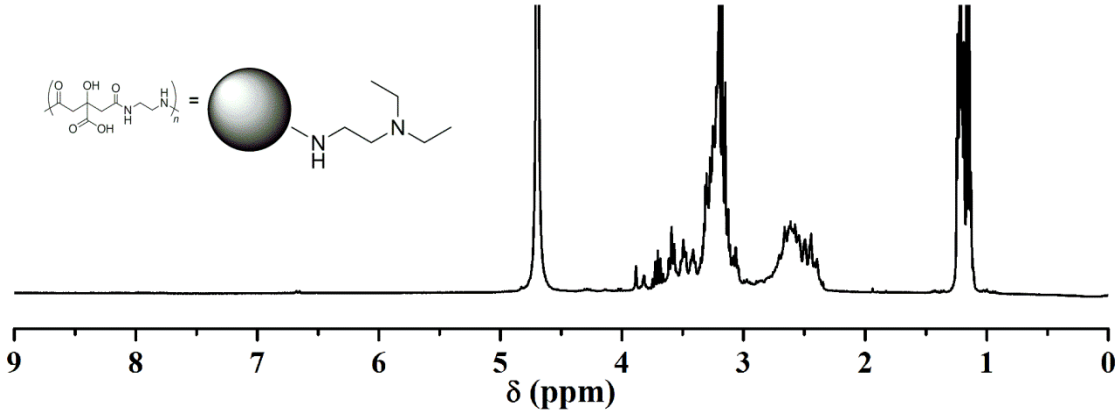

Figure 9.89. ^{1}H NMR spectrum of CDs 3b. methylene H: 3.9-2.3 ppm, N-ethyl H: 3.2, 1.2 ppm. The signal at 1.2 ppm (overlapped to CH_3 N-ethyl signal) is due to DIC impurities.

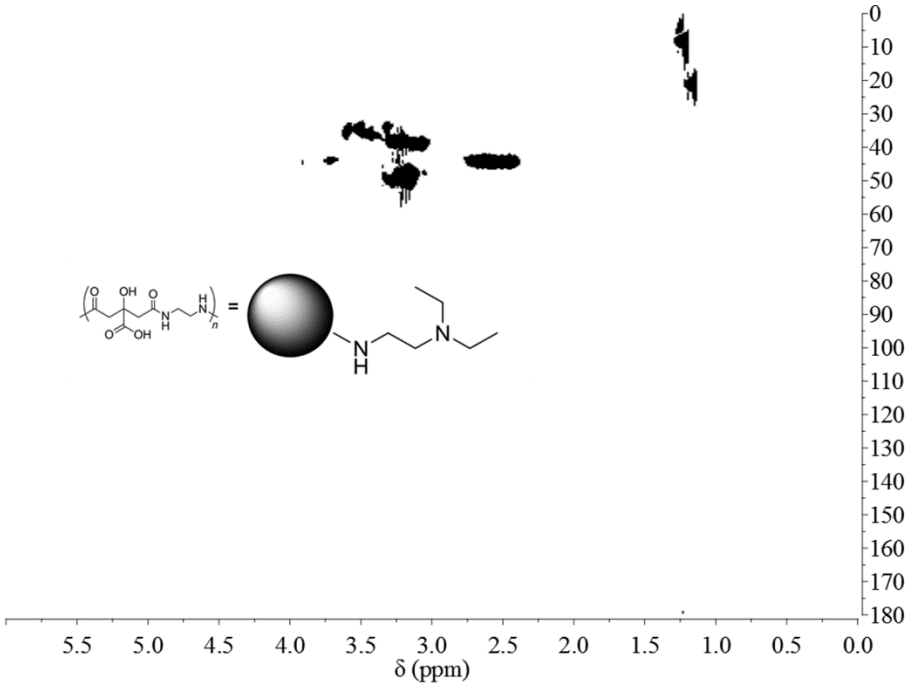

Figure 9.90. ^{1}H-^{13}C HSQC spectrum of CDs 3b.

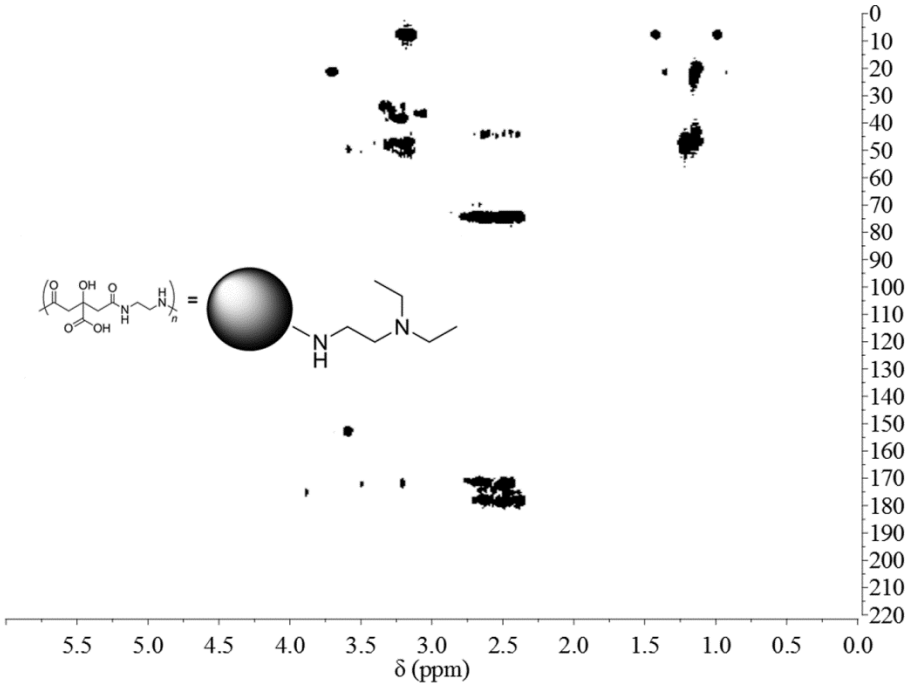

Figure 9.91. ^{1}H-^{13}C HMBC spectrum of CDs 3b.

CDs 3c

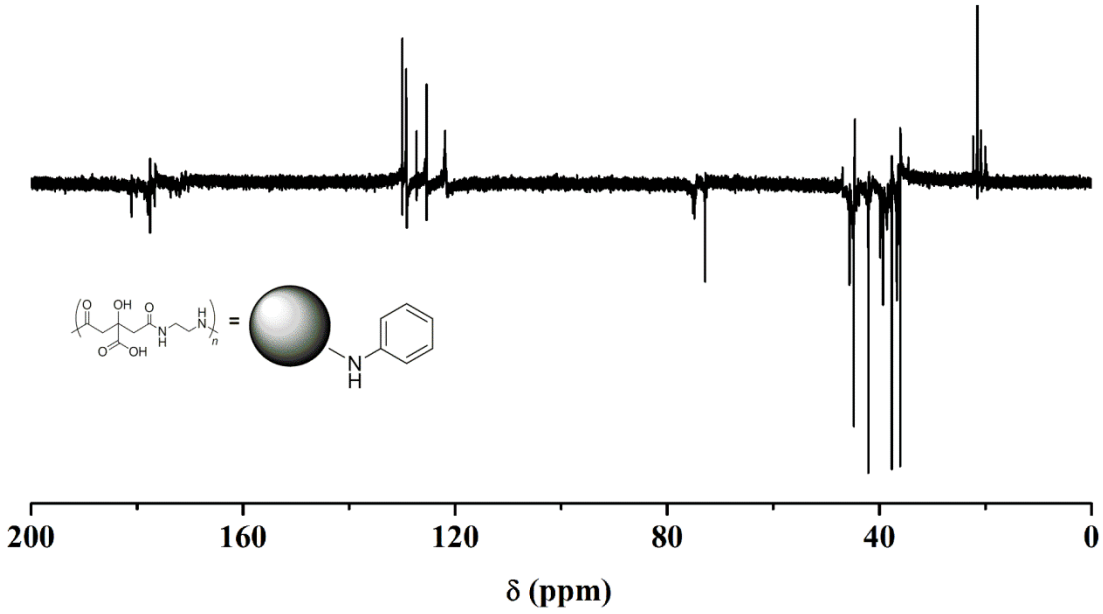

Figure 9.92. APT ^{13}C NMR spectrum of CDs 3c. Carboxylic acid and amide C: 181-170 ppm, N-phenyl C: 130-121 quaternary C: 75-72 ppm, methylene C: 46-35 ppm. The signals at 44, 21 ppm are due to DIC impurities.

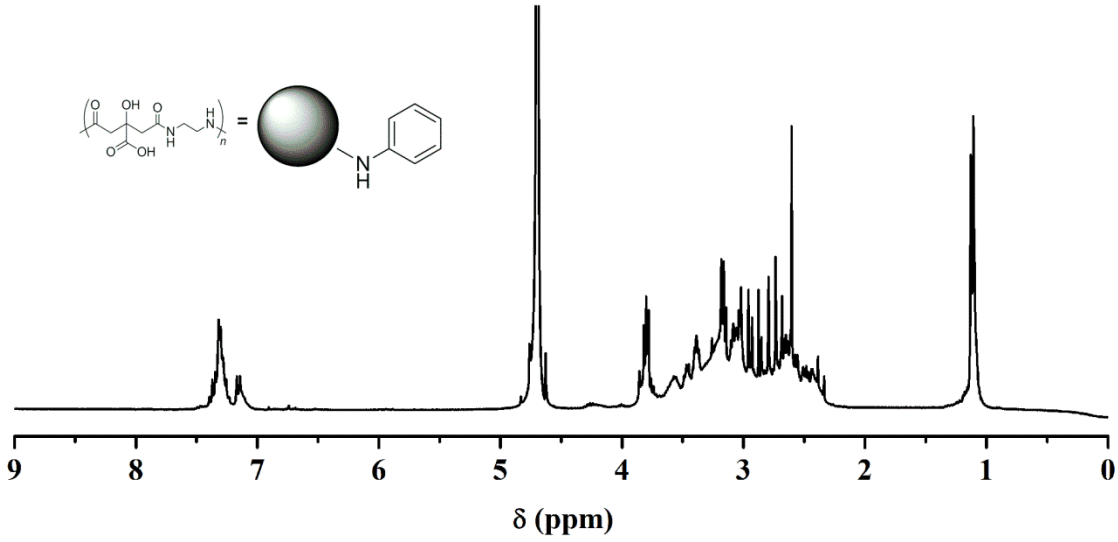

Figure 9.93. ^{1}H NMR spectrum of CDs 3c. N-phenyl: 7.5-7.1, methylene H: 3.9-2.3 ppm. The signal at 1.2 ppm (overlapped to CH_3 N-ethyl signal) is due to DIC impurities.

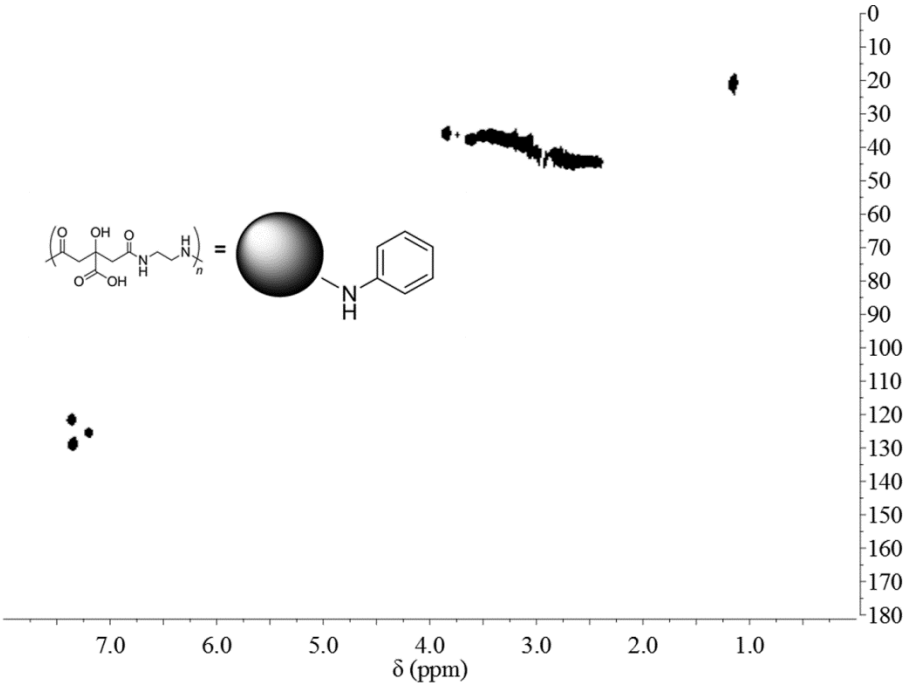

Figure 9.94. ^{1}H-^{13}C HSQC spectrum of CDs 3c.

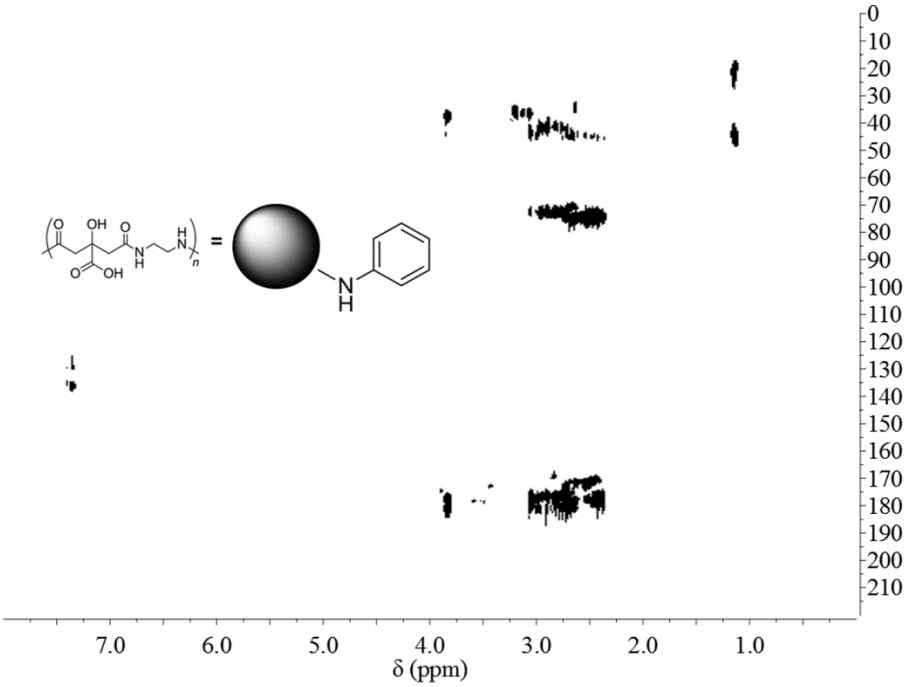

Figure 9.95. ^{1}H-^{13}C HMBC spectrum of CDs 3c.

CDs 3d

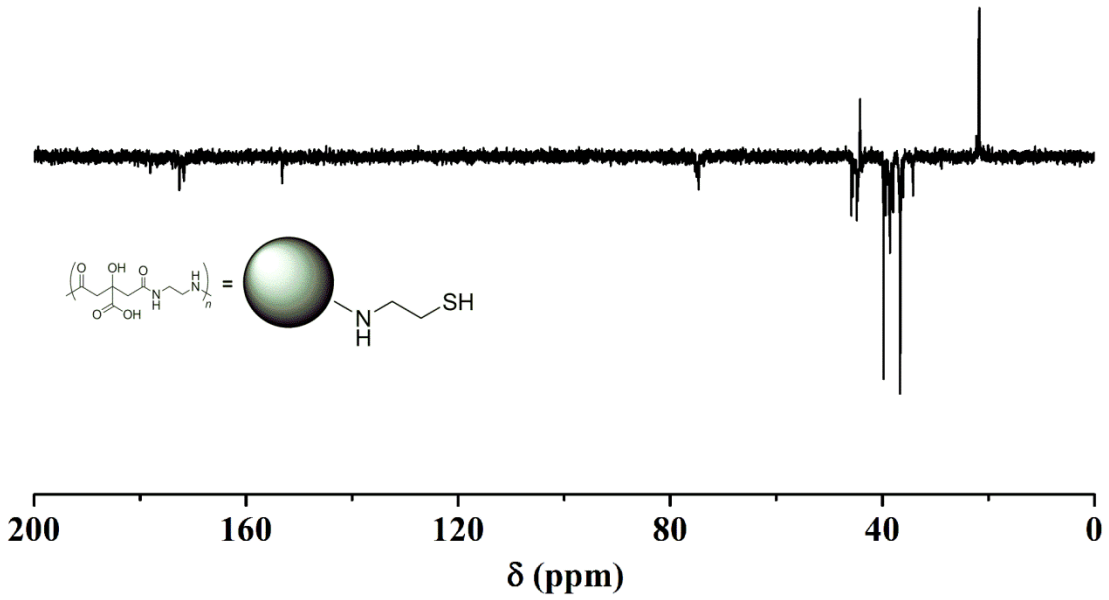

Figure 9.96. APT ^{13}C NMR spectrum of CDs 3d. Carboxylic acid and amide C: 180-171 ppm, 130-121 quaternary C: 75-73 ppm, methylene C: 46-34 ppm, N-ethanethiol C: 40, 37 ppm. The signals at 153, 44, 21 ppm are due to DIC impurities.

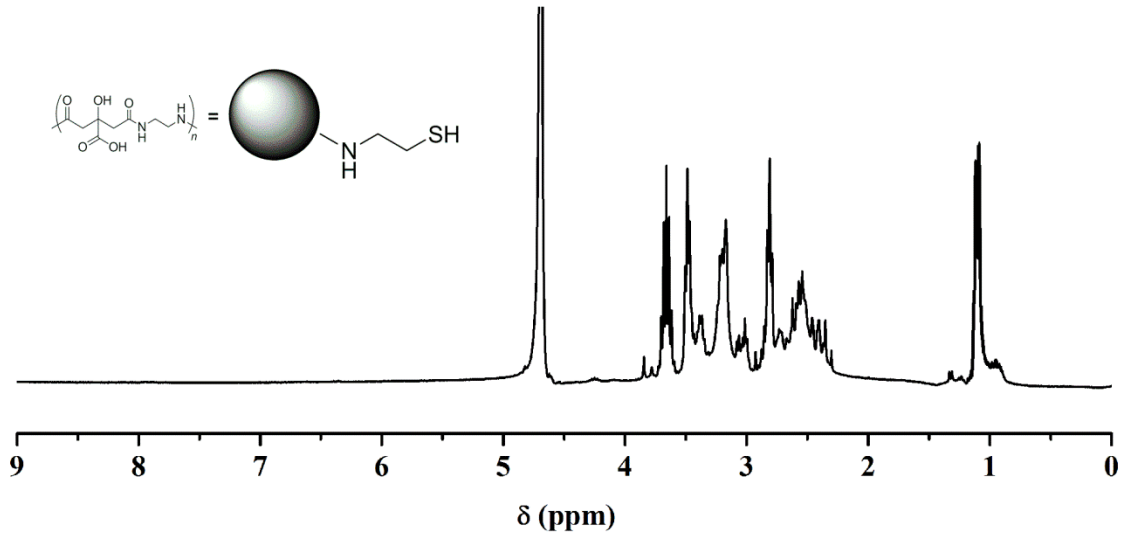

Figure 9.97. ^{1}H NMR spectrum of CDs 3d. Methylene H: 3.9-2.3 ppm, N-ethanethiol H: 3.5, 2.9 ppm. The signal at 1.2 ppm is due to DIC impurities.

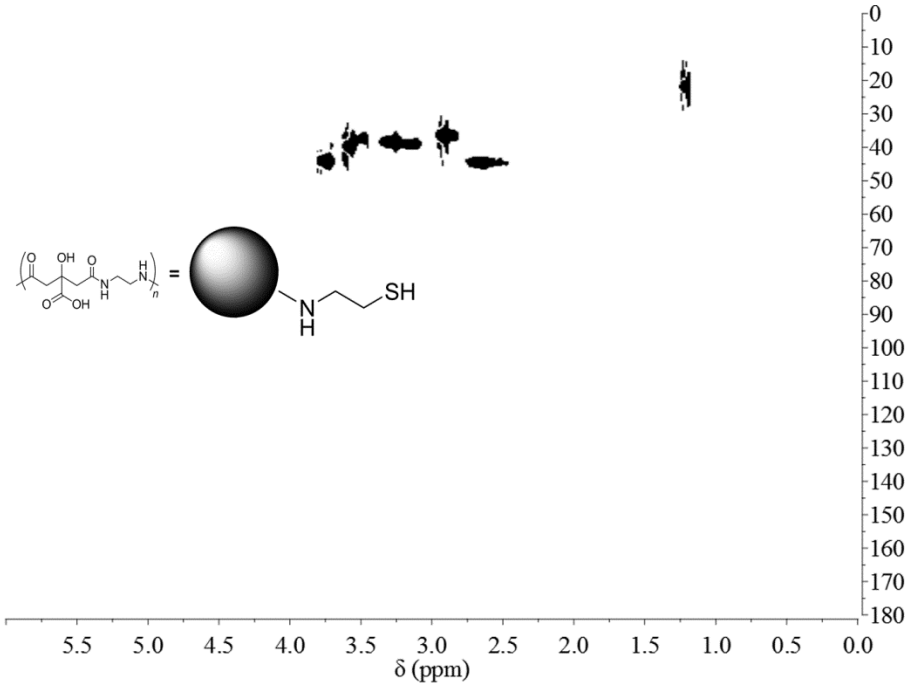

Figure 9.98. ^{1}H-^{13}C HSQC spectrum of CDs 3d.

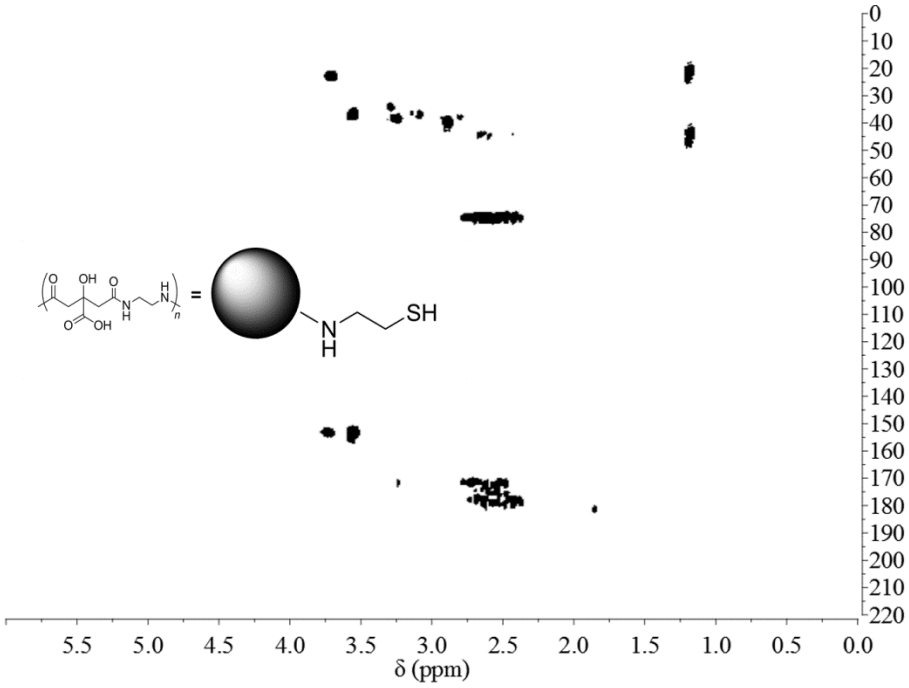

Figure 9.99. ^{1}H-^{13}C HMBC spectrum of CDs 3d.

CDs 3e

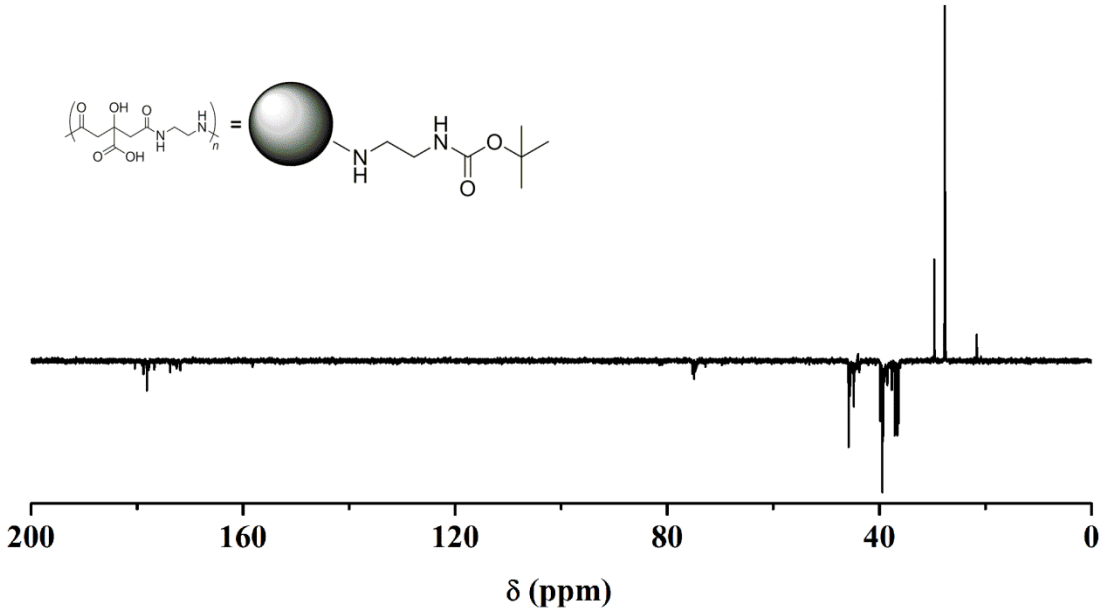

Figure 9.100. APT ^{13}C NMR spectrum of CDs 3e. Carboxylic acid and amide C: 181-171 ppm, quaternary C: 76-73, methylene C: 46-35 ppm, N-Boc carbamide C: 157 ppm, N-Boc tert-butyl quaternary C: 81 ppm, N.Boc methyl 28 ppm. The signals at 44, 21 ppm are due to DIC impurities.

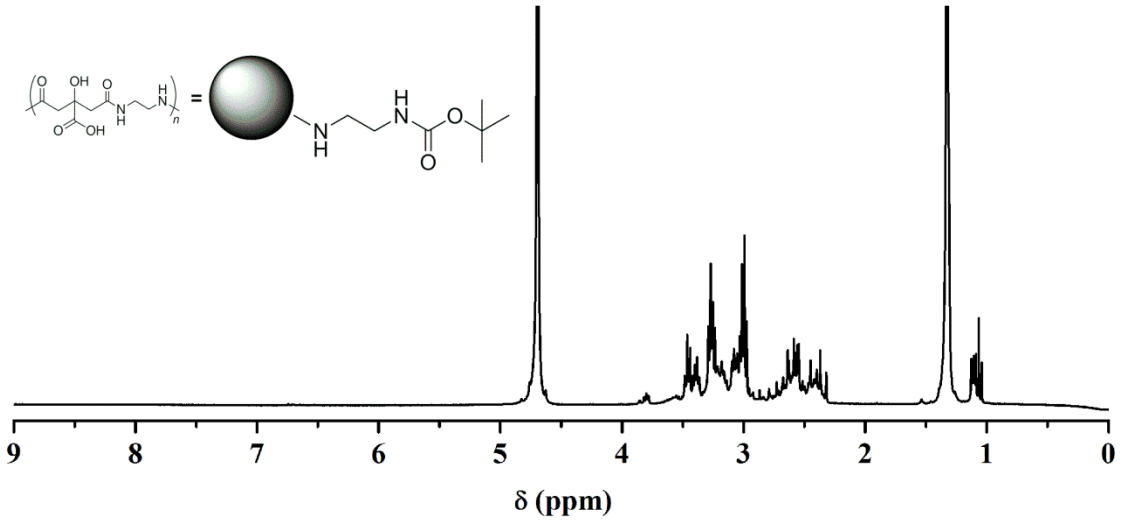

Figure 9.101. ^{1}H NMR spectrum of CDs 3e. Methylene H: 3.9-2.3 ppm, N-Boc methyl H: 1.4 ppm. The signal at 1.2 ppm is due to DIC impurities.

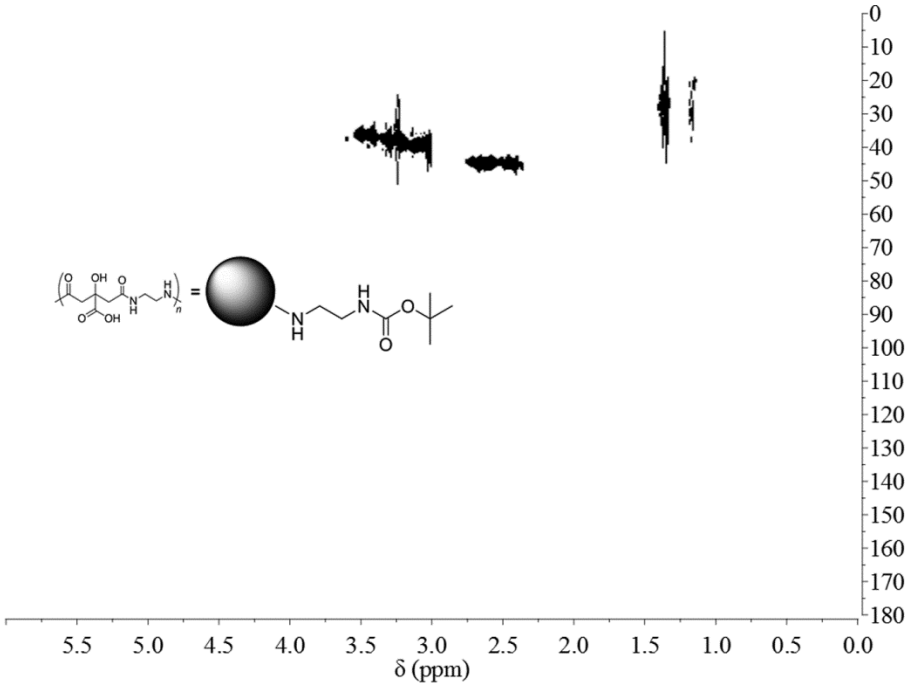

Figure 9.102. ^{1}H-^{13}C HSQC spectrum of CDs 3e.

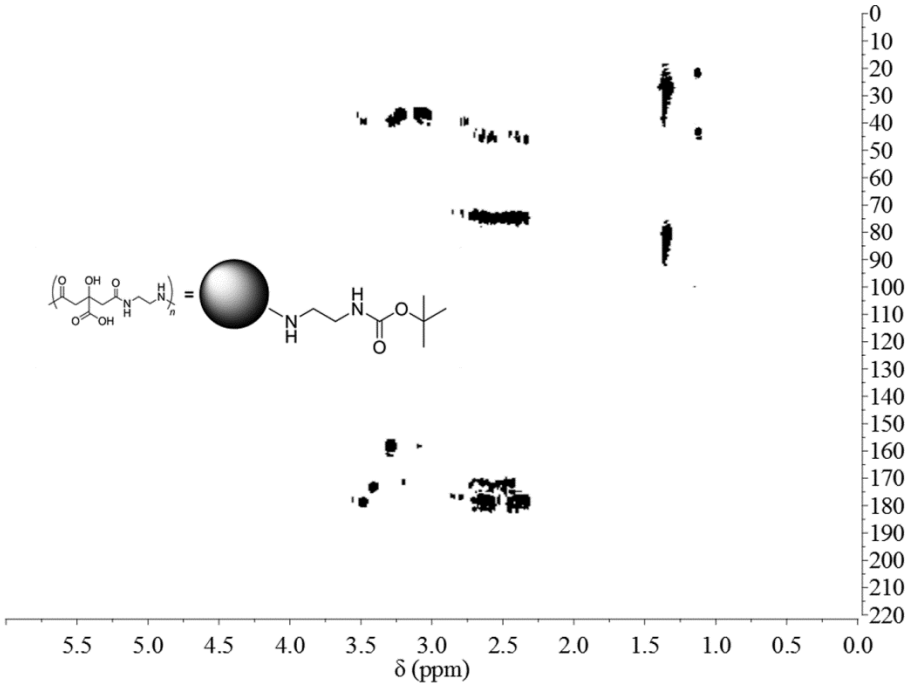

Figure 9.103. ^{1}H-^{13}C HMBC spectrum of CDs 3e.

9.3.21. UV/vis spectra of CDs 3a-e

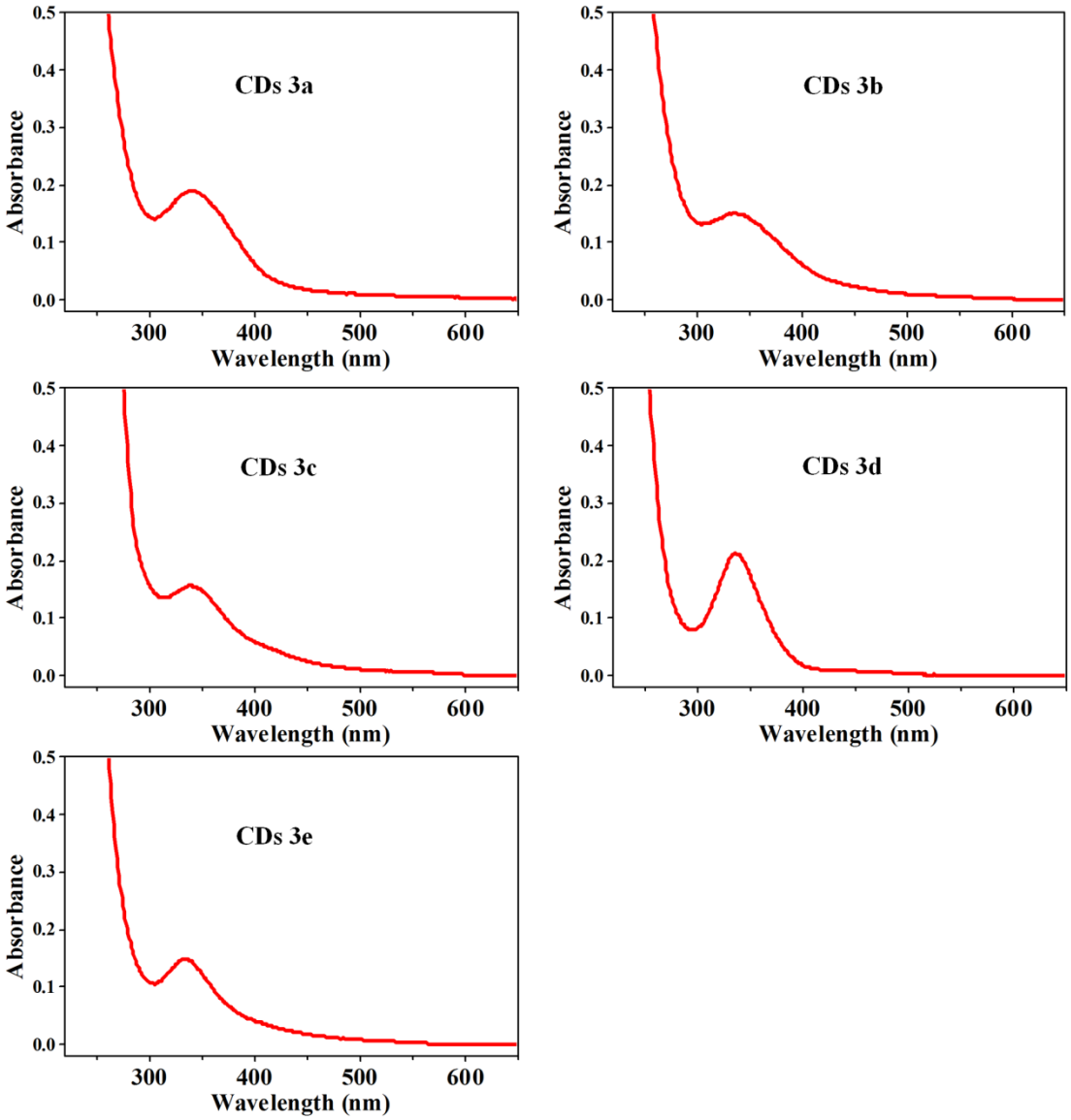

Figure 9.104. UV/vis spectra of CDs 3a-e.

9.3.22. Excitation and emission spectra of CDs 3a-e

CDs 3a

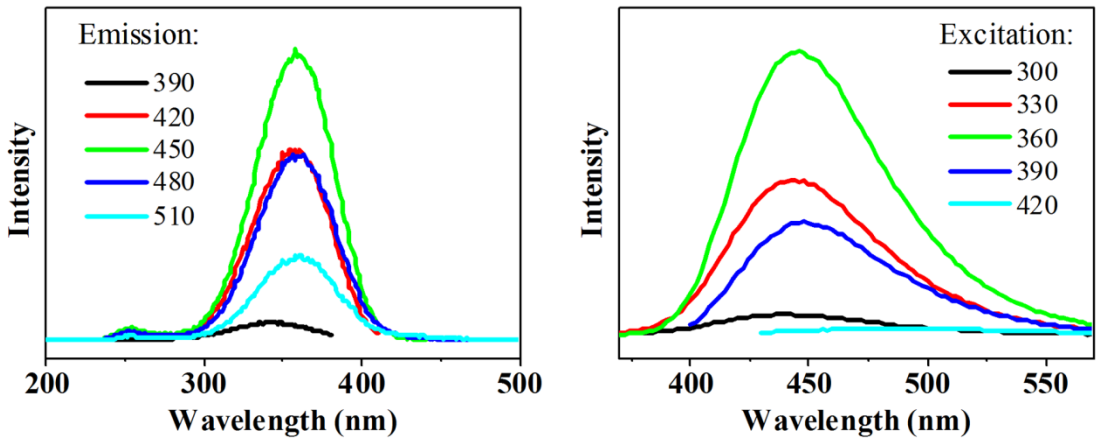

Figure 9.105. (left) excitation spectra for different emissions and (right) emission spectra for different excitations of CDs 3a.

CDs 3b

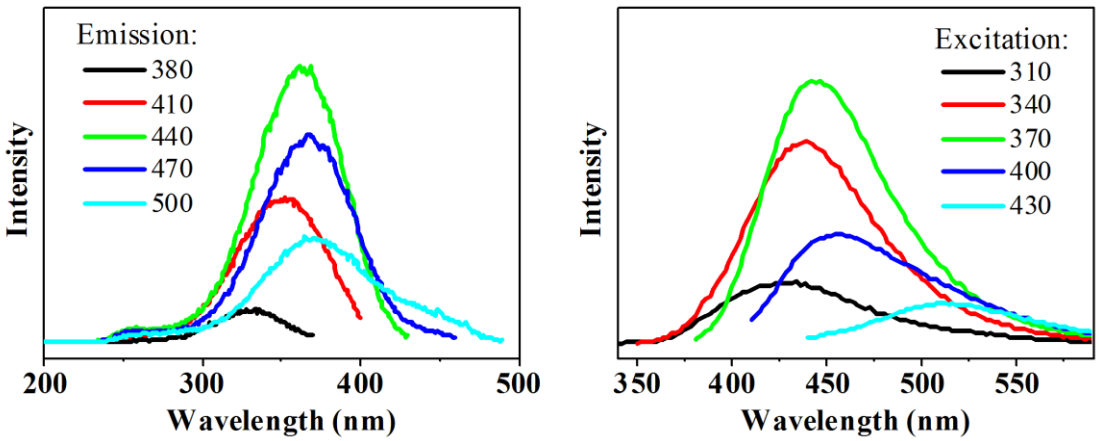

Figure 9.106. (left) excitation spectra for different emissions and (right) emission spectra for different excitations of CDs 3b.

CDs 3c

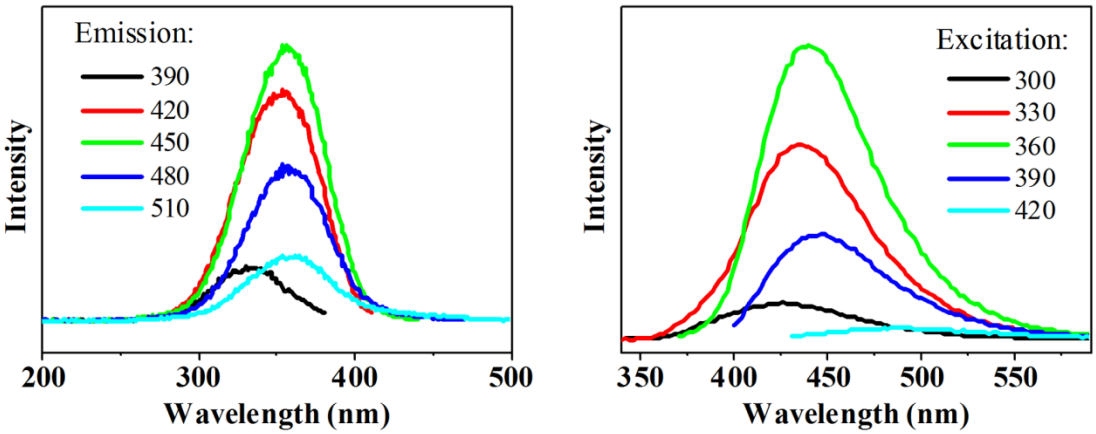

Figure 9.107. (left) excitation spectra for different emissions and (right) emission spectra for different excitations of CDs 3c.

CDs 3d

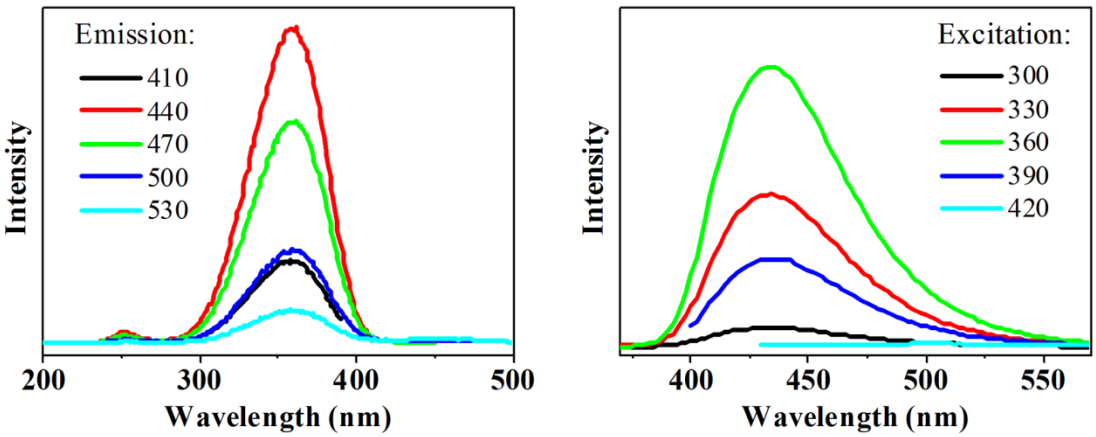

Figure 9.108. (left) excitation spectra for different emissions and (right) emission spectra for different excitations of CDs 3d.

CDs 3e

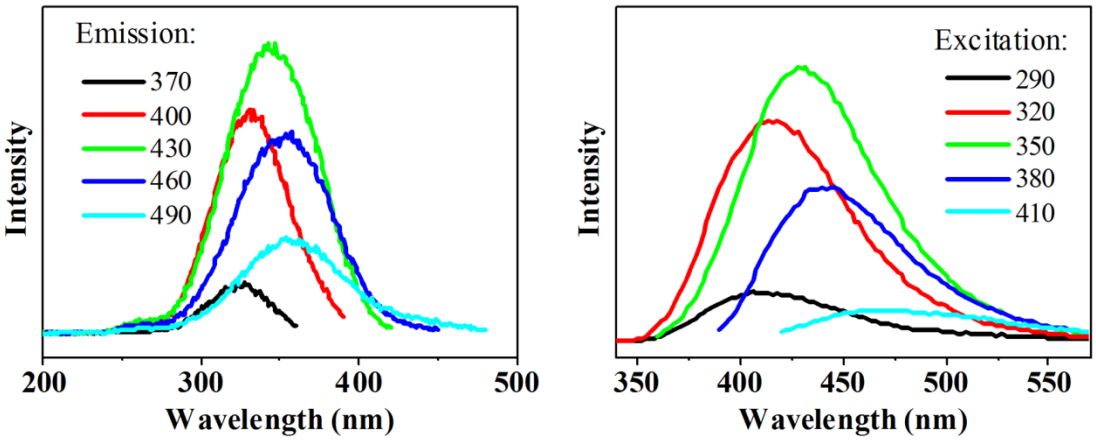

Figure 9.109. (left) excitation spectra for different emissions and (right) emission spectra for different excitations of CDs 3e.

9.3.23. Fitting for the QY calculation of CDs 3a-e

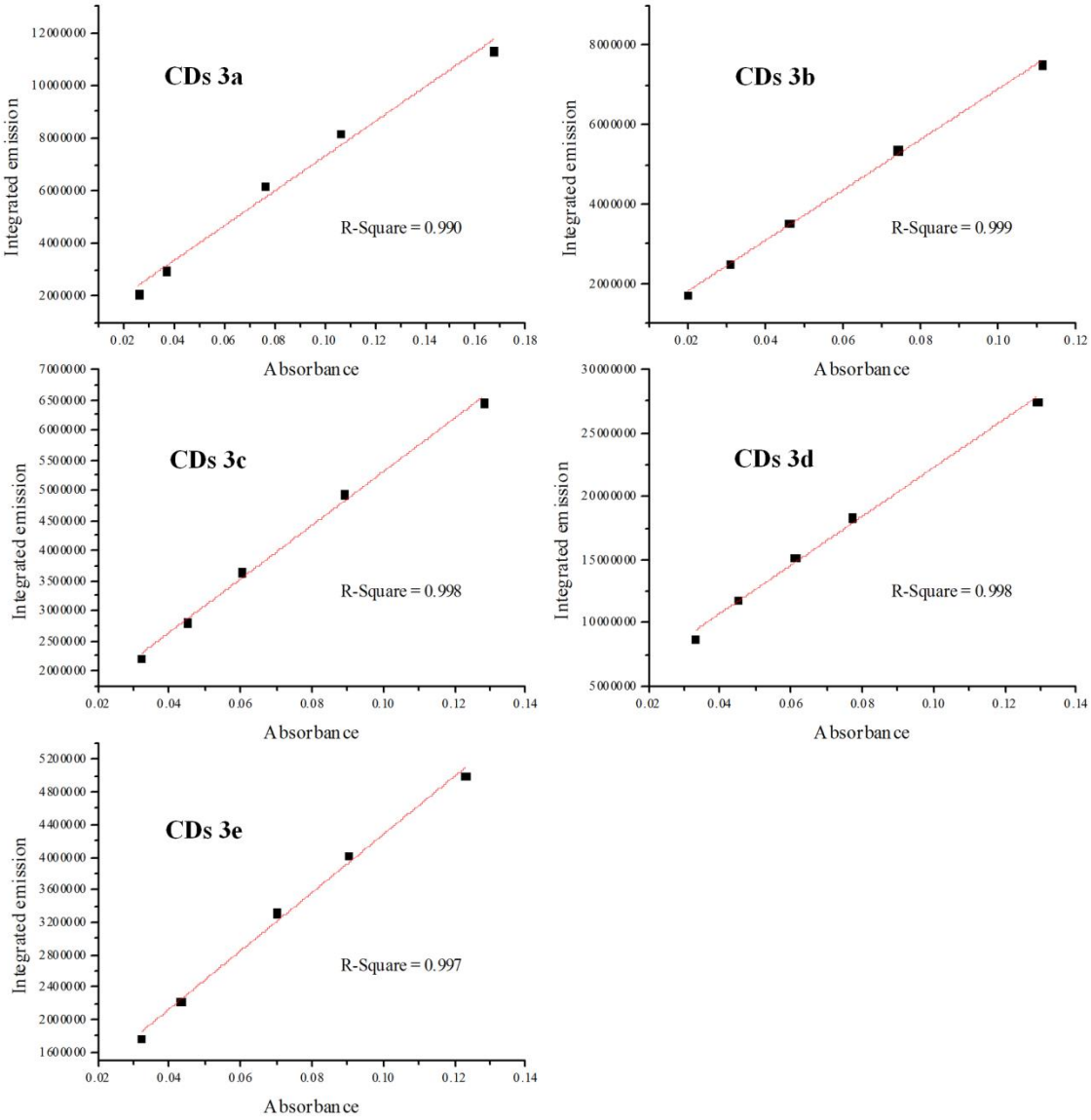

Figure 9.110. absorbance vs integrated fluorescence intensity of CDs 3a-e at different concentrations. The slope of the linear fitting was used for calculating the QY.

10. ANNEX D

10.1. Abstract

In this study, sodium borohydride ($NaBH_4$) reactivity was tested towards the CD-MoS_2 hybrid prepared in Chapter 5. The addition of $NaBH_4$ to a CD-MoS_2 dispersion was reflected in the cleavage of the thiol-molybdenum bond between CDs and MoS_2 and therefore in the loss of the covalent functionalization.

10.2. Experimental section

For the preparation of the hybrid CD-MoS_2 see chapter 5.

10.3. Results and discussion

After dispersing 10 mg of CD-MoS_2 in DMF by sonication, a centrifugation (5000 r.p.m., 5 minutes) was performed in order to precipitate the material and the supernatant was collected. As expected, no trace of CDs was detected in the supernatant by UV/vis or PL spectroscopy, being CDs firmly attached onto MoS_2 by covalent bond. Therefore, the same material was redispersed in DMF and this time few milligrams of $NaBH_4$ were added. The absorption (Figure 10.1a) and fluorescence emission (Figure 10.1b) of the dispersion were measured before and after the $NaBH_4$ addition. Interestingly, after the addition, the emission intensity of the CDs increased considerably, suggesting that the covalent bond with MoS_2 was broken and the fluorescence was not affected anymore by its quenching effect. In order to confirm this hypothesis, after the addition of $NaBH_4$ the dispersion was centrifuged as done previously and the supernatant was separated from the precipitate, which was filtered and washed with DMF and water. The IR profile of the dry precipitate does not present anymore the characteristic bands of the CDs between 1700-1600 cm^{-1} belonging to C=O stretching (figure 1.10c). On the contrary the UV/vis spectrum of the supernatant clearly shows the absorption profile of the CDs (figure 1.10d). These evidences further highlight the key role of the stable covalent bond in the occurrence of the electronic interaction between CDs and MoS_2. Additionally, it is shown that a strong reducing agent as $NaBH_4$ is able to break the thiol-molybdenum bond.

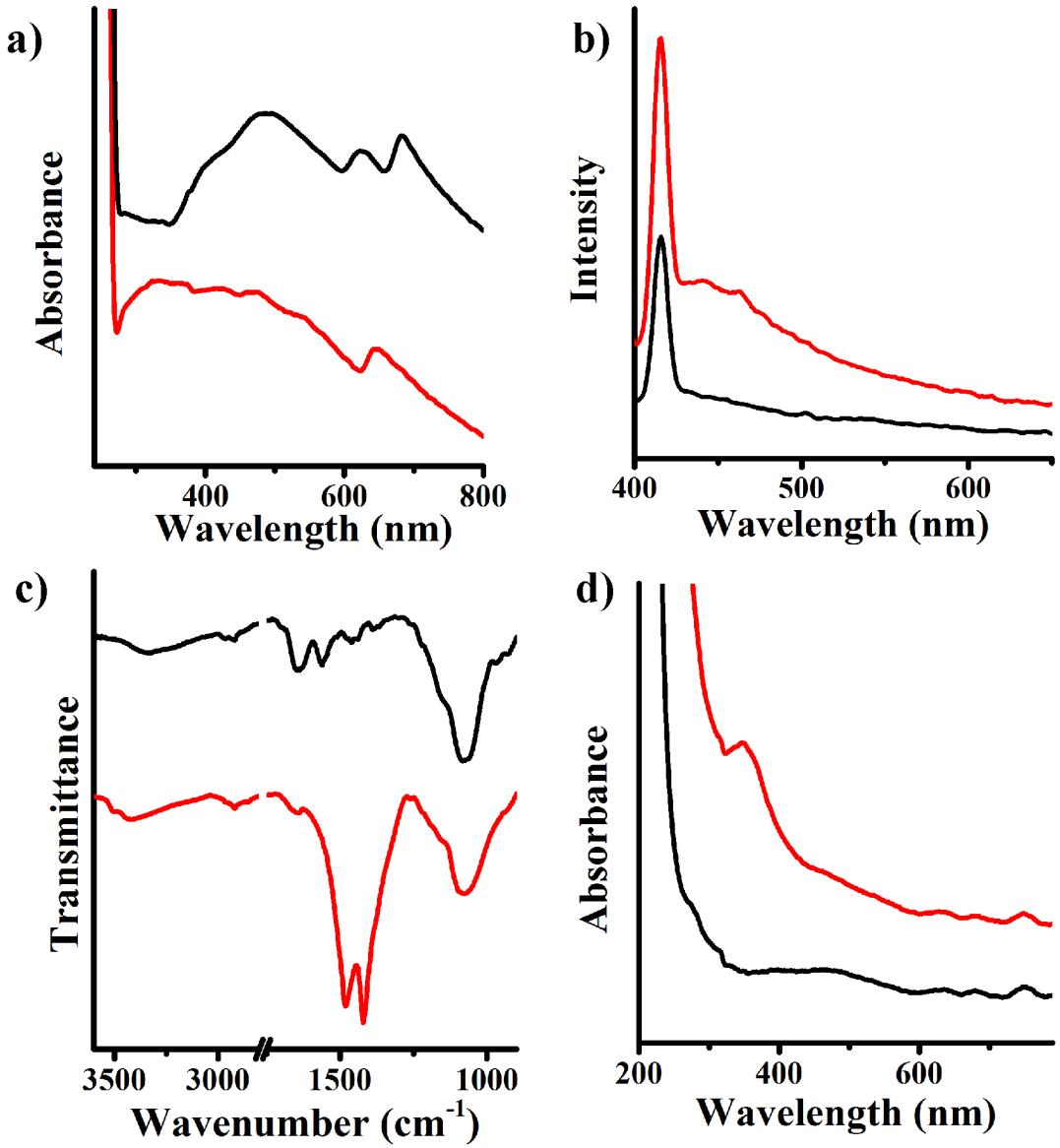

Figure 10.1. UV/Vis spectra of the CD-MoS_2 dispersion before (black) and after (red) $NaBH_4$ addition, (b) fluorescence emission spectra (λ_{exc} 370 nm) of the CD-MoS_2 dispersion before (black) and after (red) $NaBH_4$ addition, (c) IR spectra of the dry precipitate obtained by centrifugation before (black) and after (red) $NaBH_4$ addition, (d) UV/Vis spectra of the supernatant obtained by centrifugation before (black) and after (red) $NaBH_4$ addition.

11. ANNEX E

11.1. Abstract

In this study, the synthesis of fluorescent CDs is accomplished by microwave irradiation of a solid mixture of citric acid and urea. Filtration and dialysis allowed to separate the raw material by size, obtaining four different fractions. The structural characterization of the fractions was performed by infrared spectroscopy and elemental analysis, furnishing interesting information for the understanding of the nanoparticles growth process. Additionally, differences in the optical behavior were pointed out by absorption spectroscopy and steady state fluorescence spectroscopy characterization. Finally, the full dataset was interpreted under the light of the findings reported in Chapter 2.

11.2. Experimental part

11.2.1. Materials

Citric acid monohydrate (99.5%) and urea (99%) were used without further purifications. Dialysis tubes with molecular weight cut-off (MWCO) 0.5-1 KDa were bought from Spectrum Labs.

11.2.2. Characterization techniques

- The microwave-assisted reaction was performed in a CEM Discover SP reactor employed in a closed vessel.
- Elemental analyses were performed in a Thermo Flash EA 1112 instrument with ~3 mg of powder samples.
- Infrared absorption measurements were performed on powder samples pressed with KBr into pellets with a Bruker Vertex 70 spectrometer.
- UV/Vis absorption spectra were recorded on a Shimadzu UV-2401 PC spectrophotometer.
- Photoluminescence excitation and emission spectra were recorded on a Horiba Jobin Yvon Fluoromax-P, slits of excitation and emission at 1 mm. All the spectra were recorded at room temperature using 10 mm path-length quartz cuvette.

- Pico-second time-resolved fluorescence spectra were measured by the time-correlated-single-photon-counting (TCSPC) method on a Nano-Log spectrofluorometer (Horiba JobinYvon), by using a laser diode as an excitation source (NanoLED, 375 nm) and a UV-Vis detector TBX-PMT series (250-850 nm) by Horiba JobinYvon. Lifetimes were evaluated with the DAS6 Fluorescence-Decay Analysis Software.

11.2.3. Synthesis of CDs

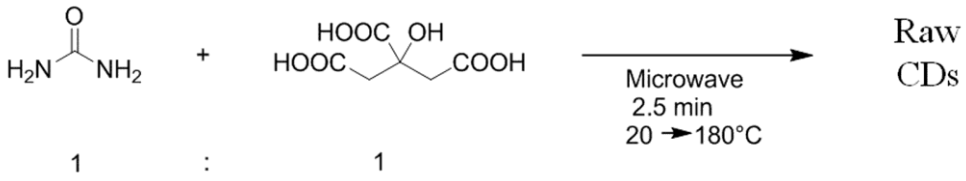

Scheme 31.1. Synthesis of raw CDs.

1 g of citric acid monohydrate in powder was mixed with 0.28 g (1 equiv.) of urea in powder in a round bottom glass equipped with magnetic stirrer. The solid mixture was irradiated by microwave (300 W, 2.5 minutes) until the temperature reached 180 °C. After cooling, 50 ml of water were poured on the as-produced material, achieving the partial dissolution. The black dispersion was filtered by filter paper. The filtrate, insoluble in water, was washed on the filter and dried in the oven, obtaining fraction **1** (Figure 11.1a). The clear solution was freeze-dried, obtaining the solid **CDs**.

11.2.4. Separation of CDs by dialysis

For the separation by size of the CDs in different fraction, two purification steps by dialysis were performed. In the first step, the CDs were dissolved in 20 ml of water and closed inside a dialysis tube with MWCO = 6-8 kDa (Figure 11.1b). The tube was soaked in a vessel filled with 0.5 liter of water. After one day, the water outside the dialysis tube was coloured by the material whose small size allowed its leakage from the tube pores. Therefore the external material was collected and dried by freeze-drying. In parallel, the dialysis tube was dialyzed against water for other three days, changing water every day, and the material left inside, consisting in the bigger size fraction (fraction **2)**, was dried by freeze-drying. The material obtained by the removal of the external water was redissolved in few milliliters and poured into a new dialysis tube (Figure 11.1c) with MWCO = 0.5-1.0 kDa, therefore with smaller pore size than the previous one. The separation was performed as before, soaking the tube in

0.5 liter of water. The smaller particles that could flow out the tube were collected after one day, removing the external water by freeze-drying (fraction **4**), while the material trapped inside was opportunely washed with water for three days, changing the water every day and finally dried (fraction **3**). Therefore, from **1** to **4** the separated fractions will have decreasing particle size.

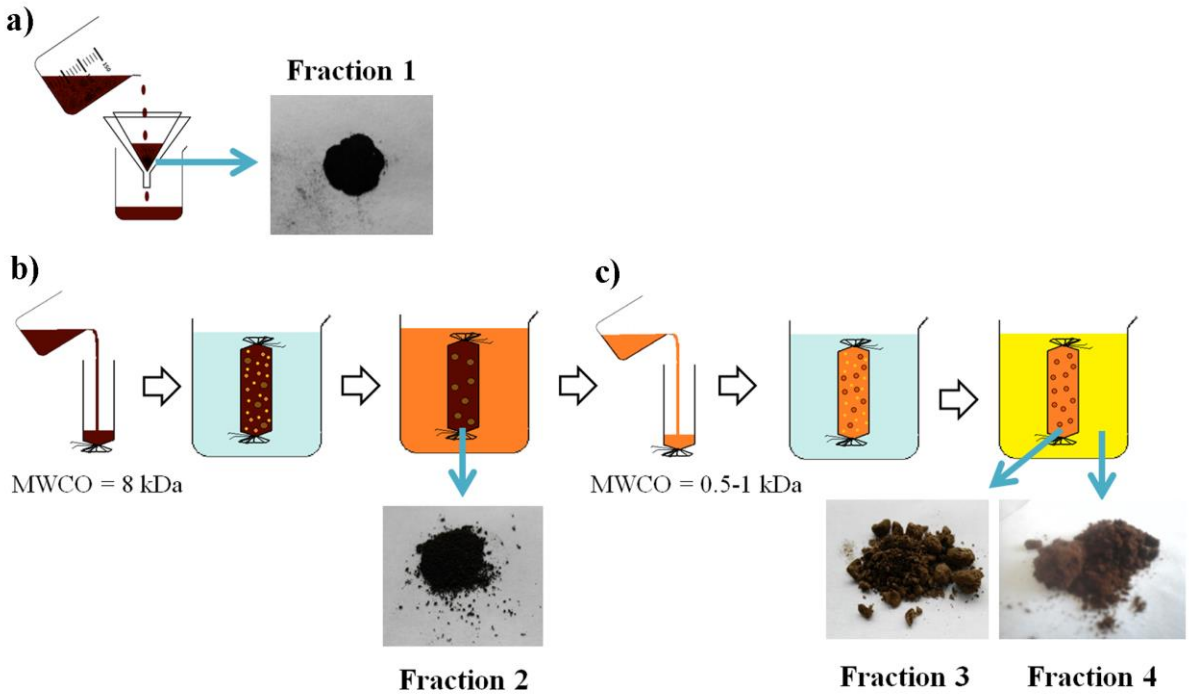

Figure 111.1. Illustration of the separation of the raw material into 4 fractions, by (a) filtration and (b,c) dialysis.

11.3. Results and discussion

Insensitive nuclei enhanced by polarization transfer (INEPT) measurements of the raw CDs in the solid state were performed in order to obtain a useful insight on the chemical structure and functional groups present on the material. Analogously to the CDs synthetized from citric acid and ethylenediamine described in the other chapters of this thesis, three set of signals are observed, corresponding to the presence of carboxylic acids and amides (180 ppm), alcohols (75 ppm) and methylenes carbons (45-25 ppm), and confirming the non-conjugated nature of the particles' structure.

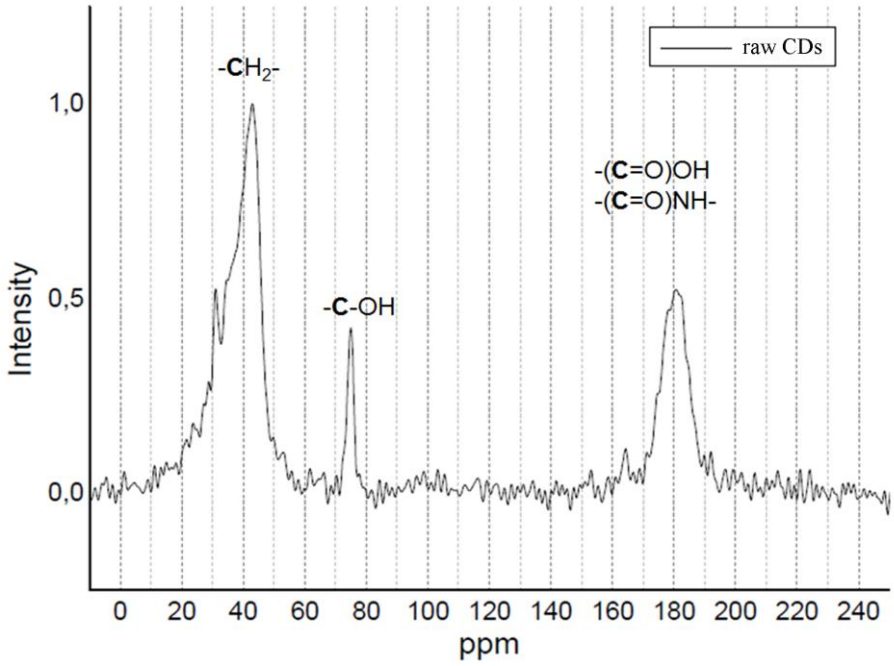

Figure 111.2. INEPT spectrum of raw CDs.

A structural comparison between the fractions was performed by IR analysis. Concerning the position of the bands, the IR spectra of the four fractions are practically equivalent, meaning that the same chemical structures are present for every particle size. Nevertheless, observing the intensities of the carboxylic acid C=O stretching (1710 cm^{-1}) and of the amide vibrational modes (1650-1550 cm^{-1}), it is evident that the ratio carboxylic acid/amide is decreasing from fraction **4** to fraction **1**. This effect should be related with the particle size and the nature of the process of growth during the synthesis. In fact, supposing that the growth is promoted by the amide bond formation and the consequent consumption of carboxylic acids, the relative intensity of the former will increase at expenses of the latter.

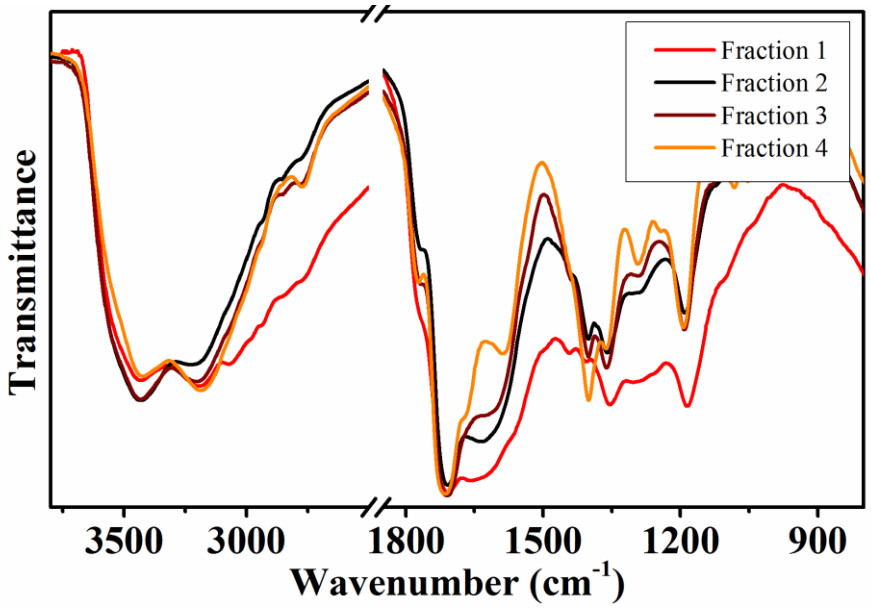

Figure 111.3. IR spectra of fractions 1-4.

The elemental analysis of fractions **1-4** supports this hypothesis. From the smaller particle size (fraction **4**) to the bigger one (fraction **1**), the weight percentage of hydrogen and oxygen decreases, in agreement with the loss of water due to the condensation reaction forming the amide bonds.

Table 111.1. C, H, O and N composition of fraction 1-4.

	Carbon (Weight %)	Hydrogen (Weight%)	Oxygen (Weight%)	Nitrogen (Weight%)
Fraction **1**	52.1	3.8	28.2	14.5
Fraction **2**	47.1	4.1	34.1	12.7
Fraction **3**	45.3	4.5	36.1	12.7
Fraction **4**	43.1	5.0	36.6	15.1

The optical properties of fractions **2-4** (fraction **1** is not soluble) were investigated in water solution by UV/Vis. spectroscopy, steady-state and time-resolved fluorescence spectroscopy. All the fractions show a characteristic absorption band located at 335 nm. This band is narrower for the smallest particles (fraction **2**), while new absorption features contributes to its broadening in fraction **3** and in particular in fraction **4**, corresponding to the bigger particle size.

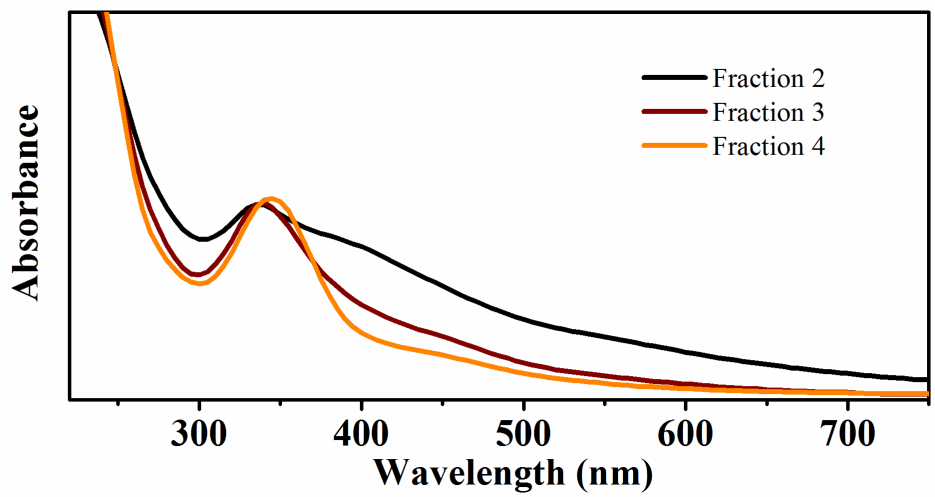

Figure 111.4. UV/Vis. spectra of fractions 2-4.

Also the fluorescence emission is affected by the size. The maximum emission for fraction **3** and **4** is found at 440 nm, obtained exciting the samples at 350 nm. Decreasing the excitation energy, the emission shows a red-shift, as well as a rapid loss of intensity. On the other hand, in fraction **2** the emission for λ_{exc} 350 nm is considerably lower with respect to fractions **3** and **4**, while exciting at lower energy, the intensity of the emission between 500-550 nm is comparable with the other samples. As a result of this, in fraction **2** the maximum emission is found for λ_{exc} 460 nm. The decrease of fluorescence intensity for λ_{exc} 350 nm from fraction **4** to fraction **2** should be ascribed to the simultaneous broadening of the absorption band, which suggests the presence of new energy levels that could furnish alternative non-radiative relaxation pathways for the electrons excited at 350 nm.

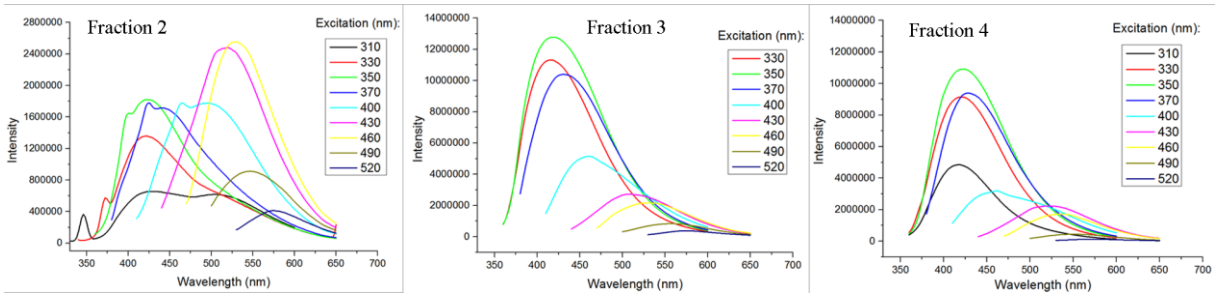

Figure 111.5. Emission spectra of fraction 2-4 (0.5 mg/ml) at different excitation wavelengths.

This observation is confirmed by the fluorescence decays of the three fractions, measured by time-resolved fluorescence spectroscopy. The fluorescence decay obtained exciting at 375 nm and plotted in logarithmic scale is linear for fraction **4** and almost linear for fraction **3**, in agreement with the occurrence of only one radiative relaxation process. Multiple relaxation

processes are occurring instead after the excitation of fraction **2**, whose decay profile is clearly convex.

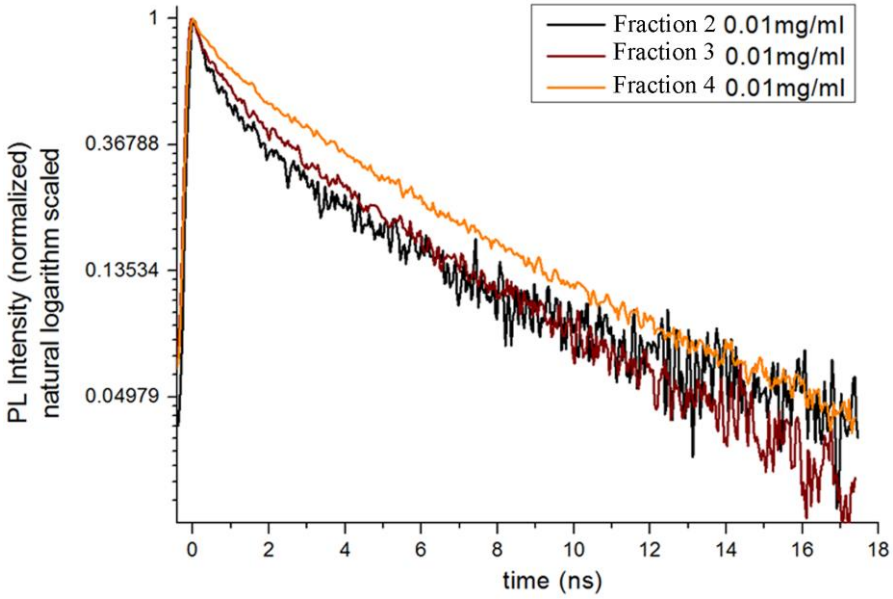

Figure 111.6. Decay profiles (in logarithm) for fractions 2-4.

11.4. Conclusions

In summary, the microwave irradiation of a solid mixture of citric acid monohydrate and urea allowed the synthesis of fluorescent particles of different sizes. A qualitative size separation was performed by filtration and dialysis by means of dialysis tubes with different pore size, obtaining four fractions. The structure and chemical composition of the fractions **1-4** were analysed by NMR, IR and elemental analysis. The results are consistent with the polymeric nature of the particle structure, whose growth is promoted (at least partially) by the amide bond formation at the expenses of the carboxylic acids and amines. Independently from the size, the fractions show the same structural features, which is not unexpected since they originated with the same reaction conditions. Fractions **2-4** exhibit typical absorption and fluorescence features of CDs, similarly to the nanoparticles described in Chapter 2 and 3. Nevertheless, the maximum emission for fractions **3** and **4**, located at 440 nm, is much less intense for fraction **2**, where the maximum emission is found instead at 540 nm. It is possible that in bigger particles the major extension and variability of the polymer structure may result in the proliferation of the energy levels, as observed in the broader absorption spectra of fraction **2**, and in the accessibility of alternative non-radiative relaxation pathways.

LIST OF SCIENTIFIC CONTRIBUTIONS

Publication 1: Supramolecular-enhanced charge-transfer within entangled polyamide chains as origin of the universal blue fluorescence of polymer carbon dots

Lorenzo Vallan, Esteban P. Urriolabeitia, Fernando Ruipérez, Jon Mattin Matxain, Ruben Canton-Vitoria, Nikos Tagmatarchis, Ana M. Benito, Wolfgang K. Maser

Journal of the American Chemical Society 2018, 140 (40), 12862-12869.

Contribution*:* experimental part (synthesis, most of the characterization), preparation of the manuscript.

Publication 2: Electronic Interactions in Illuminated Carbon Dot/MoS2 Ensembles and Electrocatalytic Activity towards Hydrogen Evolution

Ruben Canton-Vitoria, Lorenzo Vallan, Esteban Urriolabeitia, Ana M. Benito,Wolfgang K. Maser,and Nikos Tagmatarchis

Chemistry – A European Journal 2018, 24 (41), 10468-10474.

Contribution*:* experimental part (synthesis, most of the characterization) and the first article draft. Equal contribution of first and second author.

Publication 3: Interfacing transition metal dichalcogenides with carbon nanodots for managing photoinduced energy and charge-transfer processes

Lorenzo Vallan, Ruben Canton-Vitoria, Habtom B. Gobeze, Youngwoo Jang, Raul Arenal, Ana M. Benito, Wolfgang K. Maser, Francis D' Souza, Nikos Tagmatarchis

Journal of the American Chemical Society 2018, 140 (41), 13488-13496.

Contribution*:* experimental part (synthesis, part of the characterization) and the first article draft. Equal contribution of first, second and third author.

Publication 4: A versatile method for the controllable room-temperature synthesis and *in-situ* functionalization of fluorescent carbon dots ***(submitted to Angewandte Chemie International Edition)***

Lorenzo Vallan, Esteban P. Urriolabeitia, Ana M. Benito, Wolfgang K. Maser

Contribution*:* Synthesis and characterization of the materials (except NMR characterization), preparation of the manuscript.